THE EVALUATION OF SOLIDS SUSPENSION IN A PILOT SCALE MECHANICAL FLOTATION CELL

By

Andries P.P. van der Westhuizen

B.Eng. Chem. (Min. Proc.), University of Stellenbosch

A thesis submitted to the University of Cape Town in fulfilment of the requirements for

Master of Science

Department of Chemical Engineering

University of Cape Town

December 2004

SYNOPSIS

The central step in flotation is particle collection, with solids suspension together with gas dispersion and reagent mixing as necessary preconditions to particle collection. Solids suspension is therefore often identified as an important subprocess for effective flotation. Yet, surprisingly little work has been published on solids suspension in mechanical flotation cells, especially more recent studies since the advent of round mechanical flotation cells and the subsequent dramatic increases in maximum cell sizes are largely lacking. This despite Arbiter and Steininger (1962) having already proposed that what is needed is a dual correlation between a solids suspension measure and floatability on the one hand and between this solids suspension measure and system variables on the other. To this end Arbiter, Harris and Yap (1969) proposed a suspension height correlation in terms of system variables. However, suspension height has since been found not as reliable and consistent a predictor of solids suspension conditions as the critical impeller speed (N_{js}). Similarly, Schubert (1985) used critical impeller speed as their solids suspension measure. They related the floatability of a number of flotation processes relative to critical impeller speed, but did not relate is to system variables. It follows that: solids suspension is important for effective flotation, that most studies containing aspects of solids suspension are somewhat dated, and that although critical impeller speed has been found useful no correlation relating N_{js} to system conditions could be found in the flotation literature. It was therefore decided to contribute to solids suspension in flotation cells, by *evaluating solids suspension in a mechanical flotation cell.*

Fortunately, solids suspension had been the focus of many studies in the general chemical engineering literature, mostly in solid-liquid two-phase systems, but increasingly also in three-phase systems. From extensively reviewing these studies, the critical impeller speed emerged as the most consistent and commonly used solids suspension parameter. The *critical impeller speed* (N_{js}) is the impeller speed at the just suspended condition, where *off-bottom* suspension is just complete. Zwietering (1958) and a number of further studies related N_{js} to changes in particle size (d_p), solids concentration (X), solid-liquid density difference ($\Delta\rho/\rho_L$), and liquid kinematic viscosity (ν_L) as solid-liquid variables, whilst geometrical variables were also included by some. Later studies considered the effect of gas addition on N_{js} [e.g. Chapman et al. (1983)]. Due to significant differences in the design of standard stirred tanks and mechanical flotation cells (mainly impeller and stator design), it can be expected that the

critical impeller speed in a mechanical flotation cell will be influenced differently by the system variables. A 124 l (T = 0.54m) pilot scale Bateman mechanical flotation cell was selected for this study. It was decided that this cell size was sufficiently large to be representative of larger scale effects, but not too large so as to be suffering from inaccurate measurements. A detailed experimental programme was conducted to test the effect of each of the solid-liquid variables (i.e. d_p, X, $\Delta\rho/\rho_L$, ν_L) on N_{js}. The effect of geometrical variables (e.g. T, D/T, C/T) were not studied in this work. Visual observation of the tank bottom was used while applying the 1s criterion to identify the critical impeller speed.

From the *two-phase* critical impeller speed (N_{jsu}) work it followed that particle size (d_p) and especially solid-liquid density difference ($\Delta\rho/\rho_L$) had the largest effects on the critical impeller speed. These effects were also stronger than that found in most stirred tank studies. The effect of solids concentration was found to be relatively small and also smaller than most stirred tank studies. The effect of viscosity was conflicting for two particles sizes tested, but overall it was found small enough to ignore the effect of viscosity on N_{jsu}.

The three-phase critical impeller speed (N_{jsg}) work considered two aspects. Firstly, the effect of gas addition on N_{jsg}, and secondly, the effect of the solid-liquid variables under gassed conditions. Gas addition was seen to cause a linear increase in N_{jsg} and that the slope of this increase was proportional to the value of N_{jsu}. It was further seen that the effect of the solid-liquid variables were affected by gas addition, firstly increasing from ungassed to a gassing rate of 1.1 vvm (J_G = 1.0 cm/s) before decreasing on further increased air addition. However, considering the effect of the solid-liquid variables for the different gassing rates combined, they emerged as being very similar to the ungassed effects, which led to the final correlation being based on all the ungassed and gassed data combined. This analysis led to the final N_{js} correlation for both two and three-phase conditions in the tested mechanical flotation cell.

$$N_{jsg} = K_{SL'} d_p^{0.33\pm0.03} X^{0.17\pm0.03} \left(\frac{\rho_S - \rho_L}{\rho_L}\right)^{0.70\pm0.06} (\nu/\nu_w)^{0.05\pm0.04} (1 + K_G . J_G)$$

Where, $K_{SL'} = 52$, $K_G = 0.40$ (cm/s)$^{-1}$ or 0.36 vvm^{-1}

This correlation demonstrates how the off-bottom suspension condition in terms of the critical impeller speed was influenced by the full range of solid-liquid-gas variables in a mechanical flotation cell. In applying this correlation, it was seen that solids density had the largest effect

on N_{jsg}, followed by gas addition and particle size. Solids concentration and liquid kinematic viscosity had relatively very little effect on off-bottom suspension in terms of the critical impeller speed.

A secondary objective of this work was to consider solids distribution vertically in the cell and to determine whether it is related to off-bottom suspension. For this, solids concentration profiles were measured by sample withdrawal for a full range of impeller speeds (300-1100 rpm), for two particle fractions (75-106; 150-250 μm), and for both ungassed and gassed conditions (Q_G = 0, 1 cm/s = 0, 1.1 vvm). The ungassed profiles had different characteristics to the gassed profiles due to gas addition detrimentally affecting both the off-bottom suspension and the solids distribution in the tank. The rising gas bubbles were seen to contribute to the dispersion of solids in the uppermost, more quiescent areas of the cell. This effect was more significant for the finer particle size. Finally, effectiveness measures that could be derived from the concentration profiles were benchmarked against relative impeller speed. These effectiveness measures included the extent of off-bottom suspension, suspension heights, and the variation within the distribution. It was shown how definite trends emerged for these off-bottom and solids distribution measures when plotted relative to the critical impeller speed (N/N_{js}). These concentration profile studies thus confirmed the important role played by the critical impeller as a solids suspension parameter, both off-bottom and distribution.

ACKNOWLEDGEMENTS

Dr Dave Deglon, for his focus on what is important, attention to detail when it matters, and for continuously stirring this work.

Dr Malcolm Powell, for allowing me the time to focus on this work during the write-up stage, for his energy, enthusiasm and interest. The only man I know that will spent a full day sampling and inspecting steaming hot mills and then still go for his normal evening run.

All other members of the mineral processing research unit. Kenneth Maseko, for always being willing to help with my rig and other laboratory work, and your friendship. Tshikusa Lukusa and Jason Waters, who assisted me in much of the experimental work. Matthew Duddy, Gareth Smith, Dylan Campbell and Nicholas Roberts who worked with me during the early stages of this work.

My family and friends, for their support. Pa - your example inspired me. Ma, Isabel, Danie and Izak, thank you for understanding, you should see me more often from now on. Sulene, thank you for your support and encouragement, especially over the last couple of months! My other friends, ek is klaar!

Heavenly Father, for your seen and unseen guidance and strength.

TABLE OF CONTENTS

SYNOPSIS ii
ACKNOWLEDGEMENTS v
TABLE OF CONTENTS vi
LIST OF FIGURES ix
LIST OF TABLES xiii
NOMENCLATURE xiv

CHAPTER 1 INTRODUCTION 1

CHAPTER 2 LITERATURE 3

2.1 FROTH FLOTATION 5
2.1.1 Overview of Froth Flotation 5
2.1.2 The Flotation Process 6
2.1.3 Overview of Flotation Cells 11
2.2 MECHANICAL FLOTATION CELLS 13
2.2.1 Overview of Mechanical Flotation Cells 13
2.2.2 Types of Mechanical Flotation Cells 15
2.3 SUBPROCESSES AFFECTING THE COLLECTION ZONE 22
2.3.1 Hydrodynamics 24
2.3.2 Gas Dispersion 29
2.3.3 Solids Suspension 37
2.4 SOLIDS SUSPENSION IN STIRRED TANKS 47
2.4.1 Conditions for Evaluating the Effectiveness of Solids Suspension 47
2.4.2 Experimental Methods 51
2.4.3 Criteria for Identifying the Just Suspended Condition 59
2.4.4 Critical Impeller Speed Correlations (Two-Phase) 64
2.4.5 Critical Impeller Speed in Three-Phase Systems 82
2.4.6 Solids Distribution 93
2.5 SOLIDS SUSPENSION IN FLOTATION 103
2.5.1 Critical Impeller Speed, Njs 104
2.5.2 Solids Distribution 110
2.6 SCOPE AND OBJECTIVES OF THIS THESIS 115

CHAPTER 3 EXPERIMENTAL 119

3.1 EXPERIMENTAL RIG 120
3.2 VARIABLES AND MEASUREMENTS 122
3.2.1 Impeller Speed and Critical Impeller Speed 122
3.2.2 Particle Size and Solids Density 122
3.2.3 Solids Concentration 123
3.2.4 Viscosity and Liquid Temperature 124
3.2.5 Air Addition 126
3.2.6 Frother Addition and Gas Holdup 127
3.3 EXPERIMENTAL PROGRAMME AND PROCEDURES 129
3.3.1 Critical Impeller Speed 130
3.3.2 Solids Concentration Profiles 132

CHAPTER 4 CRITICAL IMPELLER SPEED 135

4.1 SOLID-LIQUID TWO-PHASE CRITICAL IMPELLER SPEED 136
4.1.1 The Effect of Solid-Liquid Variables on Njsu 137
4.1.2 Critical Impeller Speed Correlation for Two-phase conditions, Njsu 145
4.2 THREE-PHASE CRITICAL IMPELLER SPEED 150
4.2.1 The Effect of Gas Addition on the Critical Impeller Speed 151
4.2.2 Graphical Analyses of the Effect of Solid-Liquid Variables under Gassed Conditions 165
4.2.3 Numerical Analyses of the Effect of Solid-Liquid Variables under Various Gassed Conditions 170
4.2.4 Critical Impeller Speed Correlations for Two- and Three-Phase Conditions 174
4.2.5 Summary of Findings and Comparison with Literature 178
4.2.6 Application of Njsg Correlation 180
4.3 CONCLUSIONS 182
4.3.1 Two-Phase Critical Impeller Speed 182
4.3.2 Three-Phase Critical Impeller Speed 183

CHAPTER 5 SOLIDS CONCENTRATION PROFILES 187

5.1 SOLIDS CONCENTRATION PROFILES 188
5.1.1 Two-Phase Profiles at Various Impeller Speeds 189
5.1.2 Three-Phase Profiles at Various Impeller Speeds (JG = 1 cm/s) 191
5.1.3 Concentration above the Base vs. Increasing Impeller Speed 193
5.1.4 Testing the Sedimentation-Dispersion Model for Vertical Solids Distribution 195

5.2 EFFECTIVENESS OF SOLIDS SUSPENSION 199
5.2.1 Extent of Off-bottom Solids Suspension (Xm/Xms) 199
5.2.2 Extent of Vertical Solids Distribution (Suspension Heights) 201
5.2.3 Variability of Vertical Solids Concentrations (RSD) 203
5.3 CONCLUSIONS 205

CHAPTER 6. CONCLUSIONS 209

6.1 CRITICAL IMPELLER SPEED 209
6.1.1 Two-Phase Critical Impeller Speed 209
6.1.2 Three-Phase Critical Impeller Speed 210
6.2 CONCENTRATION PROFILES 212
6.2.1 Evaluation of Concentration Profiles 212
6.2.2 Effectiveness of Solids Suspension 214

REFERENCES 217

APPENDIX A. CRITICAL IMPELLER SPEED DATA 229

A.1 CRITICAL IMPELLER SPEED RAW DATA 230
A.2 CRITICAL IMPELLER SPEED TWO-PHASE DATA 233
A.3 CRITICAL IMPELLER SPEED THREE-PHASE DATA 237
A.4 CRITICAL IMPELLER SPEED TWO- AND THREE-PHASE DATA 242
A.5 MULTIPLE LINEAR REGRESSION RESULTS 245

APPENDIX B. CONCENTRATION PROFILE DATA 249

B.1 SOLIDS CONCENTRATION PROFILE TWO-PHASE DATA 250
B.2 SOLIDS CONCENTRATION PROFILE THREE-PHASE DATA 251

LIST OF FIGURES

Figure 2.1 Schematic representation of the flotation process....7
Figure 2.2 Conventional mechanical flotation cell....14
Figure 2.3 Increase in flotation cell sizes in terms of (a) volume, (b) tank diameter....15
Figure 2.4 Wemco SmartCellTM....17
Figure 2.5 Forced-aerated round flotation cells....19
Figure 2.6 Schematic of a mechanical flotation cell showing different zones in cell....23
Figure 2.7 Collection zone subprocesses in mechanical flotation cells....23
Figure 2.8 Hydrodynamic variables in a mechanical flotation cell....25
Figure 2.9 Schematic of the gas dispersion action in a mechanical flotation cell....30
Figure 2.10 Different stages of impeller flooding and gas dispersion (loading) [adapted from Chapman et al. (1983b)]....34
Figure 2.11 Balance of forces at the terminal settling velocity uT of a particle....38
Figure 2.12 Evaluating the effectiveness of solids suspension with increasing N....48
Figure 2.13 Scale of solids suspension conditions....51
Figure 2.14 Influence of sample withdrawal velocity and sampling tube tip shape on the concentration profile [Barresi and Baldi (1987a)]....55
Figure 2.15 Suspension height measurements (CH) at (a) various N/Njs, and (b) various X with N = Njs [Hicks, Myers and Bakker (1997)]....61
Figure 2.16 Solids concentration vs impeller speed for different sample heights [Ayazi Shamlou and Koutsakos (1989)]....62
Figure 2.17 Stirrers used by Zwietering....66
Figure 2.18 The dependance of the S parameter in Zwietering's equation on impeller type, impeller diameter (T/D) and impeller clearance (T/C)....69
Figure 2.19 Comparison of predicted Njs values from some correlations with that of Zwietering's correlation ('experimental') [Rewatkar and Joshi (1991)]....72
Figure 2.20 Log-log plot of Njs vs. dp Chapman et al. (1983a)....74
Figure 2.21 Solids-to-liquid mass ratio, B as a function of solids concentration, X....75
Figure 2.22 The effect of solids volume concentration on slurry apparent viscosity for different d50 particle sizes [Thomas (1965) as given in Stanley (1987)]....77
Figure 2.23 Effect of scale (T) on Njs [Chapman et al. (1983a)]....79
Figure 2.24 Influence of impeller clearance on flow patterns and suspension of solids [Nagata (1975)]....81
Figure 2.25 Increase in Njsg required for solids suspension with decrease in NPg on increased gassing for DT's [Frijlink, Bakker and Smith (1990)]....86
Figure 2.26 Increase in power addition for complete suspension (εjsg) with Njsg and QGV (data taken from Chapman et al. (1983c); cf. Table 2.10)....87
Figure 2.27 Effect of gas flow rate, QGV, on Njsg [Chapman et al. (1983c)]....89

Figure 2.28 ΔNjs vs QG for a DT impeller in a T=0.29m tank for all test conditions [Wong, Wang and Huang (1987)] 89
Figure 2.29 ΔNjs vs QG for three DT impeller sizes in a T = 0.56m tank for all test conditions [Chapman et al. (1983c)] 89
Figure 2.30 Radial concentration profiles at various impellers speeds for a Rushton turbine [Barresi and Baldi (1987a)] 94
Figure 2.31 Axial concentration profiles at (a) various impeller speeds and (b) various particle sizes [Barresi and Baldi (1987a)] 95
Figure 2.32 Semi-logarithmic plot of solids concentration vs sample height for different impeller speeds [Ayazi Shamlou and Koutsakos (1989)] 98
Figure 2.33 Critical impeller speed Njs and just suspended power density (P/V)js for various finger and bladed impellers) [Mavros (1992); data taken from Schubert, Bischofberger and Koch (1982b)] 104
Figure 2.34 Critical impeller speed (Njs = n1s) as a function of power number (NP = cP) [Schubert (1985)] ..105
Figure 2.35 The effect of air addition (qL = QGV) on (a) the just suspended power addition [(P/V)1s = (P/V)js] and (b) the critical impeller speed (n1s = Njs). [Weiss and Schubert (1989)] 107
Figure 2.36 The effect of scale on the just suspended condition: (a) Njs vs. V, (n1s = Njs); (b) (P/V)js vs. D, (d2 = D), broken lines = authors own results, line #5 = Zwietering (1958)'s results [Schubert (1985)]. 108
Figure 2.37 Diagram indicating optimal flotation conditions for different size fractions of a sylvinite ore; 1: 0.5-1.6 mm; 2: 0.125-0.50 mm; 3: -0.125 mm [Schubert and Bischofberger (1978)] 110
Figure 2.38 Solids Concentration Profiles from 42.5 m3 Wemco Cells (a) Cell 1 with forced air (b) Cell 9 with self-aeration [Yianatos et al. (2001)] 113
Figure 2.39 Solids Particle Size Profiles from 42.5 m3 Wemco Cells (a) Cell 1 with forced air (b) Cell 9 with self-aeration [Yianatos et al. (2001)] 113

Figure 3.1 Experimental rig 120
Figure 3.2 Impeller and stator mechanism 121
Figure 3.3 Determining the sugar concentrations to use for the viscosity tests 125
Figure 3.4 The viscosity of water vs. temperature [Data taken from Rogers and Mayhew (1988)] 126
Figure 3.5 Effect of frother concentration on the critical impeller speed 127
Figure 3.6 Effect of frother concentration on the average gas holdup in the tank 128
Figure 3.7 Sample withdrawal to obtain solids concentration profiles 133

Figure 4.1 The effect of particle size dp on the ungassed critical impeller speed Njsu for solids concentrations ranging between 5 and 20 wt% 139
Figure 4.2 The effect of solids concentration X on the ungassed critical impeller speed Njsu for average particle sizes ranging between 91 and 675 μm 140
Figure 4.3 The effect of relative solid-liquid density difference [(ρS-ρL)/ρL] on the ungassed critical impeller speed Njsu for solids concentrations ranging from 5 to 15% 142
Figure 4.4 The effect of kinematic liquid viscosity vL (and ρL) on the critical impeller speed Njsu for d50 = 91, 200 μm 144

Figure 4.5 The effect of kinematic liquid viscosity vL on the critical impeller speed Njsu for d50 = 91, 200 µm 145
Figure 4.6 Njsu predicted by Equation 4 12 vs. experimentally measured Njsu values (excludes viscosity work) 148
Figure 4.7 Graphical presentation of all Njs results vs. air addition rate, JG 153
Figure 4.8 Increase in Njs with air addition (JG) obtained in experimental Phase I, (a)-(d): X = 5, 10, 15, and 20 wt% 154
Figure 4.9 Increase in Njs with air addition (JG) obtained in experimental Phase II 154
Figure 4.10 Nominal increase in critical impeller speed (ΔNjs) vs. JG 156
Figure 4.11 Predicted Njsu' values using Njsu' = Njsg – a.JG vs. experimentally measured Njsu values; a = 226 rpm.(cm/s)-1 157
Figure 4.12 Ka values from graphical results in Figure 4.8 and Figure 4.9 vs. Njsu 158
Figure 4.13 Relative increase in critical impeller speed (ΔNjs/Njsu) vs. JG 159
Figure 4.14 Predicted Njsu' values using Njsu' = Njsg / (1 + K.JG) vs. experimentally measured Njsu values; K = 0.40 (cm/s)-1 160
Figure 4.15 Relative increase in critical impeller speed as a power function of (1+JG) 161
Figure 4.16 Predicted Njsu' values using Njsu' = Njsg / (1 + Jg)m vs. experimentally measured Njsu values; m = 0.52 162
Figure 4.17 Variation of Ka vs. (a) X and (b) Δρ/ρL from the graphical results given in Figure 4.8 and Figure 4.9 163
Figure 4.18 Determining the correlation coefficient for Option 4, ΔNjs / dp0.11. X0.23. (Δρ/ρL)0.62 vs. JG . 164
Figure 4.19 Predicted Njsu' values using Njsu' = Njsg - 54.dp0.11. X0.23. (Δρ/ρL)0.62.JG vs. experimentally measured Njsu values 164
Figure 4.20 The effect of particle size, dp on Njs at different gassing rates, (a) JG = 0, (b) JG = 1.0, (c) JG = 1.5, (d) JG = 2.0 cm/s 166
Figure 4.21 The effect of solids concentration, X on Njs at different gassing rates, (a) JG = 0, (b) JG = 1.0, (c) JG = 1.5, (d) JG = 2.0 cm/s 168
Figure 4.22 The effect of solids density difference, Δρ/ρL on Njs at different gassing rates, (a) JG = 0, (b) JG = 1.0, (c) JG = 1.5 169
Figure 4.23 The effect of liquid kinematic viscosity, vL on Njs at different gassing rates, (a) JG = 0, (b) JG = 1.0 cm/s 169
Figure 4.24 Numerical analyses of the effect of solid-liquid variables under various gassed and ungassed conditions (JG = 0, 1.0, 1.5, 2.0 cm/s; Or QGV = 0, 1.1, 1.7, 2.2 vvm) 173
Figure 4.25 The quality of the Njsg correlation fit obtained from the JG = 1.0 cm/s data 175
Figure 4.26 The quality of the Njsg correlation fit obtained from all three-phase data (JG > 0 cm/s) 176
Figure 4.27 The quality of Njs correlation fit obtained from the full dataset of gassed and ungassed tests (JG ≥ 0 cm/s) 177
Figure 4.28 Critical impeller speeds determined from Equation 4 28 by changing one variable at a time from a base condition (cf. Table 4.7 & Table 4.8) 181

Figure 5.1 Solids concentration profiles for dp91 (75 – 106 µm) at various N under two-phase conditions 190

Figure 5.2 Solids concentration profiles for dp200 (150 – 250 μm) at various N under two-phase conditions..190
Figure 5.3 Solids concentration profiles for dp91 (75 – 106 μm) at various N under three-phase conditions....192
Figure 5.4 Solids concentration profiles for dp200 (150 – 250 μm) at various N under three-phase conditions 192
Figure 5.5 Solids concentrations (Xh25) at a point h/T = 25% above the base vs. relative impeller speeds (N/Njs) 194
Figure 5.6 Applying the sedimentation-dispersion model to the vertical solids distribution of the (a) dp91 and (b) dp200 size fractions under two-phase conditions....196
Figure 5.7 Applying the sedimentation-dispersion model to the vertical solids distribution of the (a) dp91 and (b) dp200 size fractions under three-phase conditions....197
Figure 5.8 Average profile solids concentrations (Xm) versus increasing impeller speed 200
Figure 5.9 Extent of off-bottom solids suspension versus percentage of Njs 200
Figure 5.10 Relative suspension heights versus increasing impeller speed 202
Figure 5.11 Relative suspension heights versus percentage of critical impeller speed 202
Figure 5.12 Relative standard deviation of profile concentrations versus increasing impeller speed 204
Figure 5.13 Relative standard deviation of profile concentrations versus percentage of critical impeller speed 204

LIST OF TABLES

Table 2.1 Round Mechanical Flotation Cells Supplied as at 2004 16
Table 2.2 Hydrodynamic Dimensionless Groups in Mechanical Flotation Cells....26
Table 2.3 Hydrodynamic Parameters Used in Mechanical Flotation Cells 29
Table 2.4 Solids Suspension Conditions 49
Table 2.5 Variables and Ranges Used by Zwietering 66
Table 2.6 Critical Impeller Speed Correlations in Two-Phase Systems # 70
Table 2.7 The Effect of Impeller Clearance (C/T) on Njs and Pjs for Disc Turbines [Chapman et al. (1983a)]...79
Table 2.8 Theoretical Correlations for the Critical Impeller Speed # 82
Table 2.9 Efficiency of Different Impellers in Two-Phase Solids Suspension [Chapman et al. (1983a)] 83
Table 2.10 Effect of Gas Addition on Solids-Liquid Hydrodynamics Chapman et al. (1983c) 85
Table 2.11 Critical Impeller Speed Correlations in Three-Phase Systems 92

Table 3.1 Particle size fractions used in this testwork 123
Table 3.2 Solids Concentrations Used In This Work 124
Table 3.3 Sucrose Sugar Concentrations vs. Solution Density and Viscosity 125
Table 3.4 Air Addition Settings and Measurements 127
Table 3.5 Variables Influencing Solids Suspension and Those Tested In This Work 129
Table 3.6 Critical Impeller Speed Tests Phase I: Effect of Particle Size, Solids Concentration, and Superficial Gas Velocity 131
Table 3.7 Critical Impeller Speed Tests Phase II: Effect of Solids Density 131
Table 3.8 Critical Impeller Speed Tests Phase III: Effect of Liquid Viscosity 132
Table 3.9 Solids Concentration Profile Conditions 134

Table 4.1 Two-phase Critical Impeller Speed Correlation Results 147
Table 4.2 Comparison of Two-phase Critical Impeller Speed Results with Literature 148
Table 4.3 Rate of Linear Increase in Njs with Gas Addition, Ka, for Different Conditions (Obtained from Figure 4.8 & Figure 4.9) 155
Table 4.4 Graphical Analyses of the Effect of Two-Phase Variables at Different Gassing Rates 170
Table 4.5 Numerical Analyses of the Effect of Solid-Liquid Variables under Various Gassed and Ungassed Conditions 172
Table 4.6 Comparison of Three-phase Correlation Results with Findings from Literature 178
Table 4.7 Base Case and Increased Values used in this Case Study 180
Table 4.8 Calculated Njsg Values using Equation 4 28 and the Case Study Variable Values in Table 4.7 181

NOMENCLATURE

SYMBOL	DESCRIPTION	UNITS	BASE
a,b,c	Arbitrary exponents	-	-
A_c	Cross-sectional area	m^2	m^2
C_b	Impeller-bottom clearance, distance between bottom of the blade and the tank bottom	m	m
C_D	Drag coefficient	-	-
C	Impeller clearance, midplane off tank bottom	m	m
d_b	Bubble size	mm	m
d_p	Particle size	µm	m
D	Impeller diameter	m	m
D_S	Solids dispersion coefficient	$m^2.s^{-1}$	$m^2.s^{-1}$
F	Force	N	$kg.m.s^{-2}$
g	Acceleration of gravity	$m.s^{-2}$	$m.s^{-2}$
h_s	Suspension height of solids	m	m
H	Tank height	m	m
K	Arbitrary equation constant	-	-
M	Shaft torque	N.m (= J)	$kg.m^2.s^{-2}$
m	Mass	kg	kg
N	Impeller speed	rpm	s^{-1}
N_{hs}	Impeller speed for homogeneous solids suspension	rpm	s^{-1}
N_{js}	Critical impeller speed for solids suspension (N when the solids are just suspended off the base – also referred to as complete suspension)	rpm	s^{-1}
N_{Ar}	Archimedes number $= d_p^3(\rho_S-\rho_L).\ \rho_L^{-1}.\nu^{-2}$	-	-
N_{Fr}	Froude number $N_{Fr} = N^2D/g$	-	-
N_{hd}	Discharge head coefficient, $N_{hd} = h_d g/N^2D^2$	-	-
N_P	Power number $N_P = P/\rho_{SL}N^3D^5$	-	-
N_{Pe^*}	Modified Peclet number $= u_s.T/D_S$	-	-

N_{Qd}	Discharge *flow* coefficient, $N_{Qd} = Q_d / ND^3$, (also flow coefficient or pumping number)	-	-
N_{QG}	Airflow number, $N_{QG} = Q_G / ND^3$	-	-
N_{Re}	Reynolds number $N_{Re} = \rho_{SL} ND^2 / \mu_L$	-	-
N_{We}	Weber number, $N_{We} = \rho_{SL} N^2 D^3 / \sigma_{GL}$	-	-
P	Power, shaft	W	$kg.m^2.s^{-3}$
P_a	Probability of particle-bubble attachment	-	-
P_c	Probability of particle-bubble collision	-	-
$P_{collect}$	Probability of particle collection	-	-
P_d	Probability of particle-bubble detachment	-	-
P/V	Power density	$W.m^{-3}$	$kg.m^{-1}.s^{-3}$
Q	Volumetric flowrate	m^3s^{-1}	m^3s^{-1}
Q_{GV},	Specific air flowrate	$m^3.m^{-3}.min^{-1}$ or vvm	s^{-1}
r^2 or R^2	Coefficient of determination (Square of Pearson product moment)	-	-
RSD	Relative standard deviation (population) $RSD = \sqrt{\frac{1}{n}\sum_{i=1}^{n}(X_i - \bar{X})^2} \Big/ \bar{X}$	-	-
S	A parameter used in Zwietering's correlation	-	-
SG	Specific gravity: $SG = \rho/\rho_w \sim \rho/1000$	-	-
S_I	Impeller submergence, Z-C	m	m
T	Tank diameter	m	m
u	Velocity	m/s	m/s
u_c	Fluid circulation velocity	m/s	m/s
u_s	Relative velocity between particle and fluid (slip velocity)	m/s	m/s
u_{sh}	Hindered slip velocity of particles	m/s	m/s
u_{st}	Slip velocity of particles under turbulent conditions	m/s	m/s
u_T	Terminal settling velocity of a particle	m/s	m/s
V	Volume	m^3	m^3
V_i	Impeller swept volume, $\pi/4.D^2W$	m^3	m^3

W	Impeller width	m	m
X	Solids mass concentration	-	-
X_B	X at a point close to the base of the vessel	-	-
X_{act}	Known bulk solids concentration	-	-
X_m	Mean solids concentration in a profile	-	-
X_{ms}	Mean solids concentration in a profile under completely suspended conditions ($N \geq N_{js}$)	-	-
h	Vertical distance from the base of the vessel	m	m
Z	Liquid surface height from the base of the vessel	m	m

Greek Symbols

ε	Specific power input per mass of slurry	W/kg	$m^2.s^{-3}$
θ_{circ}	Circulation time (longest loop)	s	s
θ_{mix}	Mixing time	s	s
θ_{tt}	Tank turnover time	s	s
μ	Viscosity, dynamic (water at 20°C = 1cP = 1.002×10^{-3} Pa.s = 1.002×10^{-3} $kg.m^{-1}.s^{-1}$)	cP	$kg.m^{-1}.s^{-1}$
ν	Viscosity, kinematic (water at 20°C = 1.004×10^{-6} $m^2.s^{-1}$)	$m^2.s^{-1}$	$m^2.s^{-1}$
ρ	Density	kg/m^3	kg/m^3
σ	Surface tension	$N.m^{-1}$	$kg.s^{-2}$
σ_{rel}^2	Relative variance	-	-

$$\sigma_{rel}^2 = \frac{1}{n}\sum_{i=1}^{n}(X_i - \bar{X})^2 \Big/ \bar{X}^2$$

Subscripts

*	Indicates a modified quantity
0, u	Used sometimes to indicate ungassed conditions
1,2,3,...	Numbering
B	Refers to the base of the vessel
circ	Circulation
cd	Complete dispersion of gas

d	Discharge
eff	Effective
F	Fluid
G	Gas
g	Gassed conditions
GI	Onset of gas induction
h	Refers to vertical position from the base of the vessel
I	Impeller
i,j,n	Counting parameters
ind	Induced
js	Just suspended condition for solids
L	Liquid
p	Particle(s)
Q	Flow
S	Solid
T	Tank, or tank average values
w	Water

Abbreviations

DT	Disc turbine impeller
FT	Flat-blade turbine (paddle)
PDT	Pitched-blade disc turbine
PT	Pitched-blade turbine
HE	High efficiency axial impeller (chemineer)
Pr	Propeller impeller
APr	A-310 propeller impeller
FPr	Flat-blade propeller impeller
MPr	Marine propeller impeller
VD	Vaned disc impeller
6-	Number in front of impeller notation indicates the number of blades, e.g. 6-DT
-D, -U	A 'D' or 'U' following impeller notation indicates 'upflow' or 'downflow' rotation

	for axial impellers, e.g. PT-D, PT-U.
RTD	Residence time distribution

CHAPTER 1 INTRODUCTION

Flotation is undoubtedly the most versatile and widely used mineral beneficiation process, both in South Africa and worldwide. The central step in the flotation process is particle collection, following successful particle-bubble interaction under sufficient chemical and hydrodynamic conditions [Ralston, Fornasiero and Hayes (1999)]. Solids suspension, together with gas dispersion, and reagent mixing, are necessary preconditions to particle collection and the effectiveness of these subprocesses depends largely on the hydrodynamic conditions within the flotation cell [Schubert and Bischofberger (1998)]. Most early mechanical flotation cell hydrodynamic studies, which included aspects of solids suspension, were done by Arbiter, Harris and coworkers [Arbiter and Steininger (1962); Arbiter and Harris (1962); Arbiter, Harris and Yap (1969)], and further by Schubert and co-workers [Schubert and Bischofberger (1978); Schubert (1985)]. Solids suspension is also taken into account during flotation cell scale-up [Harris (1976); Fallenius (1976)], and coarse particle flotation [Weiss and Schubert (1989); Rodrigues, Leal Filho and Masini (2001)]. More recent publications involving aspects of solids suspension either only extend on previous work [Schubert and Bischofberger (1998); Schubert (1999)], or involves flotation work done in standard stirred tanks and not in mechanical flotation cells [Hui and Ahmed (1998a)], or only reports on industrial findings [Yianatos *et al.* (2001)].

It follows that most of the fundamental work on solids suspension had been done before the late 1980's using cell mechanisms that are mostly obsolete today and before the advent of round mechanical flotation cells. The dramatic increase in cell sizes since the introduction of round mechanical flotation cells further emphasizes the need for the better understanding of all the hydrodynamic subprocesses, including solids suspension, in the design and operation of these cells. Arbiter and Harris (1962) proposed that what is needed is a dual correlation, between an effectiveness of solids suspension criterion and system conditions on the one hand, and between the solids suspension effectiveness criterion and floatability on the other. Yet, although solids suspension is often mentioned in flotation cell design and operation, general methodologies for evaluating, or correlations for predicting, the effectiveness of solids suspension in mechanical flotation cells are not generally available from literature. In contrast, solids suspension has been the object of numerous studies in the general chemical engineering literature. However, even in these studies, there is still a need for three-phase solids suspension work. These studies are however done in standard stirred tanks and due to

the large differences in especially impeller and baffling design as well as operating conditions these results are not necessarily applicable to mechanical flotation cells, as is.

The objective of this work is therefore to contribute to the need for solids suspension studies in mechanical flotation cells. This will be done by evaluating the solids suspension conditions in a pilot scale mechanical flotation cell (124 l Bateman mechanical flotation cell) and how it is affected by changing system conditions. Considering that bubbles will not attach to unsuspended particles, off-bottom suspension conditions are expected to play a large role in mechanical flotation cell operation. The critical impeller speed (N_{js}), taken at complete off-bottom suspension conditions, is the most widely used parameter for solids suspension in stirred tanks. Schubert and co-workers measured N_{js} in mechanical flotation cells. Considering the suggestion by Arbiter and Harris (1962), their work was aimed at relating optimum floatability conditions for a number of processes to the critical impeller speed. They did not relate N_{js} to system variables. The *primary focus* of this work will therefore be to determine how off-bottom suspension (N_{js}) is affected by the solid-liquid-gas system variables, i.e. particle size (d_p), solids concentration (X), solid-liquid density difference ($\Delta\rho/\rho_L$), liquid viscosity (ν_L), as well as gas addition rate (J_G). A *secondary aspect* of solids suspension that will be considered in this work is the vertical distribution of solids as measured by concentration profiles. Concentration profiles measured during some of the critical impeller speed runs will be used to evaluate the effectiveness of solids suspension, also in terms of solids distribution.

The layout of this thesis is as follows. The literature is reviewed in Chapter 2. This review is extensive and wishes to expose the reader to the full breadth of work that has been done in the chemical engineering literature. The experimental equipment, methods, materials, and programme is considered in Chapter 3. The primary focus of this work, being the investigation of critical impeller speed in the pilot mechanical flotation cell will be done in Chapter 4, before considering the concentration profile results in Chapter 5. The conclusions of this work is summarized in Chapter 6.

CHAPTER 2 LITERATURE

CHAPTER 2 LITERATURE 3

2.1 FROTH FLOTATION 5
2.1.1 Overview of Froth Flotation 5
2.1.2 The Flotation Process 6
2.1.2.1 Conditioning 7
2.1.2.2 Collection 8
2.1.2.3 Separation 10
2.1.3 Overview of Flotation Cells 11
2.1.3.1 Mechanical Flotation Cells 11
2.1.3.2 Column Cells 11
2.1.3.3 Novel Cells 12

2.2 MECHANICAL FLOTATION CELLS 13
2.2.1 Overview of Mechanical Flotation Cells 13
2.2.2 Types of Mechanical Flotation Cells 15
2.2.2.1 Self-aerated Flotation Cells 16
2.2.2.2 Forced-aerated Flotation Cells 18

2.3 SUBPROCESSES AFFECTING THE COLLECTION ZONE 22
2.3.1 Hydrodynamics 24
2.3.2 Gas Dispersion 29
2.3.2.1 Gassed Power Draw 31
2.3.2.2 Gas Induction 32
2.3.2.3 Impeller Flooding and Loading 33
2.3.2.4 Gas Dispersion 34
2.3.2.5 Bubble Formation 35
2.3.2.6 Gas Holdup 36
2.3.3 Solids Suspension 37
2.3.3.1 Sedimentation Mechanism 37
2.3.3.2 Suspension Mechanism 40
2.3.3.3 Complete Suspension 42
2.3.3.4 Solids Distribution 43

2.4 SOLIDS SUSPENSION IN STIRRED TANKS 47
2.4.1 Conditions for Evaluating the Effectiveness of Solids Suspension 47
2.4.2 Experimental Methods 51
2.4.2.1 Methods Aimed at Measuring Off-bottom Suspension (N_{js}) 51
2.4.2.2 Methods Aimed at Measuring Solids Distribution (X_{hi} & h_s) 54
2.4.2.3 Other Methods related to Solids Suspension 57

2.4.3 Criteria for Identifying the Just Suspended Condition 59
2.4.3.1 The 1s criterion 59
2.4.3.2 100% Suspension Criterion 60
2.4.3.3 Unsuspended Layer of Solids Criterion 60
2.4.3.4 Radiation Count Rate Criterion 60
2.4.3.5 Rate of Mass Transfer Criterion 60
2.4.3.6 90% Suspension Height Criterion 61
2.4.3.7 Solids Concentration above Base Criterion 62
2.4.3.8 Variation in Vertical Solids Concentrations Criterion 63
2.4.3.9 Mixing Time vs. Impeller Speed Criterion 63
2.4.3.10 Power Number vs. Impeller Speed Criterion 63
2.4.4 Critical Impeller Speed Correlations (Two-Phase) 64
2.4.4.1 The Zwietering Correlation [Zwietering (1958)] 64
2.4.4.2 Overview of Just Suspended Correlations for Two-Phase Systems 70
2.4.4.3 Variables Affecting Solids Suspension (N_{js}) 73
2.4.4.4 Theoretical Critical Impeller Speed Correlations 81
2.4.5 Critical Impeller Speed in Three-Phase Systems 82
2.4.5.1 Impeller types and clearance 82
2.4.5.2 Effect of Solids on Gas-Liquid Hydrodynamics 84
2.4.5.3 Effect of Gas on Solids-Liquid Hydrodynamics 84
2.4.5.4 Three-Phase Critical Impeller Speed Correlations 87
2.4.6 Solids Distribution 93
2.4.6.1 Solids Concentration Profiles 94
2.4.6.2 Variation in Solids Concentration 95
2.4.6.3 Modelling Solids Distribution (Sedimentation-Dispersion Model) 96

2.5 SOLIDS SUSPENSION IN FLOTATION 103
2.5.1 Critical Impeller Speed, N_{js} 104
2.5.2 Solids Distribution 110

2.6 SCOPE AND OBJECTIVES OF THIS THESIS 115

This chapter introduces the field of froth flotation (cf. Section 2.1) before considering the machine used most extensively for froth flotation, being the mechanical flotation cell in Section 2.2. Solids suspension, as the focus of this work, is one of a number of related subprocesses in the collection zone of the mechanical flotation cell. These subprocesses affecting the collection zone is reviewed in Section 2.3. Solids suspension has been studied more extensively in stirred tanks than in mechanical flotation cells, where a shortage of solids suspension work has been identified. For this reason, solids suspension as treated in stirred tanks is considered in Section 2.4. This then serves as background in the evaluation of solids suspension work that has been published in the flotation literature, which is then considered in Section 2.5. The scope and objectives of this work is delineated in the final section of this chapter (cf. Section 2.6).

2.1 FROTH FLOTATION

This section serves as an introduction to the flotation process. After an overview of froth flotation (cf. Section 2.1.1), the flotation process is analyzed in Section 2.1.2. The last part of this section (cf. Section 2.1.3) provides a brief overview of different types of flotation cells used in industry. This section on froth flotation was partly derived with reference to reviews done by Deglon (1998) and Lewis (2003).

2.1.1 Overview of Froth Flotation

Froth flotation as a patented process is well over 100 years old and is the most widely used separation method in the mineral processing industry, responsible for the beneficiation of more than two billion tons of ore annually, consisting of over a hundred different mineral species. The first patent involving mineral flotation was granted in 1860 to Haynes who recognised differences in the wettability of mineral particles by oil and water [Anon (1998)]. This was the starting point for a number of "oil" flotation processes. Froth flotation was first used commercially at Broken Hill to treat zinc-rich lead tailings in 1909 [Griffiths (1998)]. Originally used to treat lead, zinc and copper sulphide ores, froth flotation is now applied to over one hundred different mineral species, including iron oxides, oxidised minerals such as malachite, and also non-metallic ores such as coal. The selectivity of the

process also means that complex orebodies, such as those containing lead, zinc and silver-bearing minerals can be separated into specific concentrates.

Due to its prevalence in mineral processing, inefficiencies in flotation translate into both enormous losses of revenue and unnecessary wastes of the world's valuable and steadily declining mineral reserves. These losses are expected to compound in the coming decades as, due to the preferential processing of high quality ores, mining companies are forced to treat more, more complex, and finely disseminated ore bodies. In order to address the inefficiencies in flotation processes considerable flotation research has been undertaken, especially in the three major areas of flotation reagent, flotation cell, and flotation fundamental research [Schulze (1984)]. Research into *flotation reagents* has focused on the development of new reagents and an understanding of the role of these reagents in the subprocesses of flotation. Research into *flotation cells* has focused on the development of new flotation cell technologies and improved economies of scale from a better understanding of cell hydrodynamics and the subprocesses of flotation. Research into *flotation fundamentals* affects both the aforementioned areas of research, and has focused on improving flotation efficiency through an increased understanding of the fundamental mechanisms behind the sub- and microprocesses in flotation.

2.1.2 The Flotation Process

The process of flotation selectively separates different minerals by exploiting differences in the surface properties of the various species. The addition of flotation reagents selectively renders the surfaces of mineral particles either hydrophobic or hydrophilic. The hydrophobic particles become attached to air bubbles and are carried upwards through the slurry to a froth layer that forms at the top of the flotation cell. This froth layer is removed and usually becomes the concentrate. Hydrophilic particles remain in the slurry in the flotation cell and usually discharge as the tails in conventional flotation. In *reverse* flotation, the gangue minerals are removed in the froth stream and the valuable mineral remains in the slurry discharge stream.

Froth flotation is dependent on the successful completion of a large number of interdependent sub- and microprocesses, all of which are required for a mineral particle to selectively report to the flotation concentrate. As shown in Figure 2.1 these sub- and microprocesses can largely

be divided into three stages of the process, i.e. the *conditioning stage*, the *collection stage*, and the *separation stage* as also identified by Schulze (1984). Although a particle has to go through these stages in sequence before successful recovery or rejection, it should be remembered that these stages are interdependent and occur simultaneously in a flotation cell. The conditioning, collection and separation stages will now be briefly considered in Sections 2.1.2.1 to 2.1.2.3.

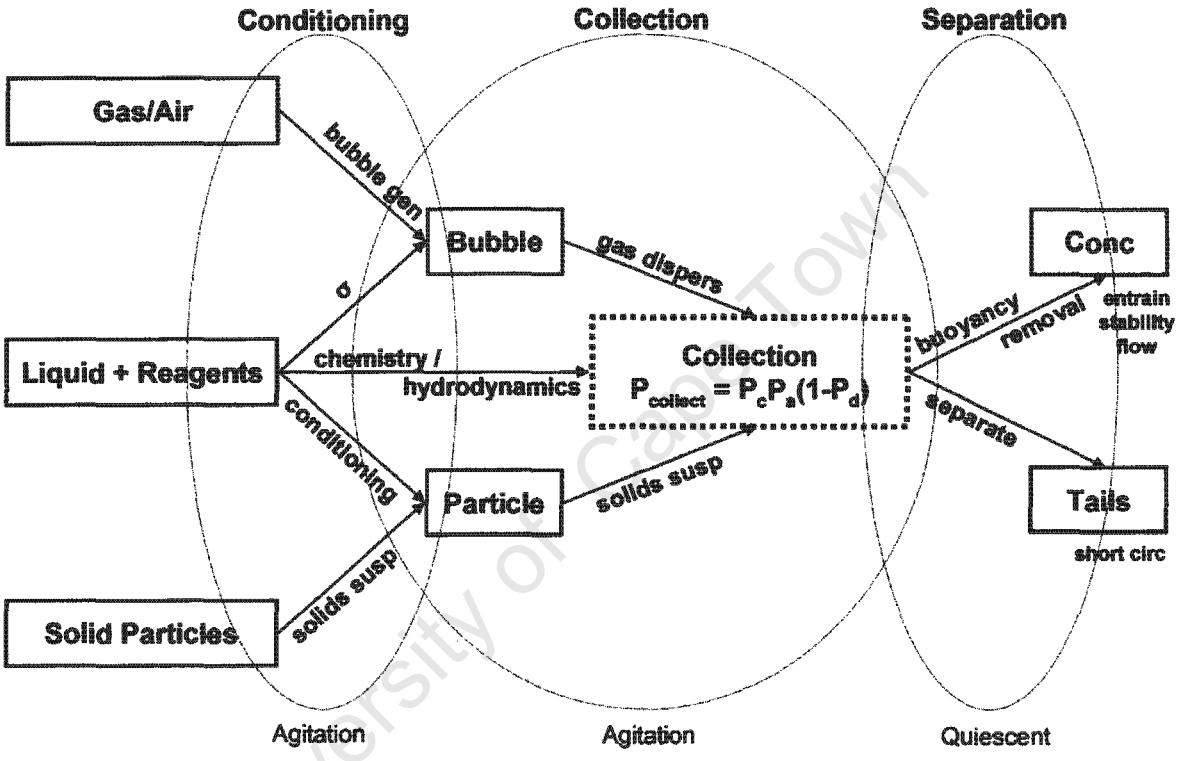

Figure 2.1 Schematic representation of the flotation process

2.1.2.1 Conditioning

Flotation is a three-phase process, which selectively concentrate solid particles in a continuous liquid medium using gas bubbles. *The aim of flotation is to separate liberated solid particles of the optimum size correctly as either hydrophobic froth or hydrophilic slurry discharge.* The liquid (normally water) carries the reagents for regulating the process and forms the continuous phase in which the process occurs under the right hydrodynamic conditions. The gas phase (normally air) forms the bubbles, which are the vehicles responsible for particle collection and removal. The action of the impeller causes *solid particles to be suspended into the liquid to form slurry*, and reagents such as collectors,

activators, depressants and frothers are added to the cell. The various reagents perform different roles in the flotation process. *Collectors* are used to render the surface of the valuable mineral hydrophobic, and therefore amenable to collection. *Activators* selectively activate certain mineral species within the slurry to allow a collector to render them hydrophobic. *Depressants* are used to suppress the natural floatability of gangue minerals in the slurry. *Frothers* reduce the gas-liquid surface tension and are added to aid in bubble formation and to stabilise the froth layer at the surface of the cell. The successful completion of the conditioning stage delivers solid particles optimally conditioned for either collection or rejection based on their surface hydrophobicities as well as optimum chemical conditions in the liquid phase for bubble formation and stability.

2.1.2.2 Collection

In order to be collected hydrophobic particles have to interact with bubbles to form particle-bubble aggregates, which are stable enough to withstand the disturbances in the slurry and buoyant enough to reach the slurry-froth interface. The prerequisite conditions of *suspended solids*, dispersed gas and sufficient turbulence set the scene for three fundamental microprocesses to occur in flotation, i.e.

1 Collision - the particle must collide with the bubble.
2 Attachment - the disjoining film separating the particle and the bubble must thin, rupture and recede to form a stable contact angle.
3 Detachment (unwanted microprocess) - the particle-bubble aggregate must be sufficiently stable to withstand external stresses in the flotation cell caused by turbulence in order to reach the froth phase for removal.

The probability of these occurring with particles has to be considered in order to evaluate the efficiency of particle collection in a flotation cell. The probability of particle collection ($P_{collect}$) can be expressed as a product of the probabilities of particle-bubble collision, P_c, - attachment, P_a and - detachment, P_d.

$$P_{collect} = P_c P_a (1 - P_d)$$

.....Equation 2-1

Probability of Particle-Bubble Collision, P_c

Collision is the process whereby conditioned and suspended particles are brought into contact with dispersed gas bubbles inside the flotation cell. The main mechanism of collision is a direct encounter between a particle and a bubble in suspension [Arbiter (1984)]. To collide with a bubble, a solid particle must have sufficient momentum to resist the tendency to follow the streamlines around the bubble [Ahmed and Jameson (1989)]. Many expressions exist for the efficiency or probability of collision, P_c, but one of the more commonly used is given by:

$$P_c \propto \frac{d_p^{\,m}}{d_b^{\,n}}$$; Where m and n vary between 1-2 and 2-3, respectively

..... Equation 2-2

While attempts at modelling collision in quiescent systems have focused on the influence of hydrodynamic forces on the probability of collision, the analysis in *turbulent* systems has focused on determining the rate of particle-bubble collisions per unit volume. The *rate of particle-bubble collisions* is a function of the numbers of particles and bubbles, particle and bubble sizes, and *specific power input* ε. Increasing ε leads to increased rates of collisions, whereas decreasing the bubble size may also increase the rate of particle-bubble collisions, mainly due to increasing the number bubbles in the turbulent system.

Probability of Particle-Bubble Attachment, P_a

Attachment between particles and bubbles is a complex interaction of both hydrodynamic and surface forces. The probability of attachment is defined as, the fraction of particles that remain attached to bubbles after collision has occurred, and is commonly modelled in terms of contact and induction times. The *contact time* is the time that a particle and a bubble are in contact for after colliding, while the *induction time* is the time taken for the disjoining film to drain, rupture and form a stable contact angle. Schulze (1989) analysed bubble deformation resulting from contact with a particle and found the contact time to be weakly dependent on the *particle-bubble relative velocity*, but found the induction time to be stronger related to this velocity. Increasing the *specific power input*, increases the relative velocities and should thus lead to increasing attachment. Schulze further showed that *sharp edged particles* can promote film drainage and reduce induction time to the order of contact time in turbulent systems. Laskowski (1993) found increasing *frother dosage* to have the most significant influence on induction time and leads to dramatic decreases in induction time.

Probability of Particle-Bubble Detachment, P_d

Detachment between particles and bubbles is an unwanted microprocess, controlled by both the stability of particle-bubble aggregates and external shear stresses in the flotation cell. The analysis of detachment is primarily of relevance to turbulent systems as detachment is negligible in quiescent systems due to appreciably lower external stresses in quiescent environments. The probability of detachment is defined as the fraction of attached particles that detaches from bubbles in the flotation cell. It has been found that detachment is strongly influenced by particle size ($P_d \propto d_p^{(3/2\text{-}7/3)}$) [Mika and Fuerstenau (1968); Woodburn, King and Colborn (1971)], is *increased by the level of turbulence* (ε) [Schulze (1982)], and is more difficult to occur with small bubbles than with larger bubbles [Holtham and Cheng (1991)].

The successful completion of the *collection stage* produces stable and buoyant particle-bubble aggregates containing the hydrophobic particles, in conditions allowing these aggregates to rise towards the froth phase, and hydrophilic particles to remain in the slurry phase.

2.1.2.3 Separation

The final separation and removal of wanted and unwanted mineral particles happens during this stage. After collection, the particle-bubble aggregate must transition towards and into the froth layer and be transported through this layer until removed from the flotation cell. At the slurry-froth interface, the particle-bubble aggregates need to separate from the hydrophilic gangue minerals, which should remain in the slurry. However, due to bubble crowding at the slurry-froth interface considerable *entrainment* of slurry into the froth occurs. Froth *stability* is very important as, liquid film drainage and rupture of bubbles with age causes some of the particles to return to the pulp from the froth (dropback). The rate of froth *flow* is dependent on a number of factors, most notably aeration rate, pulp chemistry and cell geometry. The slurry stream containing the gangue minerals is normally removed lower down in the cell. The unwanted subprocess related to slurry discharge is called *short-circuiting* and occurs when particles from the feed stream bypass the collection stage and discharge directly into the tailings stream. The successful completion of the separation phase produces a froth loaded with the hydrophilic particles and very little unattached hydrophilic particles, as well as a slurry discharge stream containing only particles that were unsuccessfully contacted with air bubbles.

2.1.3 Overview of Flotation Cells

The flotation cell has been under continuous development since the first years of the Twentieth Century, although an understanding of the role of the cell itself in the flotation process was slower to develop [Arbiter (1984)]. Many types of flotation cells have been developed. Taggart (1945) makes mention of 171 different cells, although the majority of these existed only in patent descriptions. A number of authors [e.g. Wills (1997); Skillen (1993)] have discussed the types of flotation cells in use today and the following brief overview are based on these reviews. Flotation cells can be divided into three broad categories: *mechanical cells, column cells* and *novel cells*. Each category will be briefly discussed here.

2.1.3.1 Mechanical Flotation Cells

Mechanical flotation cells are the workhorses of the flotation industry and, despite competition from a large variety of alternative flotation technologies, are still responsible for the bulk of world flotation. These cells were traditionally square but recently became cylindrical in shape with increased maximum volumes of up to 250 - 500 m^3. Mechanical agitation is delivered by an impeller mechanism, responsible for producing solids suspension, gas dispersion, and turbulence for particle-bubble contacting. As high levels of agitation are required for efficient particle suspension and gas dispersion, these flotation cells are thought to be best suited to the flotation of *fine to intermediately sized particles* due to strong detachment forces acting on coarser particles in vigorously agitated systems.

2.1.3.2 Column Cells

Column cells are a technology that has struggled to find acceptance in the minerals industry, although in recent times columns have become more widely used. A column cell is either round or square and can be up to three metres in diameter and over ten metres tall. Feed enters the cell near the top and flows downward in the cell under gravity, countercurrent to the gas, which is introduced into the cell near the bottom through gas spargers. This countercurrent flow results in good contact between the bubbles and the particles. Higher-grade concentrates can also be achieved using wash water at the top of the

cell, which helps to wash entrained gangue minerals out of the froth and back into the pulp. Due to the high grades achievable with column cells, they have become more widely used in cleaning applications.

2.1.3.3 Novel Cells

Numerous novel cell designs have been made since the inception of froth flotation, each attempting to improve on certain aspects of the subprocesses occurring in flotation. The two focus areas have been in microbubble generation and improving the particle-bubble interaction through a combination of high levels of agitation, and *decoupling* the processes of *solids suspension* and *gas dispersion.*

Section 2.1 has aimed to introduce the process of froth flotation. It follows from the overview of flotation in Section 2.1.1 that froth flotation is the most widely used mineral separation technique, responsible for the treatment of billions of tons of many ores annually. Inefficiencies in flotation thus translate into enormous losses of revenue and wastes of mineral reserves. To address inefficiencies in the flotation process, research has focused on flotation reagents, flotation cells and flotation fundamentals. The research presented in this thesis is mainly relevant to the area of flotation cell and to a lesser extent flotation fundamental research by contributing to the unravelling of the solids suspension subprocess in mechanical flotation cells. In Section 2.1.2 it was shown that the flotation process consists of many sub- and microprocesses, which can be divided as occurring during different stages of the process, i.e. conditioning, collection and separation stage. The importance of solids suspension was highlighted during the collection stage where solid particles have to interact with dispersed gas bubbles in order to be collected. Solids suspension is strongly related to the level of agitation in the cell. The level of agitation (turbulence) furthermore (in addition to bubble and particle size) has a strong influence on the collection microprocesses through its influence on the rate of particle-bubble collisions, the probability of attachment and the probability of unwanted detachment. At high levels of turbulence (ε), detachment starts to become the collection limiting microprocess. Section 2.1.3 very briefly considered different flotation machine technologies and highlighted the importance of mechanical flotation cells as being responsible for the bulk of world flotation.

2.2 MECHANICAL FLOTATION CELLS

As this study was conducted in a mechanical flotation cell, this section serves to introduce mechanical flotation cells. Section 2.2.1 presents an overview, focusing more on general design considerations and developments in mechanical flotation cells, before considering the different types of mechanical flotation cells being supplied today in Section 2.2.2. In the next section, the attention will be focused on some of the subprocesses occurring in mechanical flotation cells, of which solids suspension is an important one (cf. Section 2.3).

2.2.1 Overview of Mechanical Flotation Cells

Mechanical flotation cells are the most widely used of all flotation machines [Wills (1997)], being characterised by a mechanically driven impeller, which agitates the slurry and disperses the incoming air into small bubbles. Flotation cells are designed to produce maximum recovery of valuable minerals, at high product grades and the lowest possible cost. These machines are therefore designed such that the following objectives can be achieved simultaneously from the cell [Young (1982)]:

- Maintenance of *particles in suspension*
- Dispersion of air into small bubbles in the slurry
- Creation of adequate conditions for particle-bubble contact
- Creation of quiescent conditions towards the froth zone of the cell
- Ensuring the easy separation of particles into the concentrate and tailings streams
- Ensuring easy start-up after stoppages caused by breakdowns, power outages, etc.
- Ensuring that cell geometries fit easily into circuits (in serie configurations)
- Easy froth removal

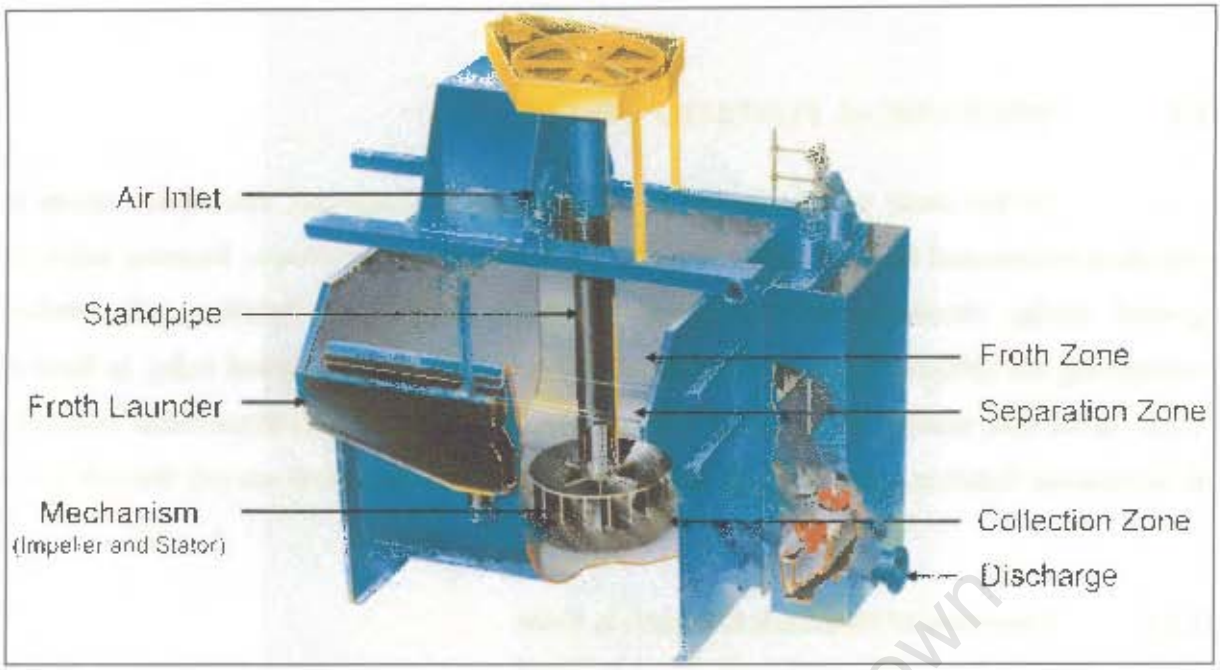

Figure 2.2 Conventional mechanical flotation cell

The benefits of increasing cell sizes were already recognised early in the development of mechanical flotation cells. Degner and Treweek (1976) discussed 'large' flotation cell design and development of up to 8.5 and 14.2 m^3 (300 and 500ft^3) and listed the following advantages:

- Reduced capital costs
- Less floor space
- Reduced operational complexity (less cells)
- Less maintenance

Degner and Treweek (1976) further qualified the aspects given above as advantages only if the following two aspects are not compromised:

- Metallurgical performance
- Solids suspension capability of the cell

The development of flotation cells through the years is discussed by Arbiter (1999), Jonaitis (1999) and Weber *et al.* (1999). The cell sizes quoted by these authors combined with the latest supplier information are graphically displayed in Figure 2.3 (a). In Figure 2.3 (b) approximate tank diameters or length, T, were included (assumed: $V \sim \pi/4.T^3$).

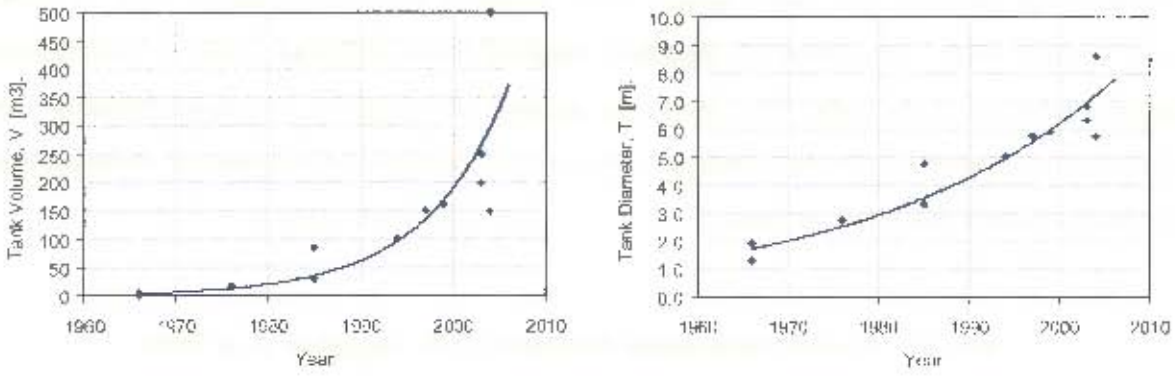

(a) (b)

Figure 2.3 Increase in flotation cell sizes in terms of (a) volume, (b) tank diameter

It follows that cell sizes have dramatically increased since the 1960's when maximum cell sizes was 1.7 to 5.7 m^3, until today with maximum design cell sizes quoted as 150 [Gilbert (2004)], 200 [Anon (2003a)], 250 [Anon (2003b)] and 500 m^3 [Anon (2004)]. This graphically demonstrates the observation by Arbiter (1999) that flotation cells have increased more than ten fold over the last two decades and 100-fold since the 1950's! The most dramatic increase in cell sizes occurred since the early 90's with the advent of round mechanical cells.

2.2.2 Types of Mechanical Flotation Cells

Mechanical flotation cells can be classified by the method of air supply to the flotation cell. At sufficient impeller speed, the rotation of the impeller causes a pressure drop in the standpipe due to vortex formation and cavitation behind the impeller blades. With *self-aerating* flotation cells this pressure drop, caused by the impeller rotation, is the only driving force for air to flow into the cell from ambient pressure. With *forced-aerated* cells, additional positive pressure is applied to the air feed to the cell by using air blowers. This requires additional energy for the air blowers but allows greater control over the air addition rate into the cell. Further classification of mechanical flotation cells can be made in terms of the design of the vessel in which the impeller mechanism is fitted. Previously all mechanical flotation cells were square or rectangular. These *conventional* cells were at first fitted together in banks of cells in series with or without dividing plates between them ('cell-to-cell' vs. 'open-flow'). As the sizes of conventional cells increased, the numbers of cells down the bank decreased until large single conventional cell units were used separately (cf. Figure 2.2).

Conventional flotation cells have largely been replaced by *round* flotation cells in recent years. Also, while, more than 10 suppliers supplied many different types of conventional flotation cells until the mid-90's, have the number of suppliers of round flotation cells decreased to around four at the moment. The current suppliers of mechanical flotation cells and their products are given in Table 2.1.

Table 2.1 Round Mechanical Flotation Cells Supplied as at 2004

Supplier	Round Cell	Air Feed	Cell volumes
Bateman	Round BQR Cell	Forced-aerated	<5 to 150 m^3
Metso Minerals	RCS™ Machines	Forced-aerated	5 to 200 m^3
Outokumpu	TankCell®	Forced-aerated	5 to 500 m^3
Wemco (Dorr-Oliver Eimco)	SmartCell™	Self-aerated	5 to 250 m^3

Self-aerated and forced-aerated flotation cells will now be discussed briefly.

2.2.2.1 Self-aerated Flotation Cells

Wemco is the only supplier of self-aerated flotation cells today. A schematic of a Wemco SmartCell™ is shown in Figure 2.4. It is clear that with this cell, the mechanism is not submerged very deep down into the pulp zone of the cell. The impeller mechanism consists of a rotor with a disperser and disperser hood fitted over it. Slurryflow from the bottom of the tank to the rotor is enhanced by a draft tube fitted below the mechanism and connected to a false bottom. This false bottom directs flow along the bottom of the tank for *solids suspension* purposes.

Degner and Treweek (1976) described the operation of Wemco self-aerated cells as follows. The rotation of the rotor generates a liquid vortex from the draft tube and extending down to the standpipe. The vacuum generated by this vortex will draw air into the standpipe and rotor core. This vacuum is strongly dependent on the rotor speed N, and the rotor submergence S_l below the slurry surface, which is the reason for the high mounting of self-aerated mechanisms. In addition to the air, is slurry drawn into the rotor from below through the draft tube. The slurry is mixed with the air before being discharged from the rotor with significant

tangential as well as radial velocity vectors. When this fluid reaches the disperser, the tangential vectors are turned into radial vectors causing high local turbulence (shear) conducive to small bubble generation and good solid-slurry mixing. Once the air-slurry mixture leaves the disperser, it enters the main fluid body of the cell and only specic separation is still to be accomplished in the relatively quiescent region above the stator mechanism.

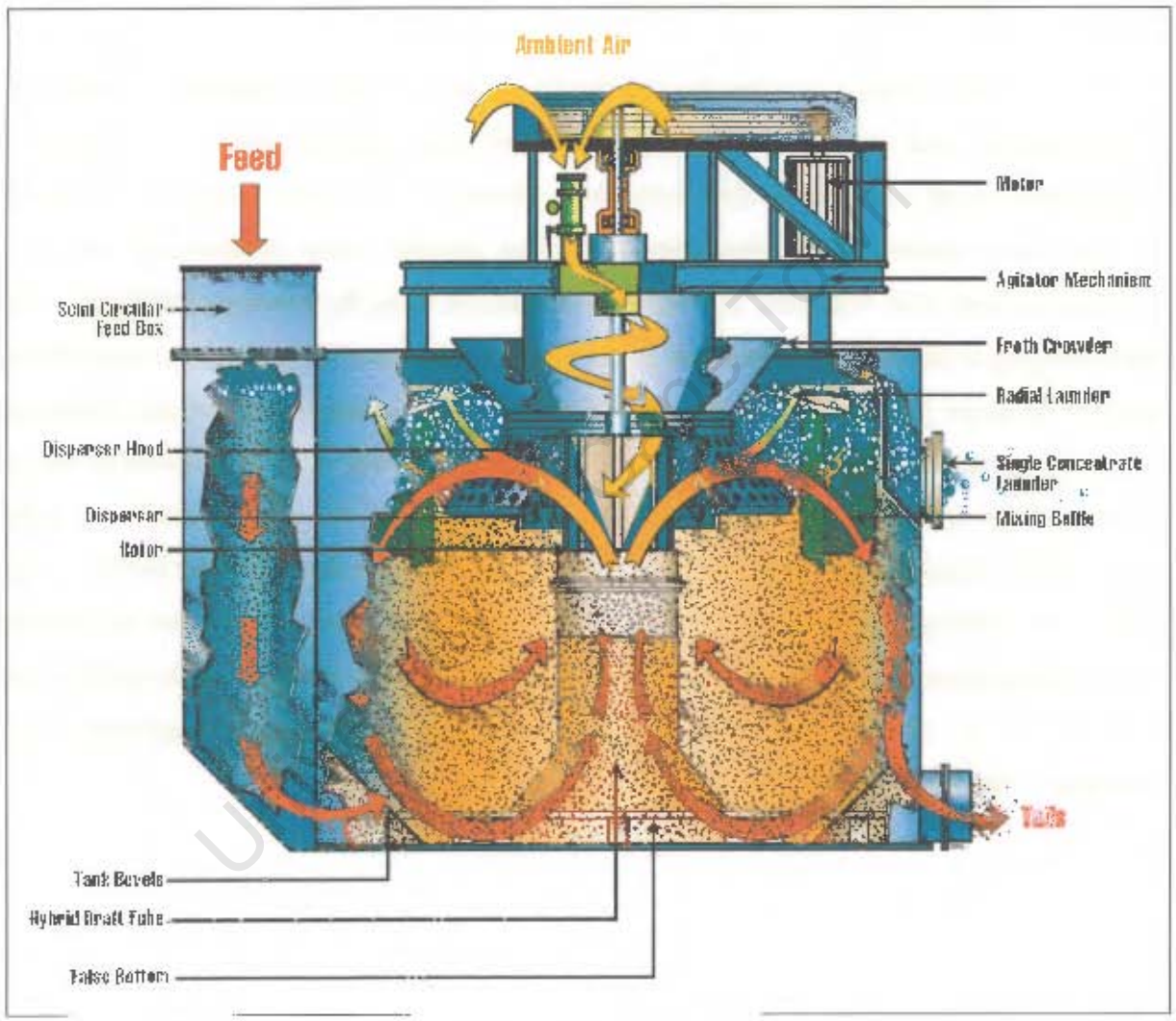

Figure 2.4 Wemco SmartCell™

Some of the collection zone benefits of the Wemco SmartCell™ can be highlighted as follows.

Wemco SmartCell™ [Anon (2003b)]

- Blowers are not required

- Rotors are located in an elevated position allowing easy startup and reduced wear
- Draft tube and bevelled tank improves
  - Hydrodynamic mixing
  - Solids suspension
  - Coarse particle recovery

2.2.2.2 Forced-aerated Flotation Cells

Forced-aerated or supercharged flotation cells are currently supplied by Bateman, Metso Minerals and Outokumpu. Examples of their round cells are shown in Figure 2.5. Remarkable overall similarity is clear from these schematics. The basic feature of the forced-air cells is the impeller mechanism consisting of an impeller-stator combination fitted low down in the tank with relatively low impeller clearances from the bottom of the tank. The supercharging of the air allows freedom in the vertical placement of the impeller mechanism, and it is therefore placed lower in the cell for effective solids suspension and gas dispersion purposes. In addition, supercharging also allows more freedom over the control of the air flowrate to the cell. Though differences in the impeller designs do exist, they all have radial blades with vertical profiles reducing the impeller diameter from the top to the bottom of the blade. The Outokumpu impeller is differentiated from the other two with the use of a double blade configuration separating the air and slurry flow through the impeller. Other differences in the forced air cells are differences in the slurry feed and discharge arrangements, froth crowding -, and froth launder arrangements.

(a) Bateman BQR Cell

(b) Metso Minerals RCS™ Cell

(c) Outokumpu TankCell®

Figure 2.5 Forced-aerated round flotation cells

Unique features of each cell's *mechanism* design are briefly given as follows.

Bateman BQR Cell [Gilbert (2004)]

- Open rotor

- Excellent solids suspension
- Good air dispersion
- Reduced power consumption

- Overhung stator
  - Easier start-up under load
  - Complete mechanism is removable
  - More stable froth-pulp interface
- Closed stator and open impeller

Metso Minerals RCS™ Cell [Anon (2003a)]

- Deep Vane DV™ Mechanism
  - Powerful radial slurry pumping to the cell
  - The only mechanism to give slurry recirculation to the upper part of the impeller
- Open stator and open impeller

Outokumpu TankCell® [Anon (2004)]

- Free flow Mechanism
  - For coarse and medium sized particles
  - Keeps the slurry in motion without excessive turbulence
- Multi-Mix Mechanism
  - For fine to medium sized particles
  - Maximum contact in the shear zone between the rotor and the stator
  - Improved recovery of especially fine particles
- Open stator and closed impeller

Apart from these 'unique' features, all the suppliers claim to provide optimum flotation performance through,

- Maximum particle-bubble contacts
- Effective *solids suspension*
- Effective air dispersion

It is thought that forced-aerated cells can be more effective in fine particle recovery due to the high levels of turbulence possible by placing the impeller mechanisms low down in the tank without disrupting the quiescent and froth zones.

As this study on solids suspension was conducted in a mechanical flotation cell, Section 2.2 specifically considered mechanical flotation cells. It started by giving an overview of mechanical flotation cells in Section 2.2.1, where it was seen that solids suspension is an important objective in the design of mechanical flotation cells. The increase in mechanical flotation cell sizes to achieve greater economies of scale was also highlighted here especially since the advent of round mechanical flotation cells in the early 90's. Scale-up normally requires a good understanding of all the subprocesses (including solids suspension) in order to be applied successfully. The different types of round mechanical flotation cells were discussed in Section 2.2.2 where they were divided into self-aerated and forced-aerated cells. The importance of solids suspension as one of the subprocesses occurring in these machines is evident from the discussion. This work was done in a forced-aerated mechanical flotation cell, which in terms of design were shown to be significantly different from the self-aerated machines. The work in this thesis is thus more related to the forced-aerated mechanical flotation cells as shown in Section 2.2.2.2.

2.3 SUBPROCESSES AFFECTING THE COLLECTION ZONE

As already discussed in Section 2.1.2, the flotation process can be divided into the stages of conditioning, collection and separation. Each of the stages consists of a number of sub- and microprocesses, which influences the effectiveness of the flotation process (cf. Figure 2.1). Compared with the mostly reagent controlled *conditioning* stage, the *collection* and *separation* stages are the main functions of a mechanical flotation cell. In terms of collection and separation subprocesses, a mechanical flotation cell can be divided into different zones as indicated in Figure 2.6. These zones are not always that clearly definable as is especially evident for the pulp phase zones (i.e. collection and quiescent zones), and only demarcate areas where certain subprocesses are expected to dominate. This study focuses on solids suspension, which is an important subprocess in the collection zone of the mechanical flotation cell. This section will therefore mainly focus on the *collection zone subprocesses* in a mechanical flotation cell. Considering the collection zone subprocesses as shown in Figure 2.7, they are *solids suspension*, *gas dispersion* and *particle collection*. These subprocesses are all regulated and controlled by the *hydrodynamic* conditions in the collection zone, which should thus form part of an overview of the collection zone subprocesses. The particle collection subprocess, consisting of the collision, attachment and detachment microprocesses was already discussed in Section 2.1.2.2. Suffice to reiterate here that increased agitation increases all the particle collection microprocesses of collision, attachment and detachment, but that detachment becomes controlling at high levels of power addition (ε). This section will thus give an overview of hydrodynamics (Section 2.3.1), gas dispersion (Section 2.3.2) and solids suspension (Section 2.3.3) in mechanical flotation cells. Later, *solids suspension* will be considered in more detail in Sections 2.4 and 2.5 of this chapter.

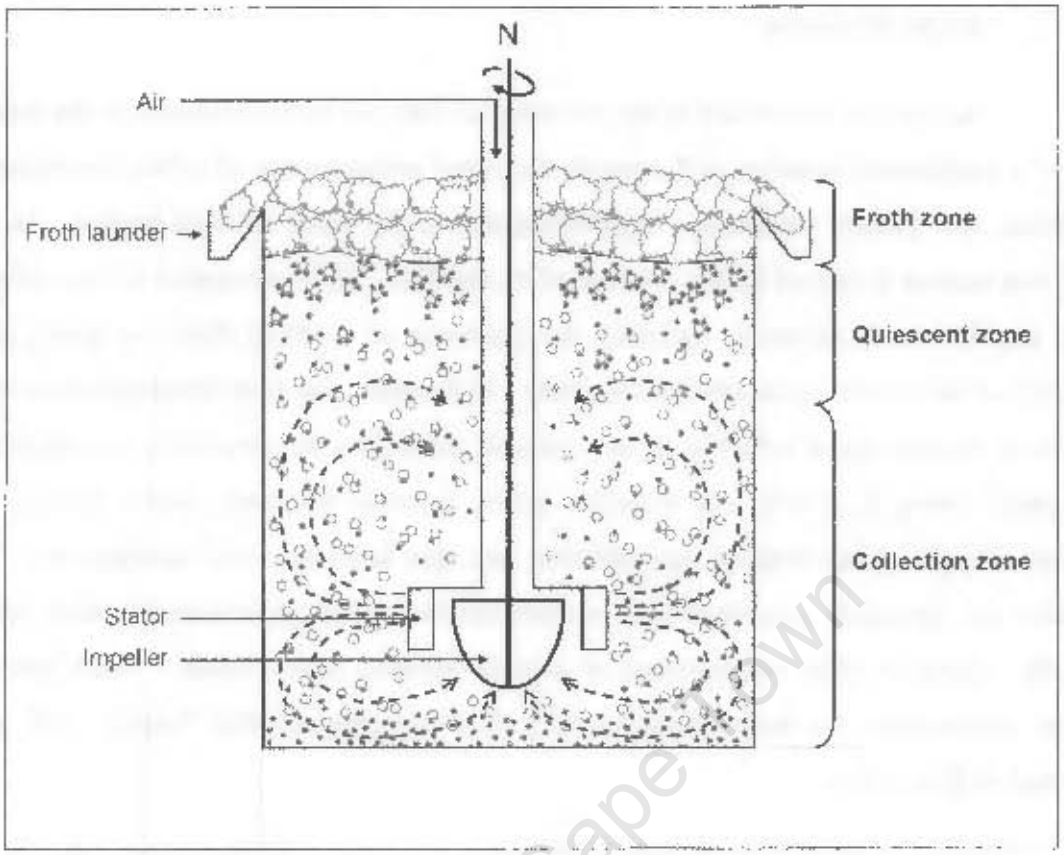

Figure 2.6 Schematic of a mechanical flotation cell showing different zones in cell

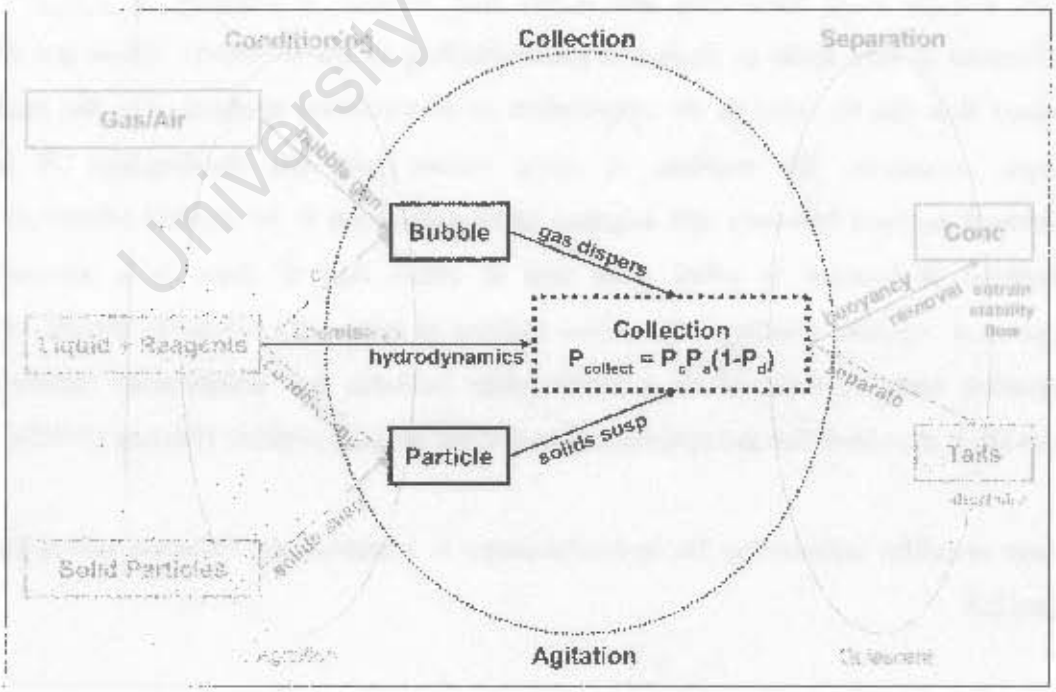

Figure 2.7 Collection zone subprocesses in mechanical flotation cells.

2.3.1 Hydrodynamics

As already mentioned in the previous section, the hydrodynamics in the collection zone of a mechanical flotation cell controls the other subprocesses of solids suspension, gas dispersion, and particle collection. Hydrodynamics is the study of fluid motion. In stirred tanks, this motion is caused by the rotation of an impeller. Hydrodynamics is thus influenced by the impeller speed (dynamic variable), the properties of the fluid (fluid variables), and the geometry of the system (geometrical variables). In flotation, the term hydrodynamics is often used more broadly when referring to any variable related to the properties or motion of the three-phase slurry in a cell, e.g. impeller speed, impeller diameter, slurry density, liquid viscosity, liquid surface tension, gas addition rate, gas holdup, power addition, etc. These variables are normally combined into certain *hydrodynamic parameters*, which are then normally related to other subprocesses or overall flotation performance. These parameters used to characterise the hydrodynamics in a mechanically agitated flotation cell will be discussed in this section.

Dimensional analysis is needed in problems that cannot be solved completely or rigorously with mathematical models [De Nevers (1991)]. It reduces the number of independent variables that has to be correlated, and in this way attempts to simplify the problem. This simplification in turn leads to increased understanding of the problem. There are different techniques that can be used in the application of dimensional analyses, i.e. the method of *governing equations*, the method of *force ratios*, and the *Buckingham Π method*. Dimensional analysis however still requires good judgement to be applied effectively. The Buckingham Π-theorem is often used and it states that if there is a dimensionally homogeneous equation relating n quantities defined in terms of r reference dimensions, then the equation may be reduced to a relationship between n-r independent dimensionless products (Π_i), provided that the reference dimensions are independent [Dickey (1992)].

The main variables influencing the hydrodynamics in a mechanical flotation cell is indicated in Figure 2.8.

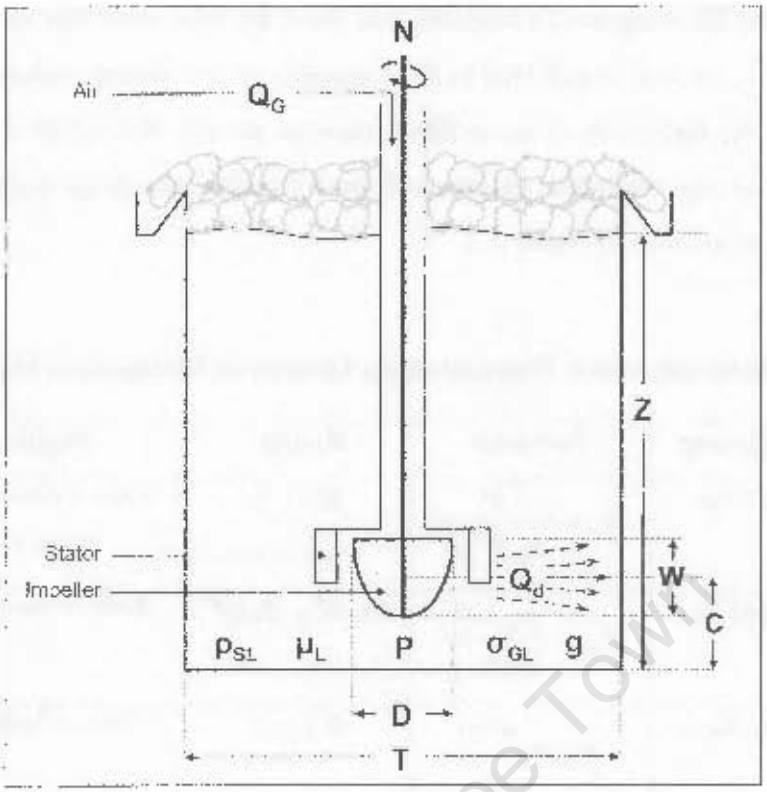

Figure 2.8 Hydrodynamic variables in a mechanical flotation cell

The thirteen hydrodynamic variables in Figure 2.8 can be divided into geometric, fluid and dynamic variables. The *geometric variables* include the tank diameter T (m), impeller diameter D (m), impeller width W (m), impeller midpoint clearance C (m), and the liquid height Z (m). The *fluid variables* include, slurry density ρ_{SL} (kg.m^{-3}), the liquid viscosity μ_L (mPa.s = 0.001 kg.m^{-1}.s^{-1}), and the gas-liquid surface tension σ_{GL} (N.m^{-1} = kg.s^{-2}). The fluid density ρ_F and viscosity μ_F should theoretically be the effective three-phase fluid values in the vicinity of the impeller but, due to difficulties of in-situ determination or estimation, are often taken as the slurry density ρ_{SL} and the liquid viscosity μ_L. The *dynamic variables* include the impeller speed N (s^{-1}), impeller slurry discharge flowrate Q_d (m^3/s), gas flow rate Q_G (m^3/s), shaft power draw P (kW = 1000 kg.m^2.s^{-3}), and the acceleration due to gravity g (m/s^2). Assuming that these variables are all related and taking power draw P to be the dependent variable, as is traditionally the case; the following correlation can be proposed [Edwards and Baker (1992)].

$$P = f\left(N, D, W, C, T, Z, \rho_{SL}, \mu_L, \sigma_{GL}, g, Q_G, Q_d\right)$$

..... Equation 2-3

It follows from the Buckingham *Π*-theorem that these thirteen variables in three independent dimensions (i.e. kg, m, and s) will lead to the formation of ten dimensionless groups as shown in Table 2.2. In the formation of these dimensionless groups, the variables are combined in such a way that the dimensionless groups will have physical meanings (often force ratios) as indicated in the last column of Table 2.2.

Table 2.2 Hydrodynamic Dimensionless Groups in Mechanical Flotation Cells

Dimensionless Group	Formula	Range[+]	Physical Meaning
Power Number (N_P)	$N_P = \frac{P}{\rho_{SL} N^3 D^5}$	0.5 – 5	Ratio of actual imposed to inertial forces on standard rotor
Reynolds Number (N_{Re})	$N_{Re} = \frac{\rho_{SL} N D^2}{\mu_L}$	$5\text{x}10^4 - 2\text{x}10^6$	Ratio of inertial to viscous forces
Froude Number (N_{Fr})	$N_{Fr} = \frac{N^2 D}{g}$	0.1 – 5	Ratio of inertial to gravitational forces
Flow Coefficient (N_{Qd})	$N_{Qd} = \frac{Q_d}{ND^3}$	0.56-1.00[++] 0.75[+++]	Ratio of actual impeller pumping rate to standard rotor pumping rate
Air Flow Number (N_{QG})	$N_{QG} = \frac{Q_G}{ND^3}$	0.01 – 0.20 0.05-0.30 [++++]	Ratio of actual air flowrate to standard rotor pumping rate
[#] Weber Number (N_{We})	$N_{We} = \frac{\rho_{SL} N^2 D^3}{\sigma_{GL}}$		Ratio of inertial to surface tension forces
Geometric Groups:			Defines the relative geometric setup
Rel. Impeller Diameter	***D/T***	1/4 -1/2*, **	
Rel. Impeller Width	***W/D***	1/10 - 1**	
Rel. Impeller Clearance	***C/T***	1/6-1/2*	
Rel. Liquid Height	***Z/T***	1/3-1.2/1*	

[+]: Data taken from Arbiter, Harris and Yap (1969), Harris (1974), Koch (1975), Mavros (1992), and Schubert and Bischofberger (1998).

[++]: Derived from data given in Weber *et al.* (1999) for Wemco impellers (may include induced slurry circulation).

[+++]: Recommended by Edwards and Baker (1992) for use with turbine agitators ($0.2 \leq D/T \leq 0.5$) for design purposes. Joshi, Pandit and Sharma (1982) gives N_{Qd} for propellers as 0.65 and 0.78 for pitched blade turbines.

[++++]: As given by Schubert and Bischofberger (1998).

[#] The Weber number as given in Mavros (1992), $N_{We} = N^2D^2/\sigma$ is not dimensionless and should be $\rho N^2 D^3/\sigma$ as given in other texts.

* Range for standard stirred tanks [Tatterson (1991); Oldshue, Herbst and Post (1995)].

** Range for mechanical flotation cells as per Harris (1974). Larger round cells, introduced after this reference have D/T values below 1/4 (~1/5).

Using the dimensional analysis results in Table 2.2, Equation 2-3 can now be slightly simplified by rewriting it in the form of dimensionless numbers as follows.

$$N_P = f\left(N_{Re}, N_{Fr}, N_{Qd}, N_{QG}, N_{We}, \frac{D}{T}, \frac{W}{D}, \frac{C}{T}, \frac{Z}{T}\right)$$

..... Equation 2-4

Power draw P is the power transfer from the impeller to the fluid, causing fluid motion, and is eventually dissipated as viscous heating of the fluid [Tatterson (1991)]. *P* is often the focus of many hydrodynamic studies in mechanical flotation cells, due to the influence that *P* has on the efficiency of turbulence controlled subprocesses (e.g. gas dispersion, and particle collection), and also on the operating cost of the process. *P* is a dependent variable that can be calculated from the power number. The ***power number*** N_P is the ratio of the imposed force by the shaft on the impeller [$F_P = M/(D/2) \alpha P/(N.D)$], compared to the resultant theoretical inertial force ($F_I = m.a \alpha \rho D^4.N^2$), which the fluid will apply to a standard rotor of unit efficiency as it rotates. Taking the ratio of these forces gives the N_P formula as given in Table 2.2 and due to its frequent use and importance is repeated here.

$$N_P = \frac{P}{\rho_{SL} N^3 D^5}$$

..... Equation 2-5

The imposed force and inertial force are always in balance during steady operation of the impeller. The N_P of an impeller is related to its design and impellers with high power numbers experience higher inertial forces from the liquid than a standard rotor and will thus dissipate more power at the same speed than an impeller with a lower N_P. Impellers scaled with geometric similitude will have the same N_P at the same N_{Re}.

The ***Reynolds number*** N_{Re} indicates the relative effect of inertial ($F=ma$) forces as compared to viscous forces ($F_\mu=\mu.du/dy \alpha \mu ND/D = \mu N$) and is used to indicate the fluid regime (i.e. laminar, transitional or turbulent) in a flow system (e.g. flow through pipes, settling particles, rotating impellers, etc). For rotating impellers, $N_{Re} < 10$ indicates laminar impeller operation, where N_P is linearly proportional to N_{Re}. All types of impellers are taken to operate in the *turbulent regime* at $N_{Re} > 10^5$ [Oldshue, Herbst and Post (1995)], where the power draw of the

impeller is independent of N_{Re} in well-baffled systems. From Table 2.2 it follows that flotation impellers are mostly operating in the turbulent regime where N_P is independent of N_{Re}. Arbiter, Harris and Yap (1969) tested a number of flotation impeller mechanisms in liquid only tests and found the power numbers for most to remain constant at $N_{Re} > 5x10^4$, as would be expected for fully turbulent well-baffled systems.

It should be reiterated here that N_P and N_{Re} were originally developed for homogeneous single-phase stirred systems. In two- and especially three-phase systems, the effective fluid density ρ_F and viscosity μ_F can normally not be determined accurately and for that reason, are often taken as the average slurry density in the tank ρ_{SL} (or sometimes ρ_L), and liquid viscosity μ_L. Notably N_P and N_{Re} are the most common dimensionless numbers affected by the fluid density and viscosity variables (Also, N_{We} depends on ρ_F). The bases used for these fluid variables (water or slurry) should thus be noted when working with N_{Re} and N_P.

As expected from the N_P correlation, Arbiter, Harris and Yap (1969) found that the power draw is increased with increasing slurry density ρ_{SL}. Arbiter *et al.* found that moderate geometrical changes in terms of tank geometry, baffling, impeller clearance C and impeller diameter D did not affect the N_P significantly. They concluded that the N_P of shrouded impellers is less influenced by geometrical variations external to the mechanism. In terms of power, it can thus be concluded that for flotation cells the N_P are mostly independent of N_{Re} (for $N_{Re} \geq 10^5$) and the geometry external to the mechanism, but are strongly influenced by the design of the impeller and stator mechanism and the effective fluid density ρ_F.

The other dimensionless numbers in Table 2.2, are normally used when referring to specific aspects of mechanical flotation cell operation. The ***Froude number*** N_{Fr} relates the inertial forces encountered by the impeller ($F_I = m.a$) to the gravitational forces g acting on the fluid ($F_g = m.g$), and in this way is strongly related to vortex formation. Vortex formation in the standpipe and impeller is important for gas induction and gas dispersion (bubble formation). The ***pumping number*** N_{Qd} (or discharge flow coefficient) gives an indication of the effectiveness of the impeller as a pump, causing bulk fluid motion and circulation. It compares the actual slurry flowrate discharged from the impeller Q_d to the theoretical fluid pumping rate of an ideal standard pumping impeller (ND^3). In order to measure the pumping rate, radial velocity measurements in the impeller discharge stream is needed. Due to the difficulty of measuring these velocities, the pumping number N_{Qd} is less often used in

mechanical flotation cells. The ***airflow number*** N_{QG} is more commonly used than the pumping number, due to the relative ease of measuring the air flowrate into the cell. Here the air flowrate is compared to the theoretical fluid pumping rate of the impeller and is often related to gas induction and dispersion, but often also to the power draw, impeller pumping capacity, and effectiveness of solids suspension. The ***Weber number*** N_{We} relates the inertial forces experienced by the impeller to the gas liquid surface tension σ_{GL}. Due to the strong influence of σ_{GL} on bubble size, N_{We} is strongly related to bubble formation and dispersion in mechanical flotation cells. However, apart from the hydrodynamic dimensionless numbers listed in Table 2.2, other parameters are also commonly used in the hydrodynamic analyses of mechanical flotation cells as shown in Table 2.3.

Table 2.3 Hydrodynamic Parameters Used in Mechanical Flotation Cells

Property	Formula	Range	Meaning
Impeller Tip Speed, u_{tip} (m/s)	$u_{tip} = \pi ND$	5.0 - 7.0	Indicate max shear rate (turbulence)
Power Intensity, P/V (kW/m^3)	$P/V = \frac{P}{V_{SLG}}$	1.0 - 3.0	Indicate average level of turbulence
Superficial Gas Velocity, J_G (cm/s)	$J_G = \frac{Q_G}{A_c}$	1.0 - 2.0	Related to the avg. gas rise velocity in the tank (J_G/φ_G)
Specific Air Flow Rate, Q_{GI} (m^3/m^3/min)	$q_{Gi} = \frac{Q_G}{V_{SLG}}$	0.04 – 1.10	The air flowrate per volume of slurry
Gas Holdup, φ_G (%)	$\varphi_G = \frac{V_G}{V_{SLG}}$	5 - 25	The fraction of the three-phase slurry occupied by gas
Shaft Torque, M (N.m)	$M = \frac{P}{2\pi N}$	-	Torque required to rotate the impeller against fluid inertia
Tank Turnover Time, θ_t (s)	$\theta_t = \frac{V_{SLG}}{N_{Qd} N D^3}$	30 - 60	The time taken to circulate the tank volume through the impeller

Data taken from Fallenius (1976), Harris (1976), Arbiter (1999), Weber *et al.* (1999), and Deglon, Egya-Mensah and Franzidis (2000).

2.3.2 Gas Dispersion

For flotation to occur, air has to be introduced into the cell in the form of bubbles, which form the carriers for hydrophobic particle collection and recovery into the froth zone

(cf. Figure 2.7). The mechanism of gas dispersion in a mechanical flotation cell is depicted in Figure 2.9, from which the turbulent nature of this subprocess is evident. Air is drawn into the low-pressure regions, which form behind the impeller blades due to rotation, to form gas cavities. At sufficient impeller speed, air from these gas cavities is entrained by the fluid vortices flowing around the impeller blades into the impeller discharge stream. Further bubble breakup occurs in the high-shear stator region.

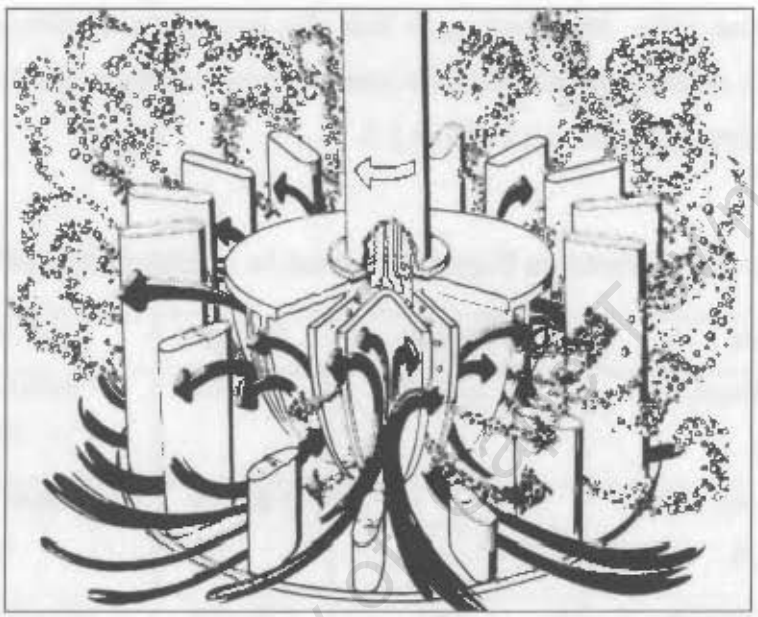

Figure 2.9 Schematic of the gas dispersion action in a mechanical flotation cell

The introduction of air into a stirred system causes a very noticeable drop in power draw. Power draw relates strongly to the hydrodynamic conditions in the cell, which as already mentioned, controls the other collection zone subprocesses of gas dispersion, solids suspension and particle collection. The effect of gas addition on the *power draw* will thus be considered in this section. The mechanism of gas dispersion can be considered in a number of ways. *Gas induction* is important for self-aerating machines, whilst forced air machines are susceptible to *impeller flooding* at too low impeller speeds and/or too high gas addition rates. The *dispersion of bubbles* throughout the cell is important for particle-bubble interaction. It is well known that bubble size as determined by *bubble formation* is very important for particle-bubble interaction (cf. Section 2.1.2.2) and thus flotation kinetics. *Gas holdup* is a measure of the volumetric concentration of gas in the three-phase slurry and is often related to hydrodynamics and flotation performance. These aspects related to gas dispersion will now receive some attention.

2.3.2.1 Gassed Power Draw

The addition of air into the system decreases the effective density ρ_{eff} around the impeller due to the presence of gas (i.e. gas holdup). The power number is thus expected to decrease with increasing gas addition rate. Schubert and Bischofberger (1978) and Schubert (1985) plotted diagrams indicating operating conditions of flotation cells in terms of power draw vs. air flow number. They suggested that the addition of gas has the following decreasing effect on the power draw.

$$N_P \propto N_{QG}^{-b}$$

..... Equation 2-6

From their results, the value of b in Equation 2-6 can be derived to vary between ~0.24 (6.6 l lab cell) and ~0.17 (6 m^3 industrial cell), with N_{QG} varying from 0.01 to 0.07. The value of b derived from the results of Fallenius (1976) on a 16m^3 cell is ~0.24, similar to Schubert *et al.* Arbiter, Harris and Yap (1969) tested a range of different impeller types, on laboratory scale, and their results show that some impellers were more affected by the addition of gas than others with b values ranging between ~0.20 and ~0.70. Joshi, Pandit and Sharma (1982) summarised a number of gassed power correlations for stirred tanks and recommended the following correlation by Hughmark (1980).

$$\frac{P_g}{P_0} \propto \frac{N_{Pg}}{N_P} = 0.1 N_{QG^*}^{-0.25} N_{Fr^*}^{-0.20}; \text{ where } N_{QG^*} = \frac{Q_G}{NV} \;\&\; N_{Fr^*} = \frac{N^2 D^4}{gWV^{2/3}}$$

..... Equation 2-7

Equation 2-7 thus predicts that b as given in Equation 2-6 has a value ~ 0.25. It thus follows that although the effect of gas on power draw is dependent on the design of the impeller most findings predict that power draw will decrease with gas addition rate to the power of approximately minus 0.25 (N_{Pg} α ~$N_{QG}^{-0.25}$).

Arbiter, Harris and Yap (1969) further found that the effect of air flowrate on N_P is magnified with increased *frother addition*. Similarly, some stirred tank P_g correlations also include the effect of surface tension (N_{We}) as summarised in Joshi, Pandit and Sharma (1982). The drop

in power draw with air addition could not be fully explained by the increase in average gas holdup φ_G in the cell, and Arbiter *et al.* therefore concluded that the gas holdup in the impeller region is higher than in the rest of the cell due to re-entrainment of gas into the impeller. There is however agreement in literature that in addition to gas re-entrainment, gassed power draw P_g is also reduced, due to the formation of gas cavities behind the impeller blades, which reduces the form drag on the impellers [Joshi, Pandit and Sharma (1982); Chapman *et al.* (1983b); Patwardhan and Joshi (1999)].

2.3.2.2 Gas Induction

Gas induction is especially important for selfaerating mechanical flotation cells. Gas induction is correlated in terms of the *impeller speed* for the onset of gas induction N_{GI}, and the induced *gas flowrate* Q_{Gind} at impeller speeds above N_{GI}. Theoretically, N_{GI} can be estimated by the application of Bernoulli's equation, using the impeller tip speed and hydrostatic head [Patwardhan and Joshi (1999)]. Sawant and Joshi (1979) found in a study on a range of gas inducing impellers, including flotation impellers, that the critical Froude number for gas induction $(N_{Fr})_{GI}$ is directly related to the relative impeller submergence (cf. Equation 2-8). Aldrich and Van Deventer (1995) later found a very similar correlation in a study on 6 and 12 bladed disc turbines. The induced gas flowrate Q_{Gind} is normally determined from a more empirical base and there is less agreement amongst different approaches. Two correlations derived for flotation impellers and listed by Patwardhan and Joshi (1999) are shown in Equation 2-9.

$$(N_{Fr})_{GI} = \frac{N_{GI}^{\,2} D}{g} = 0.21 \frac{S_I}{D} \left(\frac{\mu}{\mu_w} \right)^{0.11}$$

..... Equation 2-8

$$Q_{Gind} = 51.2\left((N_{Fr}) - (N_{Fr})_{GI}\right)^{0.83} \left(\frac{S_I}{D} \right)^{-0.50} \quad \text{; Wemco} \qquad \text{(a)}$$

$$Q_{Gind} = 0.0021\left(N^2 - N_{GI}^{\,2}\right)^{0.75} D^3 \quad \text{; Denver} \qquad \text{(b)}$$

..... Equation 2-9

The importance of the Froude number N_{Fr} and impeller submergence S_l/D for gas induction in selfaerated machines is confirmed by Equation 2-8 and Equation 2-9.

2.3.2.3 *Impeller Flooding and Loading*

In the same way that self-aerated impellers will only start to induce air above a certain impeller speed N_{GI}, will forced aerated impellers become flooded at a fixed gas flowrate Q_G as the impeller speed drops below a certain impeller speed N_F. The ***flooding condition*** occurs when the gas addition rate exceeds the gas dispersion capacity of the impeller. Under these conditions, the rotating impeller becomes largely encapsulated by gas (flooded) and has a negligible contribution to *fluid circulation* in the cell, which is *now largely gas controlled*. A significant drop in power, circulation intensity and solids suspension capacity is noticed when the impeller becomes flooded. At higher impeller speeds the power draw increases and the impeller thus becomes loaded. Under ***loaded conditions***, the impeller is able to disperse the incoming air with the slurry discharge leaving the impeller and *the impeller is thus controlling the fluid circulation patterns in the cell.*

The impeller speed N, gas flowrate Q_G and impeller diameter D, as expressed by the air flow number N_{QG} and Froude number N_{Fr} has been found to correlate the flooding condition well [Warmoeskerken and Smith (1985); Wong, Wang and Huang (1987); Hudcova *et al.* (1987)] as can be seen from Equation 2-10.

$$(N_{QG})_F = 30(N_{Fr})_F\left(\frac{D}{T}\right)^{3.5} \quad ; \textit{where } (N_{QG})_F = \frac{Q_G}{N_F D^3} \;\&\; (N_{Fr})_F = \frac{N_F{}^2 D}{g}$$

..... Equation 2-10

Hudcova *et al.* (1987)

Impeller flooding is also of relevance to *solids suspension*, due to dramatic sedimentation of solids occurring when the impeller gets flooded. The *'critical' airflow number*, where Arbiter, Harris and Yap (1969) observed drastic solids sedimentation is thought to have occurred at a point close to the flooding point of the impeller. Harris (1976), Schubert and Bischofberger (1978), and Joshi, Pandit and Sharma (1982) also expressed the effect of air on solids suspension in terms of air flow numbers.

2.3.2.4 *Gas Dispersion*

As flotation is dependent on the contacting of solid particles with gas bubbles, the dispersion of gas throughout the tank is an important aspect. Proper gas dispersion can only occur if the impeller is loaded at higher impeller speeds as shown in Figure 2.10.

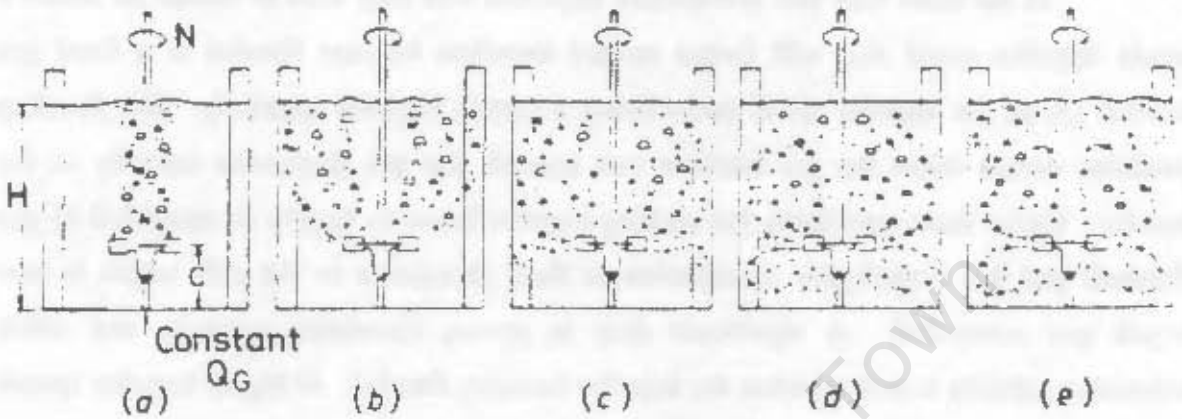

Figure 2.10 Different stages of impeller flooding and gas dispersion (loading) [adapted from Chapman *et al.* (1983b)]

(a) No gas dispersion (impeller flooded); (b) Minimal gas dispersion / bubble column (impeller flooded); (c) Gas dispersion above the impeller (impeller loaded); (d) Complete gas dispersion (impeller loaded); (e) Uniform gas dispersion (impeller loaded).

Two important points can be identified from Figure 2.10, i.e. the flooding point N_F and the just completely dispersed point N_{cd}. Although some disagreement existed in literature, N_F is taken as the (c)-(b) movement, while N_{cd} is taken as the (c)-(d) movement [Middleton, Edwards and Stewart (1980)]. Most studies have focused on the flooding point, and not many correlations exist for the point of complete dispersion of gas N_{cd}. One such study was however done by Nienow, Wisdom and Middleton (1977) using a disc turbine (cf. Equation 2-11).

$$\left(N_{QG}\right)_{cd} = \frac{1}{5}\left(N_{Fr}\right)_{cd}^{0.50}\left(\frac{D}{T}\right)^{0.50}$$

..... Equation 2-11

Comparing Equation 2-11 to Equation 2-10, it seems that N_{Fr} and D/T has a smaller effect on the completely dispersed point, than on the flooding point. Chapman *et al.* (1983b) later found a similar correlation. Dispersion of bubbles is brought about by both turbulent dispersion and bulk flow. *Turbulent dispersion* is strongly related to the power intensity,

The importance of the Froude number N_{Fr} and impeller submergence S_l/D for gas induction in selfaerated machines is confirmed by Equation 2-8 and Equation 2-9.

2.3.2.3 Impeller Flooding and Loading

In the same way that self-aerated impellers will only start to induce air above a certain impeller speed N_{GI}, will forced aerated impellers become flooded at a fixed gas flowrate Q_G as the impeller speed drops below a certain impeller speed N_F. The ***flooding condition*** occurs when the gas addition rate exceeds the gas dispersion capacity of the impeller. Under these conditions, the rotating impeller becomes largely encapsulated by gas (flooded) and has a negligible contribution to *fluid circulation* in the cell, which is *now largely gas controlled.* A significant drop in power, circulation intensity and solids suspension capacity is noticed when the impeller becomes flooded. At higher impeller speeds the power draw increases and the impeller thus becomes loaded. Under ***loaded conditions***, the impeller is able to disperse the incorming air with the slurry discharge leaving the impeller and *the impeller is thus controlling the fluid circulation patterns in the cell.*

The impeller speed N, gas flowrate Q_G and impeller diameter D, as expressed by the air flow number N_{QG} and Froude number N_{Fr} has been found to correlate the flooding condition well [Warmoeskerken and Smith (1985); Wong, Wang and Huang (1987); Hudcova *et al.* (1987)] as can be seen from Equation 2-10.

$$(N_{QG})_F = 30(N_{Fr})_F\left(\frac{D}{T}\right)^{3.5} \quad ; \textit{where } (N_{QG})_F = \frac{Q_G}{N_F D^3} \;\&\; (N_{Fr})_F = \frac{N_F{}^2 D}{g}$$

..... Equation 2-10

Hudcova *et al.* (1987)

Impeller flooding is also of relevance to *solids suspension*, due to dramatic sedimentation of solids occurring when the impeller gets flooded. The *'critical' airflow number*, where Arbiter, Harris and Yap (1969) observed drastic solids sedimentation is thought to have occurred at a point close to the flooding point of the impeller. Harris (1976), Schubert and Bischofberger (1978), and Joshi, Pandit and Sharma (1982) also expressed the effect of air on solids suspension in terms of air flow numbers.

2.3.2.4 Gas Dispersion

As flotation is dependent on the contacting of solid particles with gas bubbles, the dispersion of gas throughout the tank is an important aspect. Proper gas dispersion can only occur if the impeller is loaded at higher impeller speeds as shown in Figure 2.10.

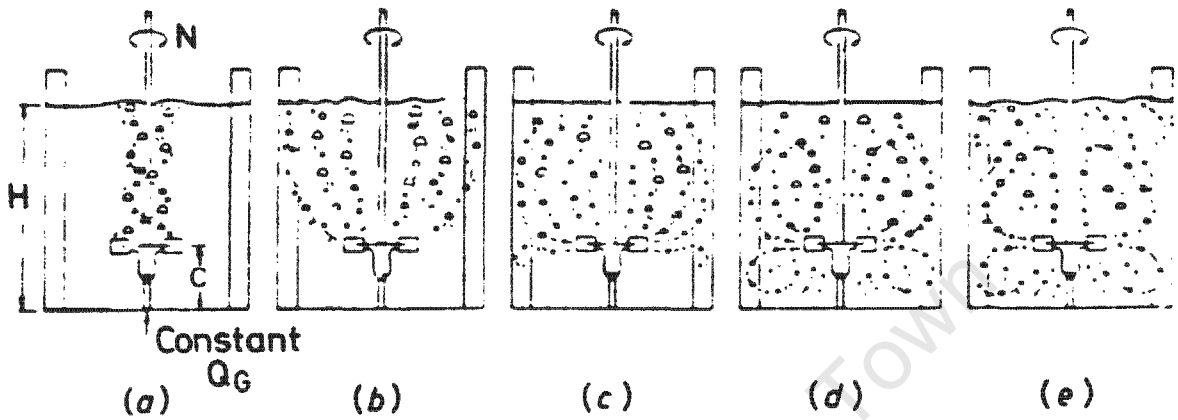

Figure 2.10 Different stages of impeller flooding and gas dispersion (loading) [adapted from Chapman *et al.* (1983b)]

(a) No gas dispersion (impeller flooded); (b) Minimal gas dispersion / bubble column (impeller flooded); (c) Gas dispersion above the impeller (impeller loaded); (d) Complete gas dispersion (impeller loaded); (e) Uniform gas dispersion (impeller loaded).

Two important points can be identified from Figure 2.10, i.e. the flooding point N_F and the just completely dispersed point N_{cd}. Although some disagreement existed in literature, N_F is taken as the (c)-(b) movement, while N_{cd} is taken as the (c)-(d) movement [Middleton, Edwards and Stewart (1980)]. Most studies have focused on the flooding point, and not many correlations exist for the point of complete dispersion of gas N_{cd}. One such study was however done by Nienow, Wisdom and Middleton (1977) using a disc turbine (cf. Equation 2-11).

$$\left(N_{QG}\right)_{cd} = \frac{1}{5}\left(N_{Fr}\right)_{cd}^{0.50}\left(\frac{D}{T}\right)^{0.50}$$

..... Equation 2-11

Comparing Equation 2-11 to Equation 2-10, it seems that N_{Fr} and D/T has a smaller effect on the completely dispersed point, than on the flooding point. Chapman *et al.* (1983b) later found a similar correlation. Dispersion of bubbles is brought about by both turbulent dispersion and bulk flow. *Turbulent dispersion* is strongly related to the power intensity,

which as already noted decreases with increasing air addition. *Bulk flow* is related to the impeller pumping capacity, which is also generally accepted to reduce with air addition, although not much is available in literature. Arbiter, Harris and Yap (1969) proposed a relationship between gas addition and the impeller discharge rate, following some work in small centrifugal pumps, in which the air and water flowrates were measured independently. The results showed that the impeller pumping capacity reduced linearly with increased introduction of gas (cf. Equation 2-12).

$Q_d = aND^3 - bQ_G$; Or in dimensionless form: $N_{Qdg} = N_{Qd} - bN_{QG}$

..... Equation 2-12

*2.3.2.5 **Bubble Formation***

Many studies have been done on the bubble size of the dispersed gas phase in stirred vessels as summarised in Mezaki, Mochizuki and Ogawa (2000). The main variables found to affect the bubble size is the surface tension of the liquid σ_{GL} and the power addition P/V into the system. In flotation cells, frother is added to reduce the gas-liquid surface tension σ_{GL}. As mentioned in Section 2.3.1, the Weber number N_{We} is the ratio of the inertial forces to the surface tension forces, and is therefore thought to be related to bubble formation and bubble size. Some have thus related the bubble diameter d_{b32} (Sauter mean) in dimensionless form, using the N_{We} of which the following is a typical example [Chatzi, Boutris and Kiparissides (1991)].

$$\frac{d_{b32}}{D} = \mathrm{K}_1 N_{We}^{-0.60} = \mathrm{K}_1 \left(\frac{\rho N^2 D^3}{\sigma_{GL}} \right)^{-0.60} \quad ; \mathrm{K}_1 = 0.046 \pm 0.002 \text{ and } d_{b32} \text{ in cm.}$$

..... Equation 2-13

It follows from Equation 2-13 that bubble size decreases with increasing Weber number, as increased N_{We} is indicative of increasing inertial forces to surface tension forces, which as expected will lead to smaller bubble sizes. Others have related the bubble diameter in non-dimensionless form directly to surface tension σ_{GL} and power addition P/V. A typical example of these correlations is given in Equation 2-14 [Parthasarathy, Jameson and Ahmed (1991)] and shows d_{b32} to decrease strongly with decreasing surface tension (d_{b32} α $\sigma_{GL}^{0.60}$)

and increasing power addition ($d_{b32} \propto P/V_i^{-0.40}$). It is interesting to note that the effect of surface tension on d_{32} is the same for both Equation 2-13 and Equation 2-14.

$$d_{b32} = K_1 \frac{\sigma^{0.60}}{(P/V_i)^{0.40}\rho^{0.20}} \quad ; \text{Where, } K_1 = 2.0 \text{ and } d_{b32} \text{ in } \mu m$$

.....Equation 2-14

2.3.2.6 Gas Holdup

Gas holdup is a complex interaction of mainly impeller speed, impeller diameter, liquid viscosity, liquid surface tension and gas addition rate. In addition to gas holdup, do these variables also manifest themselves in the dependent quantities of bubble size and power consumption. Gas holdup has been correlated both in terms of dimensionless numbers [Matsumura *et al.* (1978); Yung, Wong and Chang (1979)], and directly in terms of power draw and gas flowrate [Chapman *et al.* (1983b); Calderbank (1958)], as summarised in Mezaki, Mochizuki and Ogawa (2000).

$$\varphi_G = K_1 N_{Re}^{0.18} N_{We}^{0.25} N_{Fr}^{0.34} N_{QG^*}^{0.20} \quad ; \textit{where } N_{QG^*} = \frac{J_G}{ND} \propto \frac{Q_G}{ND^3} = N_{QG}; K_1 = 6.86 \times 10^3$$

.....Equation 2-15

Matsumura *et al.* (1978)

$$\varphi_G = K_1 \varepsilon_T^{0.31} J_G^{2/3} \quad ; \text{where } \varepsilon_T \text{ in W/kg \& } J_G \text{ in m/s; } K_1 = 1.97$$

.....Equation 2-16

Chapman *et al.* (1983b)

The effect of impeller speed (N_{Re} and N_{Fr}), surface tension (N_{We}) and air flowrate (N_{QG}) on gas holdup φ_G can clearly be seen from Equation 2-15. Yung, Wong and Chang (1979) derived a simpler equation, viz. $\varphi_G = K N_{QG}^{0.5} N_{We}^{0.65} (D/T)^{1.4}$. From the more empirical Equation 2-16, the strong dependence of φ_G on P/V and especially J_G is evident. The earlier correlation developed by Calderbank (1958) agrees very well with Equation 2-16 ($\varphi_G \propto (P_g/V)^{0.40} J_G^{0.50}$).

2.3.3 Solids Suspension

Solids suspension, as an important subprocess affecting particle collection (cf. Figure 2.7), will be considered in this section, and as the focus of this work, will be discussed further in Sections 2.4 and 2.5. In a stirred tank, solids suspension is a measure of the extent to which solid particles interacts with the fluid. In a mechanical flotation cell, it is in this interaction with the fluid that the solids also interact with the bubbles for collection purposes. Solids suspension is thus of great importance to the flotation process, as without adequate suspension of solids, the flotation of particles cannot take place (cf. Figure 2.6 and Figure 2.7). The *lifting* of solids off the base of the vessel, and the *distribution* of solids throughout the volume of the tank are two aspects related to solids suspension. The lifting of the solids off the bottom is a primary requirement of solids suspension as without it there will be no significant interaction between the sedimented solids and the rest of the fluid in the tank. The condition where all the solids are just lifted off the bottom of the vessel is called the *just suspended* or completely suspended condition. The impeller speed at the just suspended condition is commonly referred to as the *critical impeller speed* (N_{js}). A secondary requirement of solids suspension is the distribution of solids throughout the volume of the tank. The upper limit of solids distribution is a *homogeneous suspension* where solids concentrations and solids properties are constant throughout the vessel, which also implies that all solids are completely suspended from the base of the vessel. Solids suspension can be seen as a balance between two mechanisms acting on the particles, i.e. a *sedimentation mechanism* and a *suspension mechanism*, which will be considered here. The relative influence of these two mechanisms will determine the point where all the solids are just suspended off the base (at the *critical impeller speed*), or can be used to describe the vertical *distribution of solids* throughout the vessel. These measures of solids suspension and distribution will be discussed in more detail in Section 2.4, but will be briefly introduced in this section.

2.3.3.1 Sedimentation Mechanism

Intuitively it seems reasonable that solids suspension will be affected by the sedimentation properties of the solids. The most basic way in which particle settling can be considered is the terminal settling velocity of a particle u_T, which is the speed at which a

single particle will settle in a still fluid, and is determined by doing a force balance as shown in Figure 2.11.

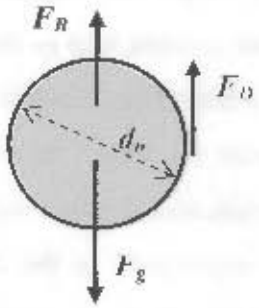

Figure 2.11 Balance of forces at the terminal settling velocity u_T of a particle

F_g = gravity force, F_B = buoyancy force, F_D = drag force

At the terminal settling velocity, the forces acting on the particle are in balance.

$$F_g = F_B + F_D \text{ ; where, } F_g = \frac{\pi}{6} d_p^{\,3} \rho_S g;\ F_B = \frac{\pi}{6} d_p^{\,3} \rho_L g;\ F_D = C_D \frac{\pi}{4} d_p^{\,2} \frac{u_t^{\,2}}{2} \rho_L \text{ (spherical part)}$$

.....Equation 2-17

Solving for u_T:

$$u_T = \sqrt{\frac{4}{3} \cdot \frac{1}{C_D} \cdot d_p \cdot \frac{\rho_S - \rho_L}{\rho_L} \cdot g}$$

.....Equation 2-18

The value of C_D depends on the particle Reynolds number $N_{Rep} = \rho_L u_T d_p / \mu_L$ as follows:

$C_D = 24/N_{Rep}$	; when $10^{-4} \le N_{Rep} \le 2$	: Laminar regime (Stokes)	(a)
$C_D = 18.5/N_{Rep}^{0.6}$	; when $2 \le N_{Rep} \le 500$	: Intermediate regime	(b)
$C_D = 0.44$	; when $500 \le N_{Rep} \le 2\text{x}10^5$	: Turbulent regime (Newton)	(c)

.....Equation 2-19

The terminal settling velocity u_T of spherical particles can be obtained through an iterative process, using Equation 2-18 and Equation 2-19. An alternative and simplified method for calculating the terminal settling velocity of spherical particles is by using the Archimedes number N_{Ar}. N_{Ar} has been related directly to the terminal settling velocity of spherical particles, and gives a good fit in all three fluid regimes (i.e. laminar, intermediate and turbulent), and does not require an iterative procedure as shown in Equation 2-20.

$$\left(N_{Rep}\right)_T = \frac{u_T d_p}{\nu_L} = \frac{N_{Ar}}{18 + 0.6 N_{Ar}^{1/2}} \quad ; \text{where } N_{Ar} = \frac{d_p^{\,3}(\rho_S - \rho_L)g}{\rho_L \nu^2}$$

..... Equation 2-20

From Equation 2-18 to Equation 2-20, the variables affecting the terminal settling velocity of particles can be identified as particle size d_p, relative solid-liquid density difference $(\rho_S-\rho_L)/\rho_L$, kinematic viscosity $\nu = \mu/\rho$, and the sedimentation force of gravity g, which is constant for stirred systems. Up until now, the terminal settling velocity of spherical particles in very dilute solids concentrations in a still fluid has been considered. For non-spherical particles, the *particle shape* can also be incorporated by means of the *particle sphericity*, being the surface area of a sphere compared to that of the particle, each having the same volume. However, as noted by Oldshue (1983a), since spheres normally settle at faster rates than other shaped particles, common conservative practice is to use the settling velocity of a sphere of the same diameter as the particle. It is further known that particles in a stirred tank won't settle at their terminal velocity. The relative settling velocity u_s between particles and fluid (also called the *slip velocity*) is further influenced by the level of turbulence in the liquid, the solids concentration in the liquid (X), and the presence of gas Q_G. However, accurate determination of the particle slip velocity u_s under these conditions are difficult and many correlations just use the accurately measurable terminal settling velocity u_T by making the reasonable assumption that the actual slip velocity u_s in the stirred system will be proportional to u_T.

The *sedimentation mechanism* is thus related to the actual slip velocity u_s of particles, caused by the acceleration of gravity g, and influenced by the following particle-fluid variables, d_p, $(\rho_S-\rho_L)/\rho_L$, ν, X, particle shape, and Q_G for three-phase systems. Ignoring particle shape the sedimentation mechanism is thus a function of the following variables.

$$\text{Sedimentation Mechanism} = \text{f}\left(d_p, \frac{\rho_S - \rho_L}{\rho_L}, g, \nu_L, X, Q_G\right)$$

..... Equation 2-21

2.3.3.2 *Suspension Mechanism*

The *suspension mechanism* is caused by the rotation action of the impeller causing fluid motion, which suspends the particles against their natural tendency to settle. Simplistically seen, the impeller produces two types of fluid motion, i.e. bulk fluid flow, and turbulent fluid motion. The bulk fluid flow is characterised by the discharge flowrate Q_d and is largely responsible for the development of fluid circulation patterns in the tank (i.e. flowlines). The turbulent fluid motion is characterised by velocity gradients (shear) and eddy motion and is responsible for the non-directional dispersing action of the fluid. The *flowrate-head* concept is often used to differentiate between the pumping and shearing action of the impeller and is derived from the analogy between the action of impellers used for agitation and those used in pumps [Edwards and Baker (1992); Oldshue, Herbst and Post (1995); Coulson and Richardson (1990)]. The flowrate-head concept thus regards the impeller in a mechanical flotation cell as being a caseless pump and aims to separate the impeller action in:

1 The rate of circulation (flowrate)
2 The intensity of turbulence (head)

The mass flowrate of the impeller discharge stream ρQ_d, can be derived from the *pumping number* or discharge flow coefficient correlation N_{Qd} (cf. Section 2.3.1) and the density of the fluid.

$$\rho Q_d \propto \rho N D^3 \; ; \; \text{Or,} \; \left(\rho Q_d = N_{Qd} \rho N D^3\right)$$

..... Equation 2-22

Equation 2-22 characterises the *flowrate* concept of impeller operation (pumping) and is characterised by the *discharge flow coefficient* N_{Qd}, which is often taken as approximately 0.75 for design purposes [Edwards and Baker (1992)]. The discharge flow from the impeller is responsible for producing bulk fluid circulation and is thus important for overall blending action in the tank. It should be noted here that the bulk fluid circulation flowrate Q_{circ} is often higher than the impeller discharge rate Q_d due to the discharge stream inducing flow in the rest of the fluid. Edwards and Baker gives the fluid circulation flowrate Q_{circ} to be about twice Q_d for design purposes.

The pressure head or virtual head h_d caused by impeller rotation is obtained when all the kinetic energy in the discharge stream is converted into pressure energy, expressed as height.

$$h_d \propto \frac{N^2D^2}{g} \; ; \text{ Or, } \left(h_d = N_{hd} \frac{N^2D^2}{g} \right)$$

..... Equation 2-23

Equation 2-23 characterises the *head* concept of the impeller action, which is responsible for the shearing action and thus the level of turbulence generated by the impeller. Similarly to the discharge flow coefficient N_{Qd} (cf. Equation 2-22), characteristic of *impeller pumping flowrate*, can a *discharge head coefficient* N_{hd} be derived (cf. Equation 2-23), characteristic of the *shearing action* produced by the impeller. The level of turbulence (shear) is most intense in the region of the impeller and decays in regions away from the impeller [Schubert (1999)]. High turbulence levels cause *dispersive* actions leading to good fluid contacting on the microscale.

Shaft power from the impeller thus produces fluid flow and fluid shearing actions. The power used by a pump impeller can be expressed as a product of the mass flowrate ρQ_d and the velocity head h_d (refer, $P = \dot{m} g \Delta h$) of the discharge stream and inserting from Equation 2-22 and Equation 2-23 gives.

$$P = \rho Q_d g h_d = N_{Qd} \cdot \left(\rho N D^3\right) . g . N_{hd} \cdot \left(\frac{N^2D^2}{g} \right) = N_{Qd} . N_{hd} \cdot \rho N^3 D^5 = N_P . \rho N^3 D^5$$

..... Equation 2-24

Dividing by $\rho N^3 D^5$:

$$N_P = N_{Qd} \cdot N_{hd}; \text{ where } N_{Qd} = \frac{Q_d}{ND^3} \text{ and } N_{hd} = \frac{h_d g}{N^2 D^2}$$

..... Equation 2-25

It can be seen from Equation 2-24 that calculating the power consumption as the product of the flowrate and the velocity head of the discharge stream leads to the power number correlation commonly used for flotation impellers. In dimensionless form, the power number (N_P) can thus be written as the product of the flow and head coefficients (cf. Equation 2-25).

From Equation 2-22 and Equation 2-23 it follows that the suspension mechanism caused by the rotation of the impeller is a function of ρ, N, D and g. The suspension mechanism (flow and especially turbulence) reduces with distance from the impeller, which is a function of tank diameter T, impeller clearance C, and liquid height Z. These parameters can thus be expected to influence the suspension mechanism in a flotation cell. Gas addition Q_G has been found to have a strong influence on the gassed power draw P_g of the impeller and by considering Equation 2-24 is related to either or both a reduction in the mass flow rate (ρQ_d) from the impeller or a reduction in the shearing action or velocity head (h_d) from the impeller. Gas flowrate is thus an important variable affecting the solids suspension mechanism in three-phase systems. Overall, it can thus be expected that the suspension mechanism would be influenced by the following variables.

$$\text{Suspension Mechanism} = f(\rho, N, D, g, T, C, Z, Q_G)$$

..... Equation 2-26

Both *empirical* and *theoretical* correlations have been developed to relate the suspension mechanism (cf. Equation 2-26) to the sedimentation mechanism (cf. Equation 2-21) aimed towards a certain *correlation objective*. The most common correlation objective is to determine an impeller speed where a certain suspension condition occurs, e.g. *the critical impeller speed.*

2.3.3.3 Complete Suspension

The critical impeller speed N_{js} is the impeller speed at the just suspended condition, when all the *solids are just completely lifted off the base of the tank.* For mechanical flotation cells, this means that *all* the solids are only available for collection purposes at or above N_{js}. Below N_{js} some sedimentation of solids start to occur in the cell. Nevertheless, other considerations such as operating costs, and the efficiency of the other subprocesses might warrant the operation of the flotation cell at speeds below (or above) the critical impeller speed. The critical impeller speed can thus be used as a relative measure for relating impeller speed in terms of solids suspension. The critical impeller speed N_{js} is not a static design speed but a dynamic speed influenced by solid-liquid, operational and design (geometry) variables. These variables were introduced in previous paragraphs to either influence the sedimentation mechanism (cf. Equation 2-21) or the suspension mechanism (cf.

Equation 2-26) acting on the solid particles. At the just suspended condition, it can be assumed that a certain balance will exist between these two mechanisms.

$$Suspension\ Mechanism_{js} = \mathrm{f}(Sedimentation\ Mechanism) \qquad \text{(a)}$$

And with N_{js} as the correlation objective,

$$N_{js} = \mathrm{f}\left(g, d_p, \frac{\rho_S - \rho_L}{\rho_L}, \nu_L, X, Q_G, D, \rho, g, T, C, Z\right) \qquad \text{(b)}$$

..... Equation 2-27

Equation 2-27 identifies possible variables to consider in the development of a correlation describing the critical impeller speed N_{js} in a mechanical flotation cell. The critical impeller speed N_{js} is normally the correlation objective and if needed can be related to power addition P_{js} by using the power number N_P correlation. As will be shown in Section 2.5.1, no correlation like that suggested by Equation 2-27 has been developed for a mechanical flotation cell. Fortunately, much work has been done on the critical impeller speed in stirred tanks. Zwietering (1958) developed one of the first comprehensive critical impeller speed correlations, which is still today the most widely used.

$$N_{js} = S d_p^{0.20} B^{0.13} \nu^{0.10} g^{0.45} \left(\frac{\rho_S - \rho_L}{\rho_L}\right)^{0.45} D^{-0.85}; \text{ for constant } D/T \text{ and } C/T$$

..... Equation 2-28

Equation 2-28 was developed for two-phase solids suspension. The effect of gas is often incorporated by the addition of a linear term to the correlation (i.e. $N_{jsg} = N_{jsu} + \mathrm{K}.Q_G$), however many have found that this is not satisfactory for a wide range of conditions, and has suggested alternative ways to demonstrate the effect of gas on the critical impeller speed. The N_{js} correlation in two- (N_{jsu}) and three-phase (N_{jsg}) conditions will be considered in detail in Sections 2.4.4 and 2.4.5.

2.3.3.4 Solids Distribution

Solids distribution considers the spatial distribution of solids throughout the cell. It is most often considered in the axial direction but can also be done in the radial direction.

In the axial direction, the maximum vertical height to which a measurable amount of solids is lifted is expressed as the suspension height, h_s. Suspension height (h_s) is thus a measure of the *vertical extent* of solids distribution without reference to homogeneity within the distribution. An h_s/T correlation in terms of impeller diameter T/D, impeller clearance C/D and power addition P/m_S was developed by Arbiter, Harris and Yap (1969). In flotation cells, the homogeneity of the solids distribution is often shown by measuring the concentration of solids at different heights in the cell to obtain an axial *concentration profile*, X_{hi} [e.g. Yianatos *et al.* (2001)]. X_{hi} thus gives a visual image of the vertical distribution of solids. It is also possible to quantify the homogeneity (variation) in the solids concentration by determining the relative standard deviation *RSD* in the measured solids concentrations. Work done in mechanical flotation cells on solids distribution will be discussed further in Section 2.5.2.

The vertical solids distribution can also be described mechanistically in terms of the opposing sedimentation (cf. Equation 2-21) and suspension (cf. Equation 2-26) mechanisms. This correlation is called the sedimentation-dispersion model for solids distribution, which has mainly had some application in high aspect ratio vessels and small stirred tanks at low X. It is however thought that the sedimentation-dispersion model can also be applied to mechanical flotation cells to mechanistically explain the axial distribution of solids in the cell, if not quantitatively at least qualitatively. In essence it considers the balance of the opposing forces of solids sedimentation in terms of the settling velocity u_s, and the solids dispersion coefficient D_S, caused by the turbulent action of the liquid. In the absence of radial concentration profiles, the sedimentation-dispersion is normally given as shown in Equation 2-29.

$$\ln\left(\frac{X_h}{X_B}\right)=\frac{u_s}{D_S}h$$

..... Equation 2-29

Solids distribution will be considered further in Section 2.4.6.

This section considered hydrodynamics, gas dispersion and solids suspension as important aspects affecting the collection zone. The collection subprocess was already discussed in Section 2.1.2.2. Solids suspension and gas dispersion are important subprocesses for particle-bubble interaction to occur. Hydrodynamic conditions influence all the subprocesses in the collection zone and thus formed the starting point of this discussion.

Hydrodynamics: *The hydrodynamics in mechanical flotation cells are influenced by a large number of fluid-, geometrical-, and dynamic variables.* ***Dimensional analyses*** *is often used to reduce the number of parameters to correlate and in so doing simplify the relations for a better understanding of the underlying principles. Power addition P is an important variable affecting the hydrodynamic conditions in a mechanical flotation cell and is a dependent variable that can be calculated using the* ***power number*** N_P. *At the high* ***Reynolds number*** N_{Re} *conditions in mechanical flotation cells,* N_P *is mostly independent of* N_{Re} ($N_{Re} \geq 10^5$) *but is influenced by the impeller and stator geometry and is strongly affected by gas addition. The* ***airflow number*** N_{QG} *is another important dimensionless number often used in flotation and is related to gas induction, gas dispersion, gassed power draw, impeller pumping with gas addition, and the effectiveness of solids suspension with gas addition. The* ***Froude number*** N_{Fr} *is related to vortex formation in the impeller and standpipe and is thus related to gas induction and dispersion. The* ***pumping number*** N_{Qd} *(also called discharge flow coefficient) describes the effectiveness of the rotating impeller as a fluid pump causing bulk circulation in the tank. However due to the difficulty of measuring fluid velocities in the discharge stream,* N_{Qd} *is less often used in flotation.* Q_d *is however directly related to gas dispersion and solids suspension by fluid circulation. The* ***Weber number*** N_{We} *relates fluid acceleration forces produced by impeller rotation (inertial forces) to surface tension* σ_{GL} *forces and is thus related to bubble formation and bubble size. In addition to these dimensionless numbers, other hydrodynamic parameters are also often used to describe the hydrodynamic conditions in mechanical flotation cells (e.g.* u_{tip}, P/V, J_G, Q_{GV}, φ_G, M, θ_{tt}).

Gas Dispersion: *Increased introduction of gas into the rotating impeller causes* ***reduced power*** *draw by the impeller. Considering a number of gassed power draw studies, it follows that the effect of gas on power draw is dependent on the impeller design but many have found power draw to decrease with gas addition to the power of approximately -0.25 within 'normal' gassing rates (i.e.* $N_{Pg} \propto \sim N_{QG}^{-0.25}$). ***Frother*** *addition also causes further increased reduction in gassed power draw. The mechanism of gas dispersion can be considered in terms of gas induction, impeller flooding, effectiveness of gas dispersion, bubble formation, and gas holdup.* ***Gas induction*** *is important for especially self-aerating flotation machines and is characterised by the minimum impeller speed for gas induction* N_{GI} *and the air flowrate induced into the cell* Q_{Gind}, *both of which are functions of the Froude number* N_{Fr} *and impeller submergence below the liquid surface* S_I. *Impeller* ***flooding*** *on the other hand might occur with forced-aerated impellers when the gas addition rate* Q_G *exceeds the impeller's gas dispersion capacity at that impeller speed. The impeller speed where flooding occurs* N_F *can be determined from a direct relation between the airflow number* N_{QG} *and Froude number* N_{Fr}. *Dramatically decreased power draw and solids suspension capacity is characteristic of the flooding point. Correlations for* ***complete gas dispersion*** *throughout the cell* N_{cd} *are less common and is thought to be due to the difficulty of determining this point accurately. Similarly, to* N_F, *can* N_{cd} *also be correlated by a relation between the airflow number* N_{QG} *and Froude number* N_{Fr}. *Gas dispersion happens through turbulent dispersion*

and bulk fluid flow, both of which are reduced by increased addition of gas. ***Bubble formation*** *is related to bubble size, which can be correlated either, in terms of the Weber number N_{We}, or in terms of power addition P/V and surface tension σ_{GL}. The* ***gas holdup*** *in the cell is the product of a fairly complex interaction of a number of variables, the most notable of which are the Froude number N_{Fr}, Weber number N_{We} and airflow number N_{QG} or more empirically in terms of power addition P/V and gas addition rate J_G.*

Solids Suspension: *The suspension or lifting of solids off the base of a flotation cell is a necessary precondition for particle-bubble contact and is the primary solids suspension step. The distribution of suspended solids throughout the vessel is the secondary solids suspension step and is also important in considering particle-bubble interaction in the collection zone. Solids suspension can be seen as a balance between a sedimentation mechanism and a suspension mechanism acting on the solids particles. The* ***sedimentation mechanism*** *is related to the settling velocity of the particles. In this way it was shown that the sedimentation mechanism is a function of the following variables, d_p, $(\rho_S-\rho_L)/\rho_L$, g, v, X, particle shape, and Q_G for three-phase systems. The* ***suspension mechanism*** *on the other hand is related to the action of the impeller. The impeller action produces both fluid flow and fluid shear motion in the cell. The fluid flow is characterised by the flow coefficient N_{Qd} and the shearing motion is characterised by the head coefficient N_{hd} of the impeller. The product of these two coefficients gives the power number N_P, showing how power consumption by the impeller is used for the production of both bulk flow and turbulence (shear) in the cell. The suspension mechanism in a mechanical flotation cell is related to both flow and turbulent fluid motion and also depends on the geometry of the cell and were thus found to be a function of the following variables, ρ, N, D, g, T, C, Z, Q_G. The suspension mechanism and sedimentation mechanisms acting on the solid particles are often* ***related to the critical impeller speed*** *where all solids are just lifted off the base the tank, which should thus be a function of all the variables already identified. The just suspended condition is strongly related to the possibility of a particle contacting a bubble for collection, yet as will be shown in Section 2.5.1, no correlation relating the just suspended impeller speed to system variables already mentioned could be found in the flotation literature. Fortunately, a commonly used correlation exists for solid-liquid solids suspension in standard stirred tanks [Zwietering (1958)] and it is thought that a similar correlation can be derived for mechanical flotation cells, which is* ***the main aim of this work****. Critical impeller speed correlations will be discussed further in the next section. A secondary aspect related to solids suspension is the distribution of solids throughout the tank. This* ***distribution of solids*** *is also determined by the interaction of the suspension and the sedimentation mechanisms as correlated through the application of the sedimentation-dispersion model. However this is less often used in stirred tanks and is thought to contribute more towards the qualitative understanding of solids distribution as measured in solids concentration profiles and will be considered further in Section 2.4.*

2.4 SOLIDS SUSPENSION IN STIRRED TANKS

The importance of flotation has been emphasised in Section 2.1; the importance of mechanical flotation cells in Section 2.2; hydrodynamics, gas dispersion and solids suspension as important subprocesses affecting the collection zone in Section 2.3. From these sections and especially from Section 2.3 it follows that solids suspension plays an important part in the collection zone. Yet in the published literature, solids suspension has not been extensively studied and correlated in mechanical flotation cells. Foretunately, many studies have been done on solids suspension in standard stirred tanks. The ***aim of this section*** is thus to consider the general chemical engineering literature in order to develop a *methodology to evaluate the solids suspension* in mechanical flotation cells, for application in this thesis. The *mechanism* of solids suspension has already been described qualitatively in Sections 2.3.3.1 and 2.3.3.2 and some quantitative correlations for considering solids suspension and solids distribution were briefly introduced in Sections 2.3.3.3 and 2.3.3.4. Solids suspension is a broad term used in general to describe both the process of suspending solids off the bottom of a vessel, as well as distributing solids throughout the volume of the tank. Different solids suspension conditions can thus be used to evaluate the *effectiveness of solids suspension*, which will be considered in Section 2.4.1. *Experimental methods* that can be used in the studying of solids suspension is briefly reviewed considered in Section 2.4.2. As will be shown in Section 2.4.1 most investigators use the just suspended condition as the reference condition for correlations of solids suspension. Different just suspended criteria or pointers have been used to identify the just suspended condition, which will be overviewed in Section 2.4.3. The impeller speed at the just suspended condition is commonly referred to as the *critical impeller speed*, N_{js}. An extensive review of N_{js} correlations will then follow, first for two-phase conditions (cf. Section 2.4.4), and then extended to three-phase conditions (cf. Section 2.4.5). The final part of this section will look at *solids distribution,* which is a secondary step in the solids suspension process (cf. Section 2.4.6).

2.4.1 Conditions for Evaluating the Effectiveness of Solids Suspension

Certain degrees of solids suspension can be identified during the solids suspension process as the impeller speed is increased from zero, with all solids sedimented on the bottom, to a relatively high impeller speed where all properties of the suspension is homogeneous

throughout the volume of the tank. These conditions normally relate, either to the *extent* of off-bottom solids *suspension*, or to the quality of the solids *distribution* throughout the tank, as shown in Figure 2.12.

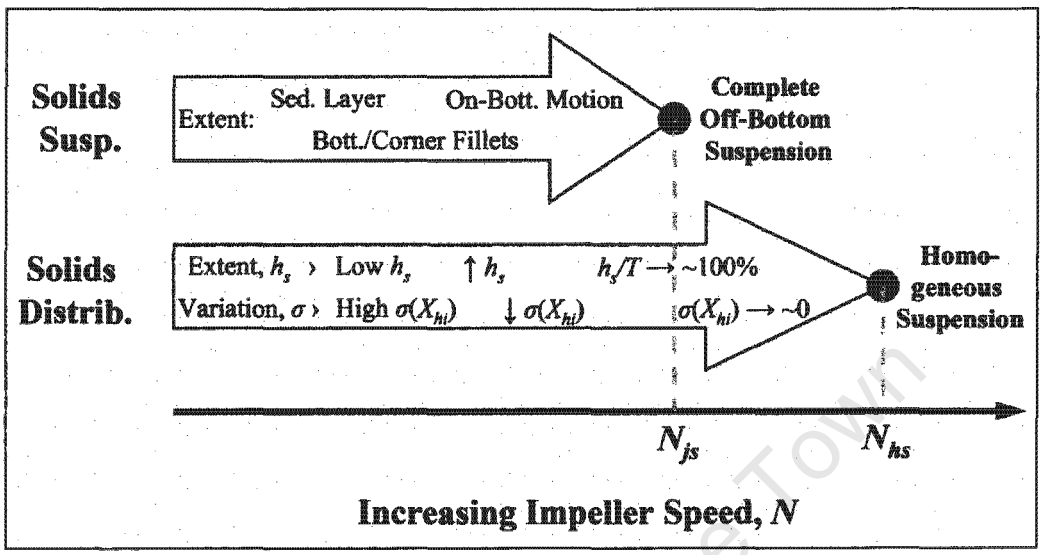

Figure 2.12 Evaluating the effectiveness of solids suspension with increasing N

Where: σ = standard deviation; X_{hi} = solids concentrations in a profile; h_s = suspension height

It follows from Figure 2.12 that solids suspension can be evaluated in terms of off-bottom suspension and/or solids distribution quality. Considering ***off-bottom solids suspension***, increasing the impeller speed leads to complete off-bottom suspension, also commonly referred to as *complete suspension* or the *just suspended* condition. The impeller speed at the just suspended condition is referred to as the *critical impeller speed* (N_{js}). Alternatively, if ***solids distribution quality*** is considered, the upper limit is a homogeneous solids suspension (N_{hs}). The solids distribution *quality* includes the *extent* of the distribution as well as the *variation* in the distribution. For a *homogeneous suspension* the solids must, firstly be suspended completely (off-bottom), secondly distributed completely throughout the volume of the tank (extent of distribution), and thirdly exhibit constant properties throughout (variation within distribution). The extent of solids distribution in stirred tanks is often expressed as relative suspension heights h_s/T, whilst the variation in the distribution can be expressed in terms of relative variance σ_{rel}^2 or relative standard standard deviation *RSD*.

Of the two suspension conditions, the critical impeller speed N_{js} has found the widest application, and is often related to other system variables as will be seen in Section 2.4.4. This just suspended condition has long been recognized as an important degree of solids

suspension [White and Summerford (1933)]. This is because until the just suspended condition is reached, the total solid surface area is not efficiently utilized and above this speed, the rate of such processes as dissolution and ion exchange increases only slowly [Nienow (1968)]. It should however be remembered that the just suspended condition relates directly to off-bottom suspension conditions, but only indirectly to solids distribution. At the point of complete suspension, small and light particles will be fairly homogeneously distributed, whereas coarse and heavy particles will remain in the lower part of the vessel, the upper part being a layer of clear liquid [Zwietering (1958)]. Apart from off-bottom suspension, is the uniformity of the solids distribution also important for some processes where a continuous and representative flow of solids from the system is required, or when the product quality is highly dependent on a constant solids concentration throughout the tank. The different *solids suspension conditions* identified here are summarised in Table 2.4 and related to the just suspended condition in terms of relative impeller speed N/N_{js}.

Table 2.4 Solids Suspension Conditions

Solids Suspension Condition	Description	Impeller speed*
Sedimented layer	Solids remain in a sedimented layer on the bottom, largely unaffected by agitation.	$N < 0.6\ N_{js}$
Bottom or Corner Fillet Formation	Solids are suspended from most of the base, with some areas still containing fillets of sedimented solids.	$N \sim 0.6\ N_{js}$ [Nienow (1992)]
Complete On-bottom motion	All particles have motion. Most are suspended off the bottom with vertical motion components, while the rest remain on the bottom, where it is being moved by the liquid.	$N \sim 0.8\ N_{js}$ [Hicks, Myers and Bakker (1997)] $N \sim 0.7\ N_{js}$ [Shaw (1992)]
Complete (off-bottom) Solids Suspension, or Just Suspended	All particles are suspended off the bottom of the vessel and experience vertical displacement.	$N = N_{js}$ [reproducibility ± 3% as per Zwietering (1958)]
Complete Solids Distribution (h_s ~ 90%)	The *extent* of solids suspension is approaching 100% (h_s = 90% is often taken), i.e. suspension height h_s approaching Z; ($Z = T$); (homogeneity not considered).	$N \sim 0.9$ to $1.5\ N_{js}$** [Hicks, Myers and Bakker (1997)]

Homogeneous Solids Suspension (Complete Uniformity)	This is the uppermost level of solids suspension and distribution. All solids are suspended off the bottom, completely distributed throughout the tank, and the variation in solids concentrations and properties are approaching zero (often taken as the point where further increases in N stops having appreciable effects on uniformity)	$N \sim 1.7\ N_{js}$ [Oldshue, Herbst and Post (1995)] $N \sim 1.5\ N_{js}$ [Shaw (1992)]

*, N_{js} is the impeller speed at the complete off-bottom suspension condition.
**, Einenkel (1980) found $h_s = 90\%$ to occur at N_{js}. However, from Hicks, Myers and Bakker (1997)'s data $h_s = 0.90.T$ occurs between 0.9 and 1.5 N_{js} depending on ρ_S, X, D/T, C/T, and number of impellers (in multiple impeller systems).

It follows from Table 2.4 that although many solids suspension conditions can be identified the just suspended condition is the most consistent condition with the least variation in impeller speed conditions. This is the attraction of using N_{js} for solids suspension correlation purposes (cf. Section 2.4.4).

Although the focus is often on the just suspended condition, some processes are run most profitably at conditions below complete suspension e.g. bottom or corner fillets, or complete on-bottom motion. Often these lower degrees of solids suspension sacrifice only slightly on process efficiency, whilst the power savings from running at lower impeller speeds can be substantial. From the N_P being constant for highly turbulent well-baffled systems, follows that P will decrease with N^3 (e.g. P drops by 50% if N drops by 20%). Whether the process run at the just suspended condition or not, doesn't deduct from the importance of the just suspended condition due to the ability of expressing all the other degrees of suspension in terms of the just suspended impeller speed. Using the just suspended impeller speed as reference, a *scale of solids suspension conditions* can be derived to relate all the solids suspension conditions (cf. Table 2.4) to N_{js} as shown in Figure 2.13. As per Table 2.4 the first four conditions relates to off-bottom solids suspension, while the last two relates to solids distribution conditions.

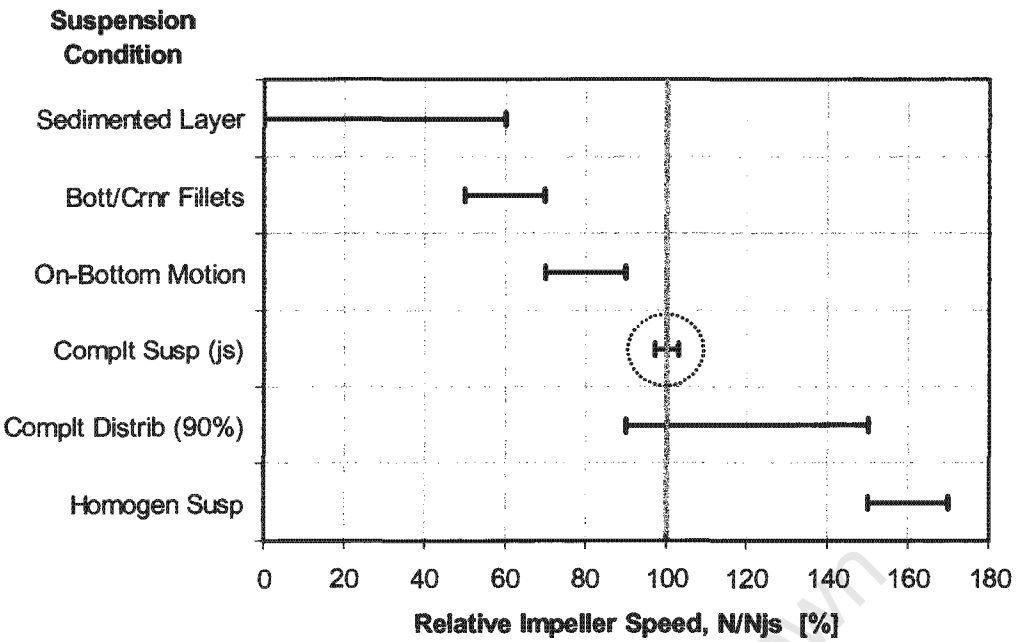

Figure 2.13 Scale of solids suspension conditions

2.4.2 Experimental Methods

In this section, some experimental methods used in the investigation of mixing and more specifically solids suspension will be reviewed. These experimental techniques can be grouped into those aimed at measuring off-bottom suspension, those aimed at measuring solids distribution and other solids suspension related methods.

2.4.2.1 Methods Aimed at Measuring Off-bottom Suspension (N_{js})

These experimental methods take their measurements of solids suspension at the tank bottom, or focus on the behaviour of solids on the bottom of the tank.

2.4.2.1.1 Visual Observation of Tank Bottom

Visual observation of the tank bottom is a very common method used in the investigation of solids suspension. This method requires the tank to be made of transparent material or at least to be fitted with transparent windows at critical locations allowing visual observations to be made. The contents of the tank are normally illuminated and the bottom is

observed through an inclined mirror [e.g. Zwietering (1958)] or a video camera [e.g. Frijlink, Bakker and Smith (1990)] fitted underneath the tank. Some [e.g. Nienow (1968)] have also observed the bottom through the sidewall; this however restricts the user to working with very low solids concentrations. The aim of the visual observation of the tank bottom is normally to identify some degree of solids suspension e.g. the just suspended condition. The *advantages* of visual observation are that it is a simple and relatively quick method, as well as being non-intrusive and therefore does not interfere with the stirring conditions during evaluation. The *disadvantages* include that it relies on the observations and interpretation of the user and can thus be criticised in terms of objectivity. It also requires the tank to be made of a transparent material, which normally restricts this method to laboratory scale testwork.

Frijlink, Bakker and Smith (1990) evaluated the method of visually observing the tank bottom. The strength and weakness of visual observation of the tank bottom lie in that only the bottom plane of a three-dimensional system is observed, although evidently the most important plane for solids suspension purposes. At the just suspended condition, off-bottom suspension conditions are the same for different systems, yet the distribution of solids might be different depending on particle, liquid, and system geometry properties. Visually identifying the just suspended condition can be demanding, sometimes very difficult, and automation will be very difficult. The location of last off-bottom suspension depends on impeller type. With axial impellers, the last solids are normally suspended from the periphery of the tank bottom, whilst for radial impellers the last solids are normally suspended from the centre of the tank bottom.

2.4.2.1.2 Contact with Tank Bottom

The contact method is mainly used to measure off-bottom solids suspension conditions in industrial-size vessels, which are normally constructed of non-transparent material. A rod normally fitted with a flat baffle at the end is inserted from the top of the tank to test for the presence of a sedimented layer or fillets of sedimented solids on the base of the tank. Care and safety precautions should be in place to prevent the rod from being caught in the impeller mechanism. The advantage of this method is that it is a simple and quick method to detect relatively high levels of solids sedimentation in industrial vessels. The safety concern of inserting a rod into a stirred vessel is one of the disadvantages of this method. The accuracy of the contact method can also be questioned, due to it only being applied to certain

points on the bottom, as well as the difficulty of detecting low levels of solids sedimentation. For this reason, it is normally only used as a rough indicator of poor solids suspension conditions in some industrial applications.

2.4.2.1.3 Ultrasonic Doppler Probe

This method uses a Doppler probe, which detects the Doppler Effect on ultrasound waves caused by moving solid particles on the base of the vessel. The Doppler probe is used from the outside on the bottom of the tank to detect solids movement and can thus be used on some industrial installations. It is also non-intrusive and thus does not interfere with the mixing conditions in the tank. Buurman, Resoort and Plaschkes (1986) used this method extensively. The selection of where to positioning the probe is important as well as calibrating the results against visual observations. Even then, the accuracy is still questionable [Nienow (1992)].

2.4.2.1.4 Radiation

Radioactive tracers have also been used by some [e.g. Rewatkar, Raghava Rao and Joshi (1991)] to determine the concentration of solids on the bottom of the tank. In this method, some of the solid particles (e.g. silica sand) are labelled with a radioactive material (e.g. radioactive gold, Au^{198}). These labelled particles emit γ-rays, which are detected with a scintillation detector placed outside the reactor on the bottom of the tank. For solids suspension work, the digital signals (count rates) on the bottom of the tank can be related to the solids concentration on the bottom and thus off-bottom solids suspension conditions. The advantage of this method lies in the non-intrusiveness of this measurement. An obvious disadvantage of this method is safety considerations and restrictions associated with the use of radioactive material.

2.4.2.1.5 Rate of Mass Transfer

In this method, a slowly dissolving solid or an ion exchange resin can be used as the solid particles in the vessel. The rate of solid-liquid mass transfer has been found to increase with increasing impeller speed as more and more solids are lifted off the base of the tank. Kneule (1956) who used the rate of solution of crystals in his work, was one of the first

to use this method to investigate solids suspension. The advantage of this method is that it gives accurate results, which can be related directly to processes such as dissolution or ion exchange. For general investigations, this method is however restrictive on the variety of systems that it can be used in, due to it requiring a sparingly dissolvable particle or ion exchange resin to be used.

2.4.2.2 Methods Aimed at Measuring Solids Distribution (X_{hi} & h_s)

These methods are applied in the bulk volume of the vessel and are normally used to give measurements of solids concentrations or solids distribution (e.g. local concentrations, concentration profiles, and suspension heights).

2.4.2.2.1 Visual Observation of Suspension Height

The suspension height h_s, also referred to as cloud height, is the height that solids are suspended to and is often measured in solids suspension work. It is thus a measure of the *extent* of solids distribution, without consideration of the variation in solids concentrations within the distribution. Suspension height h_s is often determined by non-intrusive visual observation of the clear liquid layer that normally exists at the top of the tank. The visual observation of suspension height normally requires a transparent tank, limiting its application in industrial tanks. The suspension height often fluctuates continuously at the top of the tank and visual determination of h_s thus suffers from uncertainty and lack of objectivity. Visual observation of the suspension height is also difficult under gassed conditions due to the gas bubbles interfering with the clear liquid layer at the top.

2.4.2.2.2 Sample Withdrawal

Sample withdrawal is an important technique commonly used to evaluate solids suspension and solids distributions in stirred tanks. Sample withdrawal can be used to evaluate solids concentrations at a certain point (local concentration) or a range of points to form a concentration profile. From a vertical concentration profile, the suspension height h_s can also be determined. Barresi and Baldi (1987a) used sample withdrawal extensively in their work on solids distribution in relatively dilute system ($X \leq 5\%$). They tested the effect of sample withdrawal velocity and sampling tube shape as shown in Figure 2.14. They

concluded that varying the withdrawal velocity between approximately 0.6 and 1.0 m/s had a relatively small effect on the measured solids concentrations. They however found the tip shape of the withdrawal tube to have an influence and recommended the use of a horizontal sampling tube with a 45°-profiled tip facing downwards. Barresi and Baldi further found that the average solids concentration calculated from the axial concentration profile under completely suspended conditions (X_{ms}) were generally about 10-20% lower than the known average solids concentration in the vessel (X_{act}). They attributed this to a lack of isokinetic sampling and also to the solids concentration in the layer just above the bottom of the vessel being very high but uncertain. Nienow (1992) noted that sample withdrawal methods works well, also in three-phase systems, even though it might be prone to some sampling error.

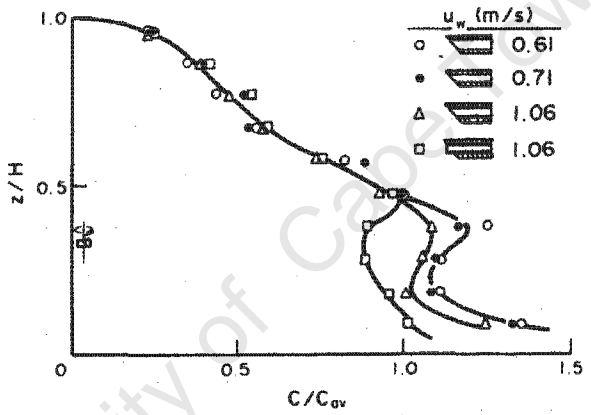

Figure 2.14 Influence of sample withdrawal velocity and sampling tube tip shape on the concentration profile [Barresi and Baldi (1987a)]

[4PBT; d_p=208 to 250μm; B=0.015; N = N_{js}; horizontal sampling tubes with 6mm ID.

2.4.2.2.3 Optical Methods

Optical methods normally employ the passing of a laser beam through a dilute suspension of solids. Compared to other light sources the laser is advantageous, since it produces a compact beam of light. In the passage of the laser through the sample, the intensity of the beam is attenuated or reduced by the presence of solid particles. The round tank is normally placed inside a rectangular tank filled with water to reduce optical distortions. The intensity of the beam is then measured on the other side of the tank using a photovoltaic receiver. The attenuation of the laser beam can be calibrated to solids concentration. These concentration measurements can easily be repeated at different heights through the vessel to produce axial solids concentration profiles. It should be remembered

that these are not point measurements as in sample withdrawal but an average along the line of the beam, and as such cannot be used to determine radial concentration profiles. The disadvantages of this method seems to include limited tank size, limited solids concentrations, and not usable in three-phase conditions. Ayazi Shamlou and Koutsakos (1989) and Bohnet and Niesmak (1980) both used He-Ne lasers and worked only with solids concentrations of up to about 6 wt% or 2 vol% in 0.225 and 0.25 m tanks. However, Godfrey and Zhu (1994) proposed a technique of carefully selecting the refractive indeces of the liquid and optically homogeneous solid, which allowed measurements at solids concentrations of between 0.2 and 30 vol.% (T = 0.154m). The advantages of optical techniques are that it is quick, accurate, and non-intrusive.

2.4.2.2.4 Ultrasonic Techniques

Ultrasonic techniques send ultrasonic sound waves through the medium in the tank from a transmitter to a receiver. The presence of solids affects both the velocity and the attenuation of the ultrasound wave as it passes through the slurry. The attenuation is measured in terms of a reduction in the amplitude of the signal reaching the receiver. In this way ultrasonic methods can be used to determine solids concentrations in both two- and three-phase slurry systems [Soong *et al.* (1995); Stolojanu and Prakash (1997)].

2.4.2.2.5 Pressure Probes

The static pressure in a slurry is influenced by the slurry density and thus the solids concentrations. Weisman and Efferding (1960) used pressure probes to measure the solids concentration in mechanical mixers. Nienow (1992) however questioned the accurace and sensitivity of this method.

2.4.2.2.6 Conductivity Probes

The conductivity of a slurry is often different from that of the liquid phase alone and is influenced by the concentration of the solids present. Conductivity probes measures the conductivity (or inverse of the resistivity) in the slurry, the results of which can then often be related to solids concentration. Application of this technique is subject to careful calibration and the influence of other factors (e.g. ionic strength in the liquid) should always

be kept in mind. Musil and Vlk (1978) used conductivity probes to measure local solids concentrations in stirred vessels.

2.4.2.2.7 Tomography

The most common method of tomography applied to mixing systems is electrical resistance tomography (ERT). It employs a number of electrodes, normally arranged as rings on different planes inside the tank. For example Wang *et al.* (1999) used a 1.5 m tank fitted with rings of 16 electrodes fitted on 8 planes on different heights in the tank. Electrical current signals are then passed through the electrodes and the potential differences over various pairs of electrodes are measured. The data is then processed by various algorithms to obtain a picture of electrical resistance fields in the plane between the electrodes. This picture of electrical resistance fields is then related to the presence and concentrations of solids in the plane. ERT can also be used to measure mixing dynamics such as mixing times in the tank by adding a high conductance pulse to the liquid and measuring the response throughout the vessel. However, obtaining high resolution, dynamic, results as well as three-phase application still seem to be somewhat challenging for this technique.

2.4.2.3 Other Methods related to Solids Suspension

These are techniques that are not direct measurements of solids suspension or distribution but can normally be related to solids suspension, even if only qualitatively.

2.4.2.3.1 Solids Residence Time Distributions, RTD_S

Residence time distributions are used extensively in the kinetic modelling of processes in continuous flow systems [e.g. Levenspiel (1972), and Oldshue (1983b)]. The solids residence time distribution, RTD_S, provides a picture of the probability of a particle leaving the system after a certain length of time. RTD_S is measured by adding a solids 'tracer' to the feed into the system and measuring the concentration of the tracer in the outlet stream as it leaves the system. Care should be taken in the selection of the tracer, to make them as representative as possible of the solids in the system. The tracer should also be easily detectable in the outlet stream. Washout curves are a slightly oversimplified but very useful method of determining RTD_S. The actual solids concentration in the outlet stream is measured

after stopping the solids feeding into the system [Nienow (1992)]. Depending on whether the discharge point is at the bottom of the tank or higher up the side a shorter RTD_S can indicate worse or better solids suspension and distribution. RTD_S is commonly compared to RTD_L and larger deviations are assumed to indicate worsening solids suspension and distribution. Therefore, RTD_S is related to the spatial distribution of solids throughout the tank, but direct correlation is difficult.

2.4.2.3.2 Mixing Time, θ_{mix}

In the perfect mixing model it is assumed that the feed into the system is instantaneously distributed throughout the tank on entry. Mixing time studies aim to measure the time that it takes for material to be spread throughout the tank volume. In this way, mixing time θ_{mix} indicates overall flow speeds and turbulence throughout the tank. For example mixing time is commonly taken as equal to 5 times the circulation time θ_{circ}. The θ_{circ} is the time it takes the fluid to circulate through the longest circulation loop in the tank and depends on impeller type and impeller clearance. Joshi, Pandit and Sharma (1982) summarised mixing time correlations. It follows that a number of different methods are used to measure θ_{mix}, including conductivity, refractive index, decolourisation, and pH measurements. Of these, conductivity measurements are most commonly used and θ_{mix} is taken as the time to reach a fraction (e.g. ~ 95 to 99.9%) of the final conductivity after adding a high conductance tracer into the feed. Rewatkar, Raghava Rao and Joshi (1991) used θ_{mix} extensively in their solids suspension work (cf. 2.4.3.9).

2.4.2.3.3 Power Draw and Torque Measurements

It was shown in Section 2.3.3.2 how the power drawn by an impeller is the product of the discharge *flowrate* and discharge *shearing* action. The bulk fluid circulation and turbulent dispersion caused by these actions of the impeller are important mechanisms in solids suspension. Rewatkar, Raghava Rao and Joshi (1991) used *power* measurements extensively in their solids suspension work (cf. Section 2.4.3.10). Accurate torque (M) measurements on the shaft, using straingauges for example, is the best way to determine the shaft power ($P = 2\pi N.M$). Electrical power is sometimes used but is prone to errors. Accounting for losses in the impeller drive mechanism (i.e. V-belts, gearbox, bearings, etc.) is the main source of error in electrical measurements. No-load power when the impeller is

running free is often used to account for these losses. However, the drive losses are not constant and most increases under increased loading.

2.4.3 Criteria for Identifying the Just Suspended Condition

In Section 2.4.1, the *just suspended* condition was identified as the most consistently identifiable degree of solids suspension in terms of the critical impeller speed N_{js}. This consistency, together with the important role that the just suspended condition has been found to play in many multiphase processes, are amongst the attractions of using N_{js} for solids suspension correlation purposes. A number of *criteria* (or pointers) that can be used to identify the just suspended condition, were developed from the experimental methods discussed in Section 2.4.2, and will be reviewed in this section.

2.4.3.1 The 1s criterion

Zwietering (1958) proposed the 1s criterion for identifying the just suspended condition as follows:

'*It was difficult to determine this point (complete suspension) exactly and objectively, because even at high stirrer speeds streaks of solid particles are always visible at the bottom. At the border between incomplete and complete suspension there are particles, which settle temporarily at the bottom and remain for a short time in a fixed position relative to each other. When such a small pile remained at rest longer than 1 or 2 seconds before being broken up the suspension was judged incomplete. When* ***no deposits remained on the bottom for more than 1 s,*** *the suspension was considered complete.*' - Zwietering (1958)

Using this criterion the critical impeller speed can be determined with a very good reproducibility of as little as 2-3% as found by Zwietering (1958) and several others who used the 1s criterion. It is difficult to apply the 1s time period exactly in practice, and refer more to a short time period in the region of 1s. Applying a 'constant' time is important to make the 1s criterion more objective and the results of different workers more comparable. The 1s criterion is the most commonly used criterion to identify the critical impeller speed.

2.4.3.2 *100% Suspension Criterion*

A *'100% suspension' criterion* has also been suggested by Staudinger and Moser (1976), where no solids are allowed to come to rest on the vessel bottom, not even for a short while. This criterion was claimed to identify the just suspended condition with a reproducibility of ±1%. However the 100% suspension criterion has not been used as widely as the 1s criterion.

2.4.3.3 *Unsuspended Layer of Solids Criterion*

This criterion measures a height, radius or volume characteristic of the unsuspended layer on the bottom of the tank with increasing impeller speed and in this way identifies the just suspended condition (N_{js}). Rieger and Ditl (1994) preferred this method to the 1s criterion, due to it depending on a number of measurements and not just one slightly subjective determination of solids suspension conditions on the base. Figure 2.15 (a) shows how the volume of the unsuspended layer ('fillet volume') changes with relative impeller speed. This method may be more accurate than the 1s criterion, but needs a 'number of measurements' and is thus not as quick as the 1s criterion.

2.4.3.4 *Radiation Count Rate Criterion*

The count rates from labelled particles on the bottom of the tank have been found to decrease with increasing impeller speed as the particles are suspended off the bottom of the tank. Beyond a certain point, the rate stops to decrease much further with increasing impeller speed. Rewatkar, Raghava Rao and Joshi (1991) took this point as the critical impeller speed for solids suspension and found the just suspended speed obtained using this criteria to agree very well within 5% to the visually observed 1s criterion critical impeller speed.

2.4.3.5 *Rate of Mass Transfer Criterion*

The rate of solid-liquid mass transfer increases with increasing impeller speed as solids are lifted from the bottom and contacted with the liquid. At a certain impeller speed, the slope of the increase drops off. This is taken as the critical impeller speed and in most

solid-liquid mass transfer processes (e.g. dissolution, ion exchange, etc.) it is the most efficient to design a stirred vessel for this condition.

2.4.3.6 90% Suspension Height Criterion

This criterion attempts to relate the suspension height h_s of the solids in the vessel to the just suspended condition. It was observed [Hirsekorn and Miller (1953); Weisman and Efferding (1960); Einenkel (1980)] that the condition where the solid particles reached 90% of the liquid height (Z), also coincided with the just suspended condition of complete off-bottom suspension N_{js}. Most of these workers used a slurry height (Z) equal to the tank diameter (T) and the 90% height criterion can thus also be expressed in terms of relative height ($h_s/T = 0.90$). However, Chapman *et al.* (1983c) reported that an h_s criterion was not useful, especially not in three-phase work. Nienow (1992) also observed that the 90% suspension height criterion results differed from those obtained by visually observing the tank bottom, especially for particles less than 300 μm. The results of Hicks, Myers and Bakker (1997) show h_s to increase with impeller speed, but that the value at N_{js} is not constant for different conditions (cf. Figure 2.15 (b)).

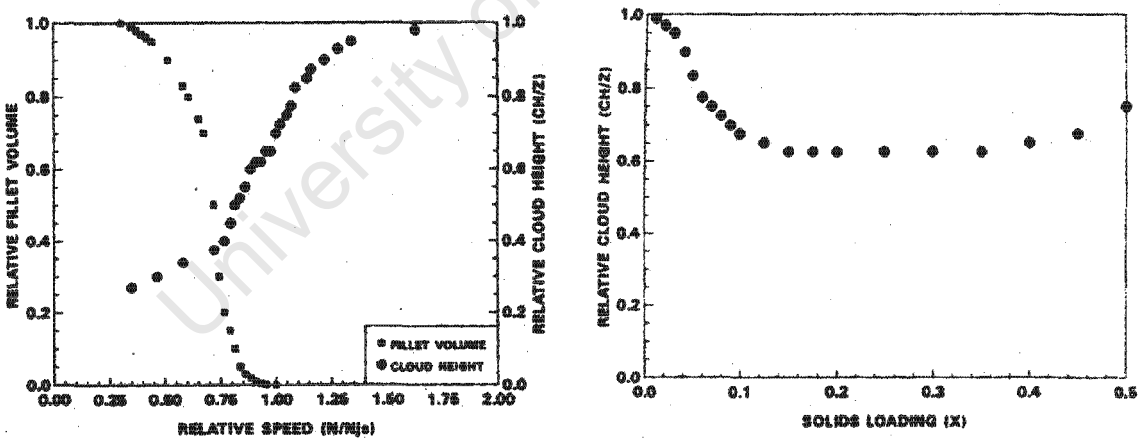

(a) (b)

Figure 2.15 Suspension height measurements (CH) at (a) various N/N_{js}, and (b) various X with $N = N_{js}$ [Hicks, Myers and Bakker (1997)]

[(a): acrylic solid, (b): ion exchange resin, HE-3 impeller, D/T=0.35, C/T = 0.25 and Z/T = 1.0]

2.4.3.7 Solids Concentration above Base Criterion

This criterion relates the variation in measured solids concentrations above the base with increasing impeller speed to the just suspended condition. The *concentration above the base* criterion considers the point where the local solids concentration at a point above the base shows a maximum [Bourne and Sharma (1974)] or a discontinuity [Musil (1976)] with increasing impeller speed. The point where the discontinuity occurs is taken as the critical impeller speed (cf. Figure 2.16). Chapman *et al.* (1983a) also used this alternative criterion (and perhaps less subjective criterion) for determining N_{js}. The change in the local solids concentration above the base with increasing N can be explained as follows. Increasing the impeller speed from low values, the particles will gradually be suspended off the base causing the concentration to increase. Eventually a point is however reached where the source of particles from the base is practically exhausted, while the upper regions of the dispersion still have very low particle hold-ups. Therefore, further increases in impeller speed will homogenise the suspension and thereby reduce the local solids concentration near the base. However, Ayazi Shamlou and Koutsakos (1989) found the trend less obvious at high X ($X \geq 6$ wt. %) and that it often gives a lower N_{js} from that obtained from visual observation of the base of the tank.

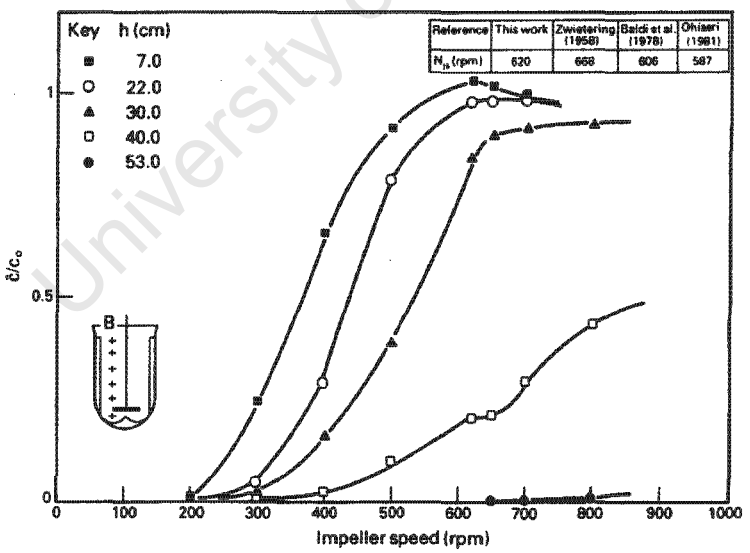

Figure 2.16 Solids concentration vs impeller speed for different sample heights [Ayazi Shamlou and Koutsakos (1989)]

($d_p = 390$ μm, $\rho_S = 2900$ kg/m^3, $\rho_L = 1000$ kg/m^3, C = 13 cm, D = 10 cm, Z = H = 65 cm, $X_{act} = C_0 = 3$ wt%)

2.4.3.8 Variation in Vertical Solids Concentrations Criterion

This criterion determines the variation in vertical solids concentrations with increasing impeller speed. With increasing impeller speed both the extent of solids distribution (h_s) increases as well as the homogeneity of solids distribution increases. It is thus expected that the variation in solids concentrations (expressed as variance σ^2, or relative standard deviation *RSD*) will decrease with increased impeller speed until a homogeneous suspension is reached as the variance in axial concentrations through the tank approaches zero. Published work that considered the variation in axial concentrations (*RSD*) suggests a decreasing trend of *RSD* vs. *N*, but that the value of *RSD* at the just suspended condition (RSD_{js}) will be system specific and not easy to generalise [Einenkel (1980); Bohnet and Niesmak (1980); Barresi and Baldi (1987a); Barresi and Baldi (1987b)]. Concentration profiles will be considered further in Section 2.4.6.

2.4.3.9 Mixing Time vs. Impeller Speed Criterion

This criterion for the measurement of N_{js}, makes use of the variation of mixing times θ_{mix} vs. impeller speed N and is described in detail by Rewatkar, Raghava Rao and Joshi (1991). In addition to identifying the just suspended condition, it is also claimed that θ_{mix} vs. impeller speed N can be used to identify the complete gas dispersion condition N_{cd} in both two and three-phase conditions.

2.4.3.10 Power Number vs. Impeller Speed Criterion

This criterion for the measurement of N_{js}, makes use of the variation of power number N_P vs. impeller speed N and is described in detail by Rewatkar, Raghava Rao and Joshi (1991). At low impeller speeds in solid-liquid agitation, the power number is decreased by the streamlining effects of solid fillets on the base. At higher speeds more solids are suspended and the effective density around the impeller increases, causing the power number to increase, until the effective density around the impeller starts to decrease again above the just suspended condition. The critical impeller speed can thus be determined graphically from these plots. The three-phase plots are furthermore also influenced by the effect of gas on impeller power draw and in addition to the critical impeller speed, can the point of complete

gas dispersion also be identified from these plots [Chapman *et al.* (1983c); Rewatkar, Raghava Rao and Joshi (1991)].

2.4.4 Critical Impeller Speed Correlations (Two-Phase) [1]

It was mentioned in Section 2.4.1 that investigations into the critical impeller speed (N_{js}) have completely dominated all work on solids suspension in stirred tanks. Zwietering (1958), who used visual observation (cf. Section 2.4.2), and defined the 1s criterion for identifying the just suspended condition consistently (cf. Section 2.4.3), completed one of the most comprehensive and influential studies on solids suspension in stirred tanks to date. For this reason, the *Zwietering correlation* will be reviewed in more detail in Section 2.4.4.1. After Zwietering, many others have tested the Zwietering equation and contributed their own findings. An overview of just suspended correlations will be given in Section 2.4.4.2. Most of the critical impeller speed correlations have been developed from semi-empirical to empirical observations. Some attempts have however been made to use more theoretical approaches to derive the just suspended correlation. These theoretical correlations have had limited success to date and will thus only be reviewed very briefly in Section 2.4.4.4. As will be shown in this section, most studies on solids suspension have been done in two-phase stirred systems. However, due to the importance of three-phase stirred processes, attempts have been made to extent the N_{js} correlation to three-phase systems, which will be considered in the next section (cf. 2.4.5).

2.4.4.1 The Zwietering Correlation [Zwietering (1958)]

The most influential work in solids suspension to date is also one of the first published on the critical impeller speed for solids suspension. Zwietering (1958) did a very extensive study, involving well over a thousand tests done on a selection of laboratory scale mixing vessels agitated by five types of stirrers at different sizes. He varied all the variables affecting solid suspension in a conventional S-L two-phase system, while measuring their effect on the impeller speed where solids are just completely suspended off the bottom (i.e. critical impeller speed). Zwietering used visual observation of the base (cf. Section 2.4.2.1.1)

[1] In this section N_{js} is used throughout to indicate the critical impeller speed. However, N_{jsu}, could also be used to indicate two-phase or 'ungassed' conditions and will be used further on in this work.

to determine the solids suspension conditions on the base of the tank. In order to make the determination of the point of complete solids suspension more objective, he introduced the 1s criterion (cf. Section 2.4.3.1).

Workers before Zwietering provided very limited quantitative information regarding the stirring conditions required for complete suspension. One of the first published works on solids suspension was done by White and Summerford (1933), who studied the distribution of sand (concentration profile) in a single unbaffled tank. Hixson *et al.* (1942) then introduced an intensity of agitation measure by considering the rate of dissolution of solids. While Hirsekorn and Miller (1953) judged the agitation as successful (or complete) when the agitator was able to suspend all the solids from their initial position of rest on the bottom of the tank. They labelled this condition as '*complete suspension.*' Hirsekorn and Miller, however, worked only in the laminar region at low Reynolds numbers ($N_{Re} < 12$) and only produced scale-up rules and no critical impeller speed correlation. Kneule (1956) also stressed the importance of the 'just suspended' or 'complete suspension' condition, in his work on the rate of solution of crystals. Furthermore, Kneule was one of the first to produce a relation indicating the required *power per unit volume* to reach and maintain this complete suspension condition. Kneule recommended equal power per unit volume for scale-up of solids suspension and related this required power input to some of the properties of the liquid and the solid. Zwietering's results however showed that the power per unit volume can be reduced during scale-up of solids suspension ($P/V \alpha D^{-0.55}$).

As already mentioned, Zwietering (1958) determined the minimum impeller speed for complete suspension in a great number of cases. This was possible by the use of visual observation, not requiring any samples to be taken and processed. He used transparent tanks, made of glass or Perspex, fitted with four baffles (width = $0.1T$) along the walls, and ranging in size between $T = 0.154$ and 0.60 m ($V_T = 2.9$ to 170 l). Zwietering and most others used cylindrical vessels filled in general to a height equal to the vessel diameter ($Z = T$). It has been found that the liquid height in the vessel (Z) does not have a significant influence on N_{js}. Five types of stirrers were used in his study, being, two paddle stirrers, a six blade disc turbine (Rushton), a vaned disc impeller and a flat blade propeller as shown in Figure 2.17. Silica sand ($\rho_S = 2600$ kg/m^3) and sodium chloride ($\rho_S = 2160$ kg/m^3) were used as solids; and as liquids, water, acetone, carbon tetrachloride, potassium carbonate solution and oil. A full list of the variables is given in Table 2.5.

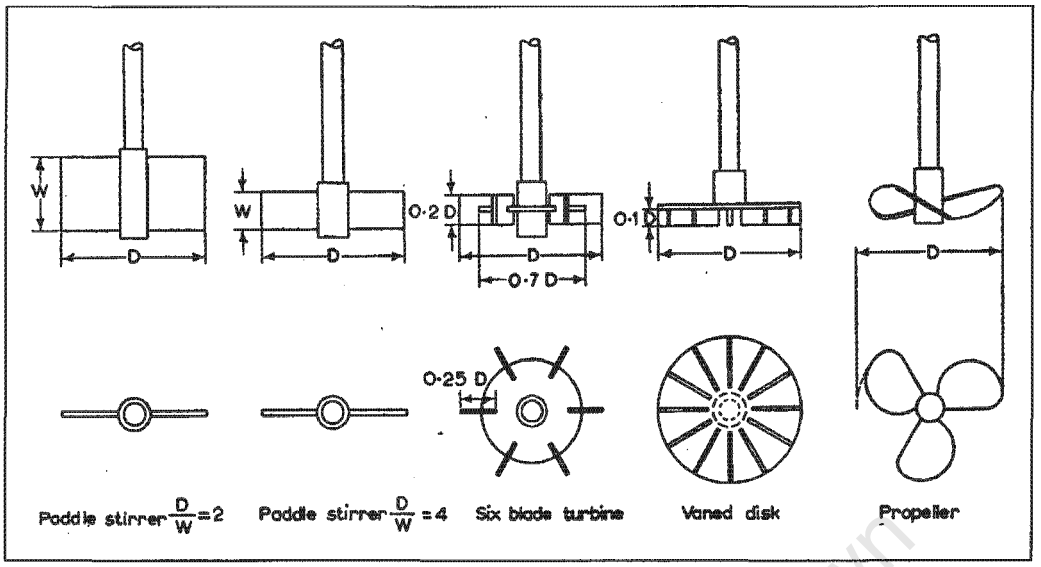

Figure 2.17 Stirrers used by Zwietering

(Paddle stirrer D/W=2: $N_P = 5.9$; Paddle stirrer D/W=4: $N_P = 2.5$; 6DT: $N_P = 6.2$; Vaned disk: $N_P = 4.6$; Propeller: $N_P = 0.5$)

Table 2.5 Variables and Ranges Used by Zwietering

Variables	Symbol	Range	Unit
Impeller speed	N	(not given)	s^{-1}
Tank diameter	T	0.154 to 0.60	m
Impeller diameter	D	0.06 to 0.22 (1/6 T to 2/3 T)	m
Impeller clearance	C	1/2 to 1/7 of T (paddle 1/10, 1/20)	m
Particle size	d_p	125 to 850 (125-150; 150-250; 250-350; 710-850)	µm
Solids to Liquid Mass Ratio (Solids Mass Fraction)*	B (X)	0.005 to 0.20 (0.005 to 0.167)	- (-)
Solids density	ρ_S	2160 (NaCl) and 2600 (silica sand)	kg/m^3
Liquid density	ρ_L	790 (acetone) to 1600 (CCl_4)	kg/m^3
Liquid viscosity (kinematic) (Dynamic liquid viscosity)*	v (μ)	$0.39x10^{-6}$ to $11.1x10^{-6}$ (0.31 (acetone) to 9.3 (oil))	m^2/s (mPa.s)
Acceleration of gravity	g	9.81	m/s^2

(Liquids used - water: $\rho_L = 1000kg/m^3$, $\mu_L = 1.0cP$; acetone: $\rho_L = 790kg/m^3$, $\mu_L = 0.31cP$; carbon tetrachloride: $\rho_L = 1600kg/m^3$, $\mu_L = 1cP$; potassium carbonate solution: $\rho_L = 1440kg/m^3$, $\mu_L = 5cP$; oil: $\rho_L = 840kg/m^3$, $\mu_L = 9.3cP$)

From the 10 variables (in three independent units), Zwietering could form a set of seven dimensionless numbers (cf. 2.3.1).

Geometric ratios : T/D, T/C, D/d_p

Reynolds number (N_{Re}) : $N.D^2.v^{-1}$

Froude number (N_{Fr}) : $N^2.D.g^{-1}$

Density ratio : $\rho_S.\ \rho_L^{-1}$

Solids to liquid ratio (B) : $m_S.m_L^{-1}$

Zwietering (1958) however noted that the disadvantage of using these dimensionless numbers is that most of them can't be varied independently, thus complicating the analysis of the experimental data. For example, impeller speed N is contained in two of the dimensionless groups and impeller diameter D in four of them. Zwietering thus decided to evaluate the effect of each variable on N_{js} independently. The silica sand in water tests (over a thousand tests) were considered separately at first to simplify the analyses. In these tests, the first six parameters in Table 2.5 could be varied. From graphical analyses (log-log plots) of the data, Zwietering found that N_{js} could well be expressed as a product function of the variables T, D, d_p and X, but not of C.

$$N_{js} = K_1 T^a D^b d_p{}^c B^e \quad ; \text{for constant } T/C$$

..... Equation 2-30

Next, Zwietering tested the effect of solid and liquid density and liquid viscosity by adding the tests done with NaCl solids, and the other liquids showed in Table 2.5.

$$N_{js} \propto \nu^{0.10}\left(\frac{\rho_S - \rho_L}{\rho_L}\right)^{0.45}$$

..... Equation 2-31

From the graphical analyses of all his data and making use of dimensional consistency checks Zwietering arrived at the following product function for N_{js}.

$$N_{js} = KT^a D^b d_p{}^{0.20} B^{0.13} \nu^{0.10} g^{0.45}\left(\frac{\rho_S - \rho_L}{\rho_L}\right)^{0.45} \quad \text{for constant T/C}$$

..... Equation 2-32

The effect of impeller clearance (*T/C*) could not be included as another product factor into the equation. Also the exponents of the other two geometrical variables *T* and *D* ('*a*' and '*b*') depended on the type of stirrer. However, their sum was found to vary around an average of minus 0.85 (varied between -0.78 and -0.94). *T* and *D* are also not normally varied independently. One can be taken as an indicator of scale (*T* or *D*), whilst a ratio of the two indicates relative impeller diameter (*D/T* or *T/D*). Zwietering opted to use *D* as an indicator of scale and *T/D* to indicate relative impeller diameter. The equation can thus be rewritten by multiplying Equation 2-32 with (D^a/D^a), as shown in Equation 2-33.

$$N_{js} = KD^{-0.85}\left(\frac{T}{D}\right)^{a} d_p^{0.20} B^{0.13} \nu^{0.10} g^{0.45}\left(\frac{\rho_S - \rho_L}{\rho_L}\right)^{0.45} \quad \text{for constant T/C}$$

Where: for propellers $a = 0.82$; for paddles $a = 1.30$; for disc turbines $a = 1.50$

.....Equation 2-33

However, *T* is often taken as the indicator of scale and *D/T* as the indicator of relative impeller diameter. This form can also be obtained from Equation 2-32, by multiplying by (T^b/T^b), leading to Equation 2-34. The exponent on *D/T*, *b*, is determined from the '*a*' values given by Zwietering, and knowing that $a + b$ was found to be equal to -0.85.

$$N_{js} = KT^{-0.85}\left(\frac{D}{T}\right)^{b} d_p^{0.20} B^{0.13} \nu^{0.10} g^{0.45}\left(\frac{\rho_S - \rho_L}{\rho_L}\right)^{0.45} \quad \text{for constant C/T}$$

Where: for propellers $b = -1.67$; for paddles $b = -2.15$; for disc turbines $b = -2.35$

.....Equation 2-34

Equation 2-33 (or Equation 2-34) is very useful in that it shows the effect of all variables (except *C/T*) on N_{js}. However, the equation constant K was not constant but depended on impeller type, relative impeller diameter (*T/D*), and relative impeller clearance (*T/C*). Zwietering thus decided to combine K, *T/D* and *T/C* into an *S* parameter, which he then determined for each type of impeller and displayed graphically. Two examples are given in Figure 2.18.

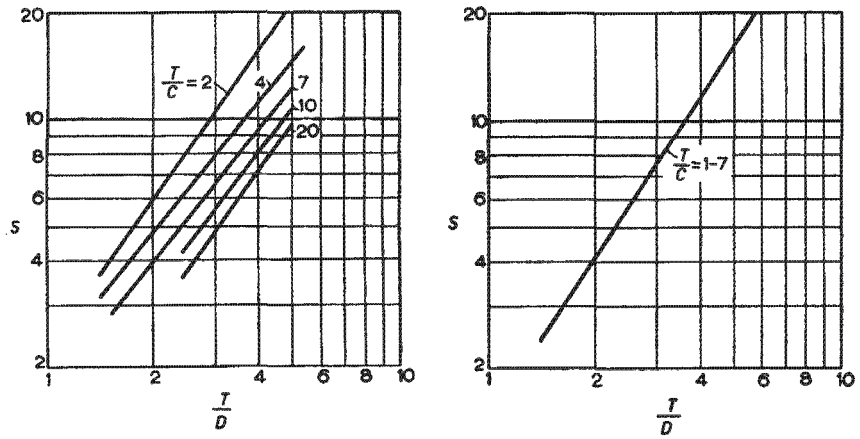

(a) paddle impeller (FT) (b) disc turbine (DT)

Figure 2.18 The dependance of the *S* parameter in Zwietering's equation on impeller type, impeller diameter (*T/D*) and impeller clearance (*T/C*)

Note: Experimental data points rarely deviated more than 10% from these lines. (a) – Paddle impeller (W/D = 1/4, $N_P = 2.5$); (b) - Disc turbine (6 bladed Rushton, $N_P = 6.2$)

This leads to the *S* parameter form of the Zwietering equation, which is most commonly used.

$$N_{js} = S d_p^{0.20} B^{0.13} \nu^{0.10} g^{0.45} \left(\frac{\rho_S - \rho_L}{\rho_L} \right)^{0.45} D^{-0.85}; \text{ Where, S = f (impeller type, T/D, T/C)} \quad \text{(a)}$$

Or *T* as the scaling parameter,

$$N_{js} = S^* d_p^{0.20} B^{0.13} \nu^{0.10} g^{0.45} \left(\frac{\rho_S - \rho_L}{\rho_L} \right)^{0.45} T^{-0.85}; \text{ Where, } S^* \text{ = f (impeller type, D/T, C/T)} \quad \text{(b)}$$

..... Equation 2-35

This *S* parameter form of the Zwietering equation thus combines all the geometric variables except for scale into one parameter (*S*). This indicates that at constant geometrical design (constant impeller type, *D/T* and *C/T*), N_{js} is only affected by the solid-liquid properties and the scale indicator (e.g. *D* or *T*). Thus, once the value of *S* has been determined for the type of impeller to be used at the relative size (*D/T*) and relative clearance (*C/T*), Equation 2-35 can be used to determine the critical impeller speed for changing liquid and solid properties as well as scale-up.

It can be seen from Figure 2.18 that the *S* parameter (and thus also N_{js}) decreases with increasing impeller diameter (decreasing *T/D*) and decreasing impeller clearance (increasing *T/C*). As per Figure 2.18 (b), Zwietering found that *S* (and thus N_{js}) for disc turbines are

independent of *C/T*. This finding was unexpected, due to all the other impellers showing N_{js} to decrease with decreasing C/T, and has since been disproved [Nienow (1968); Chapman *et al.* (1983a)]. Zwietering (1958)'s extensive study thus provided a complete correlation for critical impeller speed N_{js}, using various liquids and solid particles stirred by a variety of impeller types at various impeller sizes and clearances, whilst also allowing for scale-up. This very complete correlation has since become a yardstick against which most other work on solids suspension is measured.

2.4.4.2 Overview of Just Suspended Correlations for Two-Phase Systems

After Zwietering (1958), many others have also developed N_{js} correlations based on experimental observations. A summary of most of these two-phase critical impeller speed studies are given in Table 2.6.

Table 2.6 Critical Impeller Speed Correlations in Two-Phase Systems [#]

Reference	Exponents of Variables in the Zwietering-type Product Function $N_{js} = KT^a D^b d_p^{0.20} B^{0.13} (\Delta\rho/\rho_L)^{0.45} \nu^{0.1}$ *					
	d_p	B**	$\Delta\rho/\rho_L$	ν_L	$(D/T)^{b*}$	T^{a+b} (scale)*
Zwietering (1958)	0.20	0.13	0.45	0.1	DT: -2.35, FT: -2.15, Pr: -1.67	-0.85
Weisman and Efferding (1960)	u_T +	0.17	u_T +	u_T +	-1.67 (FT)	
Kolar (1967a)	u_T +	0.10	u_T +	u_T +	-2.24 (Pr, PT-D)	
Kneule and Weinspach (1967)	0-0.2	0.25	0.5	0-0.1	-1.7 (Pr)	
Narayanan *et al.* (1968)	0.5	0.22	0.5		-2.0 (DT)	
Nienow (1968)	0.21	0.12	0.43		-2.25 (DT)	
Gates, Morton and Fondy (1976)	0.13-0.2		0.13-0.2	0.1	-2.4	
Baldi, Conti and Alaria (1978)	0.14	0.125	0.4	0.17	-1.9 (DT)	
Herringe (1979)	0.3	0.18	0.4			-0.7 (PT-D)
Bohnet and Niesmak (1980)	0.14	0.125	0.4	0.08	-1.9 (DT)	
Einenkel (1980)	0.17-0.67	0.3	0.5		-1.7 (Pr)	

Reference	Exponents of Variables in the Zwietering-type Product Function $N_{js} = KT^a D^b d_p^{0.20} B^{0.13} (\Delta\rho/\rho_L)^{0.45} \nu^{0.1}$ *					
	d_p	B**	$\Delta\rho/\rho_L$	ν_L	$(D/T)^{b}$ *	T^{a+b} (scale)*
Chapman *et al.* (1983a)	0.15	0.12	0.4	0	DT: -2.45, PT-D: -1.67, Pr: -1.15	-0.76 (DT, PT-D, PT-U)
Buurman, Resoort and Plaschkes (1986)						-0.67 (PT-D)
Chudacek (1986)	0.52	0.08				-0.58 (PT-D)
Raghava Rao, Rewatkar and Joshi (1988)	0.11 (PT-D, PT-U) 0.15 (DT)	0.1 (PT-D, PT-U) 0.125 (DT)			-1.15 (PT-D)	
Rewatkar, Raghava Rao and Joshi (1989)	u_T +	u_T +	u_T +	u_T +	-1.15 (PT-D)	
Frijlink, Bakker and Smith (1990)						DT: -0.85, PT-D: -0.70, PT-U: -0.60
Armenante and Uehara Nagamine (1998)	0.22-0.24	0.11-0.13	0.50-0.53	0.09	DT: -2.25, FT: -2.07, PT: -1.66, HE: -1.62	-0.82 (DT, FT, PT) -0.78 (HE)
Sharma and Shaikh (2003)					-2.0 (PT)	-0.85 (PT)

NOTES TO Table 2.6

- Largely taken from Rewatkar and Joshi (1991); Summaries of correlations are also given in Bohnet and Niesmak (1980) and Chapman *et al.* (1983a); Theoretical correlations (not given here) summarised in Rieger and Ditl (1994). Experimental ranges used in these works are summarised by Chapman *et al.* (1983a), and Rewatkar and Joshi (1991).

* - Zwietering (1958)'s equation (product function as in Equation 2-32), showing T^a and D^b separately. In the table, T is shown as the variable indicating scale and D/T indicates relative impeller diameter (refer also Equation 2-33 and Equation 2-34).

** - The concentration of solids is expressed here as the mass ratio of solids to liquid, $B = m_S/m_L$. However, the mass concentration, $X = m_S/(m_S+m_L)$ is also commonly used to express solids concentration in stirred tanks. For small values of $X \leq \sim 0.05$, $B \propto X$. However, for X in the range of 0.05 to 0.50 the relation can be approximated as $B \propto X^{1.27}$. Thus to obtain the exponent for X in the latter range, the exponents on B should be multiplied by 1.27 (cf. Section 2.4.4.3.2).

+ - Terminal settling velocity u_T were used in these studies to describe the effect of these variables.

(DT = disc turbine; FT = flat-blade turbine; Pr = propeller impeller; PT-D = pitched turbine downflow; PT-U = pitched turbine upflow)

The ***variable ranges*** used by these investigators (cf. Table 2.6) are summarised in Rewatkar and Joshi (1991), and Chapman *et al.* (1983a), and will not be repeated here. Some studies can however be *criticised* for being done in very small vessels (T << 0.5m), or at very low solids concentrations (X << 10%). However, the following studies included $T \geq$ **0.5m**:

Zwietering (1958), Herringe (1979), Einenkel (1980), Chapman *et al.* (1983a), Buurman, Resoort and Plaschkes (1986), Chudacek (1986), Raghava Rao, Rewatkar and Joshi (1988), Frijlink, Bakker and Smith (1990), Armenante and Uehara Nagamine (1998), and Sharma and Shaikh (2003). Whilst, the following studies included $X \geq 10\%$: Zwietering (1958), Weisman and Efferding (1960), Kolar (1967a), Herringe (1979), Chapman *et al.* (1983a), Buurman, Resoort and Plaschkes (1986), Chudacek (1986), Raghava Rao, Rewatkar and Joshi (1988), and Frijlink, Bakker and Smith (1990).

Nienow (1992) explained the differences in N_{js} findings (cf. Table 2.6) by referring to, (a) the limited range of solids available in suitable form and quantity for study on larger scale, (b) different criteria used to identify N_{js}, and (c) the experimental determination of N_{js}, which may be imprecise. These differences in complete suspension results are compounded when power (P_{js}) is used as the measure for complete suspension, due to the dependence of power numbers on factors such as impeller geometry and in certain cases scale. Rewatkar and Joshi (1991) compared the predictions of a number of the correlations given in Table 2.6, against the Zwietering (1958) correlation ('experimental') as shown in Figure 2.19. It follows that, with the exception of the more theoretical correlation of Baldi, Conti and Alaria (1978), the other predictions form a scattogram around Zwietering's correlation. It can therefore be concluded that the Zwietering's equation is the best to use for design application, but for specific application, it will have to be tested and fine-tuned.

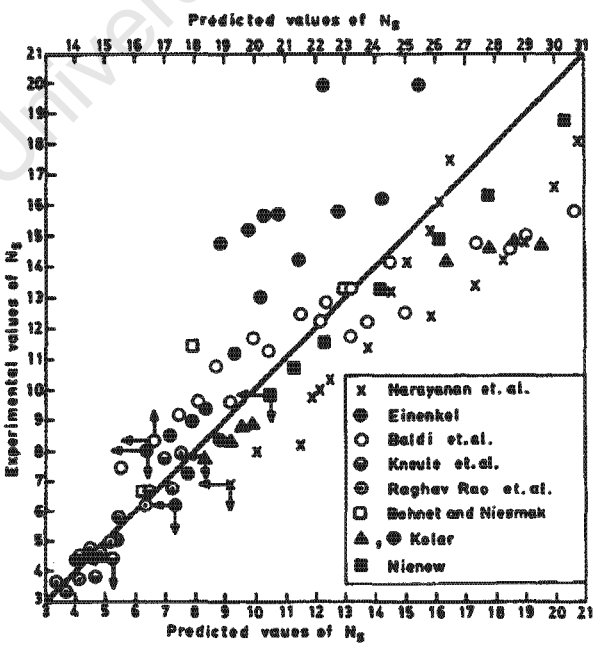

Figure 2.19 Comparison of predicted N_{js} values from some correlations with that of Zwietering's correlation ('experimental') [Rewatkar and Joshi (1991)]

2.4.4.3 Variables Affecting Solids Suspension (N_{js})

The variables given in Table 2.6, which affect N_{js}, will be briefly overviewed here.

2.4.4.3.1 Particle size, d_p

As with all the variables in the N_{js} correlation (product function), the relative effect of variations in particle size d_p on N_{js} can be determined from log-log plots as shown in Figure 2.20 as an example. As already indicated in Table 2.6, Zwietering (1958) found $N_{js} \propto d_p^{0.20}$, whilst the proportionality exponent of the other findings varied over a fairly large range of between 0.1 and 0.5.

$N_{js} \propto d_p^{0.20}$; Zwietering (1958)

..... Equation 2-36

The large variation in findings on the effect of particle size might be related to the difficulty of obtaining discrete solids size fractions and determining average particle sizes from particle size distributions. The widest range of particle sizes was studied by Herringe (1979), being 19 µm to 5000 µm, whilst most other studies included the range of 100 to 500 µm.

An important factor related to the effect of particle size is how to deal with *size distributions*. Most work on solids suspension has been done using discrete size fractions, whilst the solids encountered in industrial stirred tanks normally vary over distributions of particle sizes. Baldi, Conti and Alaria (1978) used mono-modal and bi-modal particle size fractions varying between 50 and 545 µm (X = 0.2 to 2%). They found that for N_{js} calculations, the bi-modal size fractions behaved like mono-modal size fractions of a size equal to the mass averaged size. Chapman *et al.* (1983a) investigated multi-modal size distributions further, using tri-modal and even quadri-modal size distributions at sizes varying between 92.5 and 2650 µm and confirmed Baldi's finding that these size distributions can be characterised by the mass mean diameter of the distribution (d_{50}). These results are also included in Figure 2.20 where points 'A' and 'B' shows the critical impeller speeds for a tri-modal and a quadri-modal size distribution of solids against their mass mean diameters. It can be seen that these points lie on the same line as that given by discrete size distributions. This would suggest the use of a d_{50} value when working with size distributions. However, these studies did not include very fine

particle sizes ($d_p \leq 50$ µm), where at some point solids suspension will not be a problem. Therefore, for particle size distributions in the range of 10 to 300 µm it is expected that a coarser particle size will be characteristic of the distribution, e.g. d_{80} or d_{90}.

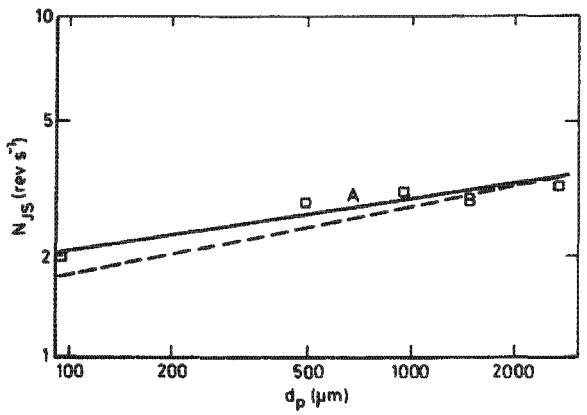

Figure 2.20 Log-log plot of N_{js} vs. d_p Chapman *et al.* (1983a)

Note: broken line = Zwietering (1958): $N_{js} \propto d_p^{0.20}$; solid line = Chapman *et al.* (1983a): $N_{js} \propto d_p^{0.15}$; Points 'A' and 'B' indicate the mass mean diameters of a tri-modal and quadri-modal size distribution; (DT, D/T=1/2, $T_{0.56}$, B=1%, $\Delta\rho$=1900kg.m^{-3})

2.4.4.3.2 Solids Concentration, B or X

Zwietering (1958) found the exponent on B to be 0.13, whilst the other findings varied mostly between 0.10 and 0.25 (cf. Table 2.6).

$N_{js} \propto B^{0.13}$; Zwietering (1958)

.....Equation 2-37

There seems to be better agreement amongst different workers on the effect of solids concentration, compared to particle size. This can partly be attributed to the accuracy of measuring and controlling the solids concentration during testwork, whilst there is always some uncertainty about the average particle size used. The range of solids to liquid mass ratios (B), varied from very low to medium solids concentrations ($0.001<B<0.50$ or $0.001<X<0.25$) [Rewatkar and Joshi (1991)].

When considering the effect of solids concentration it is important to note how the solids concentration is expressed. Most of the workers in Table 2.6 used the solids to liquid mass

ratio, $B = m_S/m_L$. However a common way of expressing solids concentration is to use the solids mass concentration, $X = m_S/(m_S+m_L)$. B vs. X is shown in Figure 2.21.

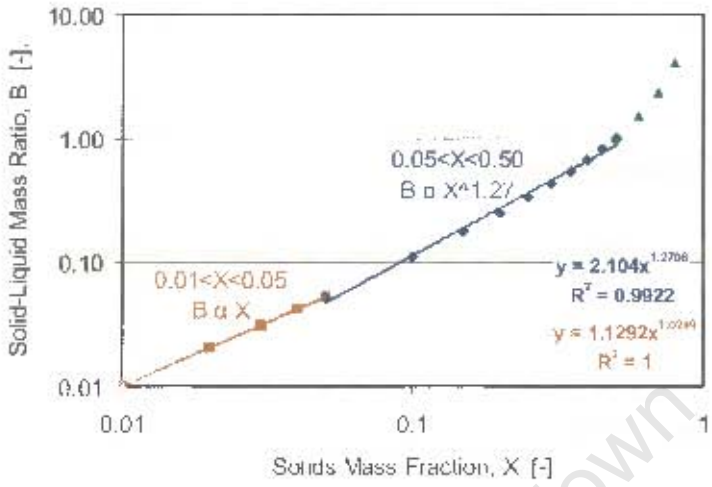

Figure 2.21 Solids-to-liquid mass ratio, B as a function of solids concentration, X

It follows from Figure 2.21 that if working at low solids concentrations up to ~5 wt%, the exponent values quoted in Table 2.6 can be used on X. However, if working at higher $X \sim 5$ to 50 wt%, the exponent on X, will be higher than the exponent on B.

$$N_{js} \propto B^{0.13} \propto \left(X^{1.27}\right)^{0.13} \propto X^{0.17}; \text{ for } 5\% \leq X \leq 50\%; \text{ Zwietering (1958)}$$

..... Equation 2-38

2.4.4.3.3 Solid-Liquid Density Difference, $\Delta\rho/\rho_L$

It follows from Table 2.6 that the relative solid-liquid density difference, $(\rho_S-\rho_L)/\rho_L$ or $\Delta\rho/\rho_L$, has a relatively large and consistent influence on the critical impeller speed. Zwietering (1958) found the exponent to be 0.45, whilst the findings of others varied mostly between 0.40 and 0.50, with only one worker [Gates, Morton and Fondy (1976)] finding the effect to be less than 0.40. From a mechanistic point of view, the large effect of solid-liquid density difference is to be expected. From a force balance (cf. Figure 2.11), it follows that density difference is the real *driving force behind phase separation*. The other solid-liquid variables merely affect the drag force and thus the rate at which this separation or sedimentation occurs.

$$N_{js} \propto \left(\frac{\rho_S - \rho_L}{\rho_L} \right)^{0.45}$$; Zwietering (1958)

..... Equation 2-39

2.4.4.3.4 Liquid kinematic viscosity, ν_L

Zwietering (1958) found the effect of liquid kinematic viscosity ν_L to be as follows.

$N_{js} \propto \nu^{0.10}$; Zwietering (1958)

..... Equation 2-40

Only some of the authors listed in Table 2.6 studied the effect of liquid viscosity and their values of the exponent on ν_L varied mostly from zero to 0.10. A number found the exponent to be zero (ν_L has no effect on N_{js}), whilst only Baldi, Conti and Alaria (1978), working with very low X ($X \leq 2\%$), found the effect to be stronger than 0.10. The effect of ν_L thus seems to be relatively small for most systems. However, for some systems the viscosity can vary over a large range (more than ten-fold), and in these cases the influence of viscosity might be important, despite the small proportionality exponent. These studies considered the liquid phase viscosity on the suspension of solids. The fluid (slurry) viscosity may however also be influenced by the presence of solids particles in the fluid as shown in Figure 2.22. It follows from Figure 2.22 that for most slurries, the slurry viscosity is only influenced significantly (more than three to four times that of water) once the solids volume concentration φ_S increases over ~25 vol%, except for very fine particle size distributions with d_{50} values of 30μm and smaller. For a slurry containing solids with an SG of three, a solids concentration of 25 vol% ($\varphi_S = 25\%$) translates to, 50 wt% solids ($X = 50\%$), or a slurry density of 1500 kg/m^3 ($\rho_{SL} \approx$ 1500 kg/m^3). Many slurry mixing systems operate below $X = 50\%$, and therefore if not containing large quantities of extremely fine solids ($d_{50} \leq \sim$ 30μm), the effect of slurry viscosity on N_{js} seems to be small.

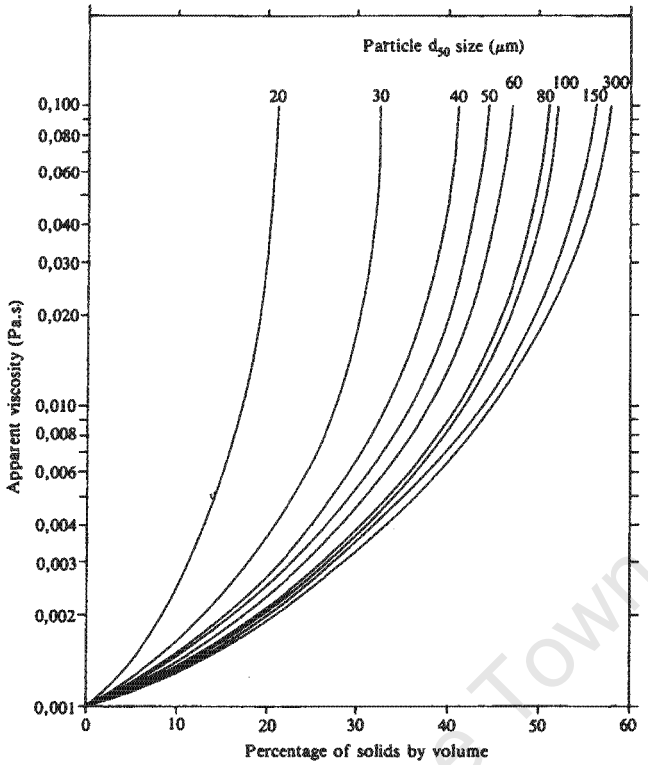

Figure 2.22 The effect of solids *volume* concentration on slurry apparent viscosity for different d_{50} particle sizes [Thomas (1965) as given in Stanley (1987)]

2.4.4.3.5 Relative impeller diameter, D/T

As already discussed in *2.4.4.1* the effect of relative impeller diameter depends on the type of impeller used. Zwietering (1958) found exponent values of minus 2.35 for disc turbines (*DT's*), minus 2.15 for flat-blade turbines (*FT's*) and minus 1.67 for propellers. Seeing that the current study focuses on radial turbine type impellers (as used in flotation cells), the propeller findings will not be discussed here.

$$N_{js} \propto \left(\frac{D}{T}\right)^{-2.35} \quad \text{for disc turbines ; Zwietering (1958)} \qquad \text{(a)}$$

$$N_{js} \propto \left(\frac{D}{T}\right)^{-2.15} \quad \text{for flat-blade turbines; Zwietering (1958)} \qquad \text{(b)}$$

..... Equation 2-41

The values of the proportionality exponent that others found for the influence of *D/T* for radial impellers varied consistently between minus 1.90 to minus 2.45 with only one worker

[Weisman and Efferding (1960)] finding the exponent less negative than minus 1.90 (cf. Table 2.6). It thus follows that increasing D (at constant T) causes N_{js} to decrease dramatically with an exponent of for example minus 2.35 as for the disc turbine. This decrease in N_{js} by increasing D, should however be put into context by also considering the effect of D on the power draw P at constant power numbers ($N_{Re} >> 10^4$).

$$P_{js} \propto N_{js}{}^3 D^5 \propto \left(D^{-2.35}\right)^3 D^5 \propto D^{-2.05}$$; for DT at constant N_P ($N_{Re} > 10^4$); Zwietering (1958)

.....Equation 2-42

Equation 2-42 seems to suggest that for *DT*'s, P_{js} can be reduced by increasing the impeller diameter D, within the range tested by Zwietering (1/6 T to 2/3 T). One should however be careful with the constant N_P assumption. As N decreases with increasing D, N_{Re} might drop below ~10^4, where N_P starts to increase with decrease in N_{Re}. Even if N_{Re} stays within the turbulent regime, N_P's have been found to increase with increasing D/T, regardless. Chapman *et al.* (1983a), for example, found the N_P for a *DT* impeller to increase in one case from 5.10 to 5.95 as D/T increased from 1/4 to 1/2, and in another case to increase from 3.15 to 4.8 as D/T increased from to 1/3 to 1/2.

2.4.4.3.6 Scale, T or D

Zwietering (1958) found N_{js} to decrease with an increase in the scale of the system,

$$N_{js} \propto T^{-0.85}$$ or $$\propto D^{-0.85}$$ for geometric similar scaling ; Zwietering (1958)

.....Equation 2-43

Some others have found the effect of scale to be influenced by the type of impeller, with PT-D and PT-U, showing smaller decreases with increasing scale. However, findings with radial impellers (e.g. DT and FT) are very close to, or slightly less than, the minus 0.85 found by Zwietering (cf. Table 2.6). Zwietering's prediction of the decrease in impeller speed with increasing scale might thus be judged as slightly optimistic and a slightly smaller value of minus 0.80, lying between that of Zwietering and Chapman *et al.* (1983a), might be safer to use for design predictions of scale-up in terms of solids suspension (cf. Figure 2.23).

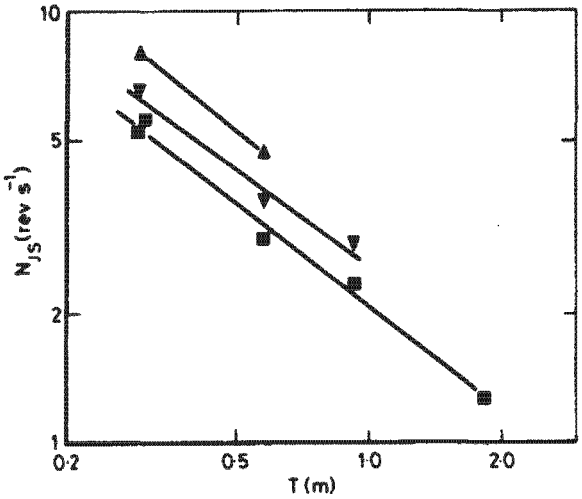

Figure 2.23 Effect of scale (*T*) on N_{js} [Chapman *et al.* (1983a)]

(D=T/2; B=0.01; silica sand; ■: DT, ▲: PT-U, ▼: PT-D)

2.4.4.3.7 Relative Impeller Clearance, C/T

Zwietering (1958) found for all the impellers tested (FT, DT, VD and Pr), as shown in Figure 2.17, that N_{js} decreased with decreasing relative impeller clearance *C/T*, except for the disc turbine DT (cf. Figure 2.18). Because the effect of *C/T* depended on impeller type and could not be fitted as a power function Zwietering decided to combine the effect of *C/T*, with the effect of relative impeller diameter *D/T*, which also depended on impeller type, as well as the correlation coefficient *K* into an *S* parameter. These *S* parameters were then presented graphically for the different types of impellers tested. Nienow (1968) later found that N_{js} reduced with decreasing *C/T*, also for DT's. Chapman *et al.* (1983a) also confirmed the decreasing N_{js} trend with decreasing *C/T* for DT's (cf. Table 2.7).

Table 2.7 The Effect of Impeller Clearance (*C/T*) on N_{js} and P_{js} for Disc Turbines [Chapman *et al.* (1983a)]

C/T [-]	N_{js} [s^{-1}]	P_{js} [W]	N_P
0.167 (1/6)	**4.28**	82	4.6
0.25 (1/4)	**4.95**	151	5.5
0.50 (1/2)	**5.90**	240	5.4

(T = 0.56 m; DT; D = T/3; X = 3%; soda glass ballotini)

From Table 2.7 it follows that in addition to N_{js} decreasing with decreasing C/T for DT's, the power number N_P was found to either stay relatively constant or to decrease with decreasing C/T. The combined effect results in a dramatic decrease in P_{js} with decreasing impeller clearance ($P_{js} = N_P.\rho.N_{js}^3.D^5$, $N_{Re} >> 10^4$). Armenante and Uehara Nagamine (1998) found that N_P generally decreased with decreasing C/T for DT's, but that after an initial decrease it started to increase at very low C/T for FT's. However, P_{js} still decreased with decreasing C/T in all cases.

The reason why the effect of impeller clearance could not be incorporated as a power function is partially related to a change in flow pattern that occur with radial impellers at low impeller clearances ($C/T \leq$ ~1/6). The two flow patterns, as observed by many [e.g. Nienow (1968), Nagata (1975), Bujalski, Nienow and Huoxing (1990)], are depicted graphically in Figure 2.24. At impeller clearances D/T above 1/5 a flow pattern is observed similar to the 'normal' radial *double-figure-of-eight* flow pattern of turbine impellers, with the discharge stream flung out horizontally from the turbine and splitting up into two streams giving vertical motion up and down the vessel wall. The downward stream scours the vessel bottom as it circulates back to the eye of the impeller. If the impeller is operating with this flow pattern, it is intuitive that the closer the impeller is to the bottom the stronger the scouring action will be. With this flow pattern, the last solids to be suspended off the bottom are from the centre of the tank. At C/T of about 1/5, slightly unstable flow patterns are observed. At C/T of 1/6 and smaller, a very different flow pattern is observed. The lower circulation loop, observed at higher clearances, now disappears. The impeller discharge stream now dips slightly towards the corner of the tank, before flowing up the tank wall and circulating back to the centre (eye) of the impeller from above. At these low clearances, the last solids to be suspended are from the periphery of the tank. Some have found this flow pattern to be very efficient for two-phase solids suspension. Nienow (1968) found that once the impeller was operating in this flow pattern a further reduction in impeller clearance only led to very small reductions in N_{js}. Armenante and Uehara Nagamine (1998) incorporated the effect of C/T into a modified Zwietering equation, but for radial impellers, it only applies to the low impeller clearance case (cf. Figure 2.24 (b)).

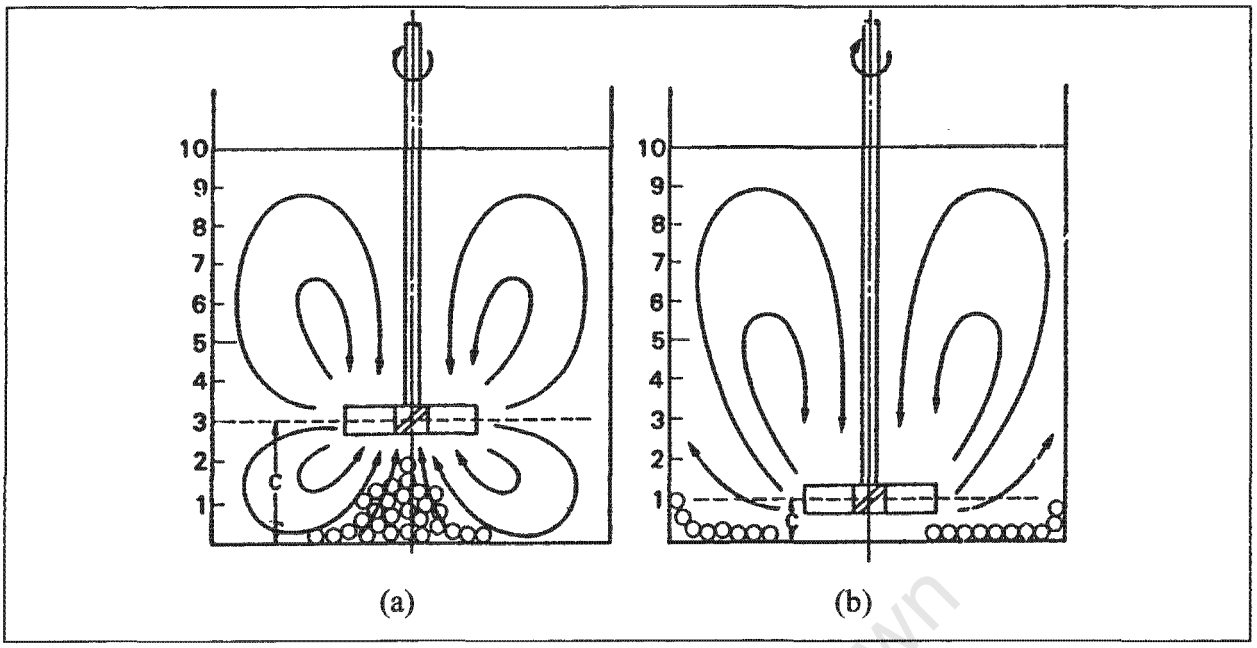

Figure 2.24 Influence of impeller clearance on flow patterns and suspension of solids [Nagata (1975)]

2.4.4.4 Theoretical Critical Impeller Speed Correlations

Though many theoretical models have been proposed, often supported by experimental data, no general agreement has been reached [Nienow (1992)]. On balance, Zwieterings empirical correlation remains the most useful in terms of estimating N_{js} [Chapman *et al.* (1983a)]. As is evident by these observations, the theoretical approaches have not achieved general acceptance and success in predicting N_{js}. For this reason, the theoretical N_{js} correlations will be reviewed very briefly here.

The aim of these theoretical correlations (mechanistic approaches) is to develop relationships between the minimum impeller speed needed to lift the solids off the bottom of the tank N_{js} (*suspension mechanisms*, cf. 2.3.3.2), and variables expected to influence solids suspension (*sedimentation mechanism*, cf. 2.3.3.1). These relationships are developed from making some simplifying assumptions and then using theoretical principles to obtain the correlation. Most mechanistic models uses one of two mechanisms involved in solids suspension, viz. the drag force acting on the particle, caused by *bulk fluid flow*, or the *turbulent* action of the fluid acting on the particle [Nienow (1992)]. These mechanisms are then applied either to particles settled on the *bottom* of the tank, or to particles already suspended in the *bulk* of the fluid

[Rewatkar and Joshi (1991)]. A summary of these mechanistic approaches are given in Table 2.8.

Table 2.8 Theoretical Correlations for the Critical Impeller Speed #

Reference	d_p^{α}	$\Delta\rho^{\beta}$	ρ_L^{γ}	μ_L^{δ}	D^{ε}	Note
Kolar (1967b)	0.177	0.5	-0.5	0	-0.667	Large N_{Ar} (large u_T)
Baldi, Conti and Alaria (1978)	0.167	0.5	-0.5	0	-0.667	
Voit and Mersmann (1985)	0.5	0.5	-0.5	0	-1	Fine particles
Buurman, Resoort and Plaschkes (1986)	0.167	0.5	-0.5	0	-0.667	
Molerus and Latzel (1987a)	-0.555	0.555	-0.444	-0.111	-0.889	$N_{Ar} \leq 40$ ($u_T \leq \sim 1.8$ cm/s; d_p=0.1mm)
Molerus and Latzel (1987b)	0.14	*	-0.14	0	-0.64	Large N_{Ar} (large u_T)
Wichterle (1988)	0.667	0.667	-0.333	-0.333	-0.667	Low N_{Ar} (low u_t)
Wichterle (1988)	-0.333	0.333	-0.667	0.333	-0.667	High N_{Ar} ($u_T \geq \sim 1.8$ cm/s; d_p=0.1mm)

Notes: The exponents in this table relates to the following correlation for N_{js}: $N_{js} = d_p^{\alpha}\Delta\rho^{\beta}\rho_L^{\gamma}\mu_L^{\delta}D^{\varepsilon}$; where D is at constant D/T and is thus a scaling parameter (T can also be used); *: Not obtainable in power form; #: Largely taken from Rieger and Ditl (1994)

2.4.5 Critical Impeller Speed in Three-Phase Systems

This section considers the effect of adding gas to two-phase solids suspension as considered in Section 2.4.4. The effect of impeller types and impeller clearance under gassed conditions will be considered first (cf. Section 2.4.5.1). In the next two sections, the effects of both gas (cf. Section 2.4.5.2) and solids (cf. Section 2.4.5.3) on hydrodynamics is briefly considered. The effects of gas as described in these sections results in increasing the critical impeller speed for gassed conditions and correlations for N_{jsg} are reviewed in Section 2.4.5.4.

2.4.5.1 Impeller types and clearance

For two-phase suspension, axial flow impellers (pumping down) have been found to be more energy efficient for solids suspension than radial turbines (cf. Table 2.9). Eventhough the just suspended impeller speeds N_{js} of the axial impellers are higher than that for the disc turbine, they still have lower just suspended power inputs $(\varepsilon_T)_{js}$. This is due to the very low power numbers of most axial impellers compared to the radial impellers (e.g. DT).

For this reason Chapman *et al.* (1983c), Wong, Wang and Huang (1987), and Frijlink, Bakker and Smith (1990) considered the use of axial impellers also for three-phase solids suspension. They found that axial impellers can still be used efficiently at very low gas addition (Q_{GV} << 0.25vvm), but on further gassing, these axial impellers lose their advantage and the disc turbine becomes more energy efficient. These axial impellers (pumping down) also become flooded very easily, which leads to dramatic sedimentation of solids. Axial impellers pumping upwards (e.g. PT-U), demonstrated very high resistances to flooding and can be considered at very high gassing rates. However, compared to axial impellers, the *disc turbine is singly the most versatile for three-phase solids suspension* [Chapman *et al.* (1983c)]. Wong, Wang and Huang (1987) came to the same conclusion by demonstrating that the effect of gas addition on the power needed for complete suspension P_{jsg} increased in the following order, 6-DT < 4-PT < 3-APr. In terms of impeller clearance, most recommend a C/T of around 1/4. As shown for two-phase (cf. Section 2.4.4.3.7) solids suspension is more efficient with small impeller clearances. However, Chapman *et al.* (1983c) found flow instabilities with $C = T/6$, whilst Frijlink, Bakker and Smith (1990) also demonstrated more stable, though slightly less efficient, operation for a disc turbine at $C/T = 0.36$ than at 0.17 (1/6). Instabilities are shown by large variations in power draw (or N_P) with relatively small changes in gas addition (or N_{QG}), whilst efficiency is measured by the power needed for complete suspension [$(\varepsilon_T)_{js}$ or $(P/V)_{js}$]. The use of a disc turbine at an impeller clearance C around $0.25.T$ is thus recommended for three-phase solids suspension.

Table 2.9 Efficiency of Different Impellers in *Two*-Phase Solids Suspension [Chapman *et al.* (1983a)]

Impeller type *	N_{js}, (s^{-1})	N_P, (-)	$(\varepsilon_T)_{js}$, (W/kg)
MPr	3.55	0.5	0.33
4-PT-D	2.75	1.4	0.35
6-PDT	2.67	2.2	0.54
6-DT	2.02	5.9	0.61
4-PT-U	3.60	1.2	0.72

(T=0.56m; D/T=1/2; X=3%; soda glass ballotini)

*: MPr = Marine propeller; 4-PT-D = Pitch-blade turbine, downflow; 6-PDT = Pitch-blade disc turbine; 6-DT = Disc turbine, Rushton; 4-PT-U = Pitch-blade turbine, upflow

2.4.5.2 *Effect of Solids on Gas-Liquid Hydrodynamics*

Solids addition has been found not to influence the liquid or gas-liquid hydrodynamics significantly, especially not in well-mixed conditions. Chapman *et al.* (1983c) demonstrated that, at the just suspended condition, solids concentration has only a small effect on the power number based on ρ_{SL}. However, as the impeller speed drops significantly below the just suspended condition, the solids start to sediment on the bottom and form a false bottom, effectively reducing the impeller clearance. As shown in Section 2.4.4.3.7, N_P decreases at low impeller clearances, and the same happens with the formation of this sedimented solids false bottom. In addition to the small effect on N_P, Chapman *et al.* (1983c), and Dutta and Pangarkar (1995) found increasing X also to have a negligible influence on gas holdup φ_G. Dutta and Pangarkar (1995) used mixing time θ_{mix} as a criterion to identify the just suspended condition and from these results it can be seen that although solids addition increases θ_{mix} marginally from the liquid, the effect of solids is less than the effect of gas addition on θ_{mix}. The marginal increase in mixing time as an indicator of bulk flow mainly, and level of turbulence to a lesser extent, thus suggests that the presence of solids do not reduce the impeller discharge rate significantly, but may contribute to some turbulence dampening. It thus follows from these observations that the effect of solids on the liquid or gas-liquid hydrodynamics in terms of power number, gas holdup, and impeller discharge rate is relatively small, but will increase the power draw with increased slurry density ($P = N_P.\rho_{SL}.N^3.D^5$) and may contribute to some turbulence dampening.

2.4.5.3 *Effect of Gas on Solids-Liquid Hydrodynamics*

The most noticeable effect of gas addition on liquid and solids-liquid hydrodynamics is the *reduction in power* draw. The drop in gassed power numbers can be seen from Table 2.10. Chapman *et al.* (1983b) demonstrated that the impeller discharge rate (causing bulk fluid circulation), as well as power draw decreases with increased gas addition. In Chapman *et al.* (1983a) it was established that particles are suspended either by bulk flow drag forces, or by turbulent eddies associated with local energy dissipation. The effect of gas addition thus causes a reduction in both the mechanisms causing solids suspension, and to counteract this, the just suspended impeller speed N_{jsg} has to be increased, as shown in Table 2.10.

Table 2.10 Effect of Gas Addition on Solids-Liquid Hydrodynamics Chapman *et al.* (1983c)

Q_{GV} [vvm]	J_G * [mm.s^{-1}]	N_{jsg} [s^{-1}]	$(N_P)_{jsg}$ ** [-]	$(\varepsilon_T)_{jsg}$ [W.kg^{-1}]
0	0	4.95	5.5	1.09
0.25	2	5.62	4.3	1.23
0.75	7	6.90	2.8	1.52
1.25	12	7.78	2.5	1.88

(T = 0.56 m; DT; D/T = 1/3; C/T=1/3; X = 3%; soda glass ballotini)

*: Convertion of Q_{GV} to J_G is dependent on vessel size, T = 0.56m in this case ($J_G = Q_{GV}/60 \times T$; where T in mm and J_G in mm/s)

**: Power number based on liquid density: $N_P = P/(\rho_L N^3 D^5)$

If the impeller speed is not increased with increased gassing, it can lead to impeller flooding, which is characterised by a sudden drop in impeller power draw and leads to dramatic solids sedimentation. As already shown in Section 2.3.2.3, the flooding condition is commonly expressed in terms of airflow number, N_{QG}. Frijlink, Bakker and Smith (1990) identified different three-phase solids suspension regimes based on airflow numbers. *Low* gas flowrates at $N_{QG} < 0.02$, *transitional* region with N_{QG} between 0.02, and 0.05 and *high* gas flowrates at $N_{QG} > 0.05$ were identified. None of the impellers studied by Frijlink *et al.* could suspend solids at N_{QG} above 0.08. In the low airflow number regime, the effect of air is relatively small, and downward pumping impellers can still be used. In the transitional airflow number regime, N_{jsg} may not be very reproducible and is related to the drop in N_P. Only radial and some upward pumping impellers can still be used in the high airflow number regime and constant or *increased power* addition is needed to keep solids suspended. Frijlink *et al.* furthermore correlated the drop in N_P with increasing gas addition, to the increase in N_{jsg} needed for solids suspension (cf. Figure 2.25), which leads to Equation 2-44.

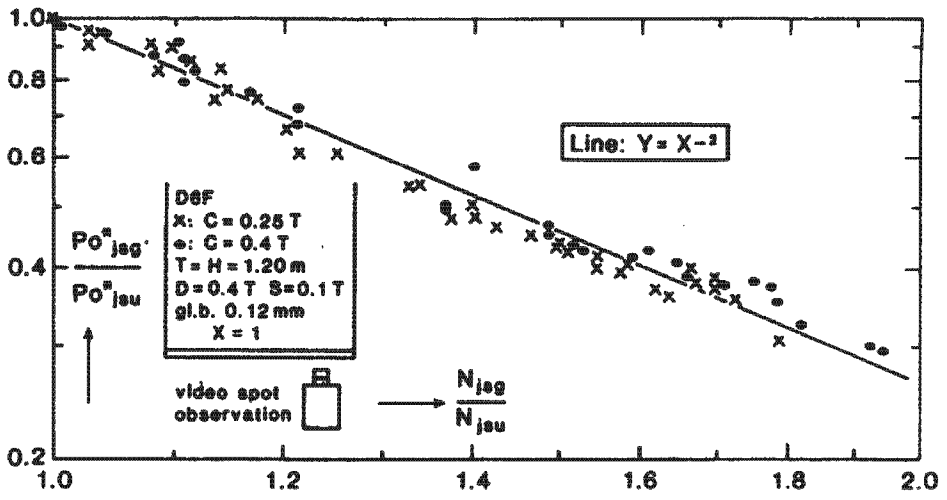

Figure 2.25 Increase in N_{jsg} required for solids suspension with decrease in N_{Pg} on increased gassing for DT's [Frijlink, Bakker and Smith (1990)]

(B = 100%; T, C, D as indicated; $Y = N_{P,jsg}/N_{P,jsu}$; $X = N_{jsg}/N_{jsu}$; For PT-D: $Y = X^{-1.1}$; For PT-U: $Y = X^{-2}$)

$$\frac{N_{P,jsg}}{N_{P,jsu}} \propto \left(\frac{N_{jsg}}{N_{jsu}}\right)^{-2} \qquad \text{(a)}$$

Alternatively, without the ratioing:

$$N_{P,jsg} \propto N_{jsg}^{-2}\ ; \qquad \text{(b)}$$

Or,

$$N_{jsg} \propto N_{P,jsg}^{-1/2} \qquad \text{(c)}$$

.....Equation 2-44

(DT's and PT-U's)

By inserting Equation 2-44 (b) into the power number correlation (P α $N_P.N^3.D^5$) at constant D, it suggests that the power addition for maintaining the just suspended condition (N_{Pjsg}) will increase linearly with the critical impeller speed, N_{jsg} (cf. Equation 2-45).

$$P_{jsg} \propto N_{P,jsg} N_{jsg}^{\ 3} \propto (N_{jsg}^{-2}) N_{jsg}^{\ 3} = N_{jsg}\ ;$$ With increased gas addition for DT's

.....Equation 2-45

This finding from Frijlink, Bakker and Smith (1990) can also be tested on the results of Chapman *et al.* (1983c) as given in Table 2.10, which leads to Figure 2.26 (a). It follows that this data also suggests that the power needed to maintain complete suspension (ε_{jsg}) increases

linearly with critical impeller speed (N_{jsg}). Figure 2.26 (b) further suggests ε_{jsg} also increases linearly with gas addition (Q_{GV}). Together, Figure 2.26 (a) and (b) suggests that N_{jsg} and Q_{GV} will also be linearly related. The effect of gas addition on N_{jsg} will be considered in the next section, where N_{jsg} correlations are considered (cf. Section 2.4.5.4).

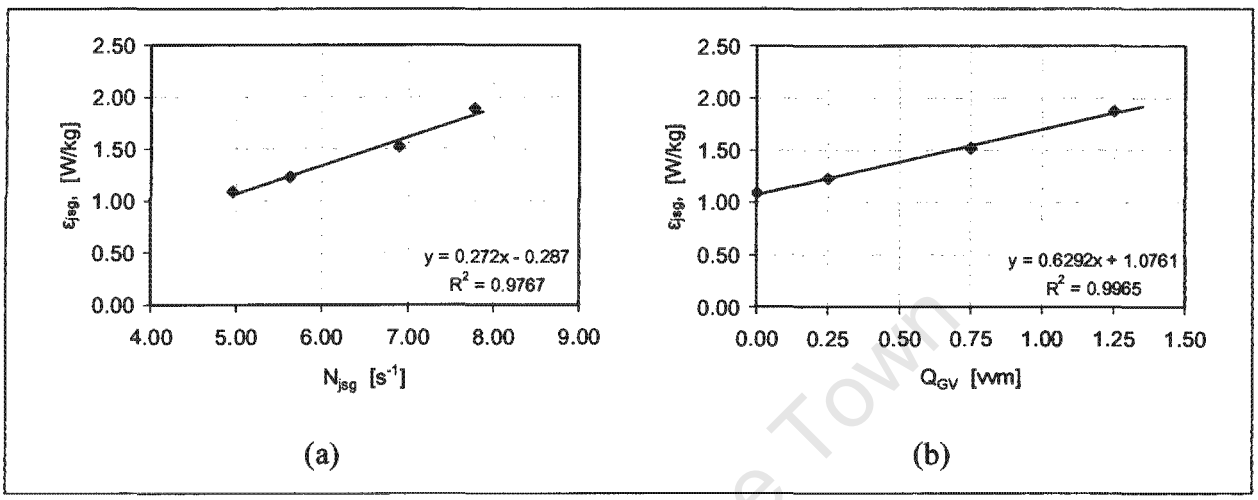

Figure 2.26 Increase in power addition for complete suspension (ε_{jsg}) with N_{jsg} and Q_{GV} (data taken from Chapman *et al.* (1983c); cf. Table 2.10)

For power to increase linearly with impeller speed, the torque on the impeller has to remain constant ($P = 2\pi N.M$; cf. Table 2.3). This lead Lehn, Myers and Bakker (1999) to investigate the relationship between N_{jsg} and M_{jsg} as a function of gas addition. His experimental results largely confirmed the expectations from Frijlink *et al.*'s findings to find a constant torque criterion with gas addition for the radial DT as well as for the PT-U but not for the PT-D impeller.

2.4.5.4 Three-Phase Critical Impeller Speed Correlations [2]

It follows from the previous section that gas addition reduces the impeller's power draw and capacity to circulate fluid. This impacts negatively on the impellers ability to suspend solids and the impeller speed therefore has to be increased to compensate for these effects. It follows that the three-phase critical impeller speed, N_{jsg}, is expected to increase

[2] In this section and in the rest of this work N_{js} will refer to critical impeller speed in general, N_{jsu} refers specifically to two-phase critical impeller speed, whereas N_{jsg} refers specifically to three-phase critical impeller speed. Many use N_{js}, to refer to two-phase critical impeller speed, which can be confusing in three-phase work.

with gas addition Q_G. This section will focus on studies aimed at incorporating the effect of gas into three-phase critical impeller speed N_{jsg} correlations. By the early 1980's Chapman *et al.* (1983a) were among the first to observe that although G-L dispersion and S-L suspension has been studied independently, there was a lack of studies considering the suspension of solid particles whilst simultaneously dispersing a gas in a liquid continuum. They thus embarked on an extensive study of S-L, L-G and S-L-G agitation aimed at providing more knowledge concerning any interactions in the mechanisms responsible for gas dispersion and solids suspension [Chapman *et al.* (1983a); Chapman *et al.* (1983b); Chapman *et al.* (1983c); Chapman *et al.* (1983d)]. Later, others also developed three-phase N_{jsg} correlations [Wong, Wang and Huang (1987); Bujalski, Konno and Nienow (1988); Rewatkar, Raghava Rao and Joshi (1991); Nienow (1992); Dutta and Pangarkar (1995); Dohi *et al.* (2003)]. All these workers used the *1s criterion* to identify the critical impeller speed N_{jsg} although some also tested other experimental methods and criteria [Rewatkar, Raghava Rao and Joshi (1991); Dutta and Pangarkar (1995)]. The findings of these three-phase N_{jsg} studies will be discussed here, whilst all the N_{jsg} correlations are summarised in Table 2.11. In the discussion, the focus will be on the results obtained with disc turbines (radial), as the impeller recommended for stable operation over a wide range of gas addition rates (cf. Section 2.4.5.1). In order to develop an N_{jsg} correlation, two aspects need to be considered. Firstly, the effect of gas addition rate on N_{jsg}, which will be considered here first, and, secondly, the effect of the other variables, already considered in the two-phase correlation (N_{jsu}), should be considered under gassed conditions, which is shown in Table 2.11.

Plotting N_{jsg} vs. Q_G for a specific test condition, N_{jsg} is often found to increase linearly with gas addition rate (cf. Figure 2.27), which leads to the following possible form for the N_{jsg} correlation, $N_{jsg} = N_{jsu} + K_a.Q_G$. However, when plotting the increase in impeller speed caused by gas addition ($\Delta N_{js} = N_{jsg} - N_{jsu}$) against the rate of gas addition for a *range of solid-liquid variables* at constant geometry, it can be seen that the results start to scatter around the linear fit (cf. Figure 2.28). In addition, changing the geometry also changes the slope of the increase in N_{jsg} with gas addition (cf. Figure 2.29). It therefore follows that it seems as if the addition of gas causes a linear increase in N_{jsg}, but that the slope of this increase (K_a) seems to be affected by other variables. Considering the three-phase correlations in Table 2.11, four options for incorporating the effect of gas addition on the N_{jsg} can be identified.

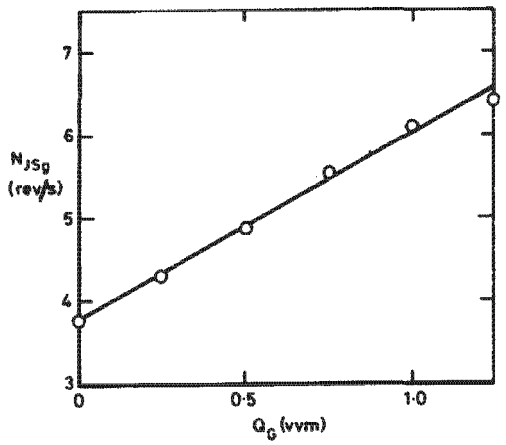

Figure 2.27 Effect of gas flow rate, Q_{GV}, on N_{jsg} [Chapman *et al.* (1983c)]

(DT; D=T/3; $T_{0.56}$; glass powder at X = 0.3%)

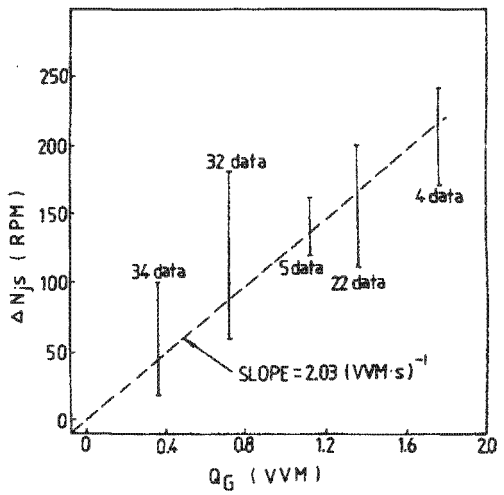

Figure 2.28 ΔN_{js} vs Q_G for a DT impeller in a T=0.29m tank for all test conditions [Wong, Wang and Huang (1987)]

($\Delta N_{js} = N_{jsg} - N_{js}$; 6-DT; D = T/3; All conditions: $1514 \leq \Delta\rho_S \leq 7642$ kg/m^3, $200 \leq$ dp ≤ 1200 µm, $0.2 \leq X \leq 20\%$)

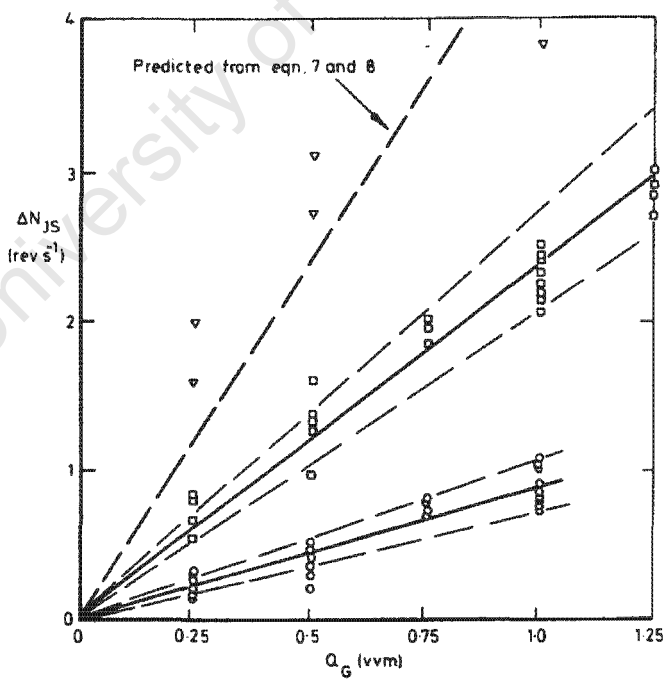

Figure 2.29 ΔN_{js} vs Q_G for three DT impeller sizes in a T = 0.56m tank for all test conditions [Chapman *et al.* (1983c)]

($\Delta N_{js} = N_{jsg} - N_{js}$; ○ D/T=1/2; □ D/T=1/3; ▽ D/T=1/4; $T_{0.56}$; All test conditions: $50 \leq \Delta\rho_S \leq 1900$ kg/m^3, $92 \leq$ dp ≤ 2650 µm, $0.3 \leq B \leq 30\%$)

Option 1:

Chapman *et al.* (1983c), Wong, Wang and Huang (1987), and Dutta and Pangarkar (1995) opted to incorporate the effect of gas addition as a constant, '*a*', multiplied by the gas addition rate Q_{GV} (cf. Equation 2-46).

$N_{jsg} = N_{jsu} + K_a.Q_{GV}$; Where K_a = constant = '*a*' for certain geometry

.....Equation 2-46

However, it was acknowledged that '*a*' varied most notably with impeller diameter [Chapman *et al.* (1983c); Dutta and Pangarkar (1995)] as can be seen from Figure 2.29, as well as impeller type [Wong, Wang and Huang (1987); Dutta and Pangarkar (1995)]. As can be seen from Table 2.11 these authors thus included '*a*' values for the different geometries. This option therefore suggests that the *nominal increase* in N_{jsg} is proportional to gas addition rate for constant geometry. Still as was seen in Figure 2.28 for constant geometry but various solid-liquid conditions, a constant slope, '*a*', shows a lot of scatter. This could suggest that a better way of incorporating the effect of gas on N_{jsg} could be found. Chapman *et al.* (1983c) fitted a power function to the effect of impeller diameter on '*a*' and found '*a*' α $(D/T)^{-2.42}$. This is almost the same relationship as they found between N_{jsu} and D/T, -2.45 (cf. Table 2.11). This may suggest that '*a*' scales similarly to the other variables as N_{jsu} does, which means that '*a*' may be proportional to N_{jsu}, i.e. $a = K.N_{jsu}$. This leads to option two.

Option 2:

Option 2 proposes that K_a can be seen as linearly related to N_{jsu}, in other words, K_a α N_{js} or $K_a = K.N_{jsu}$, cf. Equation 2-47.

$$N_{jsg} = N_{jsu} + K_a.Q_{GV} = N_{jsu} + (K.N_{jsu}).Q_{GV} = N_{jsu}(1 + K.Q_{GV}) \quad \text{(a)}$$

Or dividing by N_{jsu},

$$\frac{N_{jsg}}{N_{jsu}} = 1 + K.Q_{GV} \quad \text{(b)}$$

.....Equation 2-47

It follows from Equation 2-47 (b) that this method assumes that the *relative increase* in N_{jsg} is linearly related to the gas addition rate. Bujalski, Konno and Nienow (1988) used this option in a slightly modified form for PT-D impellers, i.e. $N_{jsg} = N_{jsu}$ $(0.82 + 0.31.Q_{GV})$. The

disadvantage of their modified form would be that N_{jsg} would not be contiguous with N_{jsu} when Q_{GV} drops to zero, cf. $N_{jsu} \neq N_{jsu}$ (0.82 + 0).

Option 3:

Option 3 was also proposed by Bujalski, Konno and Nienow (1988). In this option, it is attempted to incorporate the effect of gas as a power function. This has the advantage of treating the effect of gas, $(1+Q_{GV})$, as just another factor in the N_{js} product function. However, many have found gas addition to cause a *linear* increase in N_{jsg} and not to show a *power* relation (e.g. Figure 2.27). This is the only option that attempts to incorporate the effect of gas addition on N_{jsg} in a non-linear manner for other system conditions held constant.

$$N_{jsg} = N_{jsu}.(1+Q_{GV})^{0.11}\text{; Or dividing by } N_{jsu}\text{:}\quad \frac{N_{jsg}}{N_{jsu}} = (1+Q_{GV})^{0.11}$$

..... Equation 2-48

(Bujalski, Konno and Nienow (1988) using PT-U)

Option 4:

In this approach, the linear increase in N_{jsg} with gas addition, K_a, is taken to be a function of other variables. Rewatkar, Raghava Rao and Joshi (1991) proposed this method of incorporating the effect of gas (cf. Equation 2-49). The correlation of Dohi *et al.* (2003) as given in Table 2.11, can be seen as a more, and perhaps unnecessarily, complex variation of this method.

$$N_{jsg} = N_{jsu} + K_a.J_G\text{; Where } K_a = 132.7u_T^{0.5}D^{-1.67}T \qquad \text{(a)}$$

$$N_{jsg} = N_{jsu} + K_a.J_G\text{; Where } K_a = 330.6u_T^{0.5}D^{-0.75} \qquad \text{(b)}$$

..... Equation 2-49

(Rewatkar, Raghava Rao and Joshi (1991) using DT, PT-D, PT-U)

It follows from Option 1 to 4 that most workers agree that gas addition causes a linear increase in N_{jsg}. The value of the slope of this increase, K_a, however seems somewhat challenging to predict for various geometrical and solid-liquid system conditions. The second aspect of the three-phase critical impeller speed correlation to consider is the effect of the other system variables (everything except gas addition) under gassed conditions. These include all the variables already considered in the N_{jsu} correlation (cf. Table 2.6). Chapman *et*

al. (1983c) and Wong, Wang and Huang (1987) have found some solid-liquid variables (e.g. $\Delta\rho/\rho_L$) to have a reduced effect under three-phase conditions, whilst Dutta and Pangarkar (1995) and Dohi *et al.* (2003) proposed exponents for three-phase conditions very similar to that of Zwietering (1958) for two-phase conditions.

Table 2.11 Critical Impeller Speed Correlations in Three-Phase Systems

Reference	The effect of different variables on solids suspension as in the Zwietering type equation as modified for gassed conditions $N_{jsu} = KT^a D^b d_p^{0.20} B^{0.13} (\Delta\rho/\rho_L)^{0.45} \nu^{0.1}$; $N_{jsg} = f(N_{jsu}, Q_G)$						
	d_p	B	$\Delta\rho/\rho_L$	ν_L	$(D/T)^b$	T^{a+b} **	Q_G
Zwietering (1958)*	0.20	0.13	0.45	0.1	-2.35 (DT)	-0.85	ungassed
Chapman *et al.* (1983a)*	0.15	0.12	0.40	0	-2.45 (DT) -1.50 (PT-D)	-0.85 (DT)	ungassed
Chapman *et al.* (1983c)	0.12	0.12	0.22	0	-2.45, -2.30 (DT, Q_{GV}=0.5, 1.0) -1.45 (PT-D, Q_{GV}=0.5, 1.0)	DT: -0.75, -0.85 (Q_{GV}= 0.25, 1.0) PT-D: -0.64, -0.54 (Q_{GV} = 0.25, 1.0)	DT: $N_{jsg} = N_{js} + a.Q_{GV}$; '*a*' = 0.94 (D = T/2), 2.4 (D = T/3) $vvm^{-1}s^{-1}$; (not linear for 6-PT-D)
Wong, Wang and Huang (1987)	0.12-0.16	0.11	0.2			-0.65 (DT, PT-D, PT-D; Q_{GV} > 0.5)	DT, 4-PT-D: $N_{jsg} = N_{js} + a.Q_{GV}$; '*a*' = 2.0 (DT), 5.0 (4-PT-D) $vvm^{-1}s^{-1}$ for D/T = 1/3
Bujalski, Konno and Nienow (1988)							PT-D: $N_{jsg} = N_{js}$ $(0.82 + 0.31.Q_{GV})$; and PT-U: $N_{jsg} = N_{js}.(1+Q_{GV})^{0.11}$
Frijlink, Bakker and Smith (1990)						-0.65 (DT, Q_{GV} = const)	

Reference	The effect of different variables on solids suspension as in the Zwietering type equation as modified for gassed conditions $N_{jsu} = KT^a D^b d_p^{0.20} B^{0.13} (\Delta\rho/\rho_L)^{0.45} \nu^{0.1}$; $N_{jsg} = f(N_{jsu}, Q_G)$						
	d_p	B	$\Delta\rho/\rho_L$	ν_L	$(D/T)^b$	T^{a+b} **	Q_G
Rewatkar, Raghava Rao and Joshi (1991)	0.09 (PT-D) 0.12 (DT)				-1.61 (PT-D)	-0.81	DT, PT-D, PT-U: $N_{jsg} = N_{js} + a.J_G$; 'a' = $132.7 u_T^{0.5} .D^{1.67} .T$; (or '$a$' = $330.6 u_T^{0.5} .D^{-0.75}$)
Dutta and Pangarkar (1995) – mult imp.	0.18; 0.16 (PT-U)	0.15	0.42		-1.47, -1.39, -1.66 (DT, PT-D, PT-U; mult imp)	-0.85 (DT, PT-D) -1.0 (PT-U) (mult imp)	$N_{jsg} = N_{js} + a.Q_{GV}$ 'a' = 3.75 (DT), 4.47 (PT-D), 3.16 (PT-U) $vvm^{-1}s^{-1}$, and D/T =1/3; also 'a' = 2.75 (DT) for D/T=1/1.5
Dohi *et al.* (2003)	0.20	0.13	0.45	0.1			$N_{jsg} = N_{js}[1+0.03(J_G/u_T)^{0.2} N_{Rep}^{0.4}]$

* - Two-phase N_{js} correlations (ungassed)

** - Scaling at constant Q_{GV} (vvm); Chapman *et al.* (1983c) also gives values when scaling at constant J_G (then $Q_{GV} \propto T^{-1}$): -0.88 and -0.95 (J_G = 6, 14 mm/s) are then given for the scaling exponent for the DT

2.4.6 Solids Distribution

Solids distribution considers the *extent* of solids distribution as well as the *variation* of the distribution (cf. Figure 2.12). The extent of solids distribution is normally measured in terms of suspension height, h_s, and the homogeneity is often expressed as a relative standard deviation, *RSD*. When considering solids distribution, *solids concentration profiles* are often used to display the findings. Some solids concentration profile work done in stirred tanks will be considered in Section 2.4.6.1. Concentration profiles can be easily quantified in mainly two parameters. The first parameter is the upper level where solids are measured or in other words the suspension height h_s. As shown in Section 2.4.1, h_s only gives the *extent* of axial solids *distribution*, and has not been found to give very consistent results for various systems. The second parameter that can be derived from a concentration profile is the variation in the solids concentrations in the profile (*RSD*) in order to quantify the homogeneity of the axial solids distribution (cf. Section 2.4.6.2). Much work has been done in the modelling of the solids distribution in vessels of high aspect ratios (slurry reactors with

multiple impellers, bubble columns and three-phase fluidised beds) using the sedimentation-dispersion model. Some have applied this model also to stirred tanks, which will be considered briefly in Section 2.4.6.3.

2.4.6.1 Solids Concentration Profiles

A solids concentration profile is a plot of solids concentration measurements vs. either height or radial position. It is normally done in the vertical or axial direction, but can also be done radially. Barresi and Baldi (1987a) measured both radial and axial concentration profiles. They found the radial concentration profiles to be relatively flat, especially for the axial discharge impellers. The radial discharge impellers showed some radial profiles in the region of the impeller and below the impeller, whilst being flat above the impeller (cf. Figure 2.30). It should be noted that these radial profiles were measured in a relatively small vessel (T = 0.39 m), at very low solids concentration (B = 1.51%), and therefore one should be careful to generalise these findings. The axial profiles generally displays decreasing solids concentrations from the base to the top of the liquid, with higher impeller speeds and finer particle sizes displaying distributions that are more homogeneous.

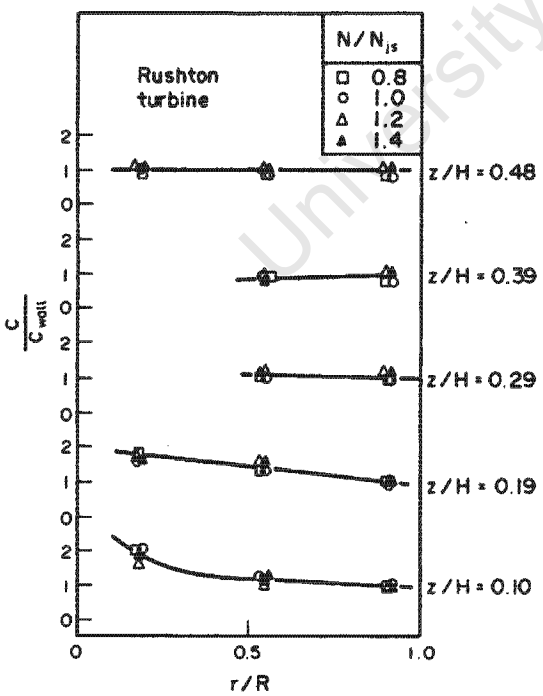

Figure 2.30 Radial concentration profiles at various impellers speeds for a Rushton turbine [Barresi and Baldi (1987a)]

(T = 0.39m; d_p = 100-177 µm; B = 1.51%)

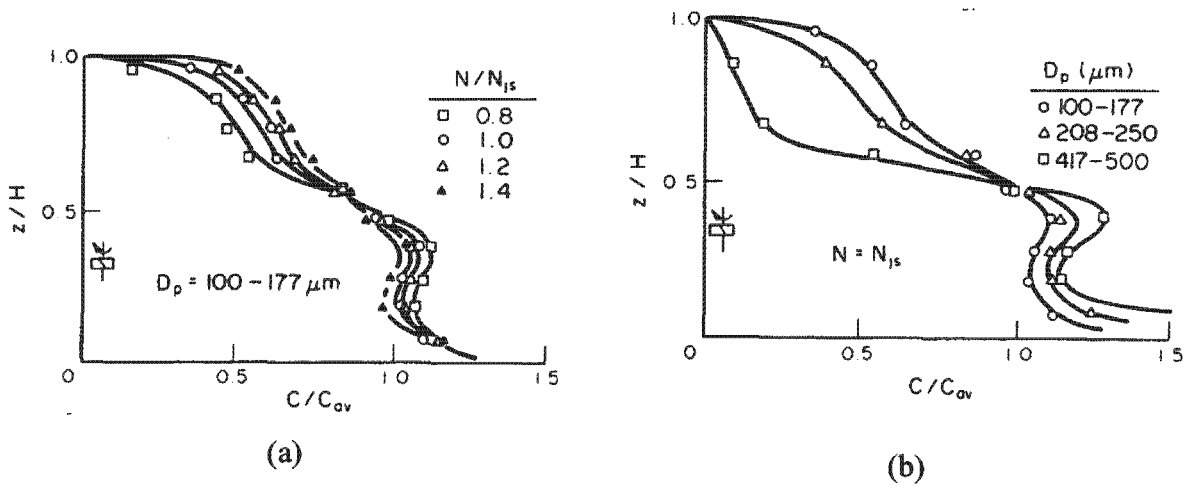

Figure 2.31 Axial concentration profiles at (a) various impeller speeds and (b) various particle sizes [Barresi and Baldi (1987a)]

(T = 0.39m; 4PT; B = 0.50%)

2.4.6.2 Variation in Solids Concentration

In order to quantify the homogeneity of the solids distribution the variation in the solids concentrations in the profile can be calculated. Bohnet and Niesmak (1980) and Barresi and Baldi (1987a) used the relative standard deviation (*RSD*) to display the variation, whilst Einenkel (1980) used the relative variance (σ_{rel}^2) as shown in Equation 2-50.

$$\sigma_{rel}^2 = \frac{1}{n}\sum_{i=1}^{n}\left(\frac{X_i}{\bar{X}}-1\right)^2 = \frac{\frac{1}{n}\sum_{i=1}^{n}(X_i-\bar{X})^2}{\bar{X}^2} = RSD^2$$

..... Equation 2-50

Using the variation in a solids concentration profile to identify the just suspended condition was already introduced in Section 2.4.3.8, as one of the N_{js} criteria. More detail will be given here on some of the studies that considered this aspect of vertical solids concentration profiles. Einenkel used *13* measuring points and used 200μm glass beads at high concentrations of 5 to 25 vol. % and suggested from his work that a *RSD* value of around 0.975 ($\sigma_{rel}^2 = 0.95$) could be compared to the just suspended condition and *RSD* = 0.25 could be compared to a homogeneous suspension. Bohnet and Niesmak used an optical method to measure the solids concentrations, which allowed them in excess of *20* measuring points, but limited the solids concentration to below 2 vol.%. From graphical results presented in their

work, it can be seen that RSD_{js} varied between 0.10 and 0.30 for different solid particles used, whilst *RSD* values at homogeneous suspension varied between 0.05 and 0.15. Comparing these findings to that of Einenkel, it seems as if there is not a common link between N_{js} and *RSD* and that RSD_{js} might depend on the number of measuring points, the solids concentration used, the particle size, and the particle density. Therefore, far a particular system a relation might be developed but it will be difficult to generalize. Bohnet and Niesmak (1980) suggested a *quality of distribution* parameter φ, [$\varphi = RSD.(X_{avg}/(X_B\text{-}X_{avg})$], whilst Barresi and Baldi (1987a) plotted their *RSD* values against a *K parameter*, [$K = N_P^{1/3}.N.D/u_T$], in attempts to make it more generic.

2.4.6.3 Modelling Solids Distribution (Sedimentation-Dispersion Model)

Attempts have also been made to model the distribution of solids in the axial direction of stirred tanks. It should however be emphasized at this point that these models are based on a number of simplifying assumptions, and has only had reasonable success in high aspect ratio vessels or in small two-phase stirred tanks at very low solids concentrations. As will be seen in the following discussion, this model is largely based on the assumption of negligible radial concentration profiles, and that solids distribution throughout the vessel is therefore mainly accomplished by turbulent dispersion. These assumptions are however questionable in large vessels and at high solids concentrations. Still, it is thought that if the aforementioned disclaimers are kept in mind, this model may be useful in describing the opposing forces at work in solids distribution.

Barresi and Baldi (1987a) and Ayazi Shamlou and Koutsakos (1989) applied the continuity equation to any horizontal plane in a stirred tank. This gives no net vertical fluid flow through the plane. Thus in the absence of radial concentration profiles, solids can not be distributed vertically by bulk fluid motion. Barresi and Baldi (1987a) found relatively flat radial profiles in a laboratory size tank at very low solids concentrations, yet for radial impellers only in the region above the impeller (cf. Figure 2.30). The absence of radial profiles led them to adopt a one dimensional vertical balance between the net flux of solid particles upwards in the vessel (down the concentration gradient) caused by turbulent diffusion (dispersion), against the downwards flux of solids under gravitational forces (sedimentation). This is called the sedimentation-dispersion model and the mass balance equation is given in Equation 2-51, where u_s is the solids settling velocity (also called the *slip*

velocity) and D_S is the turbulent dispersion coefficient for the solid particles. The first term is thus taken to characterise the sedimentation mechanism, and the second term the suspension mechanism (cf. Section 2.3.3)

$$u_s X_h + D_S\left(\frac{dX_h}{dh}\right) = 0$$

..... Equation 2-51

Rearranging Equation 2-51 gives,

$$\frac{dX_h}{X_h} = -\frac{u_s}{D_S} dh$$

..... Equation 2-52

Integrating over the height of the tank from the base leads to,

$$ln\frac{X_h}{X_B} = -\frac{u_s}{D_S} h$$

..... Equation 2-53

Replacing h on the right with D (or Z or T) as a characteristic system dimension, leads to the formation of a modified Peclet number N_{Pe*}, which is often used as a dimensionless number characterising the solids distribution in a tank. Differentiation of Equation 2-53 gives,

$$\frac{d\,ln\,X_h}{dh} = -\frac{u_s}{D_S}$$

..... Equation 2-54

Considering Equation 2-54 it follows that a plot of $\ln X_h$ vs h, will give the ratio, $-u_s/D_S$, as the slope of the line. Thus the lower the settling velocity and the higher the turbulence, the flatter the profile will be. Figure 2.32 is a typical plot of this type. Due to h being the vertical axis, the slope is taken off the vertical and not the horizontal, and '*flatter*' thus refers to more vertical.

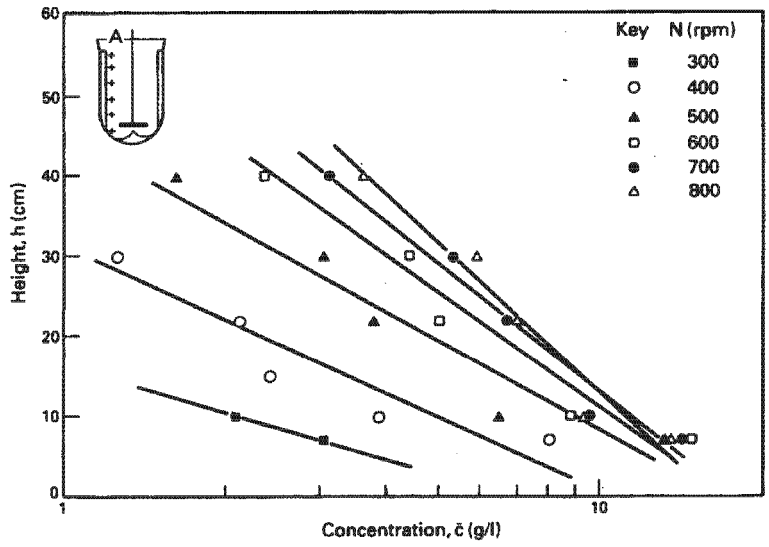

Figure 2.32 Semi-logarithmic plot of solids concentration vs sample height for different impeller speeds [Ayazi Shamlou and Koutsakos (1989)].

(d_p = 390 µm, ρ_S = 2900 kg/m^3, ρ_L = 1000 kg/m^3, D = 0.10m, C = 0.113m, T = 0.225m, Z = 0.37m, X_0 = 1 wt%)

The next step to make this model more usable would be to relate the two model variables, u_s and D_S, to other system parameters. Although the solid-liquid slip velocity, u_s, is influenced by other factors (e.g. level of turbulence, solids concentration, presence of gas, etc.) it is normally assumed reasonable to take it as being proportional to the terminal settling velocity of the particles, u_T (cf. Equation 2-55) [Barresi and Baldi (1987a); Ayazi Shamlou and Koutsakos (1989); Rewatkar and Joshi (1991)]. Relating the solids dispersion coefficient to system parameters is more difficult. Ayazi Shamlou and Koutsakos (1989) took D_S to be proportional to the liquid phase dispersion coefficient D_L, which is valid especially at the low solids concentrations they used, where there is negligible solid-solid interaction. Further assuming homogeneous, isotropic turbulence, also for the larger energy containing eddies in the range of D, they arrived at the relation given by Equation 2-56.

$$u_s \propto u_T$$

.....Equation 2-55

$$D_p \propto ND^3 \Big/ \left(T^2 H\right)^{1/3} \propto ND^2$$

.....Equation 2-56

Joshi (1981) derived the same relation as Equation 2-56. Inserting Equation 2-55 and Equation 2-56 into Equation 2-53 gives the following.

$$ln\left(\frac{X_h}{X_B}\right) \propto \frac{u_T}{ND^2}h \propto \frac{u_T}{ND}\frac{h}{D} \propto \frac{u_T}{ND}\frac{h}{T}$$

..... Equation 2-57

Equation 2-57 suggests that within the assumptions made to this point (mainly negligible radial profiles, little solid-solid interaction, and isotropic turbulence) that constant solids distribution will scale (X_h/X_B is the same at the same h/T) with constant u_T and constant impeller tip speed, $u_{tip} = \pi.N.D.$ Rewatkar and Joshi (1991) attempted to include the contribution of fluid circulation to solids distribution. Their starting point was Equation 2-58, which is similar to Equation 2-53, but with the incorporation of fluid circulation velocity u_c, which can be estimated from mixing time studies.

$$ln\frac{X_h}{X_B} = -\frac{u_s - au_c}{D_S}h$$

..... Equation 2-58

Solids Suspension in Stirred Tanks Summary

This section focused on solids suspension in stirred tanks, due to the larger amount of published solids suspension work in stirred tanks, than in mechanical flotation cells. This section thus aimed to expose the reader to the breadth of solids suspension work in the general chemical engineering literature.

The Effectiveness of Solids Suspension:

Solids suspension comprises two simultaneously occurring steps. The primary step is off-bottom suspension and the secondary step is the distribution of solids throughout the vessel. With increasing impeller speed the extent of ***off-bottom suspension*** *increases until the just suspended or complete suspended condition is reached. The impeller speed at this condition is commonly referred to as the critical impeller speed, N_{js}. The* ***distribution of solids*** *throughout the vessel also improves with increasing impeller speed. The vertical distribution of solids refers to both the extent of the distribution, and the variation within the distribution, which are commonly quantified in terms of the suspension height, h_s, and the relative standard deviaton of the concentrations within the profile (RSD). Although many solids suspension conditions referring to both off-bottom and solids distribution can be*

*identified, the **critical impeller speed** has been found to be the most significant and consistent condition to use. The other conditions can also normally be related in terms of relative impeller speed, N/N_{js}.*

Experimental Methods and N_{js} Criteria:

*A variety of methods can be used to measure solids suspension conditions. All these methods suffer from one or more of a range of disadvantages including, requires a transparent tank wall, inaccurate, intrusive, radioactive material, only usable at very low X, not usable under gassed conditions, etc. The methods that measures solids suspension conditions directly in terms of **off-bottom** conditions (e.g. visual, contact, ultrasonic, radiation, and mass transfer) and in terms of solids **distribution** (e.g. visual, sample withdrawal, optical, ultrasonic, pressure probes, conductivity probes, and tomography) are judged most suitable for studies into solids suspension. Solids suspension conditions can only be inferred from **indirect** methods (e.g. RTD_S, θ_{mix}, and P or M measurements). From these methods a number of **criteria** developed to determine the just suspended condition or the critical impeller speed (e.g. 1s, 100% suspension, unsuspended layer, radiation count rates, rate of mass transfer, 90% h_s/T, concentration above the base, variation in vertical concentrations, θ_{mix}, and N_P). Of these criteria the **1s criterion** applied by **visual** observation of the base of the tank is most often used in solids suspension studies.*

Critical Impeller Speed Correlations (Two-Phase)

*Most work in solids suspension to date has been done in ungassed, two-phase systems. **Zwietering (1958)** conducted one of the first and most comprehensive studies in solids suspension, and developed an N_{js} correlation, which is applicable under a wide range of conditions (cf. Equation 2-35).*

$$N_{js} = S d_p^{0.20} B^{0.13} \nu^{0.10} g^{0.45} \left(\frac{\rho_S - \rho_L}{\rho_L} \right)^{0.45} D^{-0.85} \; ; \; \text{Where, } S = f(\text{impeller type, T/D, T/C})$$

*Many others have also tested the effect of these solid-liquid, and geometrical variables on N_{js}. The Zwietering correlation remains one of the most widely applicable correlations. The focus of this work is on the **solid-liquid variables**. Of these, density difference and particle size have been found to have the largest effect, whilst X (or B) and v have been found to have relatively small effects. Some have even found v to have no effect on N_{jsu} within the ranges of their studies. Others have also attempt to derive the N_{js} correlation from **theoretical** or more mechanistic principles. These have been largely unsuccessful and the semi-empirical **Zwietering approach is therefore preferred**.*

Critical Impeller Speed in Three-Phase Systems

Three-phase solids suspension has not had the same attention as the two-phase correlation, and in the general chemical engineering literature, some challenges remain. In terms of ***impeller types****, the situation is very different from two-phase solids suspension. Where axial impellers have been found most effective in two-phase, the* ***radial*** *disc turbine have been found singly to be the most effective and reliable to use in three-phase conditions [Chapman et al. (1983c)]. In addition, the recommended* ***impeller clearance*** *is in the region of 25%, due to gas dispersion instabilities experienced at lower clearances. Considering the* ***effect of solids and gas on hydrodynamics*** *it has been found that the addition of solids has only a very small effect on system hydrodynamics at higher impeller speeds, mostly only related to increased power draw due to increasing slurry densities, and furthermore some turbulence dampening.* ***Gas addition*** *on the other hand has a* ***dramatic*** *influence on the system hydrodynamics. Gas addition most notably decreases the impeller* ***power*** *draw, due to decreasing the impeller discharge mass flowrate, cavity formation, and turbulence dampening effects. These effects of gas addition necessitate an* ***increase in the critical impeller speed*** *to maintain complete suspension under gassed conditions. Even the power draw for complete suspension have been found to increase linearly with gas addition.*

The increase in N_{jsg}, required with increased gassing is thus an important part of the N_{jsg} correlation. Different ways of ***incorporating the effect of gas on N_{jsg}*** *can be identified from literature:*

1. $N_{jsg} = N_{jsu} + a.Q_{GV}$; *Where a = constant for certain geometry*
2. $N_{jsg} = N_{jsu}\ (1 + K.Q_{GV})$
3. $N_{jsg} = N_{jsu}\ (1 + Q_{GV})^m$
4. $N_{jsg} = N_{jsu} + K_a.Q_{GV}$; *Where* $K_a = f$*(system variables)*

The other consideration in the three-phase correlation is the structure of the 'N_{jsu}' part of the correlation, i.e. the ***effect*** *of all the* ***other variables*** *already considered in the N_{jsu} correlation, but now* ***under gassed conditions****. Some have found some of these effects to decrease whilst others have found the effects very similar than in two-phase conditions.*

Solids Distribution:

Solids distributions are often displayed in the form of ***solids concentration profiles****. Vertical profiles are more common, although radial profiles can also be done. Solids distribution can be quantified in terms of the* ***extent of solids distribution (h_s)*** *and the* ***variation within the distribution (RSD)****. Attempts have been made to generalise both h_s and RSD findings and to relate it to N_{js}. However, although relations have been found for specific systems the generalizations are not always consistent for other systems. Finaly, attempts have also been made to* ***model vertical solids distributions*** *in stirred tanks. It has been shown in a previous section (cf. Section 2.3.3) that solids suspension is caused by interaction of a sedimentation- and a suspension mechanism. The sedimentation-dispersion model relates the*

sedimentation mechanism to the settling velocity of the particles, and the suspension mechanism to the turbulent dispersion coefficient of the solids (cf. Equation 2-53). Its application in stirred tanks is however based on a range of simplifying assumptions (including, negligible radial profiles, little solid-solid interaction, and isotropic turbulence), which is mainly true for smaller stirred vessel at low solids concentrations. It should therefore be applied carefully to other systems. Yet, it is seen as a way of demonstrating the opposing effects involved in solids distribution, if not quantitatively, then qualitatively.

$$ln\frac{X_h}{X_B} = -\frac{u_s}{D_S}h$$

2.5 SOLIDS SUSPENSION IN FLOTATION

It is well-known that the sub- and microprocesses of *solids suspension*, *feeding and dispersion of air*, *mixing* for reagent conditioning and particle-bubble collisions, and the *rising* of the loaded bubbles and *froth removal* must be accomplished in a flotation cell [Schubert (1985)]. Considering that bubbles would not collide and attach to unsuspended particles, complete suspension of solids in the pulp phase is a prerequisite for effective flotation. However increasing the agitation speed unnecessarily, decreases the bubble-solids aggregate stability, and thus reduces the floatable maximum particle size [Schulze (1984)]. These flotation subprocesses have already been considered in more detail in Sections 2.1.2 and 2.3, but these statements are repeated here to show the relevance and importance of studying solids suspension in mechanical flotation cells. However, information on the effect of *solids suspension* and energy input on flotation is sparse [Hui and Ahmed (1998a)]. This is the motivation for the thorough review of solids suspension done in Section 2.4, in order to see what knowledge and techniques developed from work done in the conventional chemical engineering literature on standard stirred systems is relevant to studies in flotation cells.

Arbiter, Harris and Yap (1969) and Harris (1976) described two ways of evaluating the effectiveness of solids suspension. The first concerns the suspension or lifting of solid particles off the bottom of the cell, i.e. the critical impeller speed, N_{js}. *Critical impeller speed* work done in mechanical flotation cells will be considered in Section 2.5.1. The second way of evaluating the effectiveness of solids suspension is the distribution of the solids throughout the tank, which is often described by concentration profiles and suspension heights. *Solids distribution* work done in mechanical flotation cells will be considered in Section 2.5.2. Other areas of mechanical flotation cell operation, which are sometimes related to solids suspension, are solids residence time distribution studies RTD_S, and the hydrodynamics of coarse particle flotation. RTD_S is strongly influenced by the effective mixing volume occupied by solid particles as well as the height of the discharge line, and is often compared to the liquid residence time. However RTD_S is very difficult to directly relate to solids suspension and observations made [Arbiter (1999); Jonaitis (1999)] and work done [Mehrotra and Saxena (1983); Yianatos *et al.* (2001)] in mechanical flotation cells will not be discussed in this section. In addition, the area of coarse particle flotation is also sometimes related to solids suspension inefficiencies, which may be either insufficient agitation causing solids not

to be suspended or over-agitation, which reduces the particle-bubble aggregate stability. This study is however aimed at quanitifying solids suspension vs. system parameters and not finding the optimum level of solids suspension for efficient flotation and thus work done by Schubert and co-workers [Schubert and Bischofberger (1978); Schubert and Bischofberger (1981); Schubert, Bischofberger and Koch (1982a); Schubert (1985)], and others [Schulze (1982); Schubert, Bischofberger and Koch (1982a); Hui and Ahmed (1998a); Rodrigues, Leal Filho and Masini (2001)], on coarse particle flotation and optimum energy input for flotation will not be considered here.

2.5.1 Critical Impeller Speed, N_{js}

Schubert, Bischofberger and Koch (1982b) determined the critical impeller speed N_{js} and the power addition for the just suspended condition $(P/V)_{js}$ for a variety of different impellers in a 54 l mechanical flotation cell at 20 vol% solids and a gas flow rate of 0.45 vvm. The impellers included finger and double finger impellers as well as triangular, bladed and double bladed turbine type impellers. They found that N_{js} and $(P/V)_{js}$ varied considerably for the different types of impellers as can be seen from Figure 2.33.

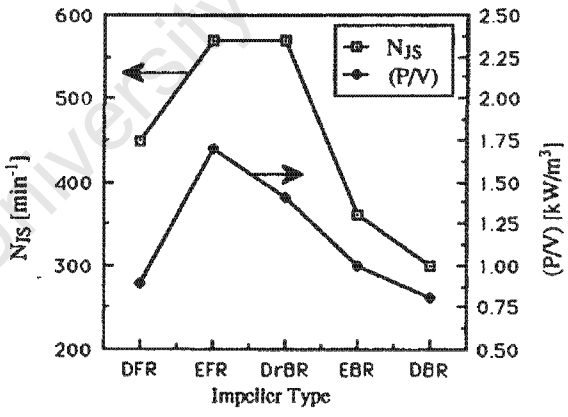

Figure 2.33 Critical impeller speed N_{js} and just suspended power density $(P/V)_{js}$ for various finger and bladed impellers) [Mavros (1992); data taken from Schubert, Bischofberger and Koch (1982b)]

(V = 54 l; φ_S = 0.20; Q_{GV} = 0.45 vvm; DFR – double finger impeller, EFR – Single finger impeller, DrBR – Triangular blade impeller, EBR – Single blade impellers, DBR – Double blade impeller)

Schubert (1985) later related the critical impeller speeds of the different types of impellers by using the power numbers of the different impellers as shown in Figure 2.34.

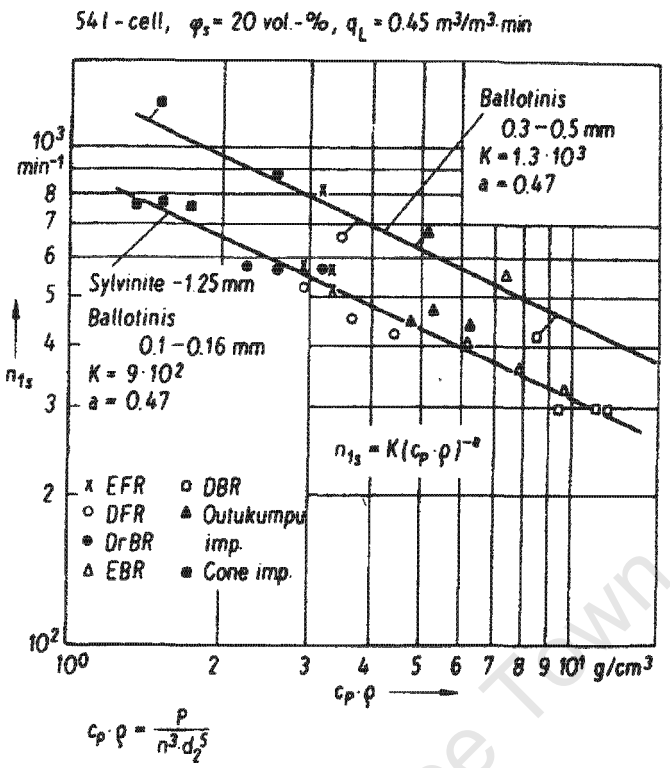

Figure 2.34 Critical impeller speed ($N_{js} = n_{1s}$) as a function of power number ($N_P = c_P$) [Schubert (1985)]

(V = 54 l; φ_S = 0.20; Q_{GV} = 0.45 vvm; DFR – double finger impeller, EFR – Single finger impeller, DrBR – Triangular blade impeller, EBR – Single blade impellers, DBR – Double blade impeller)

Figure 2.34 shows the correlation between N_{js} and N_P for seven different types of impellers (including an Outokumpu impeller). Two size fractions of glass ballotini (ρ_S = 2480 kg/m^3; 100-160 µm and 300-500 µm) and one sylvenite ore (ρ_S = 2.0 [Wills (1997)]; –1250 µm) were used in this work. They found for all the different impellers that N_{js} could be related to N_P as follows.

$N_{js} = K(N_P.\rho)^{-a}$; Where a = - 0.47

..... Equation 2-59

Schubert found 'a' to be constant at 0.47. This indicates that the just suspended speed decreases with increasing impeller power number N_P according to the following relation, N_{js} α $N_P^{-0.47}$. This type of relation provides a basis for relating the critical impeller speed for different types of impellers in the same agitation system. It is interesting to note that this relation between N_{js} and N_P for different impellers is almost exactly the same relation between N_{js} and N_P derived from Frijlink, Bakker and Smith (1990)'s results in stirred tanks for the

same impeller, but at different gassing rates, which also changed the power number, $N_{js} \propto N_P^{-0.50}$ (cf. Equation 2-44). This suggests that *critical impeller speeds* for different impellers or for the same impeller at different gassing rates can be *related by the square root of the power numbers*. The coefficient, K, depended on particle size and solids density. For the 100 – 160 µm ballotini K_1 was found $9x10^2$ and for the coarser 300-500 µm ballotini K_2 was found to be $1.3x10^3$. The constant for the even coarser sylvenite ore (-1.25mm) K_3 was found to be equal to $9x10^2$, the same as K_1. It is suggested here (in this work) that some results on the effect of d_p and ρ_S on N_{js} can be extracted from Schubert *et al.*'s work by considering these coefficients in Figure 2.34. However, due to not having sufficient details for the sylvenite ore (solids density and lower size limit), only the relation between N_{js} and d_p will be extracted here. This can be done by using the K values for the two size fractions of ballotini. From Equation 2-59 follows $N_{js} \propto K$. Thus relating K to d_p also gives the relation between N_{js} and d_p. Considering the increase in K_1 to K_2 ($9x10^2$ to $1.3x10^3$) with the corresponding increase in d_p (130 to 400µm) of ballotini gives the following relation [by considering: $(\log K_2 - \log K_1)/(\log d_{p1} - \log d_{p2})$].

$$N_{js} \propto d_p^{0.33}$$

.....Equation 2-60

Derived from Schubert (1985) for a mechanical flotation cell

This finding can be compared to that of Zwietering (cf. Equation 2-35) where $N_{js} \propto d_p^{0.20}$. It follows by comparison with Equation 2-60 that Schubert's results gave a stronger influence of d_p on the just suspended impeller speed than that found in standard stirred tanks.

Weiss and Schubert (1989) studied coarse particle flotation and considered the effect of impeller type, impeller clearance and gas flowrate on solids suspension. They developed a new type of impeller and compared the just suspended impeller speed and power draw of their new 'GR' impeller with another double finger (DFR) impeller as shown in Figure 2.35 below.

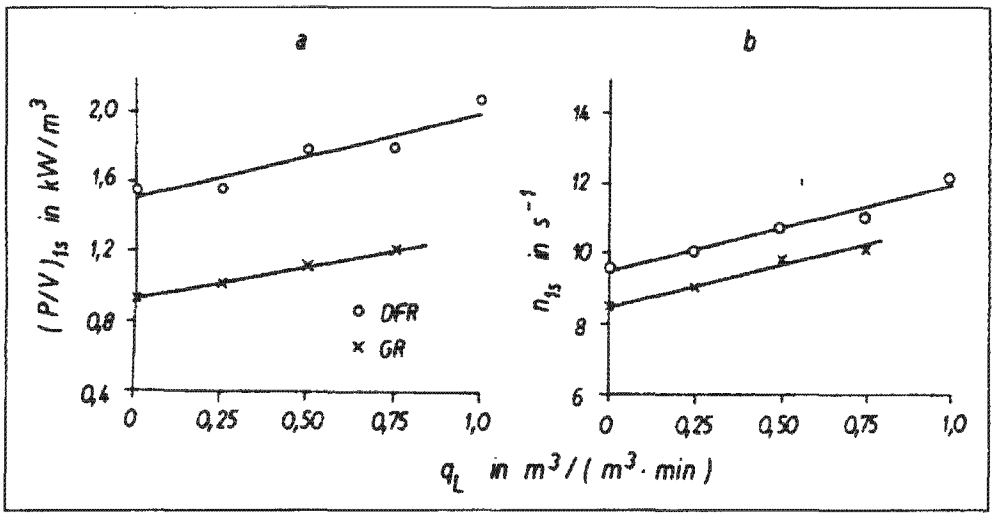

Figure 2.35 The effect of air addition ($q_L = Q_{GV}$) on (a) the just suspended power addition [$(P/V)_{1s} = (P/V)_{js}$] and (b) the critical impeller speed ($n_{1s} = N_{js}$). [Weiss and Schubert (1989)].

(54l mechanical flotation cell; C_b = 0.05T; water with 7 vol% ballotini (315-555 µm); GR – impeller type designed by the authors, DFR – double finger impeller)

It follows from the results of Weiss and Schubert as given in Figure 2.35 (b) that N_{js} increased linearly with air addition (a = 2.4 $vvm^{-1}.s^{-1}$). This is in agreement with the effect of air addition on the critical impeller speed in standard stirred tanks (cf. Figure 2.27). Also the increase in just suspended power addition $(P/V)_{js}$ with increased gassing is in agreement with findings in stirred tanks [cf. Figure 2.26 (b)]. Hui and Ahmed (1998b) also presented graphical results showing the just suspended impeller speed to increase linearly with increasing gas flowrate. It should however be noted that Hui and Ahmed [Hui and Ahmed (1998a); Hui and Ahmed (1998b); Hui and Ahmed (1999)], used a standard stirred tank fitted with a Rushton turbine for their flotation work which focused on coarse particle flotation. It can therefore be concluded mainly from the work by Weiss and Schubert (1989) that air addition causes the critical impeller in a flotation cell to increase linearly with gas flowrate Q_G for a given system.

$\Delta N_{js} = a.Q_G$; Where, $a = 2.4\ vvm^{-1}.s^{-1}$

..... Equation 2-61

Derived from Weiss and Schubert (1989) for a mechanical flotation cell

Arbiter, Harris and Yap (1969) did some air and liquid flow measurements with small centrifugal pumps in which air was introduced. They related their findings to the liquid pumping of flotation impellers and suggested the following correlation.

$Q_L = fND^3 - gQ_G$; where f and g are equation constants

..... Equation 2-62

It follows from Equation 2-62 that the liquid flow from the impeller Q_L reduces linearly with increasing air addition Q_G. Therefore, to maintain constant Q_L, the impeller speed N has to be increased by g/fD^3 x Q_G.

$\Delta N = \frac{g}{fD^3} Q_G$; for constant liquid flow Q_L from a gassed impeller

..... Equation 2-63

Comparing Equation 2-63 with Equation 2-61 it is seen that both the critical impeller speed and the impeller speed for constant fluid flow from an impeller increases linearly with addition of gas. This is further motivation that fluid flow and fluid velocity plays an important role in the suspension mechanism of solids from the bottom of a flotation cell (cf. Section 2.3.3.2).

Schubert (1985) considered the scale-up of solids suspension in pilot mechanical cells ranging from 13.5 to 72 l under two-phase and gassed conditions (Q_{GV} = 0.45 min^{-1}). Their results are shown in Figure 2.36.

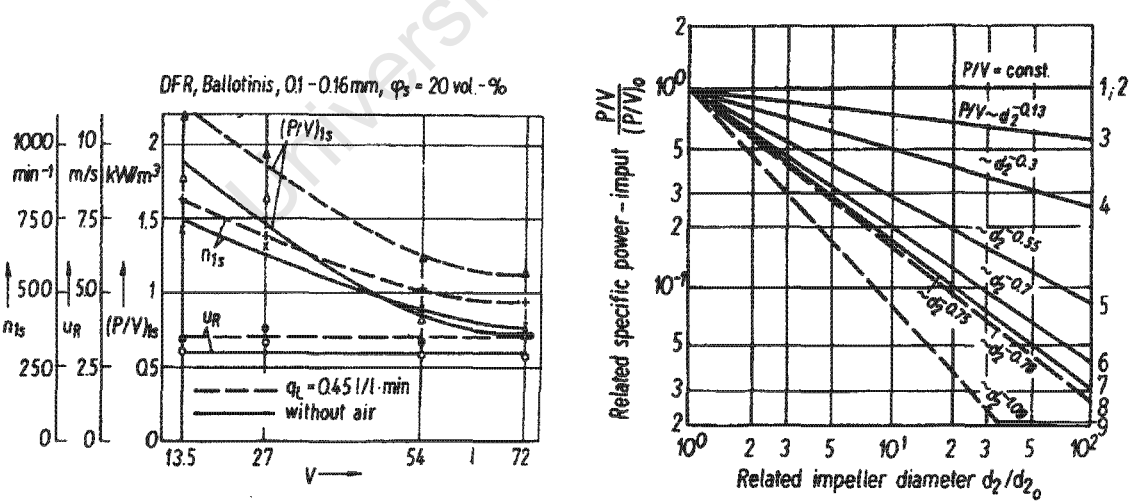

(a) (b)

Figure 2.36 The effect of scale on the just suspended condition: (a) N_{js} vs. V, ($n_{1s} = N_{js}$); (b) $(P/V)_{js}$ vs. D, (d_2 = D), broken lines = authors own results, line #5 = Zwietering (1958)'s results [Schubert (1985)]

It is shown in Figure 2.36 (a) how the critical impeller speed (N_{js}) decreased with increasing vessel volume. In Figure 2.36 (b), power addition for complete suspension, $(P/V)_{js}$, is shown versus increasing scale. The broken lines represents Schubert (1985)'s results, whilst the other lines represents results from stirred tank studies. It follows that they found a stronger decrease in power addition with increasing scale than most others, their results varying between $(P/V)_{js} \alpha D^{-0.75}$ to $(P/V)_{js} \alpha D^{-1.09}$. This can be compared to Zwietering (1958)'s result (line #5), $(P/V)_{js} \alpha D^{-0.55}$, and the scale-up rule sometimes applied of keeping power addition constant during scale-up, $(P/V)_{js} \alpha D^{0}$. It follows that Schubert (1985) found a relatively strong decrease in power addition, and thus also in critical impeller speed, with scale-up. This may be related to the relatively small range of vessel sizes that they used, 13.5 to 72 l. Using the power number relation, $P/V \alpha N^3D^2$, these power addition findings can be converted to critical impeller speed findings, giving.

$$N_{js} \alpha T^{-0.92} \text{ to } T^{-1.03}$$

..... Equation 2-64

Derived from Schubert (1985)'s results on mechanical flotation cells [Figure 2.36(b)]

These findings compares favourably with that of Zwietering $N_{js} \alpha T^{0.85}$ (cf. Equation 2-34), though somewhat stronger. It is therefore suggested that a more conservative reduction such as that predicted by Zwietering's relation for the scale-up of solids suspension in terms of critical impeller speed be used ($N_{js} \alpha T^{0.85}$) be used for mechanical flotation cells, as also implied by Harris (1976).

Schubert and Bischofberger (1978) applied their critical impeller speed measurements to indicate optimal flotation conditions for different sizes of a sylvinite ore (cf. Figure 2.37). This was done on a diagram of power addition vs. airflow number, on which a diagram of impeller speed and air flowrate could be superimposed for a specific cell (13.5 l). The N_{js}, for the coarser size fraction (0.5-1.6 mm), was indicated by the broken line, and it can be seen that the optimal flotation condition for the coarser fraction was just above the just suspended condition, with the finer fractions optimally floated at higher impeller speeds. They also developed similar diagrams for cassiterite flotation.

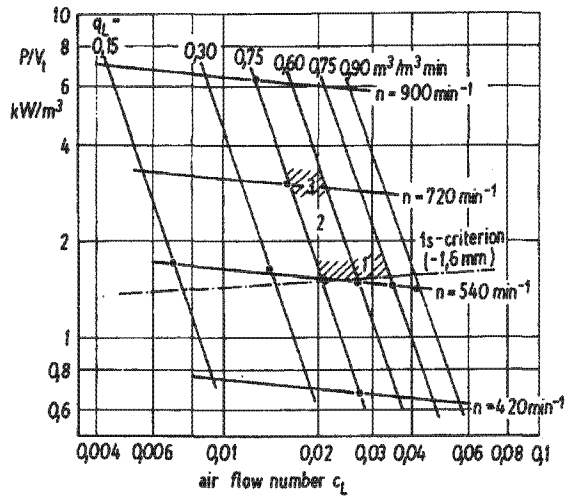

Figure 2.37 Diagram indicating optimal flotation conditions for different size fractions of a sylvinite ore; 1: 0.5-1.6 mm; 2: 0.125-0.50 mm; 3: -0.125 mm [Schubert and Bischofberger (1978)]

From a review of complete suspension work in mechanical flotation cells done mainly by Schubert and co-workers some relations between the just suspended impeller speed N_{js} and d_p, Q_{GV} and T could be extracted. Comparing these mechanical flotation cell findings to that of Zwietering (cf. Equation 2-34) it follows that the effect of d_p on N_{js} was found stronger in these studies [Schubert, Bischofberger and Koch (1982b); Schubert (1985)] than that found in stirred tanks. Air addition Q_G [Weiss and Schubert (1989); Hui and Ahmed (1998b)] seems to increase the critical impeller speed in a flotation cell linearly with the air flow rate, which agrees with what has been found in stirred tanks (cf. Equation 2-46 and Figure 2.27). The decrease in N_{js} with scale-up of tank size T [Schubert (1985)] were found to be stronger than the findings of Zwietering, and Zwietering's finding would thus be a safer, more conservative scale-up of solids suspension. It should however be noted that these flotation results are based on very limited data sets. No thorough investigation of the influence of solid-liquid-gas variables and geometrical variables on the critical impeller speed in a mechanical flotation cell could be found in this review of flotation literature.

2.5.2 Solids Distribution

Arbiter, Harris and Yap (1969) noted that even when solids dispersion appears to be complete a decreasing density gradient from bottom to top is usually evident. He states further that the theory of homogeneous isotropic turbulence applied to suspension predicts

that the solids concentration decays exponentially with height (cf. Section 2.4.6.3). Arbiter, Harris and Yap (1969) mainly considered the *dispersion* of solids in terms of solids suspension heights in two-phase solid liquid tests, but also noted when solids settled or sedimented on the bottom of the tank (below the *just suspended* condition). Using dimensional analyses and considering the work of Weisman and Efferding (1960) on suspension heights in stirred tanks, they developed the following correlation for suspension height.

$$\frac{h_s}{T} = K\left(\frac{T}{D}\right)^a\left(\frac{C}{D}\right)^b\left(\frac{P}{m_S}\right)^e d_p{}^z$$

..... Equation 2-65

Arbiter, Harris and Yap (1969) for mechanical flotation cells

Their findings on four bench scale flotation machines gave '*a*' to vary between -0.55 and 0.20, '*b*' between 0.20 and 0.40, '*e*' between 0.30 and 0.48 and '*z*' between -0.18 and -0.58. Thus, the effect of relative impeller diameter *T/D* on suspension height is conflicting. Increasing impeller clearance *C/D* increases solids dispersion in terms of suspension height. As seen in Section 2.4.4 this is opposite to off-bottom solids suspension where decreasing *C/T* improved suspension. This is one case where solids *dispersion* requirements differ from solids *suspension* requirements, i.e. for improved solids dispersion the impeller clearance should be increased where-as it should be decreased for improved off-bottom solids suspension. It should be noted that solids distribution can only really be evaluated with noting the off-bottom suspension conditions as well, i.e. whether complete or not. As expected increasing power addition P/m_S will increase the suspension height. Increasing the particle size d_p will decrease the suspension height as can also be expected. Harris (1976) reviewed this work of Arbiter *et al* and noted that this two-phase correlation was able to describe the data from different machines quite closely.

Previously, Arbiter and Steininger (1962) found that the suspension height dropped with air addition and that the drop in suspension height was related to the drop in power consumption with gas addition (P_{GLS}/P_{LS}). Similarly, they found that the introduction of air into a solid-liquid system reduces both the power consumption and the ability of the machine to suspend solids off the bottom. These effects were found to be more pronounced in the presence of a *frothing agent* and could be attributed to the lowering of the effective fluid density in the

impeller region. With narrowly sized solids fractions solids sedimented '*catastrophically*' when a certain air flow number (Q_G/ND^3) was exceeded. This sedimentation of solids coincided with a drop in the impeller power draw and is thought to be related to impeller flooding. The sedimentation of solids occurred at higher airflow numbers with decreasing particle size and solids content and occurred less abruptly with wider size distributions of solids.

In more recent reviews of large-scale mechanical flotation cells [Jonaitis (1999); Weber *et al.* (1999)], solids suspension in large flotation machines is considered qualitatively without giving any specific correlations. Jonaitis (1999) shows particle size distributions in OK-100 and OK-150 TankCell® units in the Mt. Keith Nickel operation to show that solids are adequately mixed in these cells. However, without solids concentrations accompanying these particle size distribution measurements only limited deductions can be made about the solids mixing and profiles. Weber *et al.* (1999) refers to earlier testwork done on 127 m^3 Wemco SmartCell™ machines in a copper application. These studies found the solids concentration and particle size distributions to be essentially constant throughout the cell. Weber *et al.* further quoted a case where it was claimed that a 127 m^3 unit, after some draft tube, false bottom and tank bottom modifications, was able to maintain off-bottom suspension even whilst receiving extremely coarse feeds of up to +1 inch (25mm) during extreme plant upsets!

Recently, Yianatos *et al.* (2001) did a comprehensive hydrodynamic characterization study on five parallel rougher banks consisting of nine 42.5 m^3 conventional flotation cells each on a Cu-Mo concentrator of Codelco-Chile. Solids concentration profile studies were done on the first and last cell of one of the banks and the results are shown in Figure 2.38.

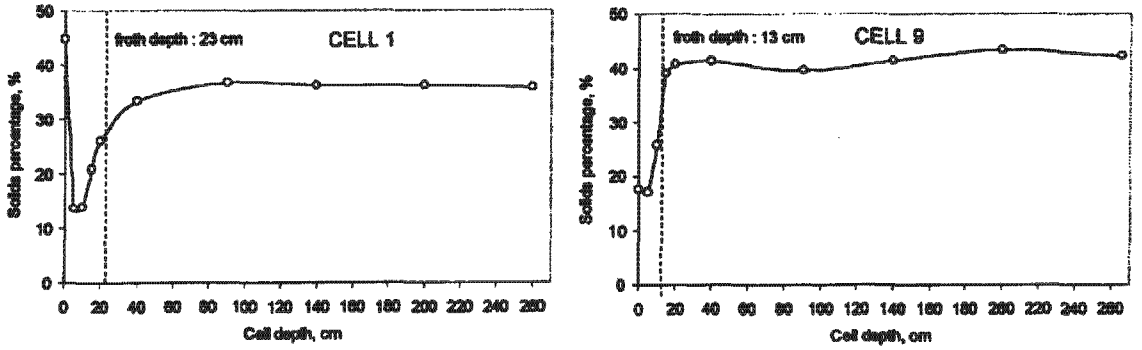

Figure 2.38 Solids Concentration Profiles from 42.5 m^3 Wemco Cells (a) Cell 1 with forced air (b) Cell 9 with self-aeration [Yianatos *et al.* (2001)]

Ignoring the froth section at the top it follows from Figure 2.38 that the solids concentration profiles were relatively flat in this work. A slight decrease is noticeable in the top section of the pulp phase and then a very slight increase from there to the bottom of the tank, which were more pronounced in the last cell of the bank than in cell 1. This would suggest that these cells had a consistent solids concentration throughout the height of the tank, suggesting that solids distribution in these 42.5 m^3 Wemco cells were very uniform. Whether or not solids were sedimented on the bottom of these cells can not be concluded directly from concentration profiles alone, but the fact that they do not show larger increases in concentrations closer to the bottom does suggests the absence of large quantities of sedimented solids on the bottom.

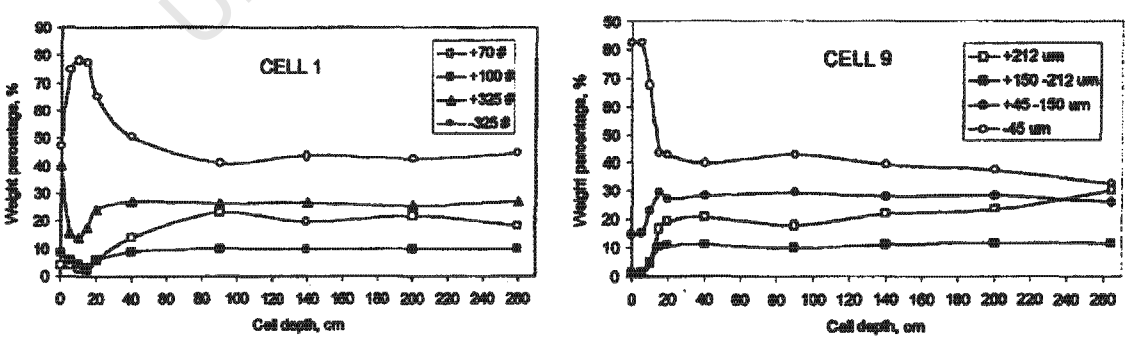

Figure 2.39 Solids Particle Size Profiles from 42.5 m^3 Wemco Cells (a) Cell 1 with forced air (b) Cell 9 with self-aeration [Yianatos *et al.* (2001)]

Once again ignoring the froth layer at the top of the cells it follows from Figure 2.39 that the particle size fraction profiles were once again relatively flat in these cells. The largest

variation is seen in the profile of the coarsest solids size fraction (+212 µm). In cell 1 the +212µm fraction decreased strongly in the upper layer of the pulp phase and in cell 9 the +212µm fraction increased strongly in the lower section of cell. These findings suggest that the solids were also consistently dispersed throughout these Wemco cells in terms of the different particle sizes. Only the coarse +212 µm fraction showed the concentration profile to drop from the bottom to the top of the cell.

It follows from this section that although many claims and observations on solids suspension and specifically solids distribution are being made, that only one correlation on suspension heights in mechanical flotation cells could be found in the published literature but no correlations for the critical impeller speed.

Solids Suspension in Flotation Summary

The following aspects related to solids suspension have been studied to some extent in the flotation literature, i.e. critical impeller speed, solids distribution, solids residence time distributions, and coarse particle flotation. RTD_S is only indirectly related to solids suspension, and coarse particle flotation falls outside the scope of this work. Mechanical flotation cell studies where critical impeller speeds were measured have mainly been conducted by Schubert and co-workers. Although these works were not designed to test the effects of different variables on solids suspension, some effects could be derived from these limited datasets. These include the effects of d_p, Q_{GV}, and scale, D. The effect of d_p in their work in a mechanical flotation cell seems stronger than that found by Zwietering and most others in stirred tanks. Gas addition (Q_{GV}) seems to cause a linear increase in the critical impeller speed, which is the same as that found in stirred tanks. In terms of scale-up, Schubert and co-workers found N_{js} to decrease stronger than that found by Zwietering and most others in stirred tanks. A more conservative decrease such as that recommended by Zwietering will thus be safer to use for the scale-up of solids suspension in stirred tanks. In terms of solids distribution, early work was done by Arbiter, Harris and co-workers. They developed a suspension height correlation, but the effects of the different variables varied significantly for different mechanisms tested. They further concluded that h_s drops with aeration, that the drop is related to the drop in power draw, and that the effect is more severe at higher frother concentrations. More recent flotation works use solids concentration profiles to display solids suspension conditions. However, most of them do not include the extent of off-bottom suspension, as the primary requirement for solids suspension.

2.6 SCOPE AND OBJECTIVES OF THIS THESIS

The overall aim of this thesis is to *evaluate solids suspension in a mechanical flotation cell.*

Sections 2.1 to 2.3 formed the *background* to this work. In these sections, the flotation process, machines and subprocesses were introduced and discussed in general. More specifically the *importance of studying solids suspension* in mechanical flotation cells was highlighted:

- Solids have to be suspended in order to interact with bubbles. Solids suspension and gas dispersion are thus necessary preconditions for flotation to occur.
- Mechanical flotation cells are unique in their designs and different from standard stirred tanks.
- Mechanical flotation cells dramatically increased in size since the advent of round mechanical flotation cells in the early 1990's. For effective scale-up, the subprocesses, including solids suspension, need to be better understood.
- Solids suspension is influenced by the dynamic action of the impeller as well as the system conditions (solid, liquid, gas, and geometrical variables). Gas addition is important for the gas dispersion subprocess, but also has a strong effect on solids suspension.

A review of flotation literature (cf. Section 2.5) highlighted the *shortage of recent solids suspension studies in mechanical flotation cells.* Early works, mostly by Arbiter and co-workers, and Schubert and co-workers, highlighted the importance of solids suspension to the flotation process. Schubert and co-workers demonstrated the relevance of the critical impeller speed as a solids suspension reference point to the flotation process, but did not develop a correlation to relate the critical impeller speed to system variables. Arbiter and co-workers, on the other hand used the suspension height as a suspension indicator and did develop a correlation for suspension height. However, suspension height has subsequently been found not to be as consistent an indicator of solids suspension conditions as the critical impeller speed. More recent publications, refer in some cases to off-bottom suspension conditions and in other cases deal with solids suspension by referring to concentration profiles. However, no dedicated studies of how solids suspension and more specifically the critical impeller speed is related to system conditions within mechanical flotation cells could be found.

Thus, due to the shortage of published solids suspension work in the flotation literature, the general chemical engineering literature was reviewed (cf. Section 2.4). Many solids suspension studies could be found in standard stirred tank systems, though most of them dealing with ungassed, two-phase conditions. It was seen that the *effectiveness of solids suspension* could be evaluated in different ways, mostly aimed at either off-bottom suspension conditions or solids distribution conditions. Methods and procedures to evaluate solids suspension were chosen as follows.

- The *critical impeller speed* (N_{js}), indicating the impeller speed at the just suspended condition, is the most widely used and consistent solids suspension parameter in stirred tank work and will thus be the main focus of this work.
- *Visual* observation of the base whilst applying the *1s criterion* is the most commonly used laboratory technique in identifying the N_{js} in stirred tanks and will thus be applied in this work.
- *Solids distribution* has also been considered in many stirred tank studies, although the findings are not as consistent as off-bottom suspension findings, and it will only be a secondary consideration in this work.
- *Sample withdrawal* was identified as a sufficiently accurate, widely applicable (also in gassed conditions and at high X), and commonly used technique in stirred tank work, and will thus be used to measure *concentration profiles* in this work.

Many studies have *correlated the critical impeller speed* (N_{js}) in stirred tanks to various system conditions. Two-phase studies (N_{jsu}) initially dominated all solids suspension work. The Zwietering correlation [Zwietering (1958)] has been found to be the most influential and widely used N_{jsu} correlation. The same correlation approach will thus be used in this work.

$$N_{jsu} = S d_p^{0.20} B^{0.13} \left(\frac{g(\rho_S - \rho_L)}{\rho_L} \right)^{0.45} \nu^{0.10} D^{-0.85}$$; Where S = f(impeller type, D/T, C/T)

..... (cf. Equation 2-35)

However not all the variables considered in the extensive study by Zwietering will be considered in this work. The effect of all the solid-liquid variables (i.e. d_p, X, $\Delta\rho/\rho_L$, ν_L) on N_{jsu} will be correlated in this work. The effect of scale (i.e. D), as well as other geometry (i.e. S parameter) will however not be considered.

A three-phase N_{jsg} correlation is however needed for application in flotation conditions. Fewer stirred tank works have considered solids suspension conditions in gassed conditions. Amongst the gassed solids suspension studies, most N_{jsg} studies have used the ungassed N_{jsu} correlation as a base to which the effect of gas is then added. The most notable effect of gas addition is to cause a linear increase in N_{jsg} with increased gas addition.

$$N_{jsg} = N_{jsu} + K_a.Q_{GV}$$

.....(cf. Equation 2-46)

However, the slope of this increase, K_a, had been found to be influenced by other system conditions. Some methods of incorporating the effect of gas into the N_{jsg} correlation in stirred tanks have been proposed. This thesis considers a number of different options and proposes an effective way to incorporate the effect of gas into the N_{jsg} correlation for a pilot scale mechanical flotation cell. Another effect that gas addition may have on the N_{jsg} correlation, is a possible influence on the effect of the solid-liquid variables (i.e. d_p, X, $\Delta\rho/\rho_L$, ν_L) under gassed conditions. Inconclusive findings have been reported in stirred tanks, with some reporting reductions in the effect of some variables with gas addition. The effect of the solid-liquid variables will thus be considered under gassed conditions here and compared with two-phase findings. The *development of a gassed N_{jsg} correlation for a mechanical flotation cell*, incorporating the effect of solid-liquid (i.e. d_p, X, $\Delta\rho/\rho_L$, ν_L) and gas variables (J_G) is thus the ***primary aim of this work***.

A ***secondary objective*** of this thesis is to evaluate the solids distribution aspect of solids suspension. Concentration profiles will be measured at different impeller speeds and for different particle sizes and gassed conditions. The findings will be mostly considered qualitatively and mechanistically. However, using concentration profiles together with critical impeller speed measurements, the effectiveness of solids suspension at various impeller speeds can be quantified in different ways. Here, the extent of off-bottom suspension (average profile concentration), the extent of vertical solids distribution (suspension height), and the variation within the vertical concentration (RSD of the vertical concentrations) will be considered.

CHAPTER 3 EXPERIMENTAL

CHAPTER 3 EXPERIMENTAL 119

3.1 EXPERIMENTAL RIG 120
3.2 VARIABLES AND MEASUREMENTS 122
3.2.1 Impeller Speed and Critical Impeller Speed 122
3.2.2 Particle Size and Solids Density 122
3.2.3 Solids Concentration 123
3.2.4 Viscosity and Liquid Temperature 124
3.2.5 Air Addition 126
3.2.6 Frother Addition and Gas Holdup 127
3.3 EXPERIMENTAL PROGRAMME AND PROCEDURES 129
3.3.1 Critical Impeller Speed 130
3.3.1.1 Critical Impeller Speed Measurement 130
3.3.1.2 Critical Impeller Speed Test Programme 130
3.3.2 Solids Concentration Profiles 132
3.3.2.1 Solids Concentration Profile Measurements 132
3.3.2.2 Solids Concentration Profile Test Programme 134

In order to evaluate solids suspension in a pilot-scale mechanical flotation cell, as outlined in Section 2.6, a large number of tests had to be conducted. The experimental rig is described in Section 3.1. In Section 3.2 the variables used and the measurements made in this testwork are described. Finally, the experimental programme and procedures used are described in detail in Section 3.3.

3.1 EXPERIMENTAL RIG

A Batequip (Bateman) pilot flotation cell was used in this testwork as shown in Figure 3.1.

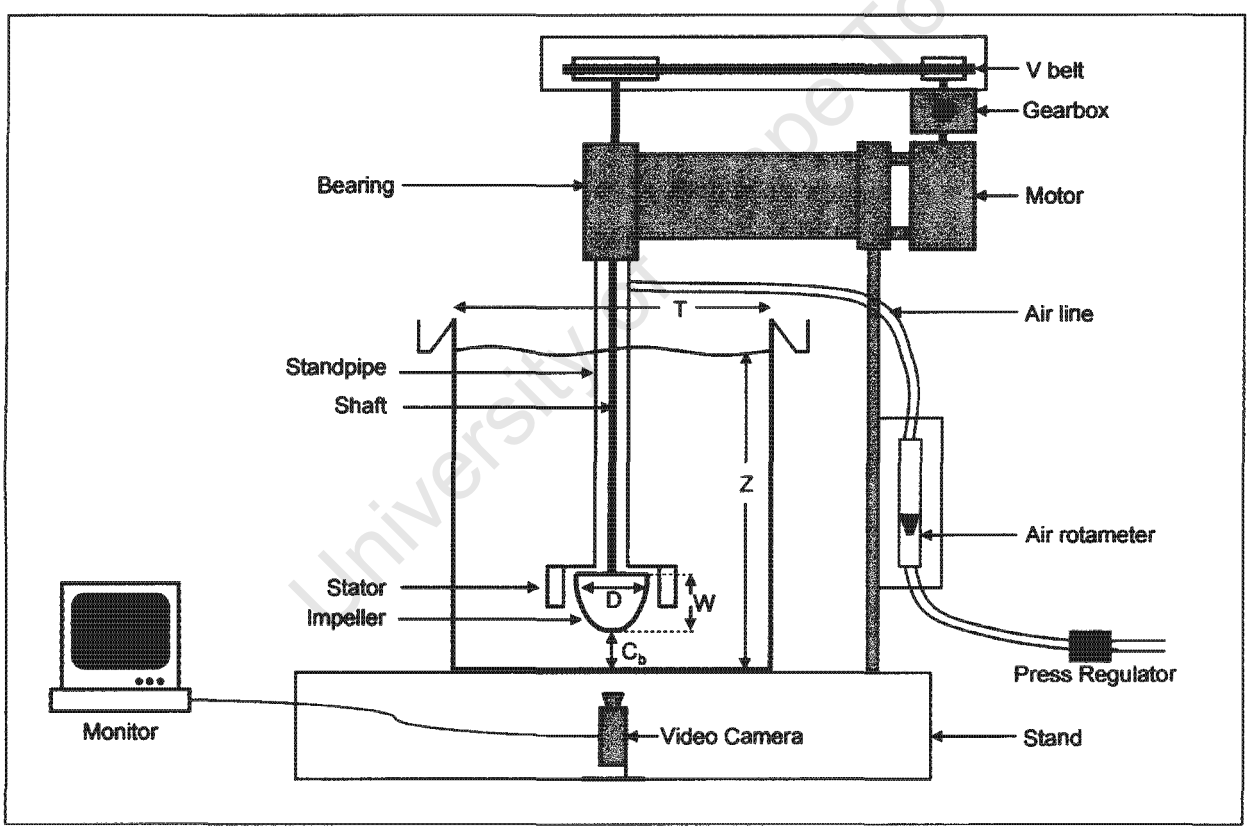

Figure 3.1 Experimental rig

The flotation cell consisted of a 124 l clear tank (T = 0.54m). The static liquid level Z was always equal to the tank diameter T ($Z = T$ = 0.54m). Slurry agitation and air dispersion was achieved by a six bladed Bateman impeller (D_{max} = 0.150 m) and stator mechanism (cf. Figure 3.2). A 1.5 kW three-phase electric motor delivered power to the impeller through an infinitely variable gearbox and V-belt drive assembly. The impeller speed was measured by

an electromagnetic pickup and displayed. Compressed air was used for air addition. The compressed air was passed through a filter to remove impurities and a pressure regulator to ensure constant air addition to the cell. The air addition rate was adjusted by a hand valve and measured by an air rotameter (metric 45G). For visually determining the critical impeller speed, a video camera was fitted below the tank to observe the suspension of solids from the cell bottom through the clear tank. For concentration profile measurements, sampling from the cell was done by sample withdrawal through a vertically adjustable sampling tube. Silica, rutile and zircon sands were used as solids. Size and solids density details of these sands are discussed in the next section. Water with 30ppm frother (MIBC) was used as the liquid in all the tests. The frother was added to ensure constant bubble size, gas dispersion and gas holdup. The impeller-bottom clearance C_b was 15% (C_b = 0.15T = 83mm), which is equivalent to a midpoint clearance C of 25% (C = 133mm = 0.25T). This clearance compares favourably to, C = 25%, recommended in Section 2.4.5.1 for three-phase solids suspension and gas dispersion and resulted in a *double-figure-of-eight* circulation pattern as given in Figure 2.24 (a). Details of the impeller-stator mechanism are shown in Figure 3.2.

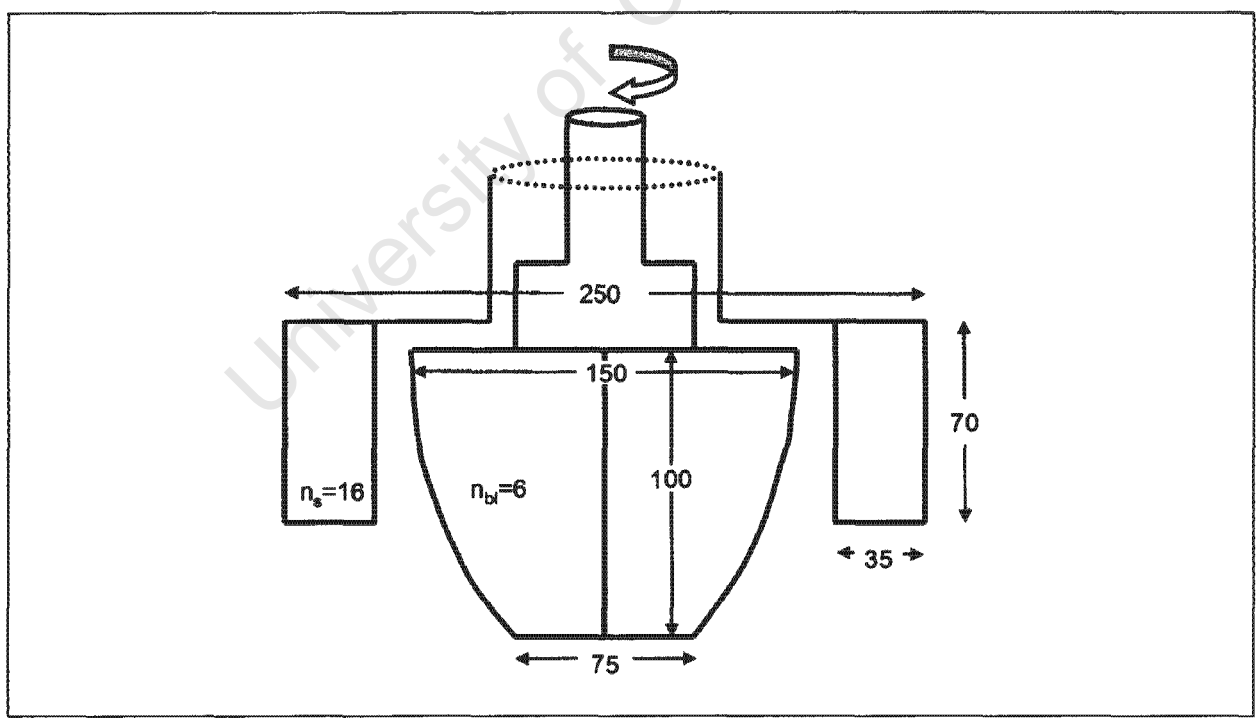

Figure 3.2 Impeller and stator mechanism

It follows from Figure 3.2 that the impeller has a non-isometric vertical profile. This means that the impeller diameter profile above and below the vertical midpoint is not the same, causing the midplane not to co-incide with the maximum diameter as in the case of propellers

and other isometric impellers. Different impeller diameters can thus be determined. In this case the maximum impeller diameter is equal to 0.150 m (D_{max} = 0.150 m), the minimum impeller diameter is equal to 0.075 m (D_{min} = 0.075 m) and the linear average diameter (measured at 10 points) is equal to 0.124 m (D_{avg} = 0.124 m). The maximum impeller diameter will be taken as the impeller diameter for calculation and comparison purposes (D = D_{max} = 0.150m). The minimum gap between the impeller and stator can be calculated from Figure 3.2 as 15mm. It should also be noted that the design of this mechanism is such that the impeller is fully enclosed by the stator above the impeller. This prevents supercharged air escaping from the impeller, but also prevents the recirculation of slurry to the upper eye of the impeller. All slurry thus circulates to the impeller from below and to allow for this, the impeller should thus be sufficiently lifted off the bottom (C_b ~ 15%).

3.2 VARIABLES AND MEASUREMENTS

3.2.1 Impeller Speed and Critical Impeller Speed

The most important variable that was measured during this work was the impeller speed. The rig had an impeller speed indicator installed that worked on an electromagnetic pickup basis. This reading was checked against a photoelectric tachometer and the readings were found to agree to within 1%. All further impeller speed measurements were taken from the rig's impeller speed gauge. The impeller speed was varied between 300 and 1100rpm, which is equivalent to N_{Re} of between 1.125×10^5 and 4.125×10^5 (based on water) and a N_{Fr} number between 0.382 and 5.14. These N_{Re} and N_{Fr} number ranges thus fall well within the ranges given in Table 2.2 for mechanical flotation cells and from the N_{Re} number being larger than 10^5 it can be assumed that the impeller operated in the fully turbulent regime (cf. Section 2.3.1). The determination of the critical impeller speed N_{js} will be discussed in Section 3.3.1.1.

3.2.2 Particle Size and Solids Density

Silica, rutile and zircon sands were used in the testwork. The silica sand ($\rho_{S,sil}$ = 2650 kg/m^3) was obtained from Consol Sand (Cape Town). The rutile ($\rho_{S,rut}$ = 4200kg/m^3) and zircon ($\rho_{S,zir}$ = 4700 kg/m^3) were needed to test for the effect of solids density on solids suspension and was obtained from a heavy sand mining operation in the Northern Cape

Province of South Africa (Namakwa Sands). The sands were sized into size fractions ranging from 75µm to 850µm as shown in Table 3.1. This was done using a 500 mm Rhologan sieve shaker. Approximately 30kg of each size fraction was needed for the testwork to ensure that solids concentrations of up to 20 wt.% could be reached. To check the purity of these sands the densities of a number of samples were checked using a pycnometer. The measured ρ_S values were very consistent and agreed well with literature values as given in Table 3.1 [Wills (1997)].

Table 3.1 Particle size fractions used in this testwork

Sand, ρ_S kg/m^3	Size Fraction µm	Mean Size µm	u_T (exp) [*3] m/s	u_T (calc) m/s
Silica, 2650	75-106	91	[*4]	0.007 [*1]
	106-150	128	0.018	0.015 [*1]
	150-250	200	0.027	0.025 [*2]
	250-500	375	0.068	0.051 [*2]
	500-850	675	0.101	0.099 [*2]
Rutile, 4200	75-106	91	0.019	0.014 [*1]
Zircon, 4700	75-106	91	0.024	0.017 [*1]

[*1]: Stokes Law: $C_D = 24/N_{Re}$; [*2]: Intermediate: $C_D = 18.5/(N_{Re})^{0.6}$; Newton's Law: $C_D = 0.44$; $u_T^2 = 4/3x1/C_D.d_p.(\rho_S-\rho_L)/\rho_L.g$ for spherical particles.; [*3]: Determined by dropping a number of particles in a 1 l measuring cylinder and measuring the time taken to settle between two heights in the cylinder; [*4]: Difficult to measure accurately

As shown in Table 3.1 terminal settling velocities were experimentally determined for some of the sand fractions. These can be compared to the calculated terminal settling velocities to check the average size and the sphericity of the particles. In general, the experimental and calculated terminal settling velocities show good agreement.

3.2.3 Solids Concentration

Tests were conducted at 5, 10, 15 and 20 wt% solids. The relationship between solids mass fraction X, slurry density ρ_{SL}, and solids density ρ_S is given by:

$$X = \frac{\rho_S(\rho_{SL} - \rho_L)}{\rho_{SL}(\rho_S - \rho_L)} \qquad \text{(a)}$$

$$\rho_{SL} = \frac{\rho_S \rho_L}{\rho_S - X(\rho_S - \rho_L)} \qquad \text{(b)}$$

..... Equation 3-1

Solids concentrations are also often given in solids volume fraction φ_S, given by:

$$X = \frac{\phi_S \rho_S}{\phi_S \rho_S + (1-\phi_S)\rho_L} \quad \text{(a)}$$

$$\phi_S = \frac{X/\rho_S}{X/\rho_S + (1-X)/\rho_L} \quad \text{(b)}$$

.....Equation 3-2

The solids concentration conditions for all test conditions are summarised in Table 3.2.

Table 3.2 Solids Concentrations Used In This Work

ρ_S [kg/m^3]	ρ_L [kg/m^3]	X [wt%]	ρ_{SL} [kg/m^3]	m_S [kg]	V_T [m^3]	φ_S [vol%]
2650	1000	5	1032	6.3	0.124	1.9
		10	1066	13.01	0.124	4.0
		15	1103	20.18	0.124	6.2
		20	1142	27.86	0.124	8.6
4200[*1]	1000	5	1040	6.34	0.124	1.2
		10	1082	13.2	0.124	2.6
		15	1129	20.66	0.124	4.0
		20[*3]	-	-	0.124	-
4700[*2]	1000	5	1041	6.35	0.124	1.1
		10	1085	13.24	0.124	2.3
		15	1134	20.73	0.124	3.6
		20[*3]	-	-	0.124	-
2650	1096[*4]	18.6	1230	27.86	0.124	8.6
	1160[*4]	17.7	1288	27.86	0.124	8.6
	1206[*4]	17.2	1331	27.86	0.124	8.6

[*1] - Rutile sand; [*2] - Zircon sand; [*3] - No tests were done here (motor limitations); [*4] - Viscosity work using sugar

3.2.4 Viscosity and Liquid Temperature

Different ways of modifying the viscosity of the liquid were considered. Using organic liquids were considered but they were thought either too expensive to use on such a large scale or too hazardous to use in this environment. Sucrose sugar was considered the safest and least expensive way of modifying the viscosity of the liquid in the tank (corn syrup is also often used). As seen in Section 2.4.4.3.4 (cf. Figure 2.22) the viscosity of a slurry containing about 20 vol.% solids (X~43%; SG_S=3) would vary between a relative viscosity of about 2-3 times that of water, except if it contains large quantities of fines resulting in the d_{50}

dropping below 30µm. It was therefore decided to use a viscosity range that goes beyond a relative viscosity of two, i.e. 2, 4 and 8 (based on relative kinematic viscosities). Dynamic viscosity measurements were done using a Brookfield viscometer to determine how much sugar to add. Liquid sugar solution densities were determined by weighing of 500ml sugar solutions accurately made up in volumetric flasks. These results are shown in Table 3.3.

Table 3.3 Sucrose Sugar Concentrations vs. Solution Density and Viscosity

Sucrose Conc [g/l]	Solution Density [kg/m^3]	Dynamic Viscosity [cP]	Kinematic Viscosity [x 10^{-6} m^2/s]
0	1000	1.00	1.00
100	1037	1.37	1.32
200	1075	1.72	1.60
300	1112	2.48	2.23
400	1150	3.79	3.30
500	1185	6.25	5.27
600	1220	11.60	9.51

Note: 1 cP = 0.001002 kg/m/s = 1.002 mPa.s = water's dynamic viscosity at 20°C

The sugar concentrations to use for kinematic viscosities of 2, 4 and 8 x10^{-6} m^2/s were determined by linear interpolation as shown in Figure 3.3 and were found to be 263, 436 and 564 gpl.

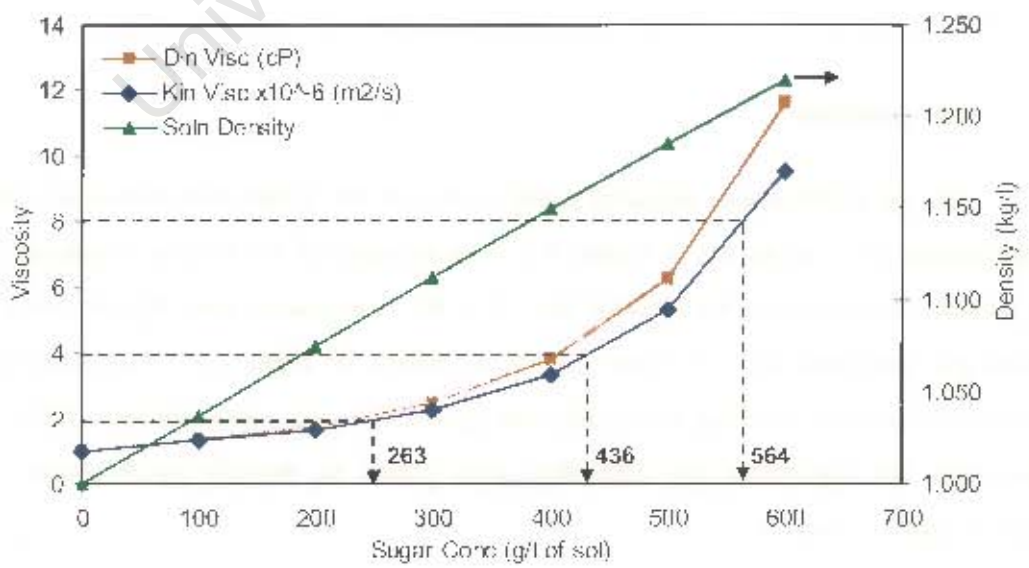

Figure 3.3 Determining the sugar concentrations to use for the viscosity tests

The viscosity of water is also influenced by the temperature of the liquid. Due to the large scale of the test tank, these tests were not done in a water bath to control the temperature of the fluid in the tank. The temperature of the liquid was however monitored using a standard mercury thermometer dipped into the tank, and controlled by a 3kW heating element and ambient cooling to remain within 20 to 25°C as far as possible. As can be seen from Figure 3.4 this variation in temperature causes the viscosity of the water to be 0.95 ± 0.05 cP. The temperature for each test was taken and the variation of viscosity due to temperature as given by the trendline equation was incorporated in the analyses.

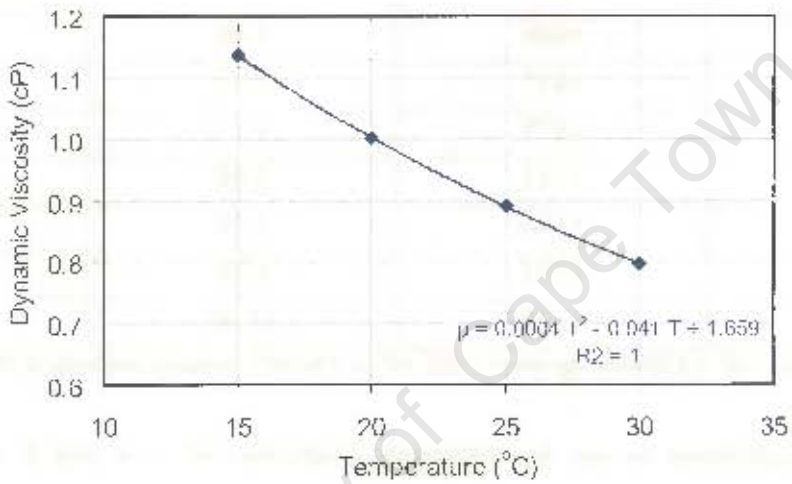

Figure 3.4 The viscosity of water vs. temperature [Data taken from Rogers and Mayhew (1988)]

3.2.5 Air Addition

The air addition was adjusted using a valve in the airline and measured with an air rotameter (metric 45G) as shown in Figure 3.1. The pressure of the feed air was kept constant using a pressure regulator on the air feed line. For the three-phase tests, the air was added at superficial gas velocities of 1, 1.5 and 2 cm/s as shown in Table 3.4. The superficial gas velocity is calculated by dividing the air flowrate Q_G by the cross sectional area of the tank A_c. It follows that the superficial gas velocities used relates to specific air flowrates varying between 1.1 and 2.2 vvm.

Table 3.4 Air Addition Settings and Measurements

Rotameter Setting [cm]	Q_G [m^3/min]	Q_{GV} [m^3/m^3/min]	J_G [cm/s]
0.0	0.000	0.00	0.0
1.5	0.138	1.11	1.0
3.5	0.207	1.67	1.5
6.0	0.276	2.22	2.0

Tank details: T=0.54m; Z=T; V_T=0.124m^3; A_c=0.229m^2; Air rotameter: metric 45G

3.2.6 Frother Addition and Gas Holdup

It is well known that frother concentration has a strong influence on bubble size, gas hold-up and impeller power consumption (cf. Section 2.3.2), which in turn also effects solids suspension. In order to determine which frother concentration to use some tests were conducted where the frother concentration was varied. These results are shown in Figure 3.5.

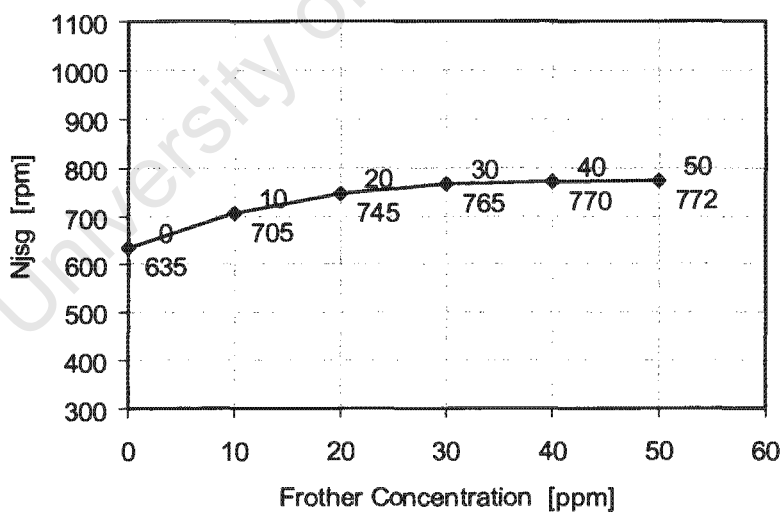

Figure 3.5 Effect of frother concentration on the critical impeller speed

(Silica, 75-106µm, X = 20%, J_G = 1 cm/s, frother = MIBC)

It follows from Figure 3.5 that increased frother additions at low frother concentrations ([MIBC] ≤ 20ppm) causes the critical impeller to increase quite dramatically. At frother concentrations of 30ppm and above the critical impeller speed remains relatively constant with increasing frother concentration. The initial frother concentration at the start of a test

was made up to be 30ppm. During the test, the frother would however evaporate. To maintain the frother concentration at or above 30ppm, the frother concentration was topped up with an additional 10ppm of frother every 30 min's. The average gas hold-up in the tank was found to follow the same trend as critical impeller speed with frother concentration and was used as a check of the frother concentration as shown in Figure 3.6 below.

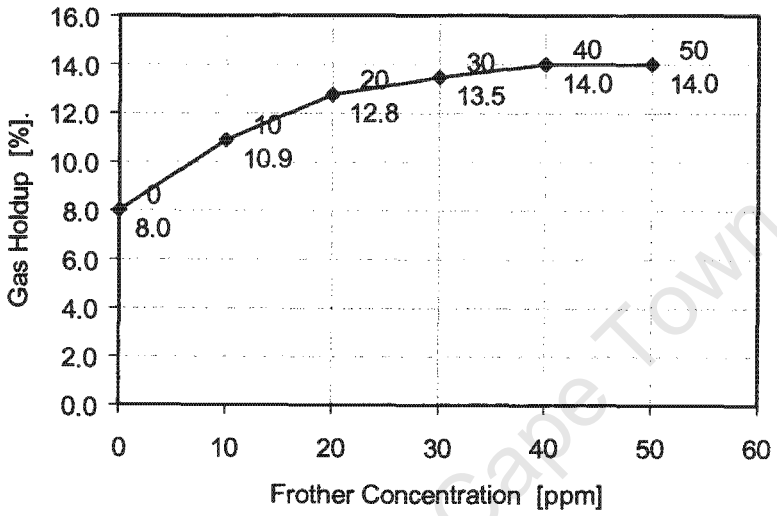

Figure 3.6 Effect of frother concentration on the average gas holdup in the tank

(Silica, 75-106μm, X = 20%, J_G = 1 cm/s, frother=MIBC)

The gas holdup was measured by measuring the expansion of slurry with gas addition (bed expansion technique). The level of the liquid (slurry) was allowed to increase above T on air addition, i.e. $Z_g \geq T$. Using a vertically mounted float on the surface of the liquid, the rise in the liquid level could be determined. This measurement gave the average gas hold-up φ_G in the tank.

3.3 EXPERIMENTAL PROGRAMME AND PROCEDURES

As outlined in the 'Scope and Objectives' in Section 2.6, this work focused primarily on off-bottom suspension in the form of critical impeller speed measurements, whilst solids distribution formed a secondary consideration in the form of concentration profiles measurements. From the literature review (cf. Table 2.6 and Table 2.11), it follows that solids suspension in stirred tanks are mainly influenced by the variables indicated in Table 3.5. The variables that were varied in this test programme are indicated in **bold** text, whilst the values of those kept constant in the programme are also indicated.

Table 3.5 Variables Influencing Solids Suspension and Those Tested In This Work

Variable	Symbol	Varied / Constant	Range / Values	Unit
Tank diameter	T	Constant	0.54	m
Impeller diameter	D	Constant	D= 0.150 (D_{max}); (D/T = 0.278)	m
Impeller clearance (midpoint) Impeller-bottom clearance	C C_b	Constant Constant	0.25 T (0.133 m) 0.15 T (0.083 m)	-
Particle size	$\mathbf{d_p}$	Varied	75-106; 106-150; 150-250; 250-500; 500-850	µm
Solids Mass Concentration	**X**	Varied	5, 10, 15, 20	wt%
Solids Density	$\boldsymbol{\rho_S}$	Varied	2650 (Silica), 4200 Rutile, 4700 (Zircon)	kg/m^3
Liquid Density	$\boldsymbol{\rho_L}$	Varied	1000, 1096, 1160, 1206 (water, 263, 436, 564 gpl sugar soln's)	kg/m^3
Kinematic **Liquid Viscosity** (Dynamic Liquid Viscosity)	**v** (µ)	Varied	1, 2, 4, 8x10^{-6} (@20°C) (1.0, 2.2, 4.4, 9.3x10^{-3})	m^2/s (mPa.s)
Acceleration of gravity	g	Constant	9.81	m/s^2
Gas Flowrate as J_G (Gas Flowrate as Q_{GV})	$\mathbf{J_G}$ (Q_{GV})	Varied	0, 1.0, 1.5, 2.0 (0, 1.11, 1.67, 2.22)	cm/s (vvm)
Frother Concentration	MIBC	Constant	30 (≥30, cf. 3.2.6)	ppm

It follows from Table 3.5 that the variables tested in this work included all the two-phase slurry variables (d_p, X, ρ_S-ρ_L and v) as well as the effect of gas addition J_G on solids suspension. The geometrical variables of impeller diameter D, tank diameter T and impeller clearance C were not tested in this work. The test procedures and test programme to test the effect of the solid-liquid-gas variables on the critical impeller speed and the solids concentration profile will be discussed in more detail in the following two sections.

3.3.1 Critical Impeller Speed

The critical impeller speed N_{js}, describes the solids suspension conditions on the bottom of the tank and is taken at that condition where the solids are just suspended off the bottom of the tank (cf. Section 2.4.4).

3.3.1.1 Critical Impeller Speed Measurement

The *critical impeller speed* for complete suspension N_{js} was determined by gradually increasing the impeller speed from 300 min^{-1} and observing the bottom of the tank from below. The base of the tank was viewed on a PC monitor, using a video camera mounted below the tank (cf. Figure 3.1). The *1s-criterion* introduced by Zwietering (1958) and commonly used by others, was used to determine the just suspended condition (cf. Section 2.4.3.1). As the impeller speed was increased, more and more solids were lifted off the bottom of the tank. Due to the flowline on the bottom of the tank returning from the tank wall to the centre (eye) of the impeller, the last solids to be suspended were in the centre of the tank. This is where the bottom of the tank was observed. At impeller speeds close to the just suspended condition, solids on the bottom of the tank would continuously be suspended and then sediment out again. At a certain impeller speed, the solids would be resuspended off the base within approximately 1s after settling out. As per the 1s criteria, this was taken as the critical impeller speed. The determination of this condition is slightly subjective and the exact point depends on the experience of the observer. The determination of the critical impeller speed was repeated in a number of tests and the results show that the average difference in N_{js} repeats by the same observer was 2%, with the maximum difference being 5%. This compares very well with the repeatability of Zwietering (1958) given as 2-3%, and Chapman *et al.* (1983a) given as repeatable within approximately ±5%.

3.3.1.2 Critical Impeller Speed Test Programme

The critical impeller speed test programme can be divided into three phases. The programme will be discussed here as planned. As will be seen when the results are discussed, it should be noted that some of the critical impeller speeds could not be achieved due to either

the electric motor reaching its maximum power output or the gearbox reaching its maximum speed output.

The aim of the *first phase* was to determine the effect of particle size d_p and solids concentration X on the critical impeller speed. The gas flowrate J_G was varied and tested throughout all phases of the test programme. The variables and ranges for this first phase of testwork are given in Table 3.6. All variables were tested under all conditions, which led to 80 tests being planned for Phase I. These 80 tests consisted of five particle sizes being tested at four percentages solids and at four superficial gas velocities (5x4x4 = 80). Phase I thus consisted of 20 ungassed and 60 gassed tests.

Table 3.6 Critical Impeller Speed Tests Phase I: Effect of Particle Size, Solids Concentration, and Superficial Gas Velocity

Variable	Range/Values
d_p [µm]	75-106; 106-150; 150-250; 250-500; 500-850
X [wt%]	5, 10, 15, 20
J_G [cm/s]	0.0, 1.0, 1.5, 2.0

The *second phase* in the critical impeller speed test programme was to test the effect of solids density on the critical impeller speed. In addition to the silica (ρ_S = 2650 kg/m^3), already tested in Phase I, tests were done using rutile (ρ_S = 4200 kg/m^3) and zircon (ρ_S = 4700 kg/m^3) as shown in Table 3.7. Again all the variables indicated in the table were tested under all conditions leading to an additional 32 tests (1x4x4x2). Phase II thus consisted out of 8 additional ungassed and 24 gassed tests.

Table 3.7 Critical Impeller Speed Tests Phase II: Effect of Solids Density

Variable	Range/Values
d_p [µm]	75-106
X [wt%]	5, 10, 15, 20
J_G [cm/s]	0.0, 1.0, 1.5, 2.0
ρ_S [kg/m^3]	(2650)*, 4200, 4700

*: ρ_S=2650kg/m^3 (silica), was already tested in Phase I

The *third phase* in the critical impeller speed test programme was to test the effect of liquid viscosity on the critical impeller speed. Silica sand of the two smaller size fractions was used in these tests and the liquid kinematic viscosity was varied in addition to 1 x 10^{-6} m^2/s (water), already tested in Phase I, also to 2, 4 and 8 x 10^{-6} m^2/s as shown in Table 3.8 below. Phase III thus led to an additional 12 tests being conducted (2x1x2x1x3), consisting of 6 ungassed and 6 gassed tests.

Table 3.8 Critical Impeller Speed Tests Phase III: Effect of Liquid Viscosity

Variable	Range/Values
d_p [µm]	75-106; 106-150
X [wt%]	20
J_G [cm/s]	0.0, 1.0
ρ_S [kg/m^3]	2650
ν_L [x10^{-6} m^2/s]	(1)*, 2, 4, 8 x 10^{-6}

*: Water (ν_L = 1x10^{-6} m^2/s), was already tested in Phase I.

In conclusion, 124 critical impeller speed tests (34 ungassed and 90 gassed) were planned to determine the effect of solid-liquid-gas variables as indicated in Table 3.5, on the critical impeller speed in a 124 l Bateman pilot flotation cell. The raw critical impeller speed data is given in Table A.1 in Appendix A.

3.3.2 Solids Concentration Profiles

An axial solids concentration profile is a plot of solids concentrations vs. slurry height in the tank, and thus describes the vertical distribution of solids in the vessel (cf. Section 2.4.6).

3.3.2.1 Solids Concentration Profile Measurements

The solids concentrations at different vertical heights X_{hi} were determined by sample withdrawal. A vertical sampling tube was used for sample withdrawal. The bottom of the tube was bent to be horizontal and oriented in a tangential direction in the same direction as impeller rotation. The tip of the sampling tube had a 45° profile to improve isokinetic sampling, as used by Barresi and Baldi (1987a). The radial position of the sampling tube was

midway between the tank wall and the outside of the stator assembly. The rate of sample withdrawal was determined to give a flow velocity in the tube which was approximately 10 times that of the terminal settling velocity of the coarsest particle as indicated in Table 3.1, viz ($u_{sampling}$ ~ 10 x 0.1 = 1 m/s). Barresi and Baldi (1987a), working at solids concentrations below 5 wt.%, found that varying the withdrawal velocity in the range of 0.61 to 1.06 m/s had a relatively small influence on the measured solids concentrations. They further found the average sampled solids concentration to be generally 10-20% lower than the known actual concentration. This was attributed to, lack of isokinetic sampling (diverted fluid / particles), the existence of slight radial profiles, and the uncertainty in sampling the solids concentration near the bottom.

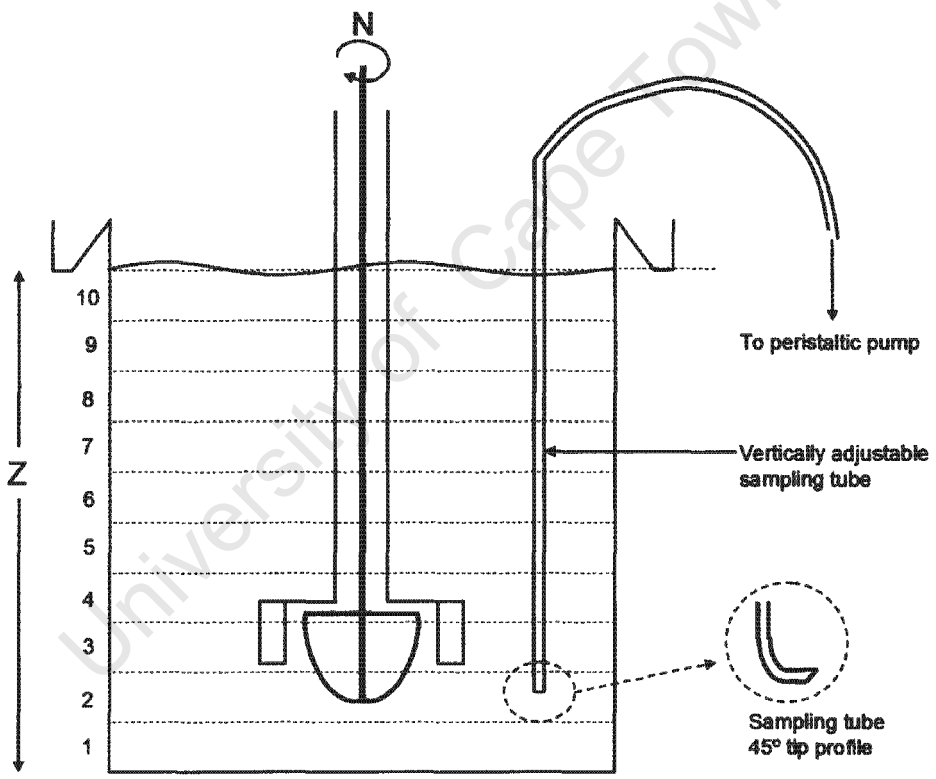

Figure 3.7 Sample withdrawal to obtain solids concentration profiles

As shown in Figure 3.7 the height of the tank was sliced into ten sections. The solids concentration in each section was determined by sample withdrawal midway between the top and the bottom of the slice as indicated in Figure 3.7. The solids concentration was determined by accurately measuring the slurry density of a relatively large withdrawn sample of approximately 3-4 l and then calculating the solids concentration using Equation 3-1 (a).

3.3.2.2 Solids Concentration Profile Test Programme

Solids concentration profiles were measured to determine how the solids distribution varies with impeller speed. This was done for two particle size fractions under both two-phase and three-phase condtions. The 75-106 and 150-250 size fractions were selected to represent a finer and coarser size fraction in a flotation cell in terms of solids suspension. The gassed profiles were done at a superficial gas velocity of 1 cm/s. These profiles were done together with the critical impeller speed measurements and co-incided with runs 29 and 77 for the ungassed and 30 and 78 for the gassed profiles. The conditions for these profiles are given in Table 3.9, and led to 10 ungassed and 12 gassed concentration profiles. The concentration profile results are given in Tables B.1 and B.2 in Appendix B.

Table 3.9 Solids Concentration Profile Conditions

Variable	Range/Values
d_p [μm]	75-106; 150-250
X [wt%]	20
J_G [cm/s]	0.0, 1.0
ρ_S [kg/m^3]	2650
ν_L [m^2/s]	1 x 10^{-6}
N [min^{-1}]	300, 450, 600, 750, 900*, N_{js}

*: Could only be obtained under the gassed conditions

CHAPTER 4 CRITICAL IMPELLER SPEED

CHAPTER 4 CRITICAL IMPELLER SPEED 135

4.1 SOLID-LIQUID TWO-PHASE CRITICAL IMPELLER SPEED 136

4.1.1 The Effect of Solid-Liquid Variables on N_{jsu} 137

4.1.1.1 The Effect of Particle Size on N_{jsu} 138

4.1.1.2 The Effect of Solids Concentration on N_{jsu} 139

4.1.1.3 The Effect of Solids Density on N_{jsu} 141

4.1.1.4 The Effect of Liquid Viscosity on N_{jsu} 143

4.1.2 Critical Impeller Speed Correlation for Two-phase conditions, N_{jsu} 145

4.2 THREE-PHASE CRITICAL IMPELLER SPEED 150

4.2.1 The Effect of Gas Addition on the Critical Impeller Speed 151

4.2.1.1 Critical Impeller Speed, N_{js}, versus Gas Addition, J_G 152

4.2.1.2 Ways of Incorporating the Effect of Gas into the N_{jsg} Correlation 155

4.2.2 Graphical Analyses of the Effect of Solid-Liquid Variables under Gassed Conditions 165

4.2.2.1 The Effect of Particle Size on N_{jsg} 166

4.2.2.2 The Effect of Solids Concentration on N_{jsg} 167

4.2.2.3 The Effect of Solids Density on N_{jsg} 168

4.2.2.4 The Effect of Liquid Viscosity on N_{jsg} 169

4.2.3 Numerical Analyses of the Effect of Solid-Liquid Variables under Various Gassed Conditions 170

4.2.4 Critical Impeller Speed Correlations for Two- and Three-Phase Conditions 174

4.2.5 Summary of Findings and Comparison with Literature 178

4.2.6 Application of N_{jsg} Correlation 180

4.3 CONCLUSIONS 182

4.3.1 Two-Phase Critical Impeller Speed 182

4.3.2 Three-Phase Critical Impeller Speed 183

This chapter discusses the development of a critical impeller speed correlation for complete off-bottom solids suspension in a mechanical flotation cell for both two- and three-phase conditions. It follows from the literature review that *no published critical impeller speed correlations could be found in the flotation literature* (cf. Section 2.5.1). Therefore, the aim of this work was to develop such an N_{js} correlation for a 124 l pilot scale mechanical flotation cell, using the methods as described in Chapter 3 . The N_{js} correlation will first be developed under two-phase conditions in Section 4.1, before developing the three-phase correlation in Section 4.2. These correlations will incorporate the effect of *solid-liquid* variables (i.e. d_p, X, $(\rho_S-\rho_L)/\rho_L$, ν_L) as well as the effect of *gas addition* (J_G) for the three-phase case. Geometrical variables (i.e. T, D/T, C/T, impeller/mechanism design) are however not considered. Both graphical, and numerical analyses methods will be employed in this chapter. Graphical methods have the advantage of visually displaying the data, allowing trendlines to be fitted to demonstrate the quality of the fitted correlation. Multiple linear regression, as the numerical method used in this chapter has the advantage of fitting coefficients to an equation optimally, to minimize the sum of squared errors in the predicted values versus the actual values. It can also quantify the confidence limits of the obtained correlation coefficients.

4.1 SOLID-LIQUID TWO-PHASE CRITICAL IMPELLER SPEED

It follows from Sections 2.4.4 and 2.4.5 by comparing Table 2.6 to Table 2.11 that most critical impeller speed work in stirred tanks have been done under ungassed, two-phase conditions. Two-phase tests are often easier and more repeatable than the three-phase tests, and comparing the ungassed tests with the gassed tests, the effect of gas addition on solids suspension can be isolated. The Zwietering correlation is commonly used to determine the ungassed critical impeller speed for complete off-bottom suspension, N_{jsu}, in *stirred tanks*.

$$N_{jsu} = S^* T^{-0.85} d_p^{\,0.20} B^{0.13} g^{0.45} \left(\frac{\rho_S - \rho_L}{\rho_L} \right)^{0.45} \nu^{0.10} \text{; where } S^* = \text{f}(D/T,\ C/T,\ \text{design}); \text{ Stirred tanks}$$

.....Equation 4-1

[Zwietering (1958)]

As already summarised in Section 2.4.4.2, many other correlations similar to Equation 4-1 have been developed for stirred tanks. Power functions such as Equation 4-1 have been found

to correlate the effects of the most commonly studied solids suspension variables on N_{js} effectively, as summarised in Section 2.4.4.3. Only the effect of impeller clearance, *C/T*, could not be incorporated as a power function due to abrupt transitions in circulation patterns as the impeller clearance is reduced. This led Zwietering and others, to introduce an *S* parameter, which can be graphically displayed as a function of *D/T*, *C/T*, and impeller design [cf. Figure 2.18; $S^* = S(T/D)^{0.85}$].

The aim of this section is to develop an equation similar to Equation 4-1 for a mechanical flotation cell. The 34 ungassed tests planned as part of Phases I, II and III of the experimental programme (cf. Section 3.3.1.2) were designed to produce the following two-phase correlation for a *mechanical flotation cell.*

$$N_{jsu} = K_{SL} d_p^{\,c} X^d \left(\frac{\rho_S - \rho_L}{\rho_L} \right)^e \nu^f \text{ ;Where } K_{SL} = \text{f}(T, D/T, C/T, \text{design}); \text{ Mechanical flotation cell}$$

..... Equation 4-2

It follows that all the solid-liquid slurry variables in the Zwietering equation (Equation 4-1) are included in Equation 4-2. The effect of geometrical variables including scale, *T*, were however not tested in this work, and therefore will the correlation coefficient, K_{SL}, be a function of these, K_{SL} = f (*T*, *D/T*, *C/T*, design). Due to the solids mass concentration, *X*, being commonly used in flotation work it was used in Equation 4-2 instead of the solids to liquid mass ratio, *B*, commonly used by Zwietering and others in their solids suspension work. Acceleration of gravity, *g*, is a constant and if included the exponent of *g* is normally taken the same as for density difference, which follows from a force balance on a settling particle as in the terminal settling velocity equation (cf. Equation 2-18). In this section, the effect of solid-liquid properties on the ungassed critical impeller speed, N_{jsu}, will be considered, first graphically (cf. Section 4.1.1), before developing the N_{jsu} correlation numerically using multiple linear regression in Section 4.1.2. Section 4.1 concludes with comparing the two-phase N_{jsu} correlation developed here for a flotation cell with stirred tank findings.

4.1.1 The Effect of Solid-Liquid Variables on N_{jsu}

The effects of particle size d_p, solids concentration *X*, solid-liquid density difference $(\rho_S-\rho_L)/\rho_L$, and liquid viscosity ν_L on the ungassed critical impeller speed, N_{jsu}, will

be displayed graphically in Sections 4.1.1.1 to 4.1.1.4 and compared with the findings in stirred tanks as already summarised in Section 2.4.4.3. As shown by Equation 4-2, the aim of these plots is to find the power function fit between N_{jsu} and each of the variables (i.e. *c, d, e, f*). Traditionally these power function relations are found by plotting N_{js} against each variable on *log-log plots* and measuring the slope. Measuring the slopes will thus give graphical estimates of the power values *c*, *d*, *e*, and *f* in Equation 4-2. In the next section (4.1.2) these power values will also be determined using multiple linear regression. Good agreement between the graphical and numerical results is a way of double-checking the value of and the confidence in the final result.

4.1.1.1 The Effect of Particle Size on N_{jsu}

As seen in Section 2.4.4.3, Zwietering (1958) found N_{jsu} α $d_p^{0.20}$, whilst the proportionality exponent found by others varied over a fairly large range of between approximately 0.1 and 0.5.

$N_{jsu} \propto d_p^{0.20}$; Stirred tanks

..... Equation 4-3

Zwietering (1958)

The two-phase, N_{jsu} vs. d_p results obtained during Phase I of the experimental programme are shown in Figure 4.1. Of the 20 runs planned, only 17 datapoints were obtained as N_{jsu} could not be reached for some of the larger particle sizes at 15 and 20 wt% solids, as the motor reached its maximum power output.

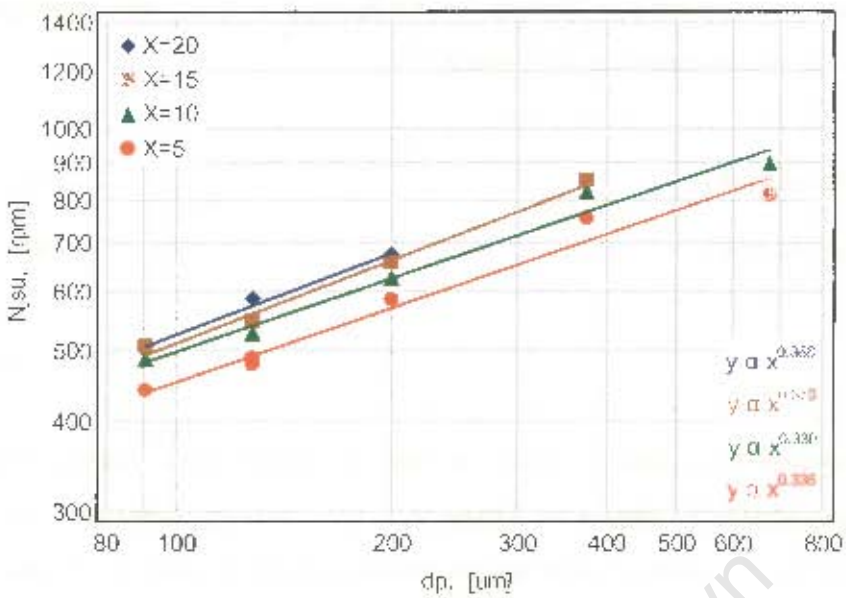

Figure 4.1 The effect of particle size d_p on the ungassed critical impeller speed N_{jsu} for solids concentrations ranging between 5 and 20 wt%

(Exp. Phase 1 (2ph): d_{50} = 91, 128, 200, 375, 675µm; X = 5, 10, 15, 20 wt%; J_G = 0; Silica sand)

It follows from Figure 4.1 that very consistent power relations between N_{jsu} and d_p had been found, varying between $N_{jsu} \propto d_p^{0.33}$ to $N_{jsu} \propto d_p^{0.38}$, for the different solids concentrations tested. Taking the average slope from the four curves gives the following relation.

$N_{jsu} \propto d_p^{0.35}$; A mechanical flotation cell (graphical analysis)

..... Equation 4-4

This effect of d_p on N_{jsu} is stronger than that found in stirred tanks by Zwietering (cf. Equation 4-3) and most others, and is thought to be related to the proximity of the stator to the impeller in a flotation cell as compared to baffles in a stirred tank which are fitted to the sides of the tank. The stator decreases fluid flow in favour of increased turbulence in the vicinity of the impeller. Fluid flow is an important suspension mechanism of especially the larger particles, with higher settling velocities.

4.1.1.2 The Effect of Solids Concentration on N_{jsu}

Zwietering (1958) found the effect of solids-liquid mass ratio B as shown in Equation 4-5(a), which can be converted to the effect of solids concentration X (cf. Equation

4-5(b)) as already demonstrated in Section 2.4.4.3.2, i.e. $B \propto X^{1.27}$. The findings of others in stirred tanks varied mostly between $B^{0.10}$ and $B^{0.25}$.

$N_{jsu} \propto B^{0.13}$; Stirred tanks (a)

$N_{jsu} \propto X^{0.17}$; Stirred tanks (b)

.....Equation 4-5

Zwietering (1958)

The relation between N_{jsu} and X found in the two-phase tests during Phase 1 of the experimental programme is shown in Figure 4.2. As already mentioned in the previous section, some of the N_{jsu} values could not be determined at X equal to 15 and 20% for the coarser particle sizes as the just suspended conditions laid above the maximum power the electric motor could deliver.

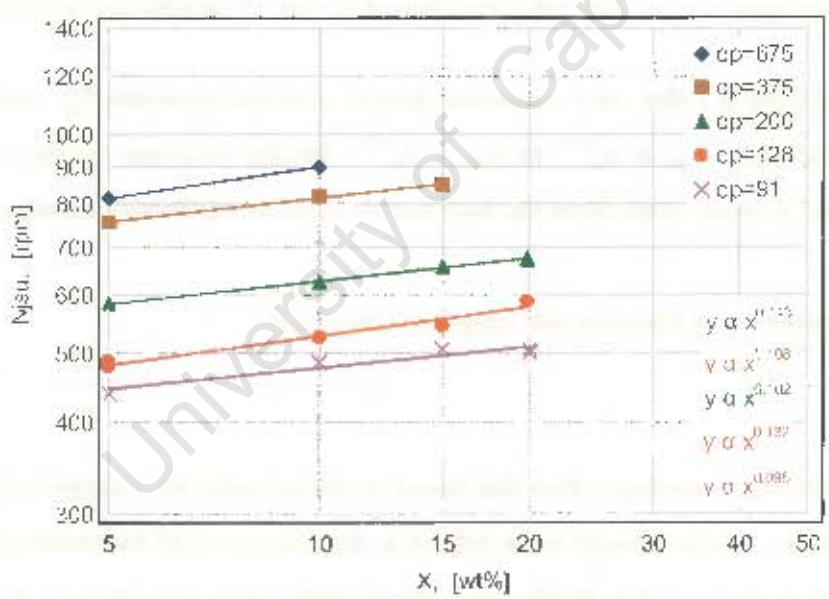

Figure 4.2 The effect of solids concentration X on the ungassed critical impeller speed N_{jsu} for average particle sizes ranging between 91 and 675 µm

(Exp. Phase 1 (2ph): d_{50} = 91, 128, 200, 375, 675µm; X = 5, 10, 15, 20 wt%; J_G = 0; Silica sand)

It follows from Figure 4.2 that fairly consistent power relations between N_{jsu} and X were obtained with the exponent varying between 0.10 and 0.14. Taking the average slope from the five curves gives the following relation.

$N_{jsu} \propto X^{0.12}$; A mechanical flotation cell (graphical analysis)

..... Equation 4-6

Comparing Equation 4-6 to Equation 4-5, it follows that the relation between N_{js} and X for this flotation cell is slightly weaker than that found by Zwietering and others in stirred tanks. The smaller effect of X in this work using a mechanical flotation cell is difficult to explain but may be related to the relatively low impeller clearance used in this work ($C/T = 0.25$ or $C_b/T = 0.15$) apart from other geometrical differences in impeller and baffling design. On balance though it can be concluded that changes in solids concentration have a relatively small influence on the critical impeller speed in a flotation cell.

4.1.1.3 The Effect of Solids Density on N_{jsu}

With respect to solids density, Zwietering (1958), and others decided to incorporate the effect of solids density in the form of relative solid-liquid density difference $[(\rho_S-\rho_L)/\rho_L]$. This is the same form that solids density affects the terminal settling velocity as already shown in Equation 2-18. Zwietering found the proportionality exponent between N_{jsu} and the relative density difference to be 0.45 as shown in Equation 4-7, whilst other findings varied mostly between 0.40 and 0.50 in a relatively narrow band.

$$N_{jsu} \propto \left(\frac{\rho_S - \rho_L}{\rho_L} \right)^{0.45}$$; Stirred tanks

..... Equation 4-7

Zwietering (1958)

The effect of solids density on N_{jsu} can be derived from the two-phase runs in Phase II of the experimental program using rutile (ρ_S = 4200 kg/m^3) and zircon (ρ_S = 4700 kg/m^3), and comparing it to the d_{p91} tests using silica (ρ_S = 2650 kg/m^3) in Phase I of the experimental program as already shown in Table 3.7. N_{jsu} could not be reached at X = 20% for rutile and zircon, which resulted in only three curves as shown in Figure 4.3 for X = 5, 10 and 15%.

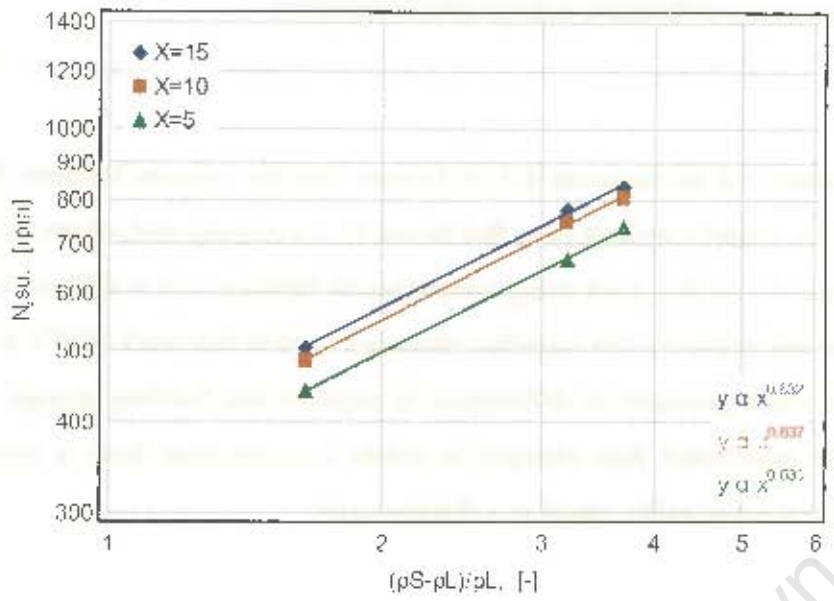

Figure 4.3 The effect of relative solid-liquid density difference $[(\rho_S-\rho_L)/\rho_L]$ on the ungassed critical impeller speed N_{jsu} for solids concentrations ranging from 5 to 15%

(Exp. Phases I & II (2ph): d_{50} = 91μm; X = 5, 10, 15 wt%; ρ_S = 2650, 4200, 4700 kg/m^3; ρ_L=1000 kg/m^3; J_G = 0 cm/s)

Although only three curves were obtained, the consistency of the proportionality exponents in the power functions in Figure 4.3 is very encouraging with the slopes varying only between 0.63 and 0.64, with an average of 0.63.

$$N_{jsu} \propto \left(\frac{\rho_S - \rho_L}{\rho_L}\right)^{0.63}$$; A mechanical flotation cell (graphical analysis)

.....Equation 4-8

From this section on the influence of solids density on the just suspended impeller speed, it follows that solids density has a large effect on the critical impeller speed. Similar to the findings on d_p, the effect of $[(\rho_S-\rho_L)/\rho_L]$ found here for a flotation cell, is also stronger than the relation found in stirred tanks. It is interesting to note that d_p and $[(\rho_S-\rho_L)/\rho_L]$ are also the two main variables affecting the particle settling velocity (cf. Equation 2-18). This supports the notion that the reason for the stronger relations between N_{jsu} and d_p, and $[(\rho_S-\rho_L)/\rho_L]$ in a flotation cell may be related to baffling arrangements in a flotation cell vs. baffles on the sides in a stirred tank. As already mentioned, the stator decreases fluid flow in favour of increased turbulence in the vicinity of the impeller. This finding suggests that fluid flow is an important

suspension mechanism of especially the larger and higher density particles, with higher settling velocities.

4.1.1.4 The Effect of Liquid Viscosity on N_{jsu}

It was seen in Table 2.6 that only some of the N_{js} investigators considered the effect of liquid viscosity in the form of kinematic viscosity, ν_L, on N_{js}. Of those that did, the findings for the power function exponent varied mostly between 0 and 0.10, with some thus finding ν_L to have no effect on N_{js}.

$N_{jsu} \propto \nu^{0.10}$; Stirred tanks

..... Equation 4-9

Zwietering (1958)

The stirred tank solids suspension work thus suggests that N_{js} is either independent of ν_L or the effect of ν_L on N_{js} is given by a relatively small proportionality exponent of not more than approximately 0.1. A small proportionality exponent indicates that only large changes in ν_L will have significant effects on N_{js}. Liquid viscosity can display large variations in some processes where viscosity thus might still have a large influence on N_{js}, despite its low proportionality exponent. If for example the power relation is given by $N_{js} \propto \nu_L^{0.10}$, then N_{js} will only be changed by more than 10% if the kinematic viscosity changes by more than 2.5 times (consider $2.5^{0.10} = 1.10$).

The liquid in flotation cells consists mainly of water. The viscosity of water is modified by liquid temperature and by dissolved components (cf. Section 3.2.4), but the effects of these in industrial flotation cells are normally relatively small. However, if the liquid is seen as a *pseudofluid* of water and fine solids, the slurry viscosity may be taken as the fluid viscosity. As already shown in Figure 2.22 (cf. Section 2.4.4.3.4), slurry viscosity is increased by solids concentration and the effect is more significant with very fine particle sizes. In flotation cells solids concentrations in the region of 40% is commonly used, which is comparable to a φ_S of just below 20 vol% given a ρ_S of 3 kg/l (cf. Equation 3-2 in Section 3.2.3). At this solids concentration the slurry viscosity is only significantly increased to more than 2 to 3 times that of water when the slurry is very fine with d_{50}'s below 40 and especially 30 µm.

With this in mind, the effect of v_L on N_{js} in a flotation cell was investigated by varying v_L up to 8 times that of water during Phase III of the experimental programme (cf. Section 3.3.1.2). These tests for two-particle sizes d_{p91} and d_{p200} at 20 wt% solids are then compared with the equivalent tests tests during Phase I of the experimental programme. The N_{jsu} vs. v_L results of these tests are displayed in Figure 4.4.

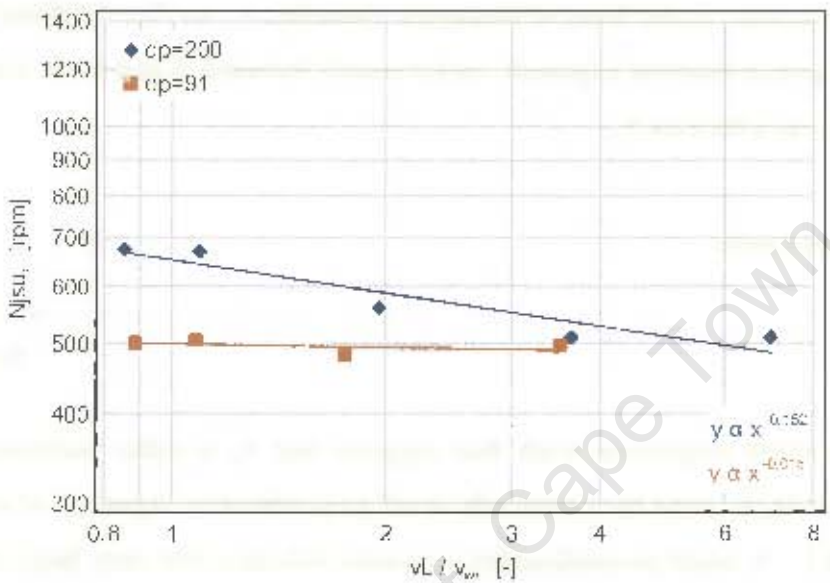

Figure 4.4 The effect of kinematic liquid viscosity v_L (and ρ_L) on the critical impeller speed N_{jsu} for d_{50} = 91, 200 µm

(Exp. Phases I and III (2ph): d_{50} = 91µm, 200µm; X = 20 wt%; ρ_S = 2650 kg/m^3; ρ_L=1000, 1160, 1206 kg/m^3; J_G = 0 cm/s; v_w @ 20°C = 1x10^{-6} m^2/s)

It can be seen from Figure 4.4 that the kinematic viscosities were slightly lower than the planned 2, 4 and 8 times that of water. This is purely a function of the liquid temperature in the tank being mostly above 20°C in the region of 25°C (cf. Figure 3.4 in Section 3.2.4). The double data points appearing at $v_L/v_w \sim 1$ is from duplicate runs. Although Figure 4.4 shows the results of N_{jsu} vs. v_L using sugar solutions it can not be used to graphically determine the effect of v_L on N_{jsu}. The reason for that being that the addition of sugar to modify v_L causes a simultaneous change in ρ_L and thus in $[(\rho_S-\rho_L)/\rho_L]$. The change in the N_{jsu} values in Figure 4.4 thus shows the combined effect of $[(\rho_S-\rho_L)/\rho_L]^e.v_L^f$. Fortunately, the effect of $[(\rho_S-\rho_L)/\rho_L]$ on N_{jsu} was already determined as shown in Equation 4-8, $N_{jsu} \propto [(\rho_S-\rho_L)/\rho_L]^{0.63}$. Removing the effect of changes in $[(\rho_S-\rho_L)/\rho_L]$ on the N_{jsu} values in Figure 4.4 leads to Figure 4.5 to show the effect of v_L alone.

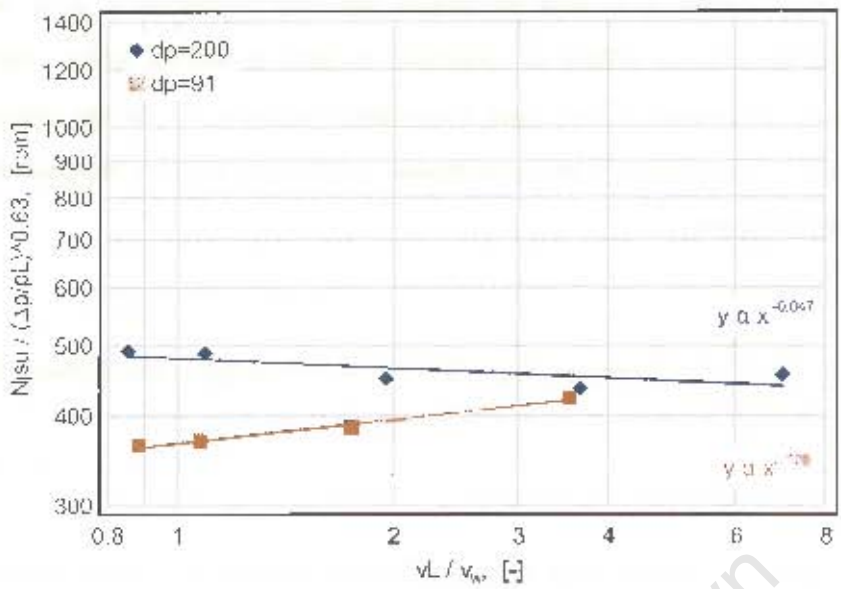

Figure 4.5 The effect of kinematic liquid viscosity ν_L on the critical impeller speed N_{jsu} for d_{50} = 91, 200 µm

(Exp. Phases I and III (2ph): d_{50} – 91µm, 200µm; X = 20 wt%; ρ_S = 2650 kg/m^3; ρ_L=1000, 1160, 1206 kg/m^3; J_G = 0 cm/s; ν_w @ 20°C = 1x10^{-6} m^2/s)

From Figure 4.5 it follows that the effect of liquid viscosity on the critical impeller speed was found to be slightly conflicting. For the finer (d_{50} = 91µm) particle size fraction the liquid kinematic viscosity caused the just suspended impeller speed to increase at a rate of $N_{jsu} \alpha \nu^{0.11}$, which is similar to that found by Zwietering ($N_{jsu} \alpha \nu^{0.10}$). However, for the coarser size fraction (d_{50} = 200µm), ν_L gave a slight decreasing effect of ν_L on N_{jsu}, ($N_{jsu} \alpha \nu^{-0.04}$), which was unexpected. These results show the effect of ν_L on N_{jsu} to be relatively small but inconclusive. In comparison, results from stirred tank work are also somewhat inconclusive with workers given the proportionality exponent of kinematic viscosity to be small but mostly variable between 0 and 0.10.

$N_{jsu} \propto \nu^{(\text{varied } -0.05 \text{ to } 0.11)}$; A mechanical flotation cell (graphical analysis)

..... Equation 4-10

4.1.2 Critical Impeller Speed Correlation for Two-phase conditions, N_{jsu}

In this section, the critical impeller speed correlation will be developed for the two-phase solids suspension tests in the pilot mechanical flotation cell using multiple linear regression. Referring back to Equation 4-2, it follows that the aim of this two-phase critical

impeller speed (N_{jsu}) section is to find the power function exponents ***c***, ***d***, ***e***, and ***f***. These exponents indicate the relative effects of variations in particle size d_p, solids concentration X, solid-liquid density difference $\Delta\rho/\rho_L$, and kinematic viscosity ν_L on the ungassed critical impeller speed N_{jsu}. The value of the correlation coefficient K_{SL} for the specific geometry used here will also be found.

$$N_{jsu} = K_{SL} d_p^{\,c} X^{d} \left(\frac{\rho_S - \rho_L}{\rho_L} \right)^{e} \nu^{f} \text{ ; where } K_{SL} = \text{f}(T, D/T, C/T, \text{design}); \text{ Mechanical flotation cell}$$

..... (cf. Equation 4-2)

Multiple linear regression can be used to fit coefficients to terms in a linear equation (e.g. $y = m_1x_1 + m_2x_2 + \ldots + m_nx_n + K$). However, Equation 4-2 is not a linear equation, but a power function. Power functions can however be linearised by taking logarithms on both sides of the equation.

$$\log N_{jsu} = \log K_{SL} + c.\log d_p + d.\log X + e.\log \left(\frac{\rho_S - \rho_L}{\rho_L} \right) + f.\log \nu \text{ ; (from Equation 4-2)}$$

..... Equation 4-11

The following numerical strategy was used for the analysis of the two-phase data. The data from all the N_{jsu} tests during Phase I and II of the experiments were analysed first (cf. first 27 entries in Table A.2). This gave the exponents for d_p, X, and $\Delta\rho/\rho_L$ as shown in Table A.12. In a second step, the viscosity tests using sugar solutions were included. In this analysis the exponents for d_p, X, and $\Delta\rho/\rho_L$ were fixed as already determined in the first step. This therefore gave the effect of viscosity during all the runs and not only the runs in Phase III. The reason for doing this is also to include the effect of temperature variations on the viscosity and not only the effect of the sugar solutions. The results from this second analysis are given in Table A.13 in Appendix A. These numerical results are summarised in Table 4.1 and compared with the graphical results obtained in the previous section.

Table 4.1 Two-phase Critical Impeller Speed Correlation Results

Analyses	Exponents of N_{jsu} Power Function $N_{jsu} = K_{SL}\, d_p^{\,c}\, X^d\, (\Delta\rho/\rho_L)^e\, v^f$				
	K_{SL}	$d_p^{\,c}$	X^d	$(\Delta\rho/\rho_L)^e$	$v_L^{\,f}$
Graphical analyses		0.35 (0.33-0.38)	0.12 (0.10-0.14)	0.63 (0.63-0.64)	-0.03 (-0.05 to 0.11)
Numerical analysis	54.1	0.35 ± 0.02	0.12 ± 0.02	0.66 ± 0.05	-0.01 ± 0.03
This Work (Proposed) [*1]	**54.1**	**0.35**	**0.12**	**0.66**	**~ 0**

[*1]: Values are given with 95% confidence intervals

It is encouraging to see that the numerical results generally agree very well with the graphical results obtained in the previous section. The graphical viscosity trends were conflicting in the previous section. The numerical results including all the tests confirm that the effect is still conflicting but so small that it can be ignored. The results from Table 4.1 can be incorporated into a two-phase critical impeller speed correlation as follows.

$$N_{jsu} = K_{SL} d_p^{\,0.35} X^{0.12} \left(\frac{\rho_S - \rho_L}{\rho_L} \right)^{0.66} ; K_{SL} = 54$$

..... Equation 4-12

A mechanical flotation cell

The quality of the fit of the predicted values from using Equation 4-12 to the experimentally measured critical impeller speed values are graphically displayed in Figure 4.6. It can be seen from Figure 4.6 that the quality of the fit is very good ($r^2 = 0.963$). Only one value (from the viscosity tests) lie outside the ± 10% deviation lines.

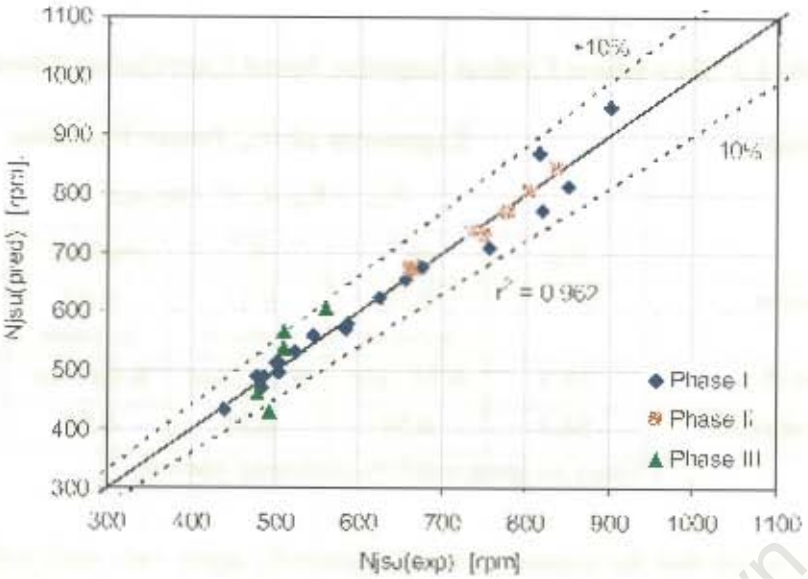

Figure 4.6 N_{jsu} predicted by Equation 4-12 vs. experimentally measured N_{jsu} values (excludes viscosity work)

Finally, the two-phase critical impeller speed findings obtained in this mechanical flotation cell can be compared to standard stirred tank results from literature (cf. Table 4.2).

Table 4.2 Comparison of Two-phase Critical Impeller Speed Results with Literature

Reference	Exponents of Variables in N_{jsu} Power Function $N_{jsu} = K\, T^a\, D^b\, d_p{}^c\, X^d\, (\Delta\rho/\rho_L)^e\, \nu^f$					
	$d_p{}^c$	$X^{d\ (*1)}$	$(\Delta\rho/\rho_L)^e$	$\nu_L{}^f$	$(D/T)^{b\ (*2)}$	$T^{a+b\ (*2,*3)}$
Zwietering (1958)	0.20	0.17	0.45	0.10	-2.35 (DT) -2.15 (FT)	-0.85
Summary of Stirred Tanks findings (cf. Table 2.6)	0.1-0.5	0.1-0.3	0.4-0.5	0-0.1	-1.9 to -2.4	-0.76 to -0.85
This Work (Proposed) [*4]	**0.35** ± 0.02	**0.12** ± 0.02	**0.66** ± 0.05	~ **0**		

[*1]: Solids concentration is often also correlated as the effect of solids to liquid mass ratio B on N_{jsu} to change from B to X the exponents were multiplied by 1.27 being the power relation between B and X over the range $5\% \leq X \leq 50\%$ as used in this work and applicable to flotation cells (cf. Section 2.4.4.3.2).;
[*2]: Dependent on impeller type; quoted here for turbine type radial impellers (e.g. DT = disc turbine, FT = flat blade turbine);
[*3]: Indicator of scale (D is also sometimes used to indicate scale);
[*4]: Values are given with 95% confidence intervals

Comparing the two-phase results from this work to that found for stirred tanks as shown in Table 4.2 it follows that solids particle size (d_p) and solids density difference ($\Delta\rho/\rho_L$) seems to

have stronger influences in a mechanical flotation cell, than found by most in stirred tank work. As already alluded to in Sections 4.1.1.1 & 4.1.1.3 it is thought that this might be related to the proximity of the stator to the impeller in a flotation cell as compared to baffles in a stirred tank, decreasing fluid flow in favour of increased turbulence mostly in the vicinity of the impeller. Variations in solids concentration (X) seems to have a relatively small influence on the critical impeller speed in flotation cells, which is also smaller than what many found in stirred tanks. As already discussed, the effect of viscosity on N_{jsu} was slightly contradicting and inconclusive, but small enough to ignore within the liquid viscosity range tested in this work ($\nu_L/\nu_w \sim 1$ to 8). This is in agreement with what some also found in stirred tank work.

In order to extend these two-phase results to three-phase conditions, gas is added into the system and the effect of these two-phase variables on N_{js}, under gassed conditions, as well as the effect of gas itself on N_{js} will be considered in the next sections.

4.2 THREE-PHASE CRITICAL IMPELLER SPEED

In this section the gassed critical impeller impeller speed (N_{jsg}) correlation for the pilot mechanical flotation cell used in this work will be developed. N_{jsg} correlations for standard stirred tanks have already been discussed in Section 2.4.5 and summarised in Table 2.11. It is evident from comparing Table 2.11 with Table 2.6, which summarises the two-phase critical impeller speed findings, that much less work has been done in three-phase environments than in two-phase, solid-liquid systems. The three-phase correlations are commonly divided into two parts. A first part, $N_{jsu'}$, which incorporates the effects of the two-phase variables (i.e. d_p, X, $\Delta\rho/\rho_L$, ν_L) under gassed conditions, and a second part, which incorporates the effect of gas addition (Q_G) on the gassed critical impeller speed.

As already mentioned in the two-phase section of this chapter, N_{jsu} for standard stirred tanks is commonly calculated using the Zwietering equation.

$$N_{jsu} = S^* T^{-0.85} d_p^{0.20} B^{0.13} g^{0.45} \left(\frac{\rho_S - \rho_L}{\rho_L} \right)^{0.45} \nu^{0.10} \text{; Where } S^* = \text{f}(D/T,\ C/T,\ \text{design})\text{; Stirred tanks}$$

..... (cf. Equation 4-1)

[Zwietering (1958)]

In this work, the effect of geometrical variables (e.g. T, D/T, C/T, design)) on the ungassed critical impeller speed N_{jsu}, were not considered. The form in which the solid-liquid variables will be incorporated under gassed conditions is thus given by Equation 4-13 (a). As was seen from Table 2.11, many have found that N_{jsg} increases linearly with gas addition (cf. Equation 4-13 (b)), although other forms of incorporating the effect of gas addition have also been proposed.

$$N_{jsu'} = K_{SL} d_p^{\ e'} X^{d'} \left(\frac{\rho_S - \rho_L}{\rho_L} \right)^{e'} \nu^{f'} \text{; Where } K_{SL'} = \text{f}(T,\ D/T,\ C/T,\ \text{design}) \qquad \text{(a)}$$

$$N_{jsg} = N_{jsu'} + K_a . Q_G \qquad \text{(b)}\ ^{(*1)}$$

..... Equation 4-13

*1: Different forms of $N_{jsg} = \text{f}(N_{jsu'}, Q_G)$ have been proposed (cf. Table 2.11): (1) $K_a = a$ = constant for given geometry; or (2): $K_a = K.N_{jsu'}$; or (3): $N_{jsg} = N_{js}(1+Q_{GF})^m$; or (4): K_a = a function of system variables, e.g. D, T, u_T, N_{Rep}, etc.

The aim of this three-phase section is summarised by Equation 4-13. Equation 4-13 (a) suggests that the ungassed critical impeller speed correlation, N_{jsu}, is used as the starting point for the three-phase correlation, N_{jsg}. The applicability of using the N_{jsu} equation as already developed in Section 4.1, to incorporate the effect of two-phase variables (e.g. d_p, X, $(\rho_S-\rho_L)/\rho_L$, ν_L) under three-phase conditions should be considered. Conflicting c, d, e, and f exponents for the two-phase variables in gassed conditions have been reported for stirred tanks (cf. Table 2.11). Chapman *et al.* (1983c) and Wong, Wang and Huang (1987) have proposed that the exponents of some of the two-phase variables reduce significantly from two-phase to three-phase conditions, whilst Dutta and Pangarkar (1995) and Dohi *et al.* (2003) used exponents very similar to that proposed by Zwietering for two-phase conditions. The other aim of this three-phase section is given by Equation 4-13 (b). Equation 4-13 (b) suggests that the effect of gas addition is incorporated separately from the two-phase effects with most finding that the addition of gas causes a linear increase in N_{jsg}. The slope of the linear increase in N_{jsg} is however not a constant under all conditions and different forms of Equation 4-13 (b) have thus been suggested for stirred tanks, and suitable forms of incorporating the effect of gas for the mechanical flotation cell used here will be considered.

This section will achieve the aim of finding Equation 4-13 for the mechanical flotation cell by first considering the effect of gas on the critical impeller speed (cf. Equation 4-13 (b)) in Section 4.2.1. Once the effect of gas has been determined, the influence of the solid-liquid variables can be considered under gassed conditions. The effect of the two-phase variables on the critical impeller speed will be considered graphically in Section 4.2.2. After graphical inspection and analyses of the data, multiple linear regression will be employed in Section 4.2.3 to fine-tune the three-phase critical impeller speed correlation numerically. The three-phase findings will then be summarised and compared with literature findings in Section 4.2.5.

4.2.1 The Effect of Gas Addition on the Critical Impeller Speed

This section will consider the form of Equation 4-13 (b), i.e. the way to incorporate the way that gas addition increases the critical impeller speed. Referring to Section 3.3.1.2 in the experimental chapter, it follows that the effect of air addition was mainly considered in Phases I and II of the experimental runs, where the conditions were

changed from ungassed (J_G = 0 cm/s), to air addition rates of J_G = 1.0, 1.5, and 2.0 cm/s. The viscosity tests during Phase III only considered either ungassed or gassed conditions (J_G = 1.0 cm/s), and will not be used here to determine the effect of gas. Two- and three-phase results of all three experimental phases are given in Table A.11 in the appendix. In Section 4.2.1.1, N_{js} will be considered graphically against J_G to see how N_{js} increases with increased air addition. Thereafter four methods, derived from literature, of incorporating J_G into the N_{js} correlation will be evaluated in turn in Section 4.2.1.2. This will lead to a decision on the form of Equation 4-13 (b) to adopt here for the pilot mechanical flotation cell.

4.2.1.1 Critical Impeller Speed, N_{js}, versus Gas Addition, J_G

When all the critical impeller speed values (N_{js}), as given in Table A.11, are plotted against gas addition, Figure 4.7 is obtained. A couple of observations can be made from this figure. *Firstly*, as expected, it can be seen that there is a general increase in N_{js} values as gas was introduced and as the gas addition rate was increased from 1.0 to 2.0 cm/s. *Secondly*, it can be seen that there are less data points at J_G = 1.5 and 2.0 cm/s. This is only partly due to the 6 additional Phase III viscosity runs that were only conducted at both J_G = 0 and 1.0 cm/s. Some of the N_{js} speeds at J_G = 1.5 and 2.0 cm/s could not be reached due to the maximum impeller speed of the gearbox (N_{max} ~ 1100 rpm) being reached first. As indicated in Table A.8, could 20 of the 28 tests planned at J_G = 1 cm/s be reached (experimental Phases I and II). On the other hand could only 14 and 12 tests be reached at J_G = 1.5 and 2.0 cm/s out of also 28 tests planned for both gassing rates (cf. Table A.9 and Table A.10). These critical impeller speeds that could not be reached occurred especially at the larger particle sizes, solids concentrations, solids densities, and gas rates. *Thirdly*, it can be seen that there is a larger spread in the N_{js} datapoints at J_G = 1 than for the ungassed tests, although the same number of tests were conducted at both conditions (34 tests, excluding repeats). This is a graphical demonstration of the fact that N_{js} is generally more difficult to determine during gassed than ungassed conditions, and that gassed N_{js} results generally have lower levels of precision than ungassed tests. This is partly the reason, for much solids suspension work, even for three-phase processes, being conducted in ungassed conditions.

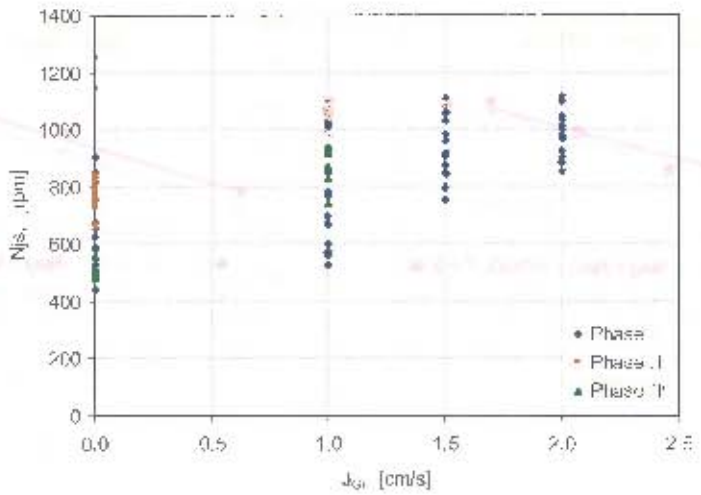

Figure 4.7 Graphical presentation of all N_{js} results vs. air addition rate, J_G

Although Figure 4.7 give a useful overview of the effects of gas addition on the N_{js} results, the specifics of the effect of gas addition on the critical impeller speed is hidden by the large number of data points obtained under different conditions being shown together. In order to focus on the way that gas addition increases N_{js}, similar conditions will be grouped together. Results from Phase I, where in addition to gas addition, the solids density and particle size was also varied, are given in Figure 4.8. Results from Phase II, where in addition to gas addition, the solids density was also varied, are given in Figure 4.9.

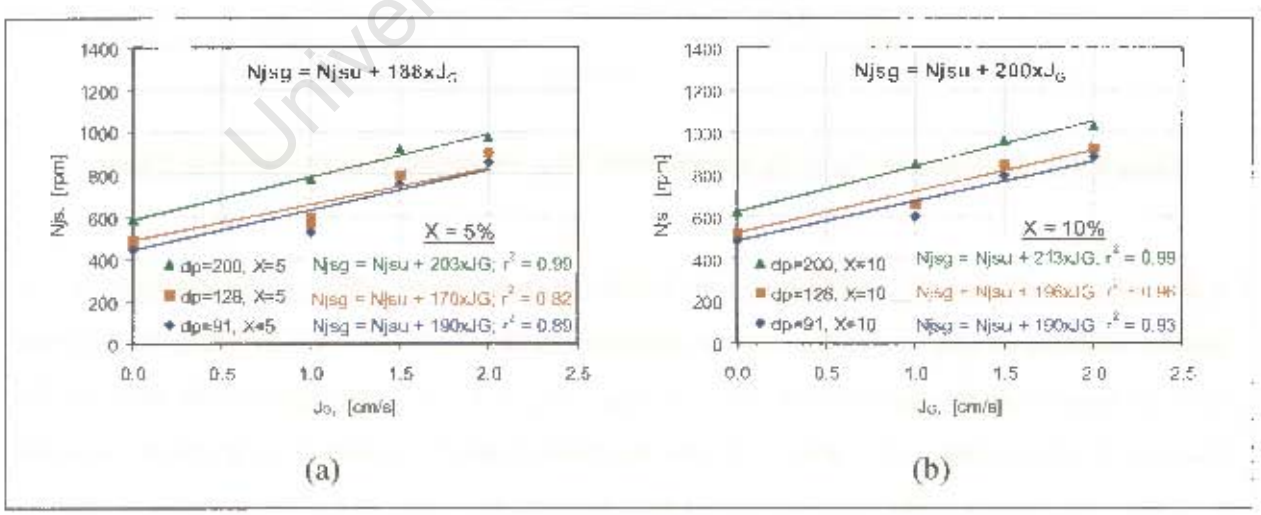

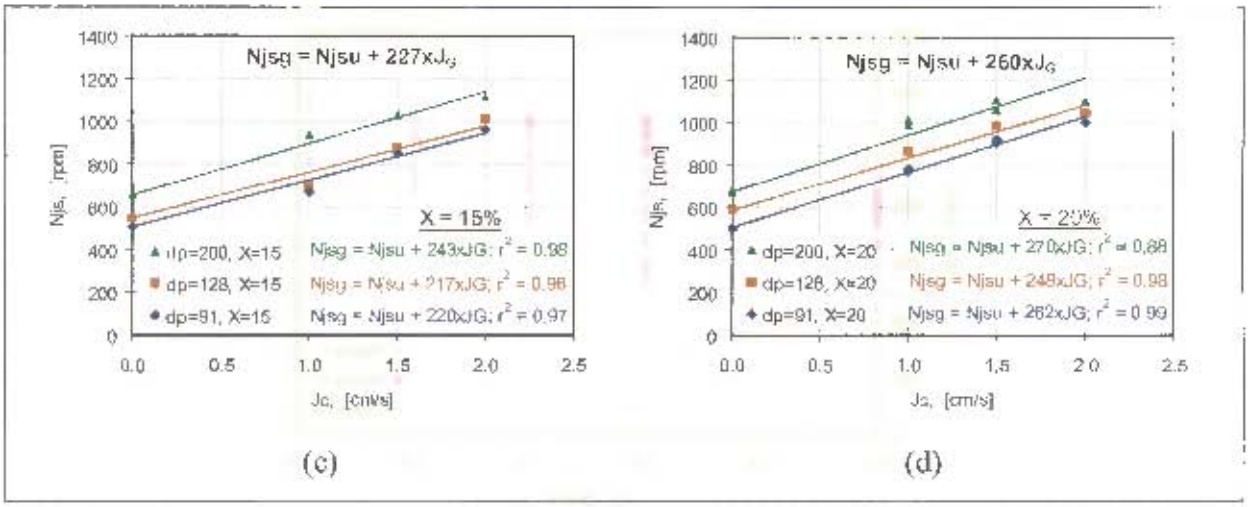

Figure 4.8 Increase in N_{js} with air addition (J_G) obtained in experimental Phase I, (a)-(d): X = 5, 10, 15, and 20 wt%

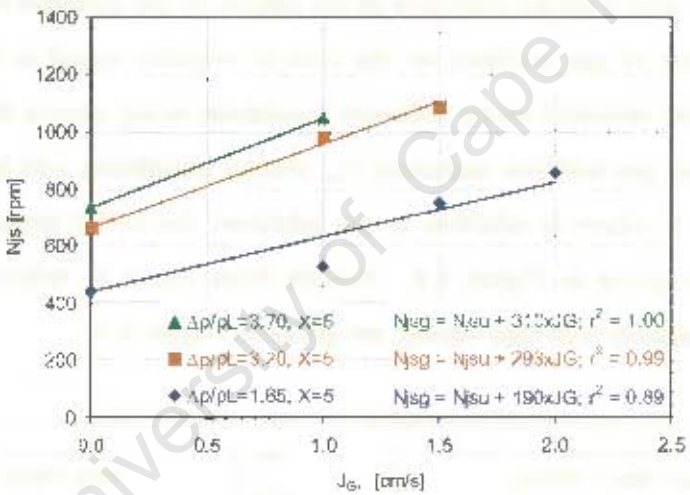

Figure 4.9 Increase in N_{js} with air addition (J_G) obtained in experimental Phase II

It follows from Figure 4.8 and Figure 4.9, which summarises the effect of gas addition on N_{js}, that the addition of gas causes the critical impeller speed (N_{js}) to increase and that the increase in N_{js} is linear with the gas flowrate (J_G), i.e. $N_{jsg} = N_{jsu} + K_a.J_G$. This agrees with many of the findings in stirred tanks (cf. Table 2.11) and the form of the N_{jsg} equation as given in Equation 4-13 (b). The slopes of the lines on the graphs indicate the value of K_a. It can be seen that K_a varies for different conditions. It is noticeable from Figure 4.8 that the value of K_a increases as solids concentration, X, increases from 5 to 20%. There is also some indication that K_a increases somewhat with d_p. Figure 4.9 indicates furthermore strong increases in K_a with increasing solids density differences, $\Delta\rho/\rho_L$. It therefore seems that the effect of gas on the

critical impeller speed increases with increasing X, d_p, and $\Delta\rho/\rho_L$. These observations will suffice for now. The K_a values indicated on Figure 4.8 and Figure 4.9 will be revisited in the next section, where different forms of Equation 4-13 (b) will be applied to the experimental dataset to see how effective each method is in incorporating the effect of gas addition into the N_{jsg} correlation.

Table 4.3 Rate of Linear Increase in N_{js} with Gas Addition, K_a, for Different Conditions (Obtained from Figure 4.8 & Figure 4.9)

#	K_a	N_{jsu}	d_p	X	$\Delta\rho/\rho_L$
1	**190**	440	91	5	1.65
2	**170**	487	128	5	1.65
3	**203**	585	200	5	1.65
4	**190**	485	91	10	1.65
5	**196**	525	128	10	1.65
6	**213**	625	200	10	1.65
7	**220**	505	91	15	1.65
8	**217**	545	128	15	1.65
9	**243**	656	200	15	1.65
10	**262**	505	91	20	1.65
11	**248**	587	128	20	1.65
12	**270**	670	200	20	1.65
13	**293**	663	91	5	3.20
14	**310**	735	91	5	3.70

4.2.1.2 Ways of Incorporating the Effect of Gas into the N_{jsg} Correlation

Four methods for incorporating the effect of gas addition, J_G, on the gassed critical impeller speed, N_{jsg}, will be evaluated in this section. In other words, different forms of Equation 4-13 (b) will be evaluated here. These four methods can be derived from correlations given in literature for stirred tanks, as summarised in Table 2.11 (cf. Section 2.4.5.4), and will be referred to as Option 1 to 4. In the following sections, these four options will be evaluated in the following way. The first step is to fit the specific $N_{jsg} = f(N_{jsu}, J_G)$ correlation to the experimental data. After determining the correlation coefficient in this way, the resultant equation for incorporating the effect of gas addition can be tested. The testing of the equation is done by turning the equation around (i.e. make N_{jsu} the subject of the equation) and calculating the ungassed critical impeller speed from the gassed measurements. These *predicted* or calculated ungassed critical impeller speeds, $N_{jsu'}$, can then be compared to the

relevant experimentally measured ungassed critical impeller speeds, N_{jsu}. The better the parity fit between $N_{jsu'}$ and N_{jsu}, the more suitable the equation will be judged to incorporate the effect of gas on N_{js}.

4.2.1.2.1 Option 1: $N_{jsg} = N_{jsu} + K_a.J_G$; $K_a = a = const$

Option 1 assumes that K_a = a, is a constant for a given geometry. Different values of a are then normally given for different types of impellers and impeller diameters. The approach of Option 1 has been followed by Chapman *et al.* (1983c), Wong, Wang and Huang (1987), and Dutta and Pangarkar (1995). This approach leads to the following form of Equation 4-13 (b), which will be tested in this section (cf. Equation 4-14).

$N_{jsg} = N_{jsu} + K_a.J_G$; Where, K_a = a = const for certain geometry (a)

Or,

$\Delta N_{js} = N_{jsg} - N_{jsu} = K_a.J_G$; Where, K_a = a = const for certain geometry (b)

.....Equation 4-14

Only one geometry was used in this work, and thus according to this option, ΔN_{js} should be a linear function of J_G (cf. Figure 4.10).

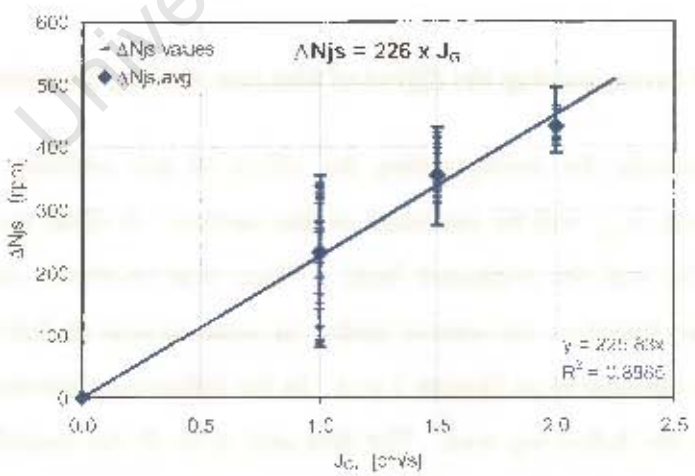

Figure 4.10 Nominal increase in critical impeller speed (ΔN_{js}) vs. J_G

It follows from Figure 4.10 that the best fitted value of 'a' to be used in Equation 4-14 (a) is equal to 226 rpm.$(cm.s^{-1})^{-1}$.

$N_{jsg} = N_{jsu} + a.J_G$; Where a = 226 rpm.(cm.s^{-1})$^{-1}$; (Or, a = 3.4 vvm^{-1}.s^{-1})

..... Equation 4-15

It follows from Figure 4.10 that the fitted line agrees reasonably with the average increases in N_{js} with gas addition. However, despite a reasonable coefficient of determination ($r^2 = 0.89$), it can be seen that many increases (ΔN_{js} values) were higher or lower than that predicted by the fitted line. The effectiveness of Equation 4-15 to incorporate the effect of gas can be evaluated by calculating $N_{jsu'}$ values from gassed N_{jsg} data points and comparing them with the equivalent N_{jsu} measurements (cf. Figure 4.11).

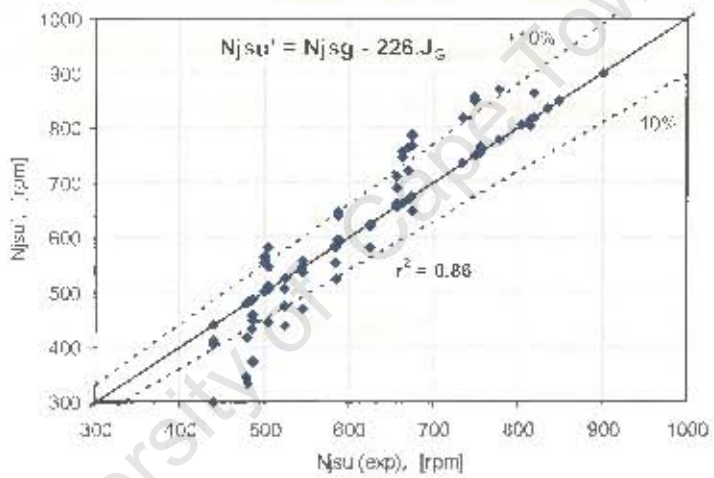

Figure 4.11 Predicted $N_{jsu'}$ values using $N_{jsu'} = N_{jsg} - a.J_G$ vs. experimentally measured N_{jsu} values; a = 226 rpm.(cm/s)$^{-1}$

The parity chart in Figure 4.11 is reasonable but not very good ($r^2 = 0.86$). Quite a number of data points fall outside the ± 10% deviation lines. It is noticeable that $N_{jsu'}$ values were underpredicted at the low end and overpredicted at the high end. This means that the effect of gas were *over*predicted at the low end and *under*predicted at the high end, using the correlation, $N_{jsu'} = N_{jsg} - 226.J_G$. The '*a*' value obtained here can be compared with that derived from graphical results presented by Weiss and Schubert (1989) (cf. Section 2.5.1). In the 54l cell they used the slope of the increase in N_{jsg} with gas addition was measured as, a = 2.4 vvm^{-1}.s^{-1}. Converting the '*a*' value obtained in this work (124 l cell) to the same units one obtains, $a = 3.4$ vvm^{-1}.s^{-1}. It therefore follows that gas addition caused a larger increase in this larger Bateman impeller, than with the smaller double finger impellers used by Weiss and

Schubert (1989). One would normally expect the smaller impeller, which operates at a higher rpm, to experience a larger nominal increase with gassing. This may be due to the much smaller impeller clearance ($C_b = 0.05T$) used by Weiss and Schubert compared to the higher impeller clearance used here ($C_b = 0.15T$).

4.2.1.2.2 Option 2: $N_{jsg} = N_{jsu} - K.N_{jsu}.J_G$

Option 2 assumes that K_a is proportional to N_{jsu} (i.e. $K_a = K.N_{jsu}$) and is thus dependent on system variables in the same way as N_{jsu}. Chapman *et al.* (1983c) found that the value of K_a was influenced by the relative impeller diameter, and found that $K_a \propto (D/T)^{-2.42}$. This is the same as the dependency they found for N_{jsu} on D/T, $N_{jsu} \propto (D/T)^{-2.45}$, for disc turbines. Thus both K_a and N_{jsu} has the same dependency on D/T from which it can be hypothesised that the same applies to all the variables that influences N_{jsu} and thus that $K_a \propto N_{jsu}$. This approach was also proposed by Bujalski, Konno and Nienow (1988) and leads to the Equation 4-16 form of Equation 4-13 (b), which will be tested here.

$N_{jsg} = N_{jsu} + K.N_{jsu}.J_G = N_{jsu}(1 + K.J_G)$; Where, K = const (a)

Or dividing by N_{jsu},

$\Delta N_{js}/N_{jsu} = N_{jsg}/N_{jsu} - 1 = K.J_G$; Where, K = const (b)

.....Equation 4-16

Whether, K_a was proportional to N_{jsu} can be tested by considering the K_a values obtained from Figure 4.8 and Figure 4.9 as summarised in Table 4.3.

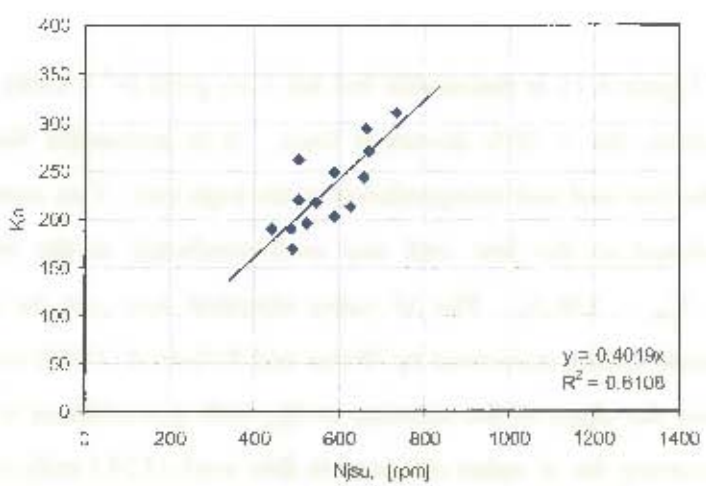

Figure 4.12 K_a values from graphical results in Figure 4.8 and Figure 4.9 vs. N_{jsu}

It follows from Figure 4.12, that the K_a values generally increased with increasing N_{jsu}, although it is not a very good linear trend. The coefficient to determine in this equation is the value of K, $K_a = K.N_{jsu}$. Figure 4.12, which considers the graphical results, suggests that the value of K should be around 0.40, but using Equation 4-16 (b) the value of K can be fitted as follows.

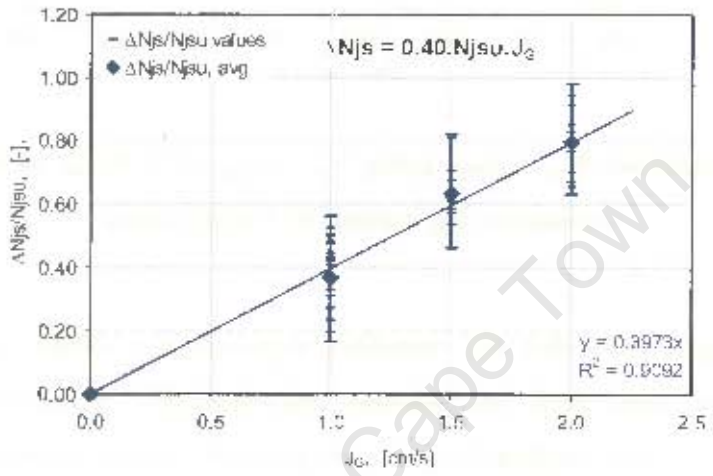

Figure 4.13 Relative increase in critical impeller speed ($\Delta N_{js}/N_{jsu}$) vs. J_G

Figure 4.13 confirms that the best-fitted value of K is indeed 0.40 $(cm/s)^{-1}$, although many ΔN_{js} values still lie above or below the fitted line. This leads to the following form of Equation 4-16 (a).

$$N_{jsg} = N_{jsu}(1 + K.J_G) \; ; \; \text{Where, } K = 0.40 \; (cm.s^{-1})^{-1} \; ; \; (\text{Or, } K = 0.36 \; vvm^{-1})$$

.....Equation 4-17

Again the effectiveness of this equation to incorporate the effect of gas addition can be tested by comparing the calculated ungassed critical impeller speeds, N_{jsu}'s, with the experimentally measured ungassed critical impeller speeds, N_{jsu}.

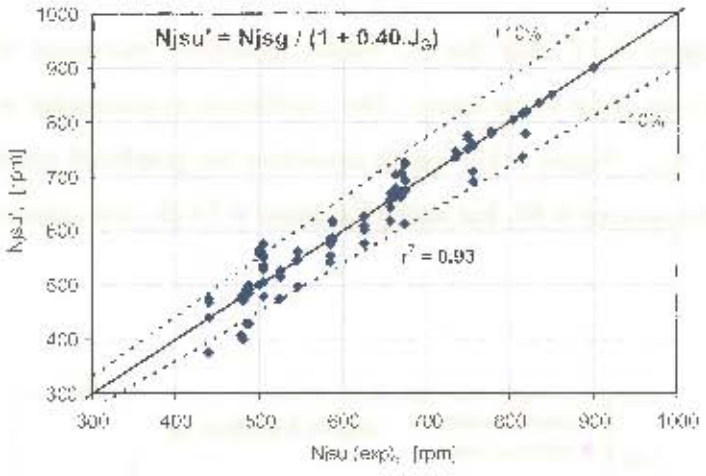

Figure 4.14 Predicted $N_{jsu'}$ values using $N_{jsu'} = N_{jsg} / (1 + K.J_G)$ vs. experimentally measured N_{jsu} values; K = 0.40 (cm/s)$^{-1}$

It follows from Figure 4.14 that the calculated ungassed $N_{jsu'}$ values using Equation 4-17 compares relatively good with the relevant experimentally measured ungassed critical impeller speeds, N_{jsu}. The predicted values are generally spread symmetrically around the parity line, with only some points at the lower end lying slightly above and below the 10% deviation lines. The improved fit compared to Option 1 is confirmed by the higher coefficient of determination, $r^2 = 0.93$. As with Option 1, this result can again be compared with that derived from graphical results presented by Weiss and Schubert (1989). It was seen in Option 1 that the impellers they used caused a lower nominal increase in the critical impeller speed. The relative increase can be determined by dividing the nominal increase, $a = 2.4$ vvm^{-1}.s^{-1}, by the ungassed critical impeller speeds of 8.5 and 9.5 s^{-1} obtained for the two types of impellers used in their work. This gives the relative increase caused by gas in Weiss and Schubert's work to vary between 0.25 and 0.28 vvm^{-1}. It follows that the relative increase in N_{js} caused by gas addition from Weiss and Schubert's work is smaller than the 0.36 vvm^{-1} obtained here. Apart from differences in the designs of the impellers they used compared to the Bateman impeller, the low impeller clearance of $C_b = 0..05.T$ might also have contributed to the smaller effect they found.

4.2.1.2.3 Option 3: $N_{jsg} = N_{jsu}(1 + J_G)^m$

Option 3 was also proposed by Bujalski, Konno and Nienow (1988) and is the only method where the effect of gas on N_{jsg} is not incorporated as a second linear term but as

another factor added onto the N_{jsu} product function. J_G can however not be added as another product term as is, and therefore $(1+J_G)$ is used to prevent the product from becoming zero when gassing is removed. This form has the advantage of considering gassing in the same manner as the other variables that influence N_{js}, i.e. on log-log basis to determine the proportionality exponent. However, most findings in literature and the findings as already given in Figure 4.8 and Figure 4.9 suggests a linear relation between N_{jsg} and J_G and not a power function. This form of Equation 4-13 (b) is given in Equation 4-18.

$$N_{jsg} = N_{jsu}(1 + J_G)^m$$

Or dividing by N_{jsu},

$$N_{jsg}/N_{jsu} = (1 + J_G)^m$$

.....Equation 4-18

The value of the exponent, m, can be determined by fitting a power function to the following plot.

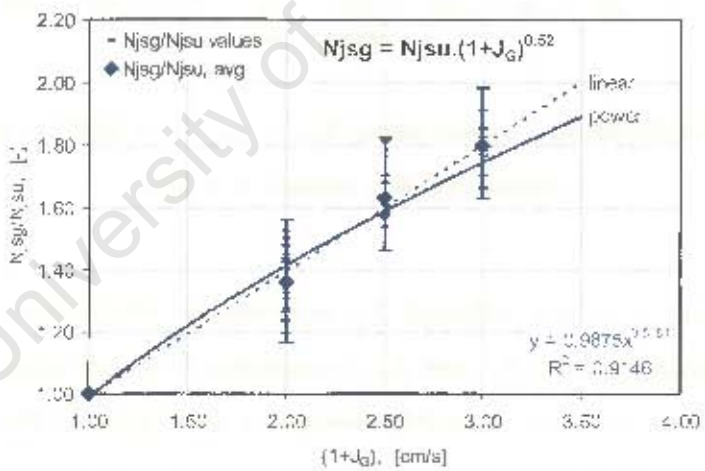

Figure 4.15 Relative increase in critical impeller speed as a power function of $(1+J_G)$

It follows from Figure 4.15 that the best fitted value of m is equal to 0.52 (cf. Equation 4-19). A linear fit similar to option 2 (dotted line) is also indicated on Figure 4.15, which can be seen to generally be in better agreement with the experimental observations. When comparing the power function fit to this line, it can be seen that a power function fit will generally be overpredicting the effect of gas at low gassing and underpredicting the effect at high gassing rates.

$$N_{jsg} = N_{jsu'}(1 + J_G)^{0.52}$$

.....Equation 4-19

Once more, the quality of this fit can be evaluated by comparing the predicted ungassed critical impeller speeds, $N_{jsu'}$, using Equation 4-19 with the experimentally measured ungassed critical impeller speeds, N_{jsu} (cf. Figure 4.16).

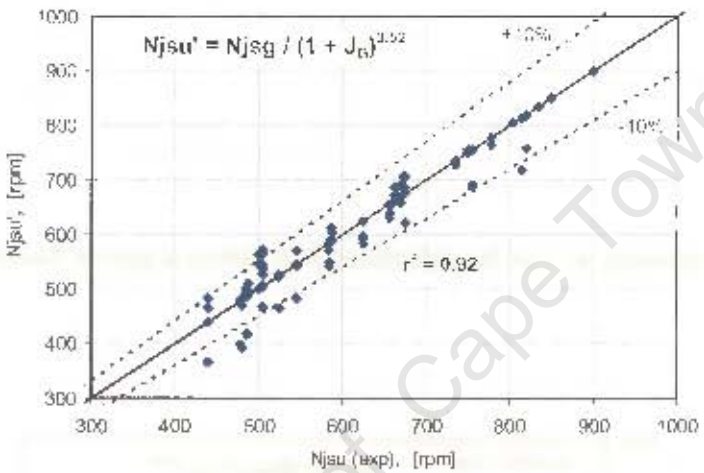

Figure 4.16 Predicted $N_{jsu'}$ values using $N_{jsu'} = N_{jsg} / (1 + Jg)^m$ vs. experimentally measured N_{jsu} values; m = 0.52

It follows from Figure 4.16 that, although the experimental observations does not suggest a power function relation between N_{jsg} and J_G, a reasonable fit is still achieved when the effect of gas is incorporated in this way. However, compared with Option 2 the quality of the parity fit is slightly reduced with slightly more points lying outside ± 10% deviation lines. The same is suggested by the very slightly reduced coefficient of determination, $r^2 = 0.92$.

4.2.1.2.4 Option 4: $N_{jsg} = N_{jsu} + K.d_p^{0.11}.X^{0.23}.(\Delta\rho/\rho_L)^{0.62}.J_G$

Option 4 proposes that K_a is equal to a product function of some system variables. Along this theme Rewatkar, Raghava Rao and Joshi (1991) has suggested that K_a is equal to a power function containing u_T, D, and T (i.e. $K_a \propto u_T^{0.5}.D^{-1.67}.T$) whilst Dohi *et al.* (2003) suggested a more complex function power function containing N_{jsu}, u_T, and N_{Rep} (i.e. $K_a \propto u_T^{-}$

$^{0.2}N_{Rep}^{0.4}$). To develop this method of incorporating the effect of gas for this work, the relation between K_a and other variables is needed. From the graphical analyses done in Figure 4.8 and Figure 4.9 it was already noticed that K_a increased with X, d_p, and $\Delta\rho/\rho_L$. It can therefore be postulated that $K_a \propto d_p^{m1}.\ X^{m2}.\ (\Delta\rho/\rho_L)^{m3}$, which leads to the following form of Equation 4-13 (b) as given in Equation 4-20.

$N_{jsg} = N_{jsu} + K_a J_G$; Where, $K_a = \mathrm{K}\ d_p^{m1}.\ X^{m2}.\ (\Delta\rho/\rho_L)^{m3}$ (a)

Or dividing by N_{jsu},

$\Delta N_{js} = N_{jsg} - N_{jsu} = K_a J_G$; Where, $K_a = \mathrm{K}\ d_p^{m1}.\ X^{m2}.\ (\Delta\rho/\rho_L)^{m3}$ (b)

..... Equation 4-20

Considering the K_a values in Figure 4.8 and Figure 4.9, it can be seen that K_a shows the largest variation with X and $\Delta\rho/\rho_L$. Taking the K_a values given on the figures and plotting the relevant ones against X and $\Delta\rho/\rho_L$ leads to.

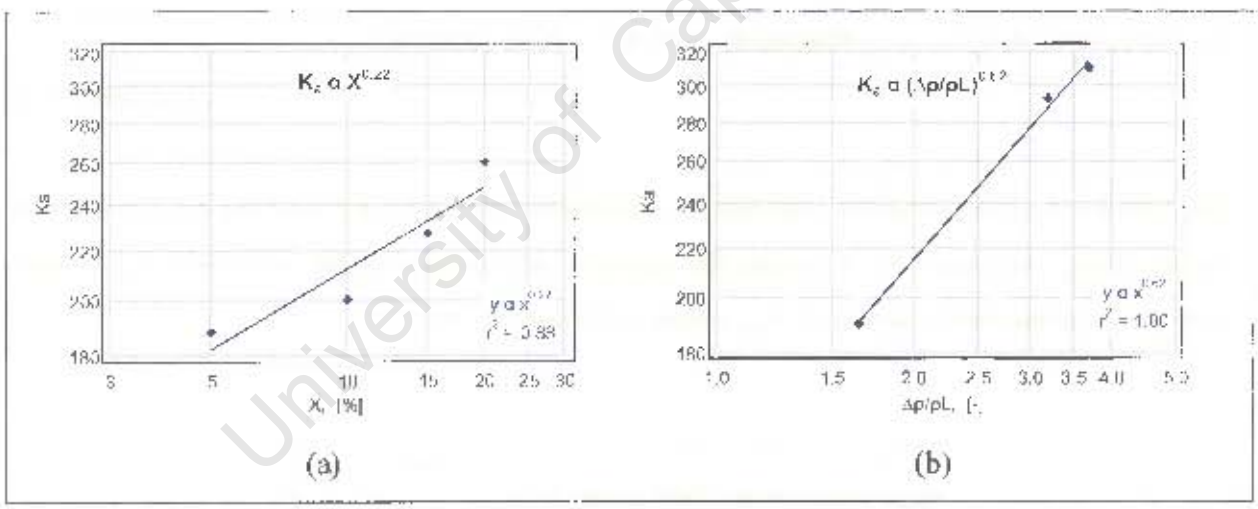

Figure 4.17 Variation of K_a vs. (a) X and (b) $\Delta\rho/\rho_L$ from the graphical results given in Figure 4.8 and Figure 4.9

By numerical analyses of the K_a data as given in Table 4.3, the dependence of d_p, X, and $\Delta\rho/\rho_L$ can be determined as, $K_a = \mathrm{K}.d_p^{0.11}.\ X^{0.23}.\ (\Delta\rho/\rho_L)^{0.62}$. This leaves the correlation coefficient, K, still to be determined. According to Equation 4-20 (b), a plot of $\Delta N_{js} / d_p^{0.11}.\ X^{0.23}.\ (\Delta\rho/\rho_L)^{0.62}$ vs. J_G will give the value of K as the slope of the fitted line (cf. Figure 4.18).

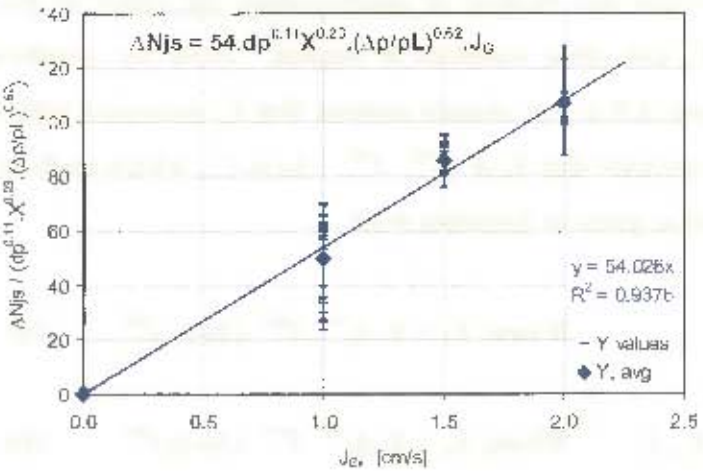

Figure 4.18 Determining the correlation coefficient for Option 4, $\Delta N_{js} / d_p^{0.11}.X^{0.23}.(\Delta\rho/\rho_L)^{0.62}$ vs. J_G

Figure 4.18 thus gives the correlation coefficient to be 54 rpm.($\mu m^{0.11}$.cm/s)$^{-1}$.

$N_{jsg} = N_{jsu} + K_a.J_G$; Where, $K_a = 54.d_p^{0.11}.X^{0.23}.(\Delta\rho/\rho_L)^{0.62}$

.....Equation 4-21

The effectiveness of using this equation to incorporate the effect gas into the N_{jsg} correlation can be tested once again by reversing the equation and comparing the calculated $N_{jsu'}$ values with the experimentally measured N_{jsu} values (cf. Figure 4.19).

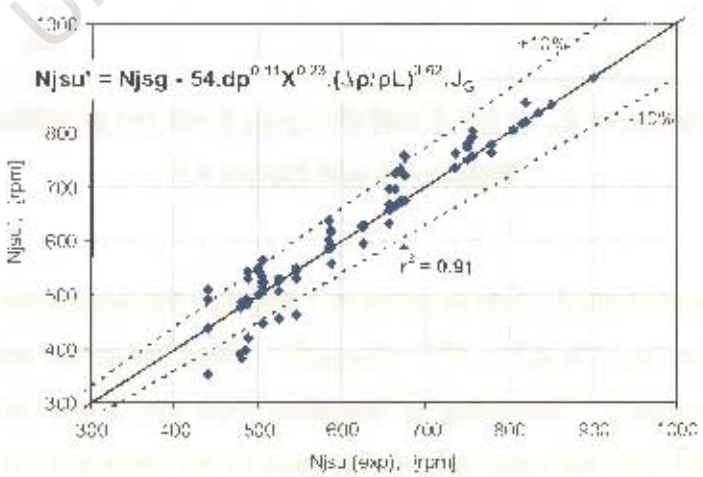

Figure 4.19 Predicted $N_{jsu'}$ values using $N_{jsu'} = N_{jsg} - 54.d_p^{0.11}.X^{0.23}.(\Delta\rho/\rho_L)^{0.62}.J_G$ vs. experimentally measured N_{jsu} values

It follows from Figure 4.19 that despite the relative complexity of Equation 4-21, it doesn't necessarily lead to a large improvement in the way that the effect of gas is accounted for. A fair number of calculated values are outside the 10% deviation lines and the r^2 value is slightly lower than both Option 2 and Option 3.

In conclusion, if all four options above are considered, a decision should be made of how to incorporate the effect of gas in this work. A number of aspects should be considered. Firstly, by considering the experimental observations on the effect of gas as shown in Figure 4.8 and Figure 4.9, it was seen that J_G caused a *linear* increase in the critical impeller speed. The slope of the linear increase was however not constant for this geometry. This observation agrees with Option 2 and Option 4. Secondly, the quality of the *parity fit* of calculated ungassed critical impeller speeds, $N_{jsu's}$ vs. experimentally measured values should be considered, and thirdly the *simplicity* of the final consideration should be considered. *Option 2* fairs the best in all these considerations and is thus selected as the way to incorporate the effect of gas addition on the critical impeller speed in this work.

$N_{jsg} = N_{jsu}(1+\mathrm{K}.J_G)$; Where, K 0.40 $(\mathrm{cm.s^{-1}})^{-1}$; (or K - 0.36 $\mathrm{vvm^{-1}}$)

.....(cf. Equation 4-17)

4.2.2 Graphical Analyses of the Effect of Solid-Liquid Variables under Gassed Conditions

Now that Equation 4-13 (b), i.e. the effect of gas addition on the critical impeller, has been correlated (cf. Equation 4-17), can the N_{jsu} part of the gassed critical impeller speed be revisited (cf. Equation 4-13 (a)). The N_{jsu} correlation, indicating the effect of two-phase variables, has already been developed in Section 4.1 (cf. Equation 4-12). The question to consider here is whether the N_{jsu} part to be used in the three-phase correlation is the same as that developed in ungassed conditions, or whether the effects of some two-phase variables change on gassing. As already mentioned, have some [Chapman *et al.* (1983c); Wong, Wang and Huang (1987)] found the effect of some two-phase variables to reduce on gassing, whilst others [Dutta and Pangarkar (1995); Dohi *et al.* (2003)] have found these effects to be very similar to that proposed by Zwietering for two-phase conditions (cf. Table 2.11). For this

reason, the effect of the two-phase variables (d_p, X, $\Delta\rho/\rho_L$, v_L) on the critical impeller speed under gassed conditions will be considered graphically in this section.

4.2.2.1 *The Effect of Particle Size on N_{jsg}*

The effect of particle size, d_p, at different gassing rates (J_G = 0, 1.0, 1.5, and 2.0 cm/s) is considered in Figure 4.20.

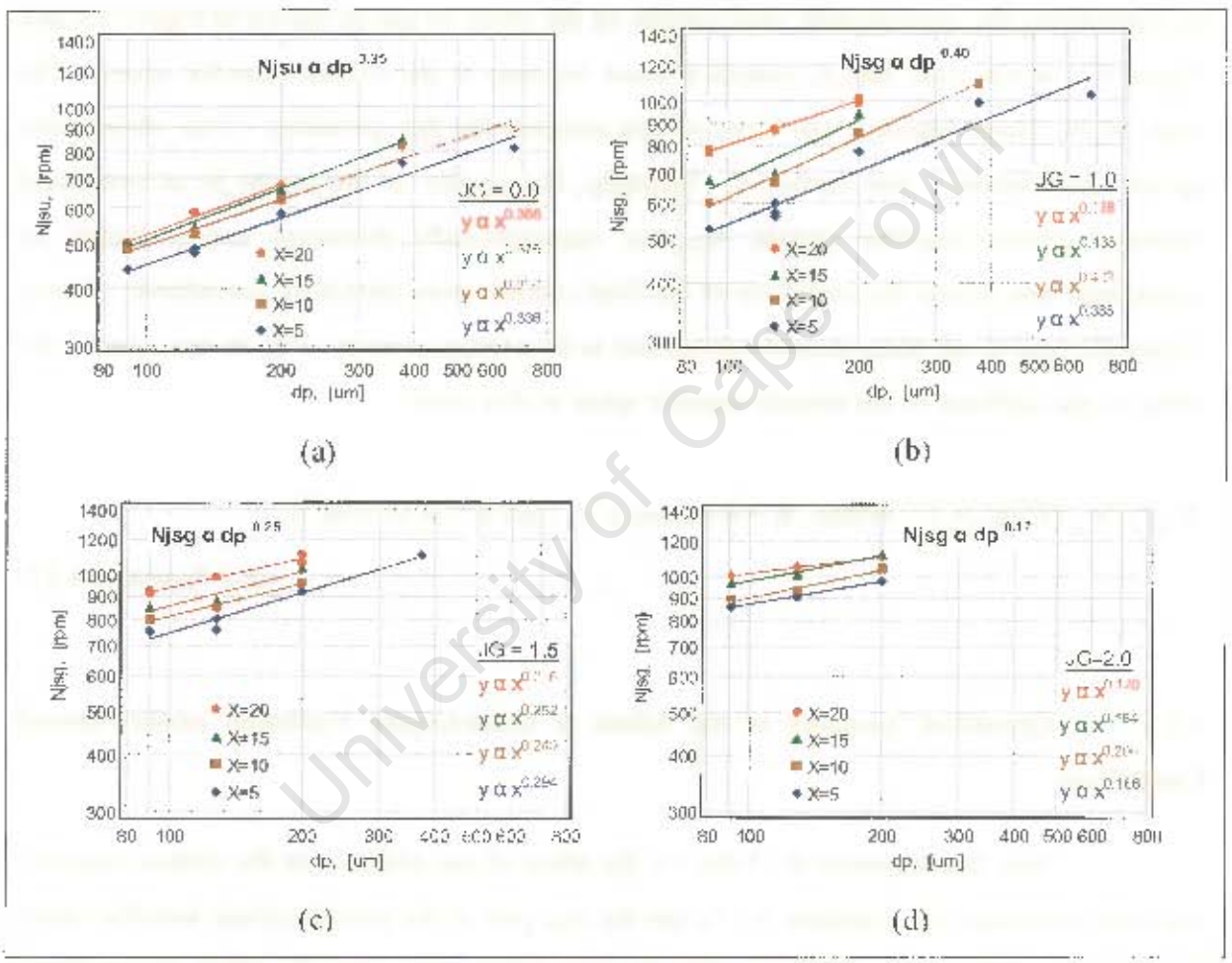

Figure 4.20 The effect of particle size, d_p on N_{js} at different gassing rates, (a) J_G = 0, (b) J_G = 1.0, (c) J_G = 1.5, (d) J_G = 2.0 cm/s

It can be seen from Figure 4.20 that the effect of d_p on N_{js} seems to increase slightly from ungassed conditions (a) to J_G = 1.0 cm/s (b), from where the effect decreases relatively quickly on further increase in J_G. It therefore follows that the relative effect of d_p on N_{js} under gassed conditions seems to vary between $d_p^{0.40}$ to $d_p^{0.17}$ depending on the gas addition rate.

From the flotation literature (cf. Section 2.5.1), a relation could be extracted from the work done by Schubert (1985).

$N_{jsg} \alpha d_p^{0.33}$; For a 54 l flotation cell in three-phase conditions

..... Equation 4-22

Extracted from Schubert (1985); $Q_{GV} = 0.45$vvm

This finding was at a volume based gas addition rate of $Q_{GV} = 0.45$ vvm. In flotation, surface based gas addition rates, J_G, are commonly used. Chapman *et al.* (1983c) found in N_{jsg} work done on different scales of stirred tanks, that the N_{jsg} relationships remained much more similar when scaling on a constant Q_{GV} basis rather than a constant J_G basis (J_G basis: $Q_G \alpha D^2$; Q_{GV} basis: $Q_G \alpha D^3$). This suggests that solids suspension (N_{jsg}) scales with the volume based gas addition rate, Q_{GV}, rather than with the surface based gas addition rate, J_G. The surface based gas addition rates used in this work of 1.0, 1.5, and 2.0 cm/s are equivalent to relatively high Q_{GV} values of 1.1, 1.7, and 2.2 $m^3/m^3/min$ (or vvm). The gas addition rate used by Schubert is equivalent to a low gassing rate of around $J_G \sim 0.5$ cm/s in this tank. By interpolation between the result obtained at $J_G = 0$ and $J_G = 1.0$ cm/s, it is expected that the effect of d_p at $J_G = 0.5$ cm/s should be around $N_{jsg} \alpha d_p^{0.37}$. The finding derived from Scubert on the effect of d_p on N_{jsg}, thus agrees very well with the finding of this work. This suggests that the effect of particle size on the critical impeller speed is most probably consistent in different flotation cells, as is the case with standard stirred tanks.

4.2.2.2 *The Effect of Solids Concentration on N_{jsg}*

The effect of solids concentration on N_{js} at different gassing rates is given in Figure 4.21.

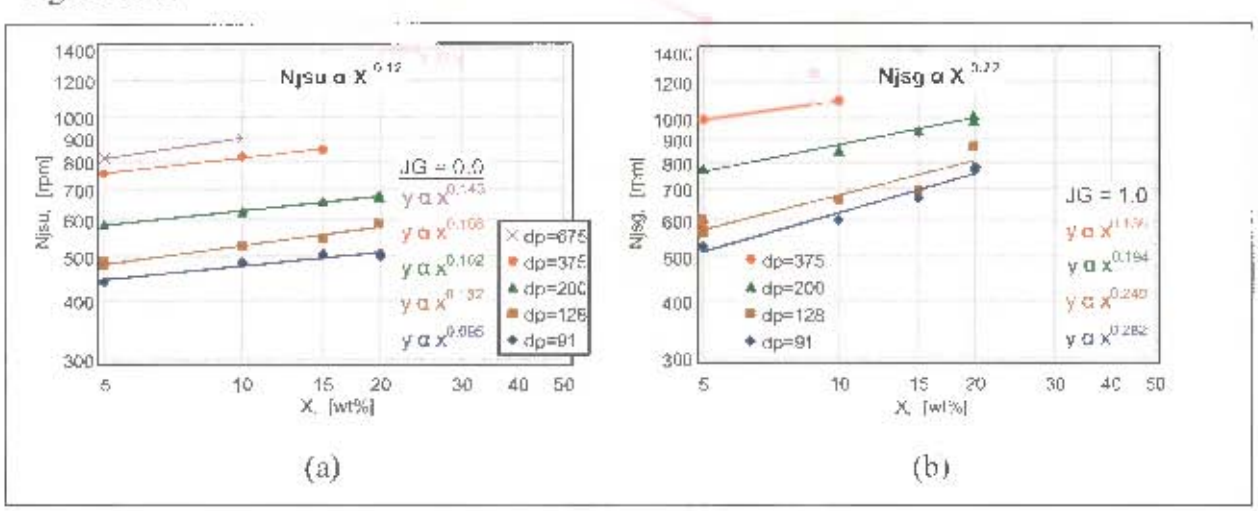

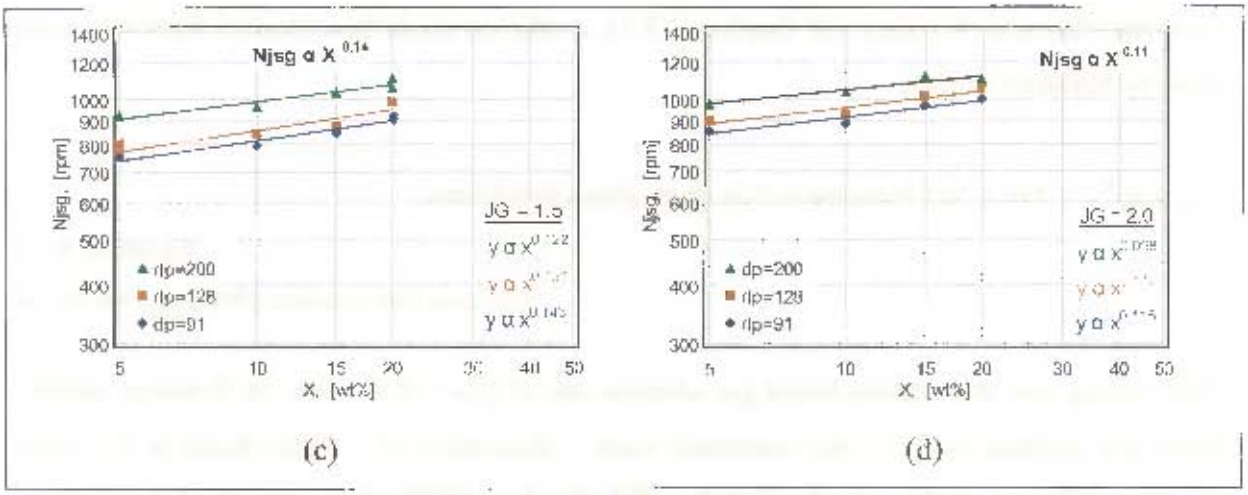

Figure 4.21 The effect of solids concentration, X on N_{js} at different gassing rates, (a) J_G = 0, (b) J_G = 1.0, (c) J_G = 1.5, (d) J_G = 2.0 cm/s

From Figure 4.21 it follows that the effect of solids concentration also seems to increase from ungassed to a gassed condition of J_G = 1.0 cm/s. As the gas addition rate is increased further, the relative effect of X decreases similarly to what was observed with d_p. No relation between N_{jsg} and X could be found in or derived from the flotation literature.

4.2.2.3 *The Effect of Solids Density on N_{jsg}*

The effect of solids density difference $\Delta\rho/\rho_L$ on N_{js} is shown in Figure 4.22.

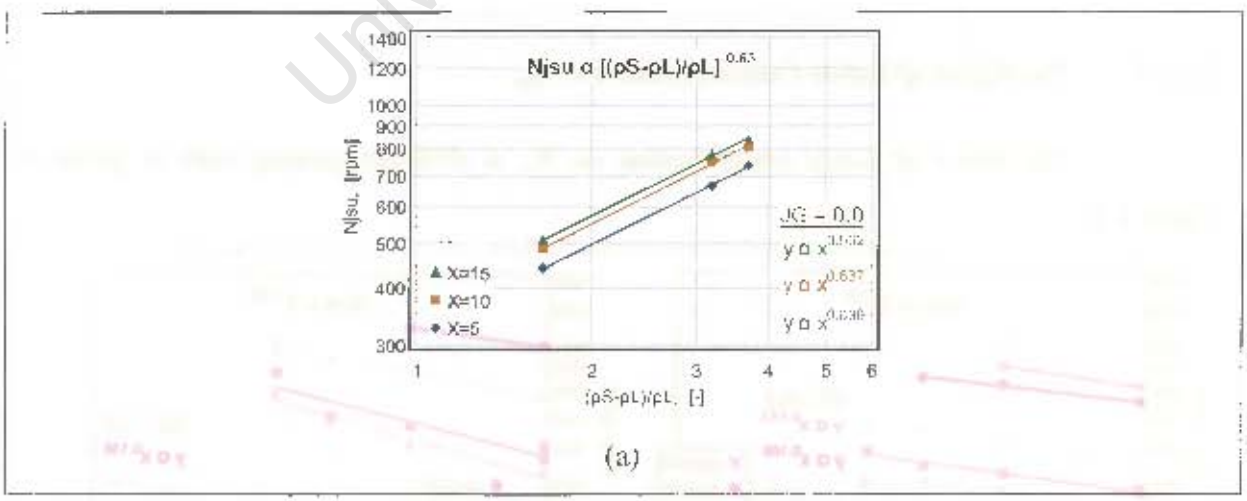

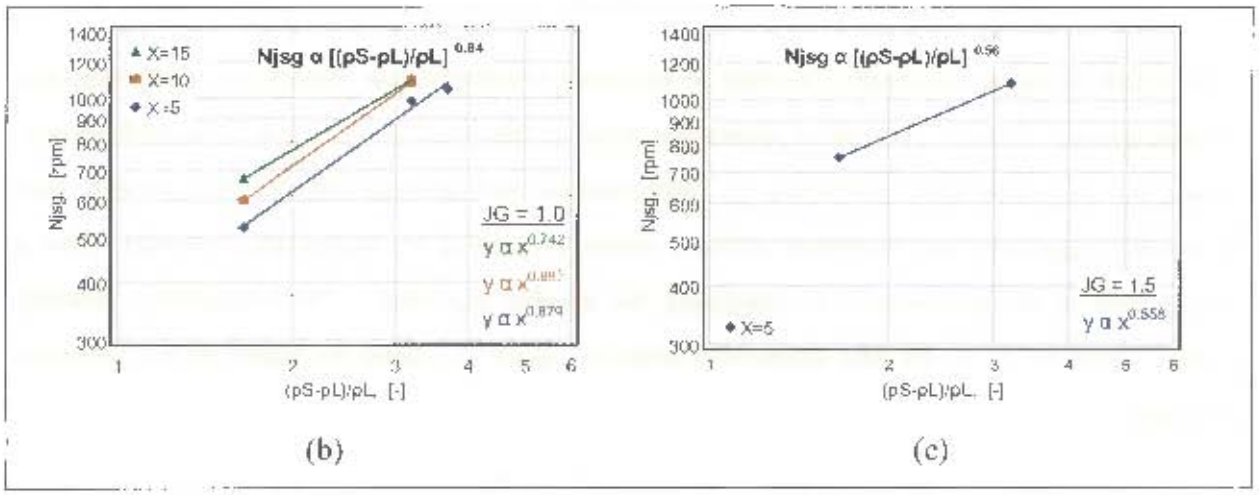

Figure 4.22 The effect of solids density difference, $\Delta\rho/\rho_L$ on N_{js} at different gassing rates, (a) $J_G = 0$, (b) $J_G = 1.0$, (c) $J_G = 1.5$

Again, as with d_p and X, the effect of $\Delta\rho/\rho_L$ seems to become stronger at the gas rate of J_G = 1.0 cm/s. On further increases in gas rates the effect of gas addion drops off once more. As already mentioned in Section 2.5.1, although Schubert (1985) give N_{js} data for two densities of materials (ballotini and sylvinite) a relation between N_{js} and ρ_S can not easily be derived due to insufficient information given on the density and particle size fraction of the sylvenity ore.

4.2.2.4 *The Effect of Liquid Viscosity on N_{jsg}*

The effect of liquid kinematic viscosity ν_L is shown in Figure 4.23.

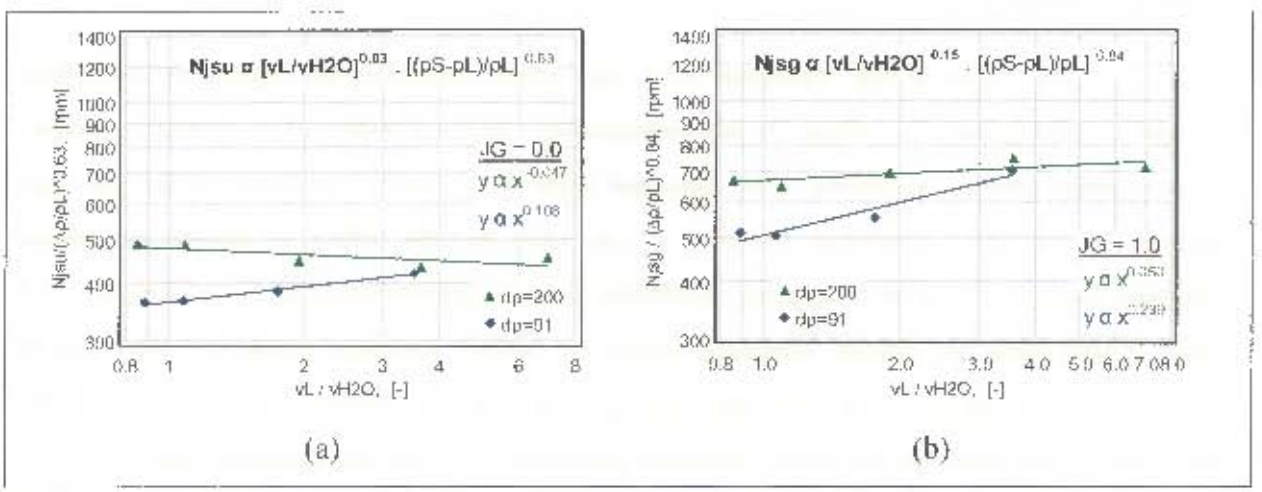

Figure 4.23 The effect of liquid kinematic viscosity, ν_L on N_{js} at different gassing rates, (a) $J_G = 0$, (b) $J_G = 1.0$ cm/s

The effect of liquid kinematic viscosity at ungassed conditions was somewhat conflicting and inconclusive. A more consistent increasing trend is observed at $J_G = 1.0$. For both partcle sizes, N_{js} increased with increasing v_L. Nonetheless, still stronger for the finer particle size fraction, suggesting that turbulent effects, which is reduced by increasing viscosity, play a larger role in the suspension of especially the smaller particles. No correlations relating liquid viscosity v_L to the just suspended impeller speed N_{js} could be found in the flotation literature.

The results of the graphical analyses of the effect of two-phase variables on the critical impeller speed under ungassed and gassed conditions can be summarised as in Table 4.4.

Table 4.4 Graphical Analyses of the Effect of Two-Phase Variables at Different Gassing Rates

Gas Addition Rate	$N_{js} \alpha d_p^c$	$N_{js} \alpha X^d$	$N_{js} \alpha (\Delta\rho/\rho_L)^e$	$N_{js} \alpha (v_L/v_w)^f$
J_G 0.0 cm/s (Q_{GV} = 0.0 vvm)	0.35 (0.33-0.38)	0.12 (0.10-0.14)	0.63 (0.63-0.64)	0.03 (-0.05 to 0.11)
J_G 1.0 cm/s (Q_{GV} 1.1 vvm)	0.40 (0.33-0.44)	0.22 (0.14-0.28)	0.84 (0.74-0.89)	0.15 (0.05 to 0.24)
J_G = 1.5 cm/s (Q_{GV} = 1.7 vvm)	0.25 (0.22-0.29)	0.14 (0.12-0.15)	0.56	-
J_G = 2.0 cm/s (Q_{GV} = 2.2 vvm)	0.17 (0.12-0.20)	0.11 (0.10-0.12)	-	-

4.2.3 Numerical Analyses of the Effect of Solid-Liquid Variables under Various Gassed Conditions

The form of the Equation 4-13 (a), which considers the effect of two-phase variables under gassed conditions is still outstanding. Some pointers of how these variables behave under gassed conditions were obtained from the graphical analyses in the previous section. From these graphical analyses it was seen that the effect of all the two-phase variables increased from the ungassed conditions to an air addition rate of $J_G = 1.0$ ($Q_{GV} = 1.1$ vvm), where after the effects decreased again on further increased aeration. The best-fit values of these exponents at different gassing rates and the statistical significance of the observations are however not easily obtained quantitatively from the graphical analyses. For this reason, numerical analyses will be employed in this section. Multiple linear regression will be used to find the best-fit coefficients under various gassing conditions. The regression

routine obtains the best-fit coefficients by minimising the sum of the squared differences between the predicted and observed values. As the name of this numerical method implies, a linear correlation is required. So before applying this technique the gassed critical impeller speed correlation should be linearised. In Section 4.2.1.2, the form of Equation 4-13 (b), which best described the effect of gas in this work was found to be Equation 4-17, which leads to the following form of the gassed critical impeller speed correlation.

$$N_{jsu'} = K_{SL'} d_p^{\,c'} X^{d'} \left(\frac{\rho_S - \rho_L}{\rho_L} \right)^{e'} \nu^{f'} \text{; Where } K_{SL'} = \text{f}(T, D/T, C/T, \text{design}) \qquad \text{(a)}$$

$$N_{jsg} = N_{jsu'} + \text{K}.N_{jsu'}.J_G = N_{jsu'}(1 + \text{K}.J_G) \text{; Where K} = 0.40 \qquad \text{(b)}$$

..... Equation 4-23

Combining Equation 4-23 (a) and (b) give Equation 4-24.

$$N_{jsg} = N_{jsu'}(1+0.40.J_G) = K_{SL'} d_p^{\,c'} X^{d'} \left(\frac{\rho_S - \rho_L}{\rho_L} \right)^{e'} \nu^{f'} (1+0.40.J_G)$$

..... Equation 4-24

Where $K_{SL'} = \text{f}(T, D/T, C/T, \text{design})$

Equation 4-24 can be linearised by taking logarithms as follows.

$$\log N_{jsg} = \log K_{SL'} + c'.\log d_p + d'.\log X + e'.\log\left(\frac{\rho_S - \rho_L}{\rho_L} \right) + f'.\log\nu + \log(1+0.40.J_G) \qquad \text{(a)}$$

Or,

$$\log \frac{N_{jsg}}{(1+0.40.J_G)} = \log N_{jsu'} : \log K_{SL'} + c'.\log d_p + d'.\log X + e'.\log\left(\frac{\rho_S - \rho_L}{\rho_L} \right) + f'.\log\nu \qquad \text{(b)}$$

..... Equation 4-25

It is important to use Equation 4-25 (b) when different gassing rates are considered together. If Equation 4-25 (a) is fitted to a dataset containing different gassing rates, the effect of changes in gassing (last term on the RHS) will incorrectly be attributed to the other coefficients (i.e. c', d', e', f'). Equation 4-25 (b) first removes the effect of gas addition before fitting the coefficients. It should also be noted that the way in which the gassed critical impeller speed is linearised (cf. Equation 4-25) is dependent on the way that the effect of gas

is incorporated into the three-phase critical impeller speed correlation (cf. Option 1 to 4 in Section 4.2.1.2).

Another point that should be discussed before considering the results of the numerical analyses is the strategy that was used in the numerical analyses of the data. All numerical analyses of datasets were done in the following two-step manner. The effects of d_p, X, $\Delta\rho/\rho_L$ were considered during Phases I and II of the experimental programme (cf. Section 3.3.1.2). As a first step, the coefficients of these variables will thus be fitted by considering data from Phases I and II. The effect of viscosity was tested by adding Phase III to the above. In this second analysis, all the tests in Phases I, II, and III are considered. However, the exponents of d_p, X, $\Delta\rho/\rho_L$ are fixed as found in the first step and this analyses thus only considers the effect of viscosity. The reason for considering viscosity on the full dataset and not only the Phase III reduced dataset is in order to incorporate the viscosity effects due to temperature variations, which occurred in all runs, in addition to the sugar tests.

The results of these analyses on different datasets are given in Section A.5 in the Appendix and is summarised in Table 4.5 and displayed graphically in Figure 4.24.

Table 4.5 Numerical Analyses of the Effect of Solid-Liquid Variables under Various Gassed and Ungassed Conditions

	$N_{jsg} = K_{SL'} \cdot d_p^{c'} X^{d'} (\Delta\rho/\rho_L)^{e'} (v_L/v_w)^{f'} (1 + 0.40 J_G)$				
Dataset	$K_{SL'}$	c'	d'	e'	f'
J_G = 0.0 cm/s (Q_{GV} = 0.0 vvm)	54.1	0.35 ±0.02	0.12 ±0.02	0.66 ±0.05	-0.01 ±0.03
J_G = 1.0 cm/s (Q_{GV} = 1.1 vvm)	28.7	0.39 ±0.05	0.25 ±0.05	0.85 ±0.11	0.13 ±0.05
J_G = 1.5 cm/s (Q_{GV} = 1.7 vvm)	80.7	0.27 ±0.05	0.14 ±0.03	0.61 ±0.13	-
J_G = 2.0 cm/s (Q_{GV} = 2.2 vvm)	185	0.17 ±0.04	0.11 ±0.03	-	-
All Gassed ($J_G > 0$)	53.1	0.31 ±0.04	0.18 ±0.03	0.73 ±0.09	0.11 ±0.05
All Ungassed & Gassed	51.6	0.33 ±0.03	0.17 ±0.03	0.70 ±0.06	0.05 ±0.04

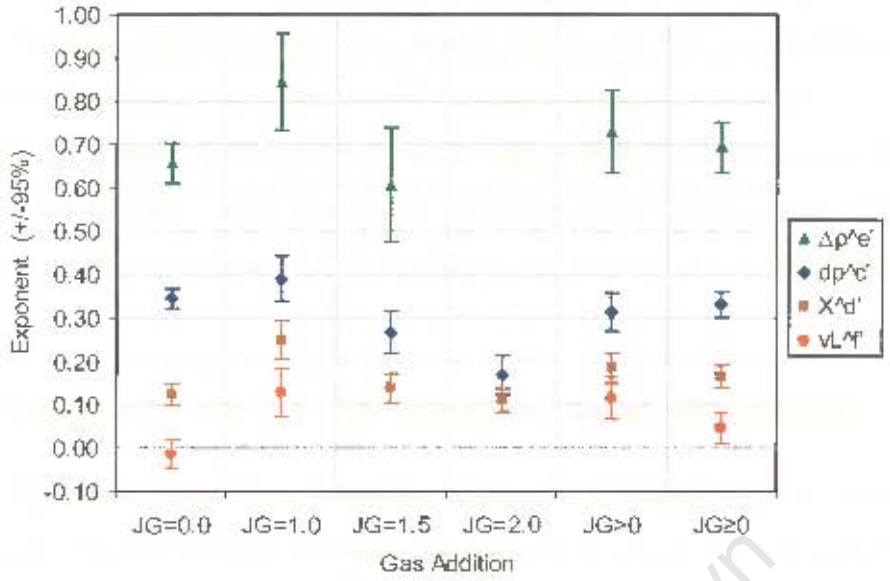

Figure 4.24 Numerical analyses of the effect of solid-liquid variables under various gassed and ungassed conditions (J_G = 0, 1.0, 1.5, 2.0 cm/s; Or Q_{GV} = 0, 1.1, 1.7, 2.2 vvm)

It is important always to check that numerical results agree with what was observed graphically in order to ensure that numerical results are reflective of reality and not just a numerically optimum combination. It is therefore encouraging when comparing Table 4.5 (numerical) & Table 4.4 (graphical) to see that the exponent results are very similar. The ungassed results (J_G = 0 cm/s) were already discussed in Section 4.1 but is included here as reference. Considering the exponents of particle size (d_p), solids concentration (X), solids density difference ($\Delta\rho/\rho_L$), and kinematic viscosity (ν_L/ν_w) for J_G = 0, 1.0, 1.5, 2.0 cm/s, similar trends are observed. All the exponents increased from ungassed to J_G = 1.0, where after it decreased on further increased gassing. The increase from ungassed to J_G = 1.0 (Q_{GV} = 1.1 vvm) is interesting. In stirred tanks, Chapman *et al.* (1983c) and Wong, Wang and Huang (1987) have proposed that the effect of some two-phase variables reduce in gassed conditions, whilst Dutta and Pangarkar (1995) and Dohi *et al.* (2003) proposed exponents very similar to that of Zwietering (1958) for ungassed conditions (cf. Table 2.11). It should be noted that these increases in the effects of all the two-phase variables from ungassed to a gassing rate of 1 cm/s are significant for all variables except d_p at the 95% confidence level. Above J_G = 1.0 the effect of all the two-phase variables started to decrease relatively quickly. It can further be noted that the 95% confidence intervals on the gassed results are wider than for the ungassed condition, which is indicative of the increased difficulty of doing solids suspension work under gassed conditions. In the last two columns of Figure 4.24 data from different

gassing rates were also analysed together. In the first instance, all gassed results were considered together ($J_G > 0$) and in the second case the full dataset of both ungassed and gassed tests ($J_G \geq 0$) were considered together. The results from these combined gassing rates are averaged values from the different gassing rates and the confidence in the values will also increase due to these results being based on larger data sets. The critical impeller speed correlations that can be derived from these results will be considered in the next section.

4.2.4 Critical Impeller Speed Correlations for Two- and Three-Phase Conditions

Now that the effect of two-phase variables have been considered under gassed conditions (Table 4.5 and Figure 4.24), can the complete critical impeller speed correlation (cf. Equation 4-24) be tested for both gassed and ungassed conditions. From the numerical analyses in the previous section, a number of correlations can be drawn. The ungassed correlation ($J_G = 0.0$) was already considered in Section 4.1.2. The ungassed correlation will however be compared to the gassed correlations, which will be tested here. *Firstly*, the correlation developed for a constant gassing rate of 1 cm/s ($J_G = 1.0$), will be tested here. All the variables tested during ungassed conditions ($J_G = 0.0$) were also tested at this gassing rate and the total number of tests at each condition is very similar (i.e. datasets are similarly sized; cf. Tables A.12 to A.15). Correlations for constant gassing rates of 1.5 and 2.0 cm/s will not be tested here because the number of tests were less (not all N_{jsg} values could be reached), and not all variables could be considered at these higher gassing rates. *Secondly*, the correlation developed from all the gassed runs together ($J_G > 0$) will be tested, and *thirdly* the correlation developed from the full dataset, of gassed as well as ungassed tests ($J_G \geq 0$), will be tested.

From Table 4.5 the following N_{jsg} correlation is obtained for a constant gassing rate of J_G = 1.0 cm/s (Q_{GV} = 1.1 vvm).

$$N_{jsg} = K_{SU} d_p^{0.39} X^{0.25} \left(\frac{\rho_S - \rho_L}{\rho_L} \right)^{0.85} (\nu / \nu_w)^{0.13} (1 + K_G J_G);$$

Where, $K_{SU} = 28.7$; $K_G = 0.40$ (cm/s)$^{-1}$

..... Equation 4-26

Only for $J_G = 1.0$ cm/s ($Q_{GV} = 1.1$ vvm)

If this correlation is applied to the experimental results obtained at J_G = 1.0 cm/s, the parity chart as shown in Figure 4.25 is obtained.

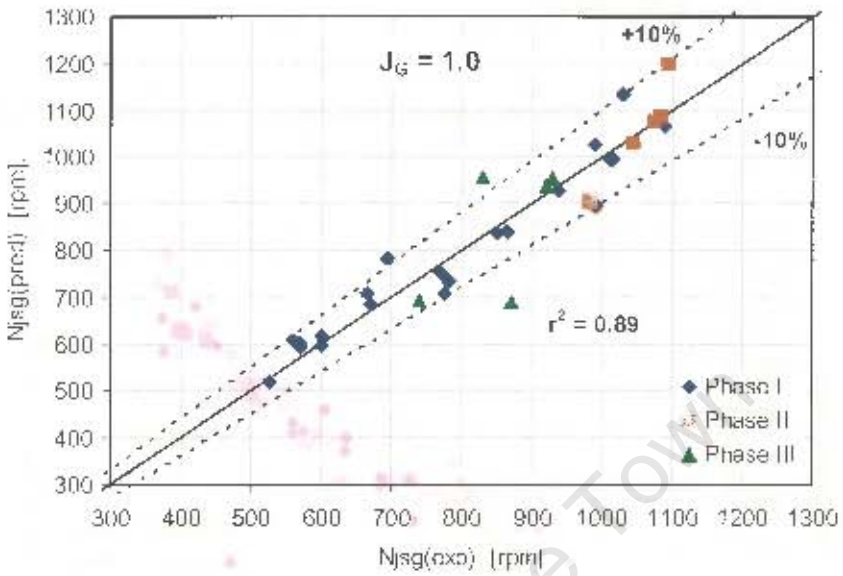

Figure 4.25 The quality of the N_{jsg} correlation fit obtained from the J_G = 1.0 cm/s data

It follows from Figure 4.25 that a relatively good fit is obtained when applying Equation 4-26 to the J_G = 1.0 cm/s data. Only 3 data points are outside the ± 10% deviation lines, two of which are from the viscosity work in Phase III. The coefficient of determination, r^2, of 0.89 also indicates a reasonably good fit. The quality of the fit of this equation obtained at J_G = 1.0, is however not as good as the quality of the fit of the ungassed equation (cf. Figure 4.6), where r^2 was 0.96 and only 1 viscosity datapoint deviated outside ± 10% of experimentally observed. This is very normal when comparing two- and three-phase solids suspension work, and is also expected when considering the wider confidence limits of the results obtained at J_G = 1.0 compared to J_G = 0.0 (cf. Figure 4.24).

From Table 4.5 the correlation fitted from considering all the three-phase data combined (J_G > 0) is given by Equation 4-27, and testing this correlation against the experimentally observed values under gassed conditions leads to the parity chart given in Figure 4.26.

$$N_{jsg} = K_{SL'} d_p^{0.31} X^{0.18} \left(\frac{\rho_S - \rho_L}{\rho_L} \right)^{0.73} (\nu/\nu_w)^{0.11} (1 + K_G J_G);$$

Where, $K_{SL'} = 53.1$; $K_G = 0.40$ (cm/s)$^{-1}$

..... Equation 4-27

Only for gassed conditions ($J_G > 0$); Gassing range, Q_{GP}: 1.1 to 2.2 vvm

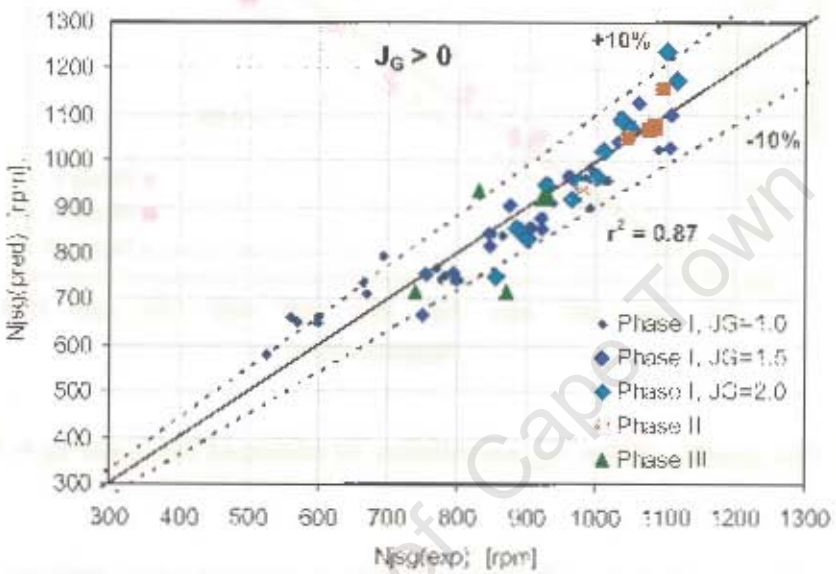

Figure 4.26 The quality of the N_{jsg} correlation fit obtained from all three-phase data (J_G > 0 cm/s)

It is interesting to see that even though the exponents of the solid-liquid variables are influenced by gas rate, a fit of all the data combined still gives a relatively good fit as shown in Figure 4.26. Most of the predicted values are within the 10% deviation lines and evenly spread around the parity line. It seems as if there is some trend to overpredict the critical impeller speeds slightly at the lower end, which in this work will be the finer particle sizes at a gas rate of 1 cm/s during Phase I. Overall, the fit is reasonably good as also indicated by the coefficient of determination ($r^2 = 0.87$).

Finally, the correlation developed by considering all the critical impeller speed data in this work combined can be taken from Table 4.5 as given in Equation 4-28, and testing this correlation against the full dataset of gassed and ungassed tests leads to the parity chart in Figure 4.27.

$$N_{jsg} = K_{SL} d_p^{0.33} X^{0.17} \left(\frac{\rho_S - \rho_L}{\rho_L} \right)^{0.70} (\nu/\nu_w)^{0.05} (1 + K_G . J_G) \text{; Where, } K_{SL} = 52,\ K_G = 0.40\ (\text{cm/s})^{-1}$$

..... Equation 4-28

For both gassed and ungassed conditions ($J_G \geq 0$); Gassing range, Q_{GP}: 0 to 2.2 vvm (J_G: 0 to 2 cm/s);
K_{SL} = f (T, D/T, C/T, imp. design); K_G = f (C/T, imp design)

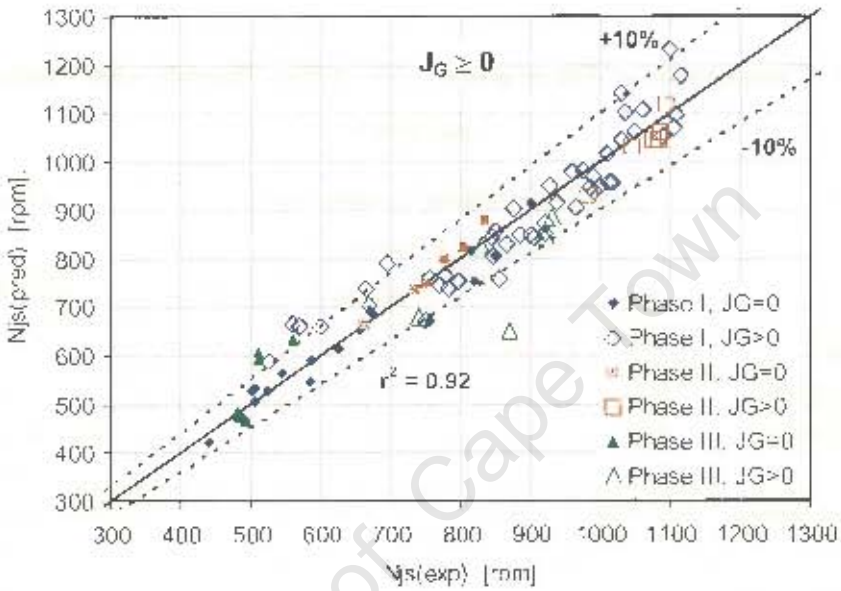

Figure 4.27 The quality of N_{js} correlation fit obtained from the full dataset of gassed and ungassed tests ($J_G \geq 0$ cm/s)

It follows from Figure 4.27 that the correlation for two- and three-phase tests combined, as given by Equation 4-28, gives a good fit to the experimentally measured critical impeller speeds. Again, the predicted values are spread relatively symmetrically about the parity line with most of the 92 predictions within the 10% deviation lines. Apart from one gassed viscosity test outlier (Phase III, JG>0), the other points falling outside the 10% deviation lines are relatively close to these lines. There seems to be some over prediction of values at the lower end. These overpredicted values consist of gassed tests during Phase I (Phase I, JG>0), which will be the finest silica fraction under gassed conditions, as well as some ungassed test from the viscosity tests during Phase III (Phase III, JG=0). Overall, as also indicated by the coefficient of determination ($r^2 = 0.92$) this correlation gives a good fit to all the measured data.

4.2.5 Summary of Findings and Comparison with Literature

In this section, the two- and three-phase correlations developed in this work will be summarised and compared against stirred tank findings from literature. The two-phase correlation given by Equation 4-12, together with the three-phase correlations tested in the previous section (cf. Equation 4-26 to Equation 4-28) is summarised in Table 4.6 and compared with stirred tank findings from Table 2.11.

Table 4.6 Comparison of Three-phase Correlation Results with Findings from Literature

Reference	Effect Two-Phase Variables on N_{jsg} $N_{jsg} \propto d_p^{c'} X^{d'(*2)} (\Delta\rho/\rho_L)^{e'} v^{f'}$				Effect of Gas [*3]
	$d_p^{c'}$	$X^{d'(*2)}$	$(\Delta\rho/\rho_L)^{e'}$	$v_L^{f'}$	$N_{jsg} = f(N_{jsu}, Q_{GV})$
Zwietering (1958) [*1]	0.20	0.17	0.45	0.1	$Q_{GV} = 0$
Chapman *et al.* (1983a) [*1]	0.15	0.15	0.40	0	$Q_{GV} = 0$
Chapman *et al.* (1983c)	0.12	0.15	0.22	0	$\Delta N_{js} = a.Q_{GV}$; a = const; (a = 0.94, 2.4) [*4]
Wong, Wang and Huang (1987)	0.12-0.16	0.14	0.20		$\Delta N_{js} = a.Q_{GV}$; a = const; (a = 2.0, 5.0) [*4]
Bujalski, Konno and Nienow (1988)					$N_{jsg} = N_{jsu}.(0.82 + 0.31.Q_{GV})$; Or: $N_{jsg} = N_{jsu}.(1+Q_{GV})^{0.11}$
Rewatkar, Raghava Rao and Joshi (1991)	0.09-0.12				$N_{jsg} = N_{jsu} + K_a.J_G$ $K_a = 132.7.u_T^{0.5}.D^{1.67}.T$; Or: $K_a = 330.6.u_T^{0.5}.D^{0.75}$
Dutta and Pangarkar (1995)	0.18	0.21	0.42		$\Delta N_{js} = a.Q_G$; a = const; (a = 3.75, 4.47, 3.16, 2.75) [*4]
Dohi *et al.* (2003)	0.20	0.13	0.45	0.1	$N_{jsg} = N_{jsu}.[1+0.03(J_G/u_t)^{0.2}.N_{Rep}^{0.4}]$
Gassed Stirred Tank Range	**0.09-0.20**	**0.13-0.21**	**0.20-0.45**	**0-0.10**	
Derived from Flotation literature: [Schubert (1985)]; Weiss and Schubert (1989)	0.33				$\Delta N_{js} = a.Q_{GV}$; a = 2.4 $vvm^{-1}.s^{-1}$ Or, $N_{jsg} = N_{jsu}.(1 + K.Q_{GV})$; K = 0.25 to 0.28 vvm^{-1}; K = 0.28 and 0.31 $(cm/s)^{-1}$
This Work (J_G=0 cm/s) [*1,*5]	**0.35 ±0.02**	**0.12 ±0.02**	**0.66 ±0.05**	**-0.01 ±0.03**	$J_G = 0$
This Work (J_G=1 cm/s) [*5]	**0.39 ±0.05**	**0.25 ±0.05**	**0.85 ±0.11**	**0.13 ±0.05**	$N_{jsg} = N_{jsu}.(1 + 0.40.J_G)$ Or, $N_{jsg} = N_{jsu}.(1 + 0.36.Q_{GV})$
This Work (All Gassed) [*5]	**0.31 ±0.04**	**0.18 ±0.03**	**0.73 ±0.09**	**0.11 ±0.05**	
This Work (Two- and Three-phase combined) [*5]	**0.33 ±0.03**	**0.17 ±0.03**	**0.70 ±0.06**	**0.05 ±0.04**	

Notes to Table 4.6

*1: Two-phase, $N_{js\mu}$, correlations

*2: Solids concentration is often also correlated as the effect of solids to liquid mass ratio B on $N_{js\mu}$, to change from B to X the exponents were multiplied by 1.27 being the power relation between B and X over the range $5\% \leq X \leq 50\%$ as used in this work and applicable to flotation cells (cf. Section 2.4.4.3.2).

*3: In solids suspension the effect of gas addition is most commonly incorporated in terms of the tank volume normalised gas flowrate, Q_{GV}, in $m^3/m^3/min$ or vvm. To convert: $Q_{GV} = J_G / Z \times 60$ s/min x 0.01 m/cm.

*4: 'a' was found to be constant for constant geometry, but changed with impeller type and impeller diameter (D/T)

*5: Values are given with 95% confidence intervals

The two-phase findings, included for reference in Table 4.6, have already been discussed and compared to two-phase literature findings in Section 4.1.2. Here, the discussion and comparison will focus on the three-phase correlations results. That is, the effects of variables under gassed conditions and the effect of gas itself. As with the two-phase results, the effects of particle size and solids density under gassed conditions have been found to be stronger than reported in stirred tanks. As speculated before, this may be attributed to the proximity of the stator mechanism to the impeller, leading to increased turbulence in the impeller region and reduced fluid flow further away for solids suspension. Another interesting finding from this work compared to literature, is the increase in the effect of all solid-liquid variables from ungassed conditions to a gassing rate of $J_G = 1.0$ cm/s (or $Q_{GV} = 1.1$ vvm). Considering the 95% confidence limits, it can be seen that these increased effects are very significant. Reductions in the effects of these solid-liquid variables to below the two-phase conditions only occurred (relatively quickly) on further increased gassing to $J_G = 2.0$ cm/s (or $Q_{GV} = 2.2$ vvm). No reports of increased effects of solid-liquid variables could be found in stirred tank work. Reports have only been made, about reductions in the observed effects of some variables from ungassed to gassed conditions [Chapman *et al.* (1983c); Wong, Wang and Huang (1987)]. Chapman *et al.* (1983c) reported this reduction to be relatively strong for the solids density difference, for which the exponent almost halved, and to a lesser extent for particle size (cf. Table 4.6). Solids density difference, $\Delta\rho/\rho_L$, and particle size d_p, remain the variables with the largest exponents, also for gassed conditions. Although having smaller exponents than, $\Delta\rho/\rho_L$, and d_p, it can be seen that the effect of solids concentration, X, and liquid kinematic viscosity increased significantly from ungassed to gassed conditions. The two-phase viscosity results showed conflicting but relatively small trends with kinematic viscosity, which could be best fitted by making N_{js} independent of viscosity ($f = 0.0$). However, under gassed conditions viscosity consistently caused N_{jsg} to increase. The value of this exponent for all the gassed conditions together (i.e. 0.11) is almost the same as the upper limit found in two-phase work, i.e. 0.10. The relations as given in the last row of Table 4.6

were developed by considering all the tests (two- and three-phase) combined. Overall, this correlation gives good predictions under all conditions (cf. Figure 4.27), and is therefore recommended for general two- and three-phase use.

4.2.6 Application of N_{jsg} Correlation

In this section, the N_{jsg} correlation will be applied to different conditions. This will serve as a brief demonstration case study of how to use the N_{jsg} correlation. The N_{jsg} correlation, which was developed from all the two- and three-phase data combined, will be used here (cf. Equation 4-28). Two sets of variable values were selected for this case study (cf. Table 4.7). A *base case* condition was selected to represent a low critical impeller speed condition in a mechanical flotation cell. *Increased values* were then selected to represent high values for each variable, which may be likely in a mechanical flotation cell. Calculating the critical impeller speeds using these variable values leads to the critical impeller speeds given in Table 4.8. To demonstrate the effect of each variable, N_{jsg} values were calculated by changing only one variable at a time from the base case condition. The dramatic effect of moving all variables together from a set of low N_{jsg} variables to a set of high N_{jsg} variables is also given. It should be noted that although each variable is likely to vary within these ranges, it is highly unlikely in reality that *all variables* will vary *together* from the low base case to the increased values. The increased critical impeller speeds caused by changing each variable on its own from the base case is shown graphically in Figure 4.28. The *large effects* of solids density followed by gas addition and particle size can clearly be seen. The *very small effects* of solids concentration and kinematic viscosity are also evident.

$$N_{jsg} = K_{SL} d_p^{0.33} X^{0.17} \left(\frac{\rho_S - \rho_L}{\rho_L} \right)^{0.70} (\nu/\nu_w)^{0.05} (1 + K_G . J_G) \text{; Where, } K_{SL} = 52,\ K_G = 0.40 \text{ (cm/s)}^{-1}$$

..... (cf. Equation 4-28)

Table 4.7 Base Case and Increased Values used in this Case Study

	d_{90} [#] [μm]	X [wt.%]	$\Delta\rho/\rho_L$ [-]	ν/ν_w [-]	J_G [cm/s]
Base Case Values	53	30	1.65 [*1]	1	0.5 [*3]
Increased Values	150	50	4.60 [*2]	4	2.0 [*4]

[#]: Characteristic size for upper 20% of solids, where solids suspension problems may be expected; [*1]: The average density of silica; [*2]: The average density of chromitite [Wills (1997)]; [*3]: Equivalent to $Q_{GV} = 0.56$ vvm; [*4]: Equivalent to $Q_{GV} = 2.2$ vvm.

Table 4.8 Calculated N_{jsg} Values using Equation 4-28 and the Case Study Variable Values in Table 4.7

N_{jsg} Condition	N_{jsg0} [rpm]	N_{jsg} [rpm]	N_{jsg} / N_{jsg0} [-]
Base Case (0)	639	**639**	1.00
Increase d_{90} only	639	**884**	1.38
Increase X only	639	**695**	1.09
Increase $\Delta\rho/\rho L$ only	639	**1303**	2.04
Increase v only	639	**683**	1.07
Increase J_G only	639	**959**	1.50
All Variables Combined	639	**3140**	4.91

[1]: Due to N_{jsg} being a product function of variables, is the combined relative effect of all the variables, the product of the relative effects of each variable on its own.

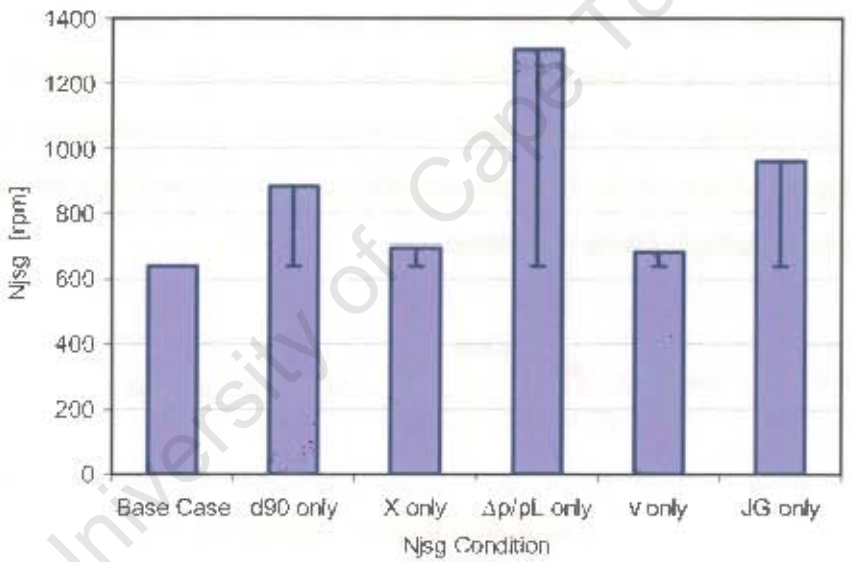

Figure 4.28 Critical impeller speeds determined from Equation 4-28 by changing one variable at a time from a base condition (cf. Table 4.7 & Table 4.8)

4.3 CONCLUSIONS

This chapter formed the *primary aim* of this thesis, i.e. the development of an N_{js} correlation for a mechanical flotation cell. In this way, off-bottom solids suspension, and how it was affected by the solid-liquid-gas variables in the 124l pilot mechanical flotation cell that was used in this study, was evaluated. This was achieved in this chapter by first considering two-phase solids suspension and then solids suspension under gassed conditions.

4.3.1 Two-Phase Critical Impeller Speed

The aim of this section was to investigate the effects of d_p, X, $\Delta\rho/\rho_L$, and ν_L on N_{jsu}. These findings can be compared with a large body of stirred tank N_{jsu} work and specifically to the work of Zwietering (1958). The N_{jsu} correlation also forms the basis from which the N_{jsg} correlation can be developed. The following N_{jsu} correlation was developed by first considering the effects of the different variables graphically and then developing the final correlation through multiple linear regression.

$$N_{jsu} = K_{SL} d_p^{0.35\pm0.02} X^{0.12\pm0.02} \left(\frac{\rho_S - \rho_L}{\rho_L} \right)^{0.66\pm0.05} ; \; K_{SL} = 54 \text{ and } N_{jsu} \text{ in rpm}$$

..... (cf. Equation 4-12)

A mechanical flotation cell (this work); $K_{SL} = f$ (T, D/T, C/T, imp. design)

The following specific observations could be made about the N_{jsu} results.

- Good agreement between graphical results and numerical results were obtained, which validated the numerical fit.
- Narrow 95% confidence limits were obtained for the effects of the solid-liquid variables, which confirmed the high accuracy at which two-phase critical impeller speed work can be done.
- The effect of viscosity was found to be conflicting, with an increasing trend observed for the smaller 75-106 µm size fraction ($N_{jsu} \propto \nu_L^{0.11}$) and a decreasing trend observed for the coarser 150-250 µm size fraction ($N_{jsu} \propto \nu_L^{-0.05}$). This may reflect a difference in the suspension mechanism for finer and coarser particles under two-phase conditions. If finer particles are suspended more by turbulent

action and coarser particles more by fluid flow drag, these positive and negative trends would be expected (increased viscosity decreases turbulence and therefore is an increase in impeller speed required for the fine particles; increased viscosity increases drag, cf. Equation 2-19, and therefore can the impeller speed be reduced for the coarser particles).

- The two-phase correlation fitted the experimental data very well with only one predicted value outside the 10% deviation lines and a good coefficient of determination ($r^2 = 0.963$).
- The effect of particle size ($N_{jsu} \alpha d_p^{0.35}$) is stronger than that found by Zwietering ($N_{jsu} \alpha d_p^{0.20}$) and most others in stirred tanks ($N_{jsu} \alpha d_p^{0.10}$ to $N_{jsu} \alpha d_p^{0.50}$).
- The effect of solid-liquid density difference found here ($N_{jsu} \alpha \Delta\rho/\rho_L^{0.66}$) is stronger than found by Zwietering ($N_{jsu} \alpha \Delta\rho/\rho_L^{0.45}$) and all others in standard stirred tanks ($N_{jsu} \alpha \Delta\rho/\rho_L^{0.40}$ to $N_{jsu} \alpha \Delta\rho/\rho_L^{0.50}$).
- The larger influence of particle size and especially solid-liquid density difference is thought to be related to the proximity of the stator to the impeller in a flotation cell decreasing the fluid flow from the impeller in favour of increased turbulence. Particle size and density difference are the two main variables influencing the terminal settling velocity of a particle (cf. Equation 2-18).
- The effect of solids concentration ($N_{jsu} \alpha X^{0.12}$) was found to be small, smaller also than found by Zwietering ($N_{jsu} \alpha X^{0.17}$) and most other findings ($N_{jsu} \alpha X^{0.10}$ to $N_{jsu} \alpha X^{0.30}$) in stirred tanks.
- Although conflicting trends were observed for viscosity, was the overall effect of viscosity found to be small enough to ignore in the two-phase work, which disagrees with Zwietering ($N_{jsu} \alpha \nu_L^{0.10}$) but agrees with some others [Chapman *et al.* (1983a)] in stirred tank work.

4.3.2 Three-Phase Critical Impeller Speed

The aim of this section was two-fold. Firstly, the *effect of gas addition on* N_{jsg} should be determined, and secondly the effect of the *other solid-liquid variables* should be tested *under gassed* conditions.

Gas addition was seen to cause a *linear increase* in N_{jsg}, but the rate of the increase *varied* for different conditions. Four options for incorporating the effect of gas was evaluated, i.e. linear

with a constant slope, ($N_{jsg} = N_{jsu} + a.J_G$), linear with the slope proportional to N_{jsu}, ($N_{jsg} = N_{jsu} + K.N_{jsu}.J_G$), a power relation, ($N_{jsg} = N_{jsu}(1 + J_G)^m$), linear with the slope being a function of system variables, ($N_{jsg} = N_{jsu} + K_a.J_G$; where K_a = f (system variables)). Option 2, where the slope of the linear increase caused by gas addition was taken as proportional to N_{jsu} was selected as the best way in this work to account for the effect of gas. This lead to.

$$N_{jsg} = N_{jsu}(1 + K.J_G)\ ;\ \text{Where, } K = 0.40\ (\text{cm.s}^{-1})^{-1}\ ;\ (\text{Or, } K = 0.36\ \text{vvm}^{-1})$$

..... (cf. Equation 4-17)

Air addition had a stronger effect on N_{jsg} in this work than the effect taken from Weiss and Schubert (1989), which varied between K = 0.25 to 0.28 vvm^{-1}. The very low impeller clearance, $C_b = 0.05T$, they used might have contributed to the smaller effect of air addition they observed in addition to differences in the impellers they used (double finger impellers) compared to this work.

Secondly, the *effects of the other solid-liquid variables* were considered under *different gassed conditions* (cf. Figure 4.24).

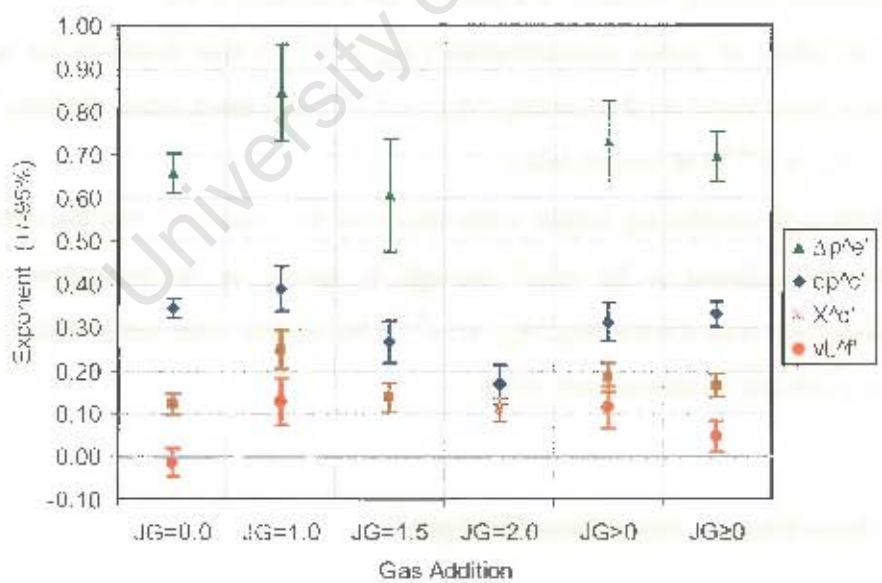

Cf. Figure 4.24 Numerical analyses of the effect of solid-liquid variables under various gassed and ungassed conditions (J_G = 0, 1.0, 1.5, 2.0 cm/s; Or Q_{GV} = 0, 1.1, 1.7, 2.2 vvm)

It followed that:

- Good agreement between the graphical observations and numerical results validated the numerical analyses.
- The effect of all solid-liquid variables consistently increased from ungassed to a gassing rate of 1 cm/s, before starting to decrease relatively quickly as the gassing rate was increased further.
- The increased effect of the solid-liquid variables at a gassing rate of 1 cm/s or 1.1 vvm were unexpected but were significant at the 95% confidence level for all variables except d_p. In stirred tank work, the effects of solid-liquid variables are either taken as very similar as two-phase or decreasing for some variables, most notably $\Delta\rho/\rho_L$ [Chapman *et al.* (1983c); Wong, Wang and Huang (1987)].
- Where kinematic viscosity (ν_L) gave contradicting effects on N_{jsu} for the finer (positive) and the coarser (negative) size fractions in the two-phase work, it now caused the critical impeller speed to increase for both size fractions. Still the increase was larger for the finer particle fraction, which may again indicate a larger influence of turbulent action on the suspension of the finer particles.
- Although, the gassing rate affected the influence of solid-liquid variables on N_{jsg}, were the average effects of these solid-liquid variables for all gassed conditions combined ($J_G > 0$) very similar to the two-phase findings ($J_G = 0$). It was therefore decided to base the final N_{jsg} correlation for use in three-phase (and two-phase) conditions on all the data combined ($J_G \geq 0$ cm/s), which gave,

$$N_{jsg} = K_{SL} d_p^{0.33\pm0.03} X^{0.17\pm0.03} \left(\frac{\rho_S - \rho_L}{\rho_L} \right)^{0.70\pm0.06} (\nu/\nu_w)^{0.05\pm0.04} (1 + K_G J_G);$$

Where, $K_{SL} = 52$, $K_G = 0.40$ (cm/s)$^{-1}$ or 0.36 vvm^{-1}

.....(cf. Equation 4-28)

For both gassed and ungassed conditions ($J_G \geq 0$); Gassing range, Q_{GV}: 0 to 2.2 vvm (J_G: 0 to 2 cm/s);
K_{SL} = f (T, D/T, C/T, imp. design); K_G = f (C/T, imp design)

- The three-phase correlation predicted the experimental observed N_{js} values very well with most predictions lying within 10% or very close to 10% of the experimental values. The good fit is also confirmed by the good coefficient of determination ($r^2 = 0.92$).
- Similarly to the two-phase findings, the effects of particle size and especially solid-liquid density difference found here, were stronger than that found in stirred tank work. Again, this is thought to be related to the proximity of the stator to the

impeller in a flotation cell, decreasing the fluid flow from the impeller in favour of increased turbulence, which effect is more limited to the impeller region only than the further reaching effect of fluid circulation.

- The average effect of particle size on N_{jsg}, $N_{jsg} \propto d_p^{0.33}$, is the same as that extracted from Schubert (1985) in a 5l mechanical flotation cell at a gassing rate of $Q_{GV} = 0.45$vvm. The good agreement implies that these findings are generic for different flotation cells (as is the case in stirred tanks) and that the effect of particle size in flotation cells are generally higher than in stirred tanks.
- The effects of both solids concentration and kinematic viscosity increased from the two-phase correlation, where both were low compared to stirred tank findings, to being very similar to average stirred tank findings under gassed conditions.

CHAPTER 5 SOLIDS CONCENTRATION PROFILES

CHAPTER 5 SOLIDS CONCENTRATION PROFILES..... 187

5.1 SOLIDS CONCENTRATION PROFILES.....188
5.1.1 Two-Phase Profiles at Various Impeller Speeds.....189
5.1.2 Three-Phase Profiles at Various Impeller Speeds (J_G = 1 cm/s).....191
5.1.3 Concentration above the Base vs. Increasing Impeller Speed.....193
5.1.4 Testing the Sedimentation-Dispersion Model for Vertical Solids Distribution.. 195
5.2 EFFECTIVENESS OF SOLIDS SUSPENSION.....199
5.2.1 Extent of Off-bottom Solids Suspension (X_m/X_{ms}).....199
5.2.2 Extent of Vertical Solids Distribution (Suspension Heights).....201
5.2.3 Variability of Vertical Solids Concentrations (*RSD*).....203
5.3 CONCLUSIONS.....205

This chapter discusses solids concentration profiles that were measured in a 124l pilot scale mechanical flotation cell as used in this work. In the previous chapter, *complete off-bottom suspension conditions* as characterized by the critical impeller speed (N_{js}) were related to solid-liquid system conditions and gas addition. The critical impeller speed is important for the performance of many multiphase processes, as is evident from the large body of work that has been done on the critical impeller speed in standard stirred tanks. However, some processes are not only influenced by the extent of off-bottom solids suspension, but also by *the distribution of solids throughout the vessel*. In this chapter, the axial (or vertical) distribution of solids in the tank is considered. Although the critical impeller speed was the main focus of this thesis, some concentration profile measurements were also done. Four sets of concentration profiles, consisting of a finer and coarser particle size fraction under two-phase and gassed conditions, will form the main discussion in this chapter. The mostly qualitative discussion and *analyses* of these four sets *of concentration profiles* at different impeller speeds will be done in Section 5.1. Axial solids concentration profiles focus on the vertical distribution of solids. When concentration profiles are however used in conjunction with critical impeller speed measurements, a more complete quantitative picture of the *effectiveness of solids suspension* can be determined by deriving some effectiveness measures from the concentration profiles, which will be discussed in Section 5.2.

5.1 SOLIDS CONCENTRATION PROFILES

A number of axial solids concentration profiles will be considered in this section. The solids concentration profile data is given in Appendix B. The profiles formed part of four sets of profiles done at impeller speeds ranging from 300 rpm to a maximum of approximately 1100 rpm. Two particle size fractions (75-106μm, 150-250μm) were tested under both two- and three-phase conditions (J_G = 0, 1 cm/s). These particle sizes are commonly encountered in flotation and were selected to present a finer and a coarser feed in terms of solids suspension. For gassed conditions, the gas flowrate of 1 cm/s (or 1.1 *vvm*) were selected as it is commonly used in flotation cells. For each of the four conditions, the solids concentrations (X) were measured at ten relative vertical heights (h/T) in the tank to form vertical *solids concentration profiles* (cf. Figure 5.1 to Figure 5.4). As per the convention used by Arbiter, Harris and Yap (1969) and others, h/T will be used here to indicate relative height as an alternative to h/Z. Using the tank diameter, T, has the advantage of being a fixed value,

whereas the top of the pulp phase, Z, may be variable during operation. Vessels with different aspect ratios (H/T) can also be compared directly on this basis. In this work $Z = T$, and h/T thus reached '1.0' at the top of the slurry in the tank. The two-phase profiles will be discussed in Section 5.1.1 and the three-phase profiles in Section 5.1.2. A potential N_{js} criterion linking solids concentration profile measurements to off-bottom suspension is the 'concentration above the base' criterion, which will be tested in Section 5.1.3. In Section 5.1.4 the sedimentation-dispersion model will be briefly considered to aid in the mechanistic discussion of vertical solids distribution. This model attempts to model the vertical distribution of solids in a vessel as a balance between the opposing mechanisms of upward turbulent dispersion, and downward particle settling, and has mainly found some application in high aspect ratio vessels such as columns.

5.1.1 Two-Phase Profiles at Various Impeller Speeds

In this section, the two-phase concentration profiles will be introduced and discussed. The two-phase concentration profile data is given in Table B.1 in Appendix B. The two-phase profiles were done together with critical impeller speed runs 77 and 29 as indicated in Table B.1. The profiles as displayed in Figure 5.1 and Figure 5.2 plot the measured solids concentrations, X, on the horizontal axis versus the relative height in the cell, h/T, on the vertical axis. The impeller speeds (e.g. 300rpm) as well as the percentages of critical impeller speed (e.g. 60%N_{js}) are indicated on these figures for each concentration profile. The bulk solids concentrations line (X_{act} = 20%) represents the theoretical vertical profile for the condition where the solids are completely suspended and homogeneously distributed throughout the tank.

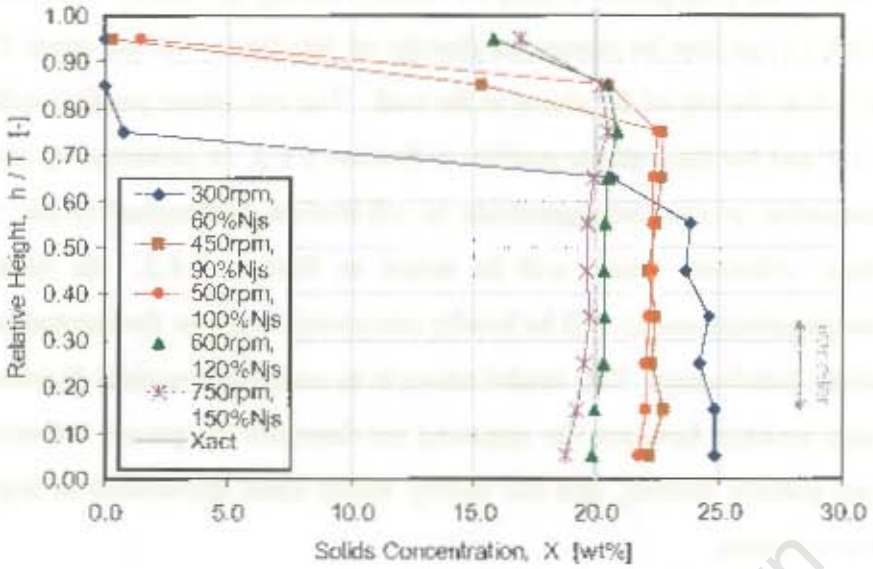

Figure 5.1 Solids concentration profiles for d_{p91} (75 – 106 µm) at various N under two-phase conditions

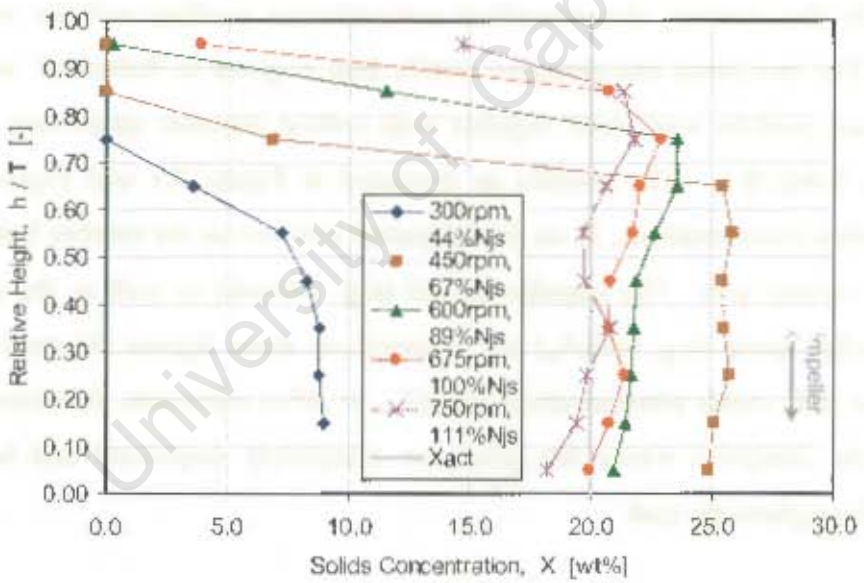

Figure 5.2 Solids concentration profiles for d_{p200} (150 – 250 µm) at various N under two-phase conditions

It should be noted that N_{js} for the finer d_{p91} size fraction (cf. Figure 5.1) was 500 rpm and 675 rpm for the coarser d_{p200} fraction (cf. Figure 5.2). This causes the percentage of critical impeller speed (%N_{js}) to be lower for the coarser compared to the finer size fraction at the same impeller speed. It is therefore expected that the extent of off-bottom suspension will be lower for the coarser size fraction than for the finer fraction at the same impeller speed. The

extent of off-bottom suspension for each size fraction will be evaluated at different impeller speeds in Section 5.2.1. It can be seen from Figure 5.1 and Figure 5.2 that the solids concentrations in the profiles remain relatively uniform from the bottom of the tank up to a certain height before dropping off rapidly. It follows that the *suspension height* (h_s) to which solids are distributed vertically in the tank can easily be extracted from these concentration profiles. At $N = N_{js}$ (100% N_{js}) solids were just noticeable at $h/T \approx 0.95$, indicating that a relation between suspension height and N_{js} may exist. These suspension height (h_s) observations will be analyzed further in Section 5.2.2. It is also noticeable how the profiles approaches the homogeneous suspension line (X_{act}) as the impeller speed increases, especially at N above N_{js}, and especially for the finer particle size fraction (cf. Figure 5.1). At relative impeller speeds below 50 percent of critical (cf. Figure 5.2) solids concentrations up the tank are very low and most of the solids are clearly still sedimented on the base. At 100 percent of critical impeller speed the solids are well distributed although slightly above the bulk concentration with a drop-off in concentrations at the very top. It can be seen from Figure 5.1 how a homogeneous suspension is approached as the impeller speed is increased to 150 percent of critical. This agrees well with observations already made in Table 2.4 (cf. Section 2.4.1) that a homogeneous suspension is normally approached as the relative impeller speed is increased to approximately 150 to 170 percent of the critical impeller speed, N_{js}, depending on particle properties and concentration [Oldshue, Herbst and Post (1995); Shaw (1992)]. Comparing Figure 5.2 to Figure 5.1 it follows that slightly more variations in the vertical concentrations of the coarser d_{p200} fraction are also noticeable compared to the finer d_{p91} fraction. Variation in the vertical concentrations as measured by the *RSD* will be considered further in Section 5.2.3.

5.1.2 Three-Phase Profiles at Various Impeller Speeds (J_G = 1 cm/s)

In this section, the three-phase concentration profiles for the d_{p91} (75-106μm) and d_{p200} (150-250μm) fractions at a gassing rate of J_G = 1 cm/s (or 1.1 *vvm*) obtained at various impeller speeds ranging from 300 to approximately 1100 rpm will be introduced and discussed. The three-phase concentration profile data is given in Table B.2 in Appendix B. These profiles were done together with critical impeller speed runs 78 and 30 as indicated in Table B.2. The profiles are displayed graphically in Figure 5.3 and Figure 5.4.

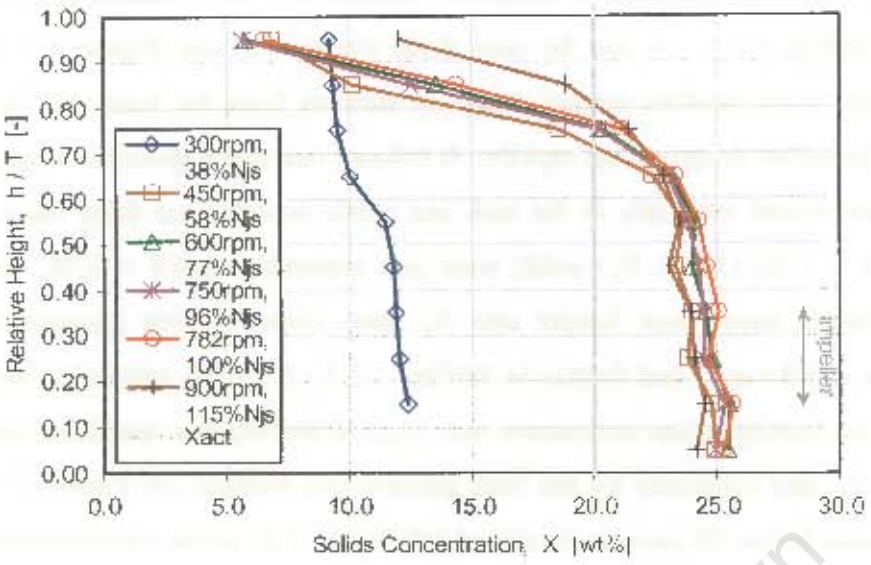

Figure 5.3 Solids concentration profiles for d_{p91} (75 – 106 μm) at various N under three-phase conditions

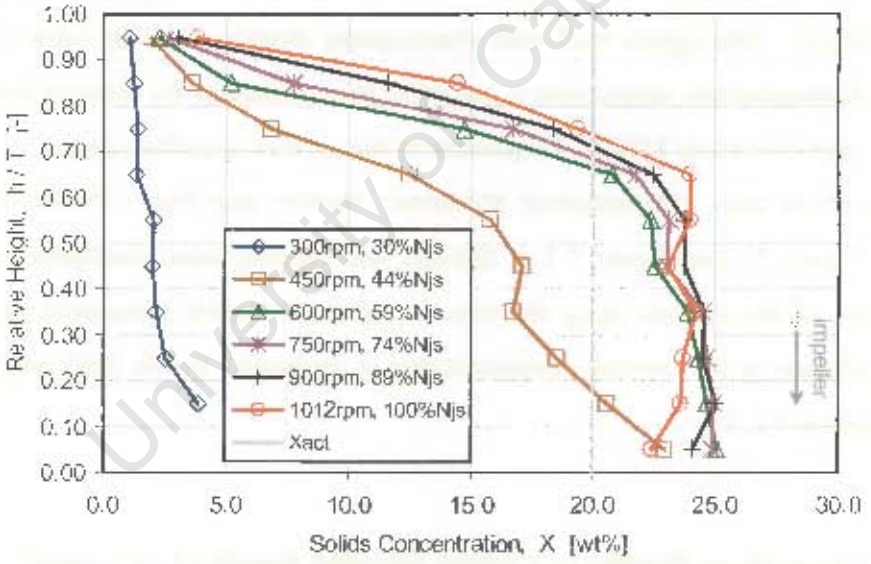

Figure 5.4 Solids concentration profiles for d_{p200} (150 – 250 μm) at various N under three-phase conditions

The three-phase profiles, shown in Figure 5.3 and Figure 5.4, display somewhat different characteristics compared to the two-phase profiles in Figure 5.1 and Figure 5.2. The effects of gas on the solid-liquid hydrodynamics were already considered in Section 2.4.5.3. The introduction of gas causes both a reduction in turbulent dispersion, through increased turbulence dampening by the presence of gas, as well as a reduction in the impeller discharge

mass flowrate, through the reduction of the effective slurry density and the formation of gas cavities behind the impeller blades. Solids are suspended off the bottom and distributed throughout the tank by a combination of turbulent dispersion and fluid circulation. The presence of gas thus reduces both these mechanisms of solids suspension and it is therefore expected that the effectiveness of solids suspension at the same impeller speed will deteriorate with increased gas addition. The reduction in off-bottom suspension can be seen by comparing the percent of critical impeller speed ($\%N_{js}$) values at the same impeller speed (N) from the ungassed (Figure 5.1 and Figure 5.2) to the gassed (Figure 5.3 and Figure 5.4) conditions. This reduction in percent critical is the result of the *gassed* critical impeller speeds, N_{jsg}, being higher (782 and 1012 rpm) than the *ungassed* critical impeller speeds, N_{jsu}, (500 and 675 rpm). The reduction in the effectiveness of solids distribution can be seen from comparing both the position and the shape of the three-phase profiles with that of the two-phase profiles. In terms of position, the lower sections of the three-phase profiles are generally further above the homogeneous suspension line (X_{act}) than for the two-phase profiles. This indicates less vertical distribution of solids with more solids remaining in the lower sections. The shape of the curves indicates slightly decreasing slopes in the lower sections with the drop-off in vertical solids concentrations occurring at lower levels than for ungassed cases, which are indicative of turbulence dampening and reduced circulation caused by the addition of gas. A further noticeable feature of the three-phase profile is that although it generally starts to drop-off at lower levels than the comparable two-phase profile the drop-off is less rapid than for two-phase with the solids concentrations at the top generally not dropping off to zero as for many two-phase profiles. This additional solids distribution effect in the case of the three-phase profiles is due to rising bubbles having a solids dispersion effect, which can be seen to be more significant for the finer particles (cf. Figure 5.3) than for the coarser size fraction (cf. Figure 5.4).

5.1.3 Concentration above the Base vs. Increasing Impeller Speed

It can be noted, especially in the two-phase solids concentration profiles in Section 5.1.1, but also to some extent in the three-phase profiles in Section 5.1.2 that the vertical concentrations in the lower sections of the profiles are relatively uniform, and changes with increasing impeller speed. This concentration above the base is determined by the interaction between the extent of off-bottom suspension and the extent of solids distribution. As more solids are suspended from the base the concentration above the base

increases, and as the solids are distributed higher up in the cell, this concentration above the base tends to decrease. As already discussed in Section 2.4.3 this *concentration above the base criterion* has been used and tested by some as an alternative method for identifying N_{js} [Chapman et al. (1983c); Ayazi Shamlou and Koutsakos (1989)]. This criterion equates the point where a plot of solids concentration above the base vs. impeller speed shows a maximum or a discontinuity to the just suspended condition (N_{js}). This criterion can be tested for the two- and three-phase profiles in the previous two sections by choosing a point above the base (e.g. h/T = 25%) and plotting the solids concentrations at this height (X_{h25}) vs. increasing impeller speed. Plotting the values as given in Table B.1 and Table B.2 leads to the plots as given in Figure 5.5.

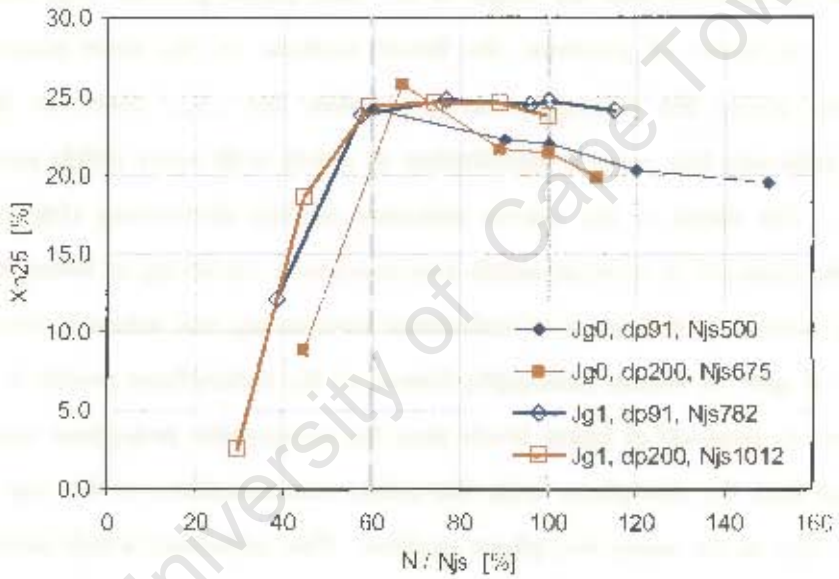

Figure 5.5 Solids concentrations (X_{h25}) at a point h/T = 25% above the base vs. relative impeller speeds (N/N_{js})

It follows from Figure 5.5 that plotting the solids concentrations at a relative height of 0.25 T above the base against impeller speed did form discontinuities in the curves as predicted. However, it is clear that these discontinuities occurred relatively consistently at points far below N_{js} and not at N_{js}. The discontinuities for the three-phase curves occurred at a point close to 60% of N_{js} and it seems that the same applies for the two-phase condition. This finding is in agreement with the finding of Ayazi Shamlou and Koutsakos (1989), who also found that the concentration above the base criterion often gave a predicted N_{js} value lower than that obtained from visual observation.

5.1.4 Testing the Sedimentation-Dispersion Model for Vertical Solids Distribution

The sedimentation-dispersion model for vertical solids distribution has already been introduced in Section 2.4.6.3 in the Chapter 2. Barresi and Baldi (1987a) and Ayazi Shamlou and Koutsakos (1989) modelled the distribution of solids vertically in stirred tanks by applying the sedimentation-dispersion model. Both used relatively dilute solids concentration systems ($X \leq 6$ wt.%) in small vessels ($T \leq 0.39$ m). The sedimentation-dispersion model relies on the assumptions of, negligible radial profiles, negligible solid-solid interaction and isotropic turbulence. These assumptions were approximately met in these works. In the current study, a larger tank ($T = 0.54$ m) and a higher solids concentration ($X = 20\%$) were used. Applying the sedimentation dispersion model here is therefore not expected to agree with an *idealized turbulent suspension* as referred to by Schubert (1999) in his discussion of the sedimentation-dispersion model. Still, the sedimentation-dispersion model will be applied here to the results obtained. This while keeping in mind that although not incorporated into this model the contribution of bulk fluid circulation to solids distribution should not be forgotten, especially at larger scale, higher solids concentrations, and gassed conditions.

The basic balance equation from which the sedimentation-dispersion model is derived is as given in Equation 5-1 (sedimentation flux vs. dispersion flux of solids).

$$u_s X_h + D_S\left(\frac{dX_h}{dh}\right) = 0$$

..... Equation 5-1

With some manipulation of Equation 5-1, it can be written as Equation 5-2, showing how the change in solids concentration with height is determined by the ratio of the solids slip velocity, u_s, and the solids dispersion coefficient, D_S.

$$\frac{d\ln X_h}{dh} = -\frac{u_s}{D_S}$$; Where u_s = solids sedimentation velocity; D_S = solids dispersion coefficient

..... Equation 5-2

Schubert (1999) used modified Peclet numbers, $N_{Pe^*} = u_s T/D_S$, to define three different types of vertical solids distributions. High u_s and low D_S ($N_{Pe^*} > 100$) will lead to all solids remaining on the bottom of the tank. Low u_s and high D_S ($N_{Pe^*} < 0.1$) will lead to a constant vertical solids distribution. Ratios of u_s and D_S between these extremes will lead, under *idealized turbulent suspension* conditions, to exponential decays in solids concentrations from the bottom of the tank.

Equation 5-2 thus suggests that a plot of ln$X$ vs. h will give the ratio u_s / D_S as the slope. Ayazi Shamlou and Koutsakos (1989) did the same (cf. Figure 2.32). It should be remembered that they worked in a smaller vessel at very low solids concentrations (X = 1 wt.%). Plotting the natural logarithms of the solids concentrations against height for the two-phase profiles already discussed in Section 5.1.1, Figure 5.6 is obtained.

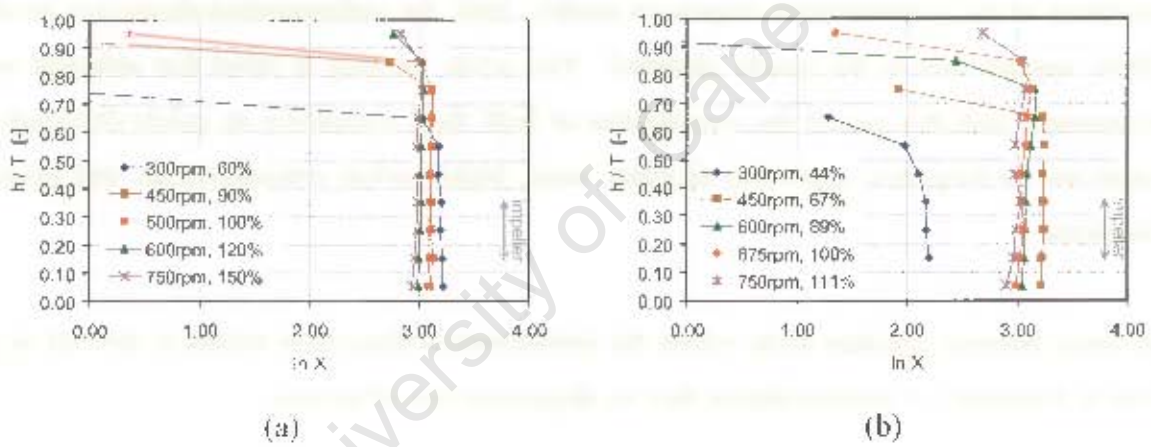

Figure 5.6 Applying the sedimentation-dispersion model to the vertical solids distribution of the (a) d_{p91} and (b) d_{p200} size fractions under two-phase conditions

It can be seen from Figure 5.6 (a) and (b) that most of the data points gave very uniform vertical profiles, and thus by applying Equation 5-2 that, d.ln$X$ / dh = u_s / D_S ~ 0. It follows that in most of the profiles tested, the upward turbulent dispersion coefficient (D_S) was totally controlling and much larger than the solids slip velocity (u_s), leading to very uniform vertical profiles. It should be noted that slope of d.ln$X$ / dh, as referred to by Equation 5-2, is the slope *off the vertical* due to the orientation of the axes in Figure 5.6. Only at very low impeller speeds and higher up in the cell does the slip velocity of the solids become controlling causing the solids concentrations to drop off. Overall, the application of the sedimentation-dispersion model to two-phase suspension conditions at high solids

concentration and turbulence can be evaluated as to provide mechanistic insight into the opposing processes of sedimentation and dispersion. However, due to the very flat profiles observed in most of the tank at impeller speeds above 60% of N_{js} its practical value is limited.

The three-phase solids concentration profiles as already discussed in Section 5.1.2, will now be considered in terms of the sedimentation-dispersion model. The model is still the same as that used for the two-phase conditions; however, equating upwards solids dispersion to turbulent diffusion action of the impeller only, will now change. The additional dispersion effect of gas bubbles, as observed in three-phase bubble columns [Smith and Ruether (1985); Reilly et al. (1990)] and three-phase fluidized beds [Kim, Kim and Han (1992); Matsumoto et al. (1997)] should now also be considered in addition to the impeller action. It is however thought that the dispersion of solids by air will only become prevalent under lower turbulent conditions as existing in the upper parts of a mechanical flotation cell.

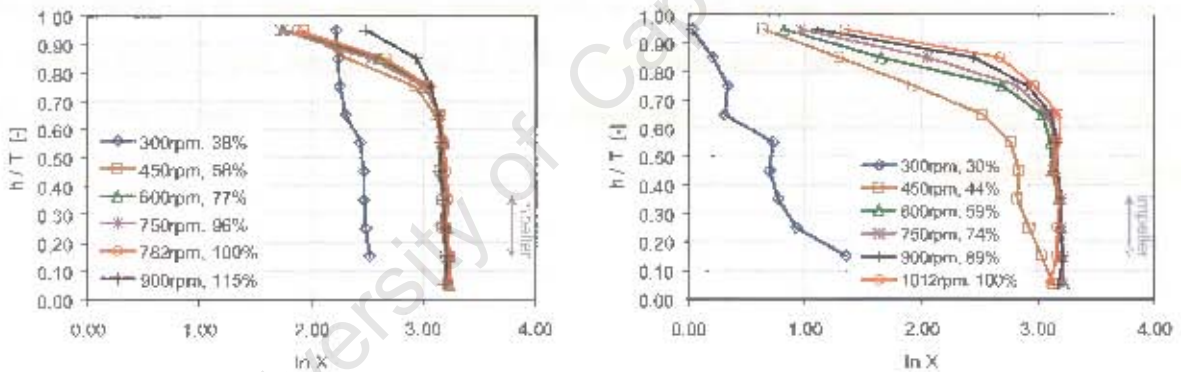

Figure 5.7 Applying the sedimentation-dispersion model to the vertical solids distribution of the (a) d_{p91} and (b) d_{p200} size fractions under three-phase conditions

Applying the sedimentation-dispersion model to the three-phase profiles for the d_{p91} and d_{p200} size fractions leads to Figure 5.7 (a) and (b). Considering Figure 5.7 (a) and (b) it can be seen that most of the plots at higher impeller speeds above approximately 60% of N_{js} gave very flat slopes (off the vertical) in the lower 60% of the tank with increased slopes in the upper 30% of the cell. This indicates that the dispersing action was controlling in the lower part of the cell, with the solids slip velocity starting to compete higher up in the cell. The dispersing action in the lower part of the cell is due to the rotation of the impeller at these relatively high speeds, and the very flat profiles indicate that the impeller action was totally controlling over

the solids slip velocity. However, the solids drop-off occurred consistently at lower levels than in the two-phase cases, pointing to the turbulence dampening effect of the gas. In the upper 30% of the cell, the profiles dropped off at almost constant slopes, but not as sharply as in the two-phase cases, with solids being dispersed in all cases to the very top of the cell. This indicates the dispersing action in the upper part was mostly due to the rising gas bubbles. Only at very high impeller speeds (e.g. 115% of N_{js}) can it be seen that the dispersing action of the impeller is extended into this upper section of the cell. On the other hand, at very low impeller speeds (N < 50% of N_{js}), the rising gas bubbles become the main dispersing action against solids settling. The larger gas bubbles that form at these low impeller speeds also have larger dispersing actions. However, under these conditions most solids are settled out on the bottom of the tank.

Overall, it was shown how the sedimentation-dispersion model, mechanistically, explains the opposing effects at work in solids distribution. Its practical application to model vertical solids distribution however seems limited in mechanical flotation cells. It is further thought important to acknowledge the solids dispersion effect of the rising gas bubbles as this effect is at the top of the cell, below the froth, and might interact with separation and recovery into the froth (entrainment).

5.2 EFFECTIVENESS OF SOLIDS SUSPENSION

In Section 5.1 the solids concentration profiles obtained for the four different test conditions were discussed mostly qualitatively to give a better mechanistic understanding of solids suspension and specifically solids distribution as measured by concentration profiles. In this section, quantitative measures of the effectiveness of solids suspension as derived from the concentration profiles will be evaluated both in terms of increasing impeller speed (N), and increasing percentage of critical impeller speed (N/N_{js}). The four different test conditions had different critical impeller speeds (N_{js}), and it will be shown how the effectiveness of solids suspension is normalized if benchmarked in terms of percentage of critical impeller speed (N/N_{js}). The solids suspension *effectiveness* criteria that will be quantified here are *extent of off-bottom suspension* (cf. Section 5.2.1), *extent of axial solids distribution* (cf. Section 5.2.2), and *variability of axial solids concentrations* (cf. Section 5.2.3).

5.2.1 Extent of Off-bottom Solids Suspension (X_m/X_{ms})

The extent of off-bottom solids suspension can be determined from concentration profiles done at different impeller speeds by calculating the mean solids concentration from each profile (X_m). As more and more solids are suspended off the bottom, X_m will increase until all the solids are suspended at or above the just suspended condition. Within sampling error, X_m will remain constant at a constant mean suspended value of X_{ms} at or above N_{js}. Comparing X_{ms} to the actual bulk solids concentration X_{act}, which was known in this work, indicated that the relative sampling error was generally less than five percent (cf. Tables B.1 & B.2). The average profile concentration under complete off-bottom conditions, X_{ms}, was taken at the just suspended condition in this work but can also be taken at any point above. Plotting the mean profile concentrations (X_m) against increasing impeller speed (N) results in Figure 5.8 from which it can be seen how the average profile concentrations (X_m) generally increase with increasing impeller speed (N) until the solids are full suspended. However these fully suspended conditions (N_{js}) occur at different impeller speeds and it is difficult to identify a general trend off this figure. Figure 5.9 plots the extent of off-bottom solids suspension (X/X_{ms}) against percentage of critical impeller speed (N/N_{js}). In so doing, much clearer trends emerge. As per definition, off-bottom solids suspension is complete ($X_m/X_{ms} \sim 1$) when the critical impeller speed is reached ($N/N_{js} = 100\%$). Below N_{js}, the extent of solids

sedimentation ($1-X_m/X_{ms}$) can be derived from this figure. The extent of solids sedimentation increases relatively slowly until the impeller speed drops to around 60 percent of N_{js}, below which solids sedimentation becomes much more drastic. In gassed conditions the fraction of sedimented solids increases rapidly from less than ten percent, whilst for ungassed conditions the fraction of sedimented solids increases rapidly from around 20 percent as the impeller speeds drops below 60 percent of N_{jsg} (J_G = 1 cm/s) and N_{jsu} respectively. This would suggest that in order to prevent significant sanding and associated losses in a flotation cell, it should be operated above at least 60 percent of the gassed critical impeller speed ($N > 0.60 \times N_{jsg}$).

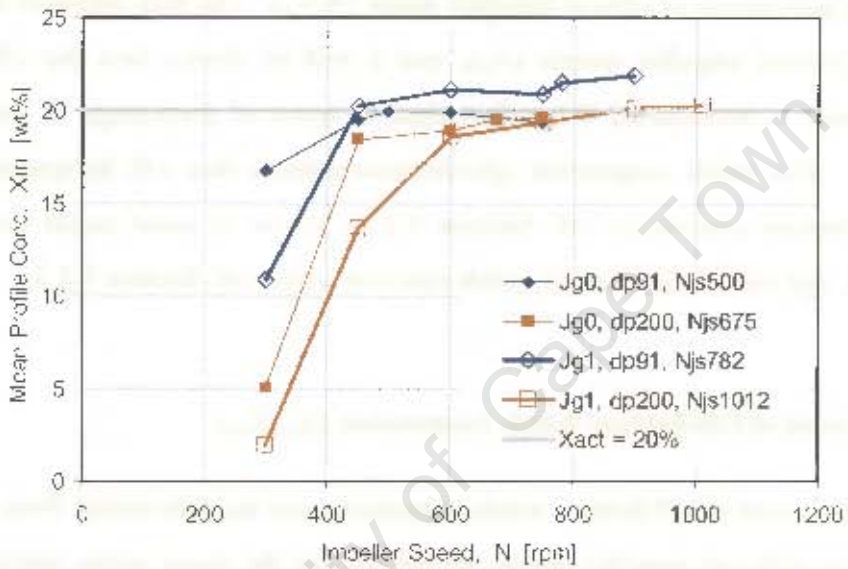

Figure 5.8 Average profile solids concentrations (X_m) versus increasing impeller speed

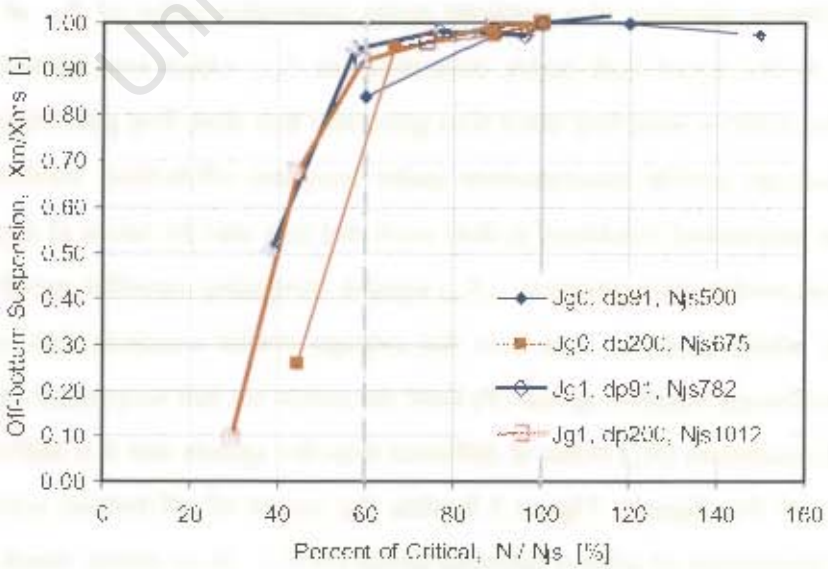

Figure 5.9 Extent of off-bottom solids suspension versus percentage of N_{js}

5.2.2 Extent of Vertical Solids Distribution (Suspension Heights)

The suspension height (h_s) is a solids suspension effectiveness measure that quantifies the extent of vertical distribution of solids rather than off-bottom suspension of solids. Similarly, concentration profiles are also measures of solids distribution rather than off-bottom suspension. In this regard Arbiter, Harris and Yap (1969) suggested that off-bottom suspension conditions, whether complete or not, should always be noted together with solids distribution measures, in order to obtain a more complete picture of the effectiveness of solids suspension, both off-bottom and distribution. The suspension height h_s is per definition the upper height from the base to which solids are distributed to in a vessel. It is sometimes measured visually and is also referred to as cloud height. However, the visual measurement is somewhat subjective and very difficult under three-phase conditions. In this work the suspension heights were determined from the concentration profiles (cf. Tables B.1 & B.2). Relatively sharp drop-offs were already noted in the profiles higher up in the tank and the suspension height was taken as the height where the profile dropped below a certain concentration. Here this detection concentration was taken as $X = 10$ percent, which was half the bulk solids concentration. Suspension heights are often made relative by dividing it by the tank diameter (h_s/T) [Arbiter, Harris and Yap (1969)]. When plotting the relative suspension heights (h_s/T) vs. impeller speed (N), Figure 5.10 is obtained. As can be expected, h_s for the four different test conditions increases with increasing N until the solids reach the top of the liquid surface ($h_s/T = Z/T = 1$) at high impeller speeds. Figure 5.11 shows how h_s/T changes versus percentage of critical impeller speed (N/N_{js}). As with extent of off-bottom solids suspension, the suspension height drops off dramatically as the impeller speed drops below 60 percent of N_{js}. It is further noticeable that the suspension height (h_s) consistently reached a height equivalent to 90 percent of the tank diameter (T) as the critical impeller speed is reached. As already discussed in Section 2.4.3.6, this finding is in good agreement with the 90% suspension height criterion proposed by some to identify the just suspended condition in standard stirred tanks. Weisman and Efferding (1960) and Einenkel (1980) have proposed the 90% suspension height as an alternative N_{js} criterion to the visual 1s criterion, whilst Chapman et al. (1983c) and Hicks, Myers and Bakker (1997) have found that the relation between $h_s/T = 90\%$ and the directly observed N_{js} is not always that consistent. Still it is thought that the 90% suspension height criterion may be worth considering in testing solids suspension conditions in industrial scale flotation cells, but should always be checked against

some other direct measurement of the conditions on the bottom of the tank, eg visual, contact with the tank bottom, ultrasound, or radiation.

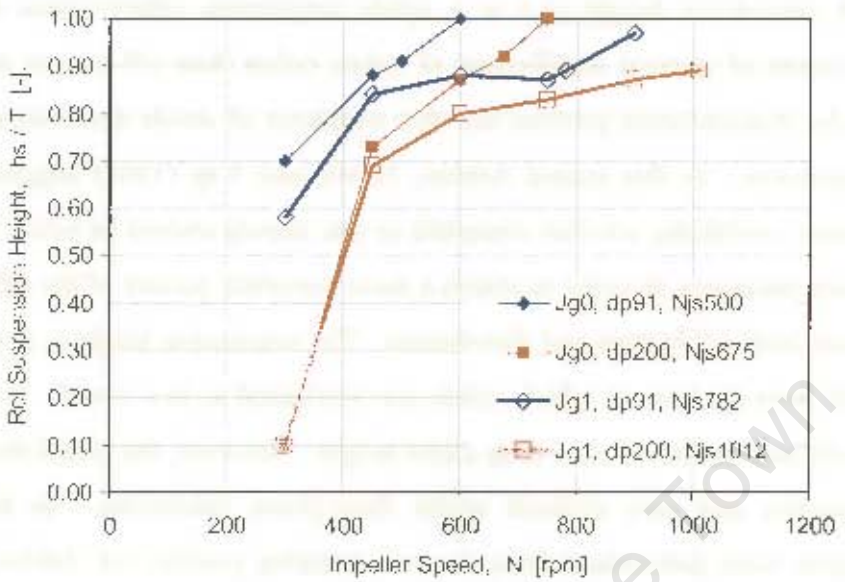

Figure 5.10 Relative suspension heights versus increasing impeller speed

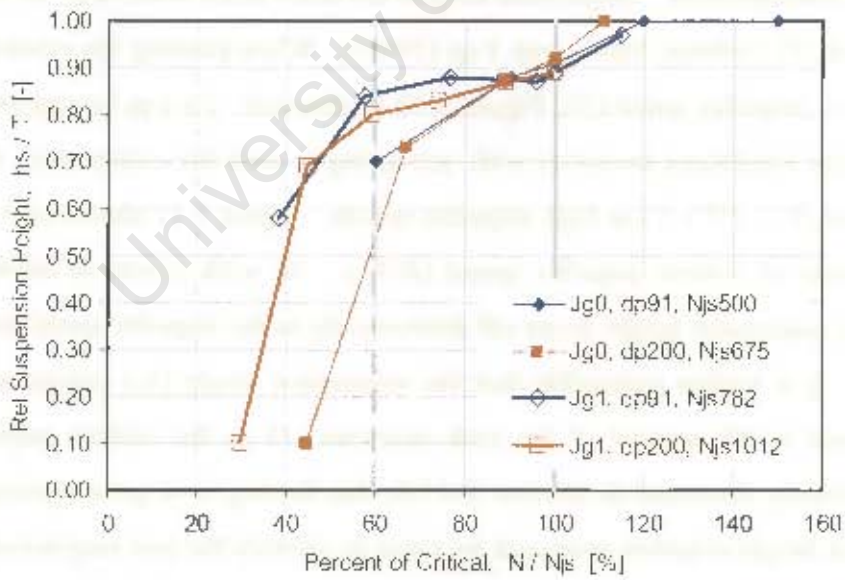

Figure 5.11 Relative suspension heights versus percentage of critical impeller speed

5.2.3 Variability of Vertical Solids Concentrations (*RSD*)

Finally, the variation of the solids distribution can be considered by calculating a relative standard deviation *RSD* of the solids concentrations in each profile (Tables B.1 & B.2). It should be remembered that only 'measurable' solids concentrations were included in these profiles and not the sedimented solids on the bottom of the tank as the sedimented layer will normally not be sampled. Plotting the calculated *RSD* values of the concentrations in the profiles versus increasing impeller speed (N), Figure 5.12 is obtained. The *RSD* value is a measure of the variation of the solids concentrations within the distribution. When low *RSD* values are reached, which remains constant with increasing impeller speed, the homogeneous suspension condition is normally assumed. It can be seen that the two-phase *RSD* values are initially higher but then decreases more quickly with increasing impeller speed compared to the three-phase *RSD* values. The three-phase *RSD* values on the other hand, are initially lower at very low impeller speeds due to the dispersing action of the rising gas bubbles, but then remains constant or decreases at a much slower rate versus increasing impeller speed due to the presence of gas inhibiting both the fluid circulation and the turbulent dispersion actions produced by the impeller. Figure 5.13 shows the *RSD* values from each profile versus relative impeller speed (N/N_{js}). Once again, the usefulness of benchmarking solids suspension conditions versus percentage of critical impeller speed becomes clear as all conditions display approximately the same *RSD* value when the critical impeller speed is reached. In this work the *RSD* value at the just suspended condition was in the region of 30%. Others working in two-phase standard stirred tanks [Einenkel (1980); Bohnet and Niesmak (1980); Barresi and Baldi (1987a)] have also reported that they observed consistencies in the calculated variation in solids concentrations in profiles obtained at the just suspended condition (cf. Section 2.4.3.8). However, the actual *RSD* value at the just suspended condition does depend amongst other things on the number of measurements in the profile, and the repeatability of the sampling; and a generally applicable value does not seem to exist. For a given system this *RSD* value may be found and might be useful in indirectly identifying the just suspended condition. However, this criterion is not widely established, *especially not for gassed conditions*, and as seen for the finer particle size fraction under gassed conditions, the same *RSD* values of close to 30% are obtained, even with the impeller speed dropping to almost 50% of critical.

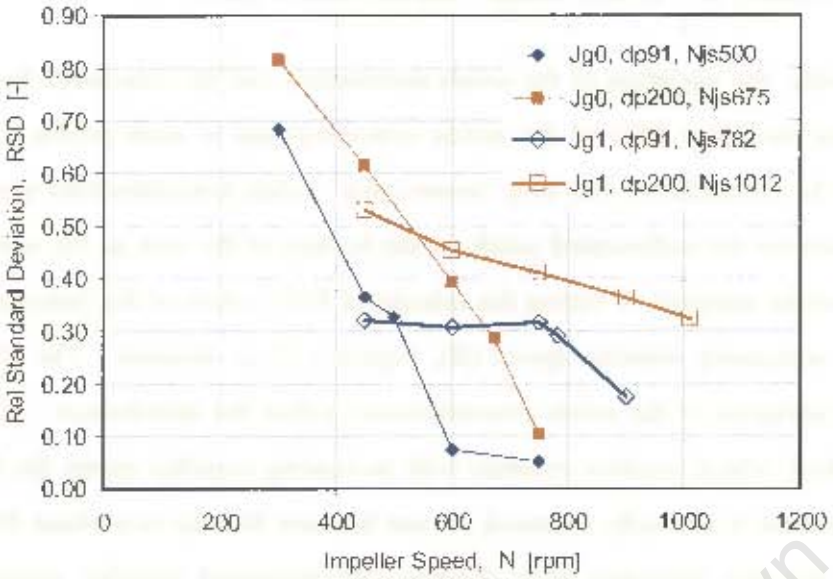

Figure 5.12 Relative standard deviation of profile concentrations versus increasing impeller speed

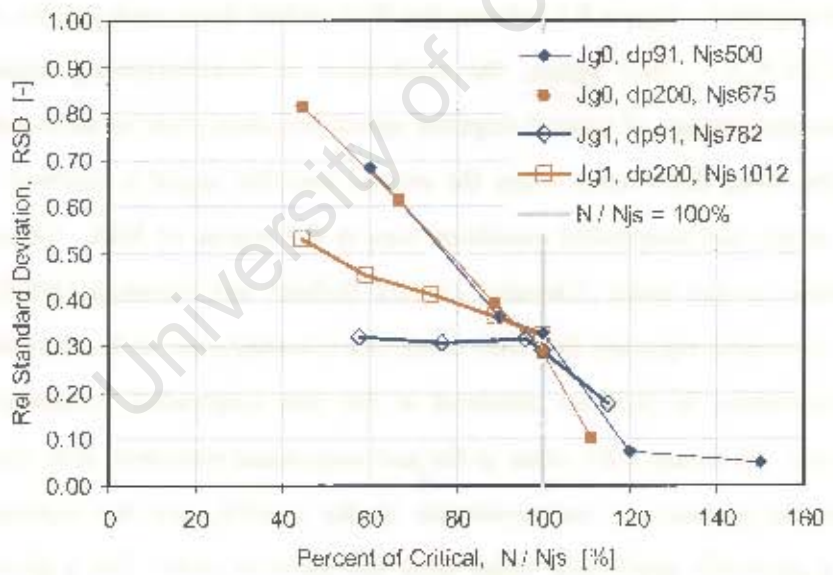

Figure 5.13 Relative standard deviation of profile concentrations versus percentage of critical impeller speed

5.3 CONCLUSIONS

The aim of this chapter was to evaluate the solids distribution aspect of solids suspension in a pilot scale mechanical flotation cell and to determine whether it can be related to off-bottom suspension conditions in terms of the critical impeller speed. As outlined in the 'Scope and Objectives' of this work (cf. Section 2.6), concentration profiles formed a secondary objective after the primary objective of characterising off-bottom suspension in terms of the critical impeller speed, which was addressed in Chapter 4. In this chapter, concentration profiles were measured at a full range of impeller speeds for two solids size fractions (75-106μm, 150-250μm) under both two- and three-phase conditions (J_G = 0, 1 cm/s). The concentration profiles obtained under the different conditions were then discussed mostly qualitatively and mechanistically, before considering some solids suspension measures (i.e. extent of off-bottom, suspension height, and variation within the profiles) by which the effectiveness of solids suspension and distribution can be quantitatively evaluated and related to off-bottom suspension conditions.

Considering the concentration profiles versus impeller speed, the following observations were made.

- At the same impeller speed the coarser solids fraction were less distributed and showed more variation than the finer size fraction.
- The two-phase profiles generally displayed uniform solids concentrations up to certain height above which it dropped off rapidly (suspension height).
- At the critical impeller speed, the solids are distributed relatively homogeneously throughout the tank, although above the average bulk concentration in most of the tank, with a sharp drop-off in concentration at the very top of the tank ($h \sim 0.90T$).
- A homogeneous suspension was approached for the finer size fraction as the relative impeller speed was increased to 150 percent of critical. This agrees well with observations by Oldshue, Herbst and Post (1995) and Shaw (1992).
- The introduction of gas caused the critical impeller speed to increase and the extent of *off-bottom* suspension for the three-phase profiles was thus less at the same impeller speed if the impeller speed dropped below the gassed critical impeller speed.

- The effectiveness of solids *distribution* was also reduced with gassing. The concentrations in the lower parts of the profiles were generally higher and further above the bulk average concentration and the drop-off in concentrations occurred at lower heights than for the two-phase profiles. The reduced solids distribution with gassing is thought to be related to turbulence dampening and reduced fluid circulation caused by the presence of gas.
- The drop-offs in solids concentration at the top of the cell were however not as steep as those obtained for two-phase conditions, indicating that the rising gas bubbles were contributing to solids distribution in the upper regions of the tank. The dispersing effect of the gas bubbles could be seen to be stronger for the finer particle size fraction. It is thought that this dispersing action of the gas bubbles in the upper regions of the tank may be affecting the *separation* between valuable and gangue particles that should be occurring in this region below the froth and may thus be contributing to entrainment in mechanical flotation cells.
- In testing the '*solids concentration above the base*' N_{js} criterion it was seen that some criterion does seem to exist but that it related to a relative impeller speed far below the critical impeller speed (~ 60 % of N_{js}). Similarly, Ayazi Shamlou and Koutsakos (1989) also found that this criterion predicts N_{js} values below the visually observed values.
- The sedimentation-dispersion model, developed for small stirred tanks at low solids concentrations and negligible radial concentration profiles, aided in the mechanistic discussion of the opposing effects of the downward solids sedimentation flux versus the upwards solids dispersion flux [Schubert (1999)]. Its practical application to model the solids distribution in larger flotation cells, operating at higher solids concentration and radial profiles does however seem limited.
- For the two-phase profiles the sedimentation-dispersion model indicated that the turbulent dispersion action of the impeller is totally controlling in most of the cell, causing uniform vertical profiles, up to the suspension height where the impeller action reduces abruptly and the sedimentation of particles become controlling leading to sharp drop-offs in solids concentrations.
- In three-phase conditions the dispersion action is not only due to the impeller action, but also due to the dispersing action of the rising gas bubbles, which will

become significant in low turbulent conditions, such as those normally existing in the quiescent region at the top of the cell.

- For most of the three-phase profiles (at impeller speeds between approximately 60% and 100% of critical impeller speed) the sedimentation-dispersion model indicated two regions to exist vertically in the cell. In the lower approximately 60% of the tank the dispersing action of the impeller was controlling leading to almost vertical profiles, although turbulence dampening caused the solids concentrations to drop slightly. In the upper approximately 30% of the cell, the dispersing action of the impeller dropped off and was replaced by the dispersing action of the rising gas bubbles.
- As the impeller speed is increased significantly above N_{jsg} (e.g. $\geq$ 115% of N_{jsg}) the dispersing action of the impeller starts to expand into this upper region of the tank, superseding the dispersing action of the bubbles, and resulting in very uniform vertical profiles to extend further up into the top section of the cell.

The effectiveness of solids suspension was further quantified in terms of the extent of off-bottom suspension, suspension height, and the variability of the concentrations within the distribution.

- When plotting the extent of off-bottom suspension against relative impeller speed rather than impeller speed, consistent trends emerged for the different conditions tested.
- The extent of off-bottom suspension decreased dramatically for all conditions as the relative impeller speed dropped below 60% of critical. This suggests that in order to prevent significant sanding losses a flotation cell should be operated above at least 60 percent of the gassed critical impeller speed ($N > 0.60 \times N_{jsg}$).
- The extent of off-bottom suspension was determined in this flotation cell (batch) by plotting average profile concentrations versus increasing impeller speed. This method may also be useful in continuous industrial flotation cells.
- Similarly to the extent of off-bottom suspension, the extent of solids distribution in terms of suspension heights, displayed consistent trends for the different conditions tested, when plotted against relative impeller speed (% of N_{js}) rather than impeller speed (N).
- Similarly to Weisman and Efferding (1960) and Einenkel (1980) it was found that the suspension as derived from the concentration profile consistently reached 90%

as the critical impeller speed was reached. This 90% suspension height criterion ($h = 0.90T$) thus show some promise to be used in industrial mechanical flotation cells, but should be applied with caution due to many finding it not to give very consistent results of off-bottom suspension conditions [Chapman et al. (1983c); Nienow (1992)]. It should therefore always be checked against some other direct measurement of the conditions on the bottom of the tank, eg visual, contact with the tank bottom, ultrasound, or radiation.

- The variation in vertical solids concentrations in terms of the relative standard deviation, showed consistent results for the two-phase conditions, when plotted against relative impeller speed, but not for the three-phase conditions. In this work the *RSD* value at the just suspended condition was in the region of 30%. Others [Einenkel (1980); Bohnet and Niesmak (1980); Barresi and Baldi (1987a)] working in stirred tanks have also observed consistencies, but their RSD values are different. For gassed conditions this RSD value also seems less significant for relating solids variation with the just suspended condition.
- The consistent trends that were obtained when the effectiveness of off-bottom as well as solids distribution were benchmarked against critical impeller speed (an off-bottom suspension condition) demonstrated the importance of the critical impeller speed as a general measure of solids suspension conditions in a vessel, both off-bottom and solids distribution. This is thus a further motivation for using the critical impeller speed for solids suspension correlation purposes, as was done in Chapter 4.

CHAPTER 6. CONCLUSIONS

The *overall aim* of this thesis was to *evaluate solids suspension* in a 124l pilot scale mechanical flotation cell. Different solids suspension parameters were considered and the *critical impeller speed*, which relates to the complete off-bottom suspension condition, was selected as the primary parameter for evaluating solids suspension conditions. A number of *concentration profiles* were also measured to extend the evaluation of solids suspension from off-bottom suspension conditions to include solids distribution aspects. The conclusions reached in Chapters 4 and 5 are summarised here.

6.1 CRITICAL IMPELLER SPEED

The *primary objective* of this work was to develop a solids suspension correlation relating the critical impeller speed (N_{js}) to solid-liquid-gas system variables. In so doing the effects of particle size (d_p), solids concentration (X), solids density ($\Delta\rho/\rho_L$), liquid kinematic viscosity (ν_L), and gas addition (J_G or Q_{GV}) on off-bottom solids suspension would be determined. Geometrical variables (T, D/T, C/T) were not considered in this work. Schubert and co-workers [Schubert (1985); Weiss and Schubert (1989)] also measured critical impeller speeds in mechanical flotation cells but did not develop a correlation of how this important off-bottom suspension condition is affected by system parameters. In this work, the N_{js} correlation was developed in two stages, first for solid-liquid, two-phase and then for three-phase conditions. This approach is also commonly followed in stirred tanks and assists in isolating the effect of gas on N_{js}.

6.1.1 Two-Phase Critical Impeller Speed

The two-phase critical impeller speed correlation developed in this work shows how the critical impeller speed under ungassed conditions (N_{jsu}) is influenced by the main solid-liquid variables that has been found to influence solids suspension in stirred tanks.

$$N_{jsu} = K_{SL} d_p^{0.35\pm0.02} X^{0.12\pm0.02} \left(\frac{\rho_S - \rho_L}{\rho_L} \right)^{0.66\pm0.05} \quad ; K_{SL} = 54 \text{ and } N_{jsu} \text{ in rpm}$$

.....(cf. Equation 4 12)

A mechanical flotation cell (this work); K_{SL} = f (T, D/T, C/T, imp. design)

The N_{jsu} correlation fitted the experimental observations very well with almost all predictions lying within 10% of the experimentally measured values and a good coefficient of determination (r^2 = 0.963). The effects of particle size and especially solid-liquid density difference on N_{jsu} were found stronger than that found by Zwietering (1958) and most others in stirred tanks. This is thought to be related to the proximity of the stator to the impeller in a flotation cell, reducing fluid circulation in favour of increased turbulence in the impeller region. Particle size and solid-liquid density difference are the two main variables influencing the settling velocity of particles. The effect of solids concentration was within the range, but towards the lower end of stirred tank findings. Similarly, kinematic viscosity was found to have a small influence on N_{jsu}. Viscosity gave somewhat conflicting effects for two particle sizes tested, decreasing for the coarser 150-250 µm and increasing for the finer 75-106 µm size fraction. This may suggest that coarser particles are suspended more by fluid flow drag and finer particles more by turbulent actions, which will cause viscosity to have these conflicting effects on N_{jsu}. However, numerical analyses suggested that on balance viscosity effects should be ignored in the two-phase work. This disagrees with Zwietering ($N_{jsu} \alpha \nu_L^{0.10}$) but agrees with some others [e.g. Chapman *et al.* (1983a)] also finding viscosity to have a negligible effect on N_{jsu}.

6.1.2 Three-Phase Critical Impeller Speed

The aim of this section was two-fold. Firstly, the *effect of gas addition on* N_{jsg} should be determined, and secondly, *the effect of the other solid-liquid variables* should be tested *under gassed conditions.*

Gas addition was seen to cause a *linear increase* in N_{jsg}, but the rate of the increase *varied* for different conditions. It was found that the effect of gas is best accounted for by assuming the linear increase to be proportional to the ungassed critical impeller speed (N_{jsu}).

$$N_{jsg} = N_{jsu}(1 + \mathrm{K}.J_G) \; ; \; \text{Where, K} = 0.40 \; (\mathrm{cm.s^{-1}})^{-1} \; ; \; (\text{Or, K} = 0.36 \; \mathrm{vvm^{-1}})$$

.....(cf. Equation 4 17)

In comparison, data from Weiss and Schubert (1989) showed that air addition had a slightly smaller effect (K = 0.25 to 0.28 $\mathrm{vvm^{-1}}$) in a smaller 54l cell using double finger impellers at a very low impeller clearance, C_b = 0.05. It is thought that the impeller type and the low

impeller clearance they used contributed to the smaller effect of air addition derived from their data.

The *effects of the other solid-liquid variables* were found to be influenced by gas addition and varied under *different gassed conditions*. The effects of all solid-liquid variables consistently increased from ungassed conditions to a gassing rate of 1 cm/s (1.1 vvm), where after the effects decreased on further gassing up to 2 cm/s (2.2 vvm). However, all the gassed conditions combined (1.1 to 2.2 vvm) gave exponents comparable to the ungassed effects. It was therefore thought best to develop the final correlation based on all the ungassed and gassed tests combined (0 to 2.2 vvm).

$$N_{jsg} = K_{SL'} d_p^{0.33\pm0.03} X^{0.17\pm0.03} \left(\frac{\rho_S - \rho_L}{\rho_L}\right)^{0.70\pm0.06} (\nu/\nu_w)^{0.05\pm0.04} (1 + K_G J_G);$$

Where, $K_{SL'} = 52$, $K_G = 0.40$ (cm/s)$^{-1}$ or 0.36 vvm^{-1}

.....(cf. Equation 4 28)

For both gassed and ungassed conditions ($J_G \geq 0$); Gassing range, Q_{GV}: 0 to 2.2 vvm (J_G: 0 to 2 cm/s);
$K_{SL'}$ = f (T, D/T, C/T, imp. design); K_G = f (C/T, imp design)

This three-phase correlation predicted the two and three-phase experimentally observed N_{js} values very well with most predictions lying within 10% or very close to 10% of the experimental values. The good fit was also confirmed by the good coefficient of determination (r^2 = 0.92). Similarly, to the two-phase findings, particle size (d_p) and especially solid-liquid density difference ($\Delta\rho/\rho_L$) were found to have the largest influences on the gassed critical impeller speed, and that their effects were also larger than that found in gassed stirred tank work. Again, as with the two-phase findings, this was thought to be related to the proximity of the stator to the impeller, increasing turbulence levels around the impeller, but decreasing fluid circulation with further reach for solids suspension purposes. The effect of particle size on N_{jsg}, $N_{jsg} \propto d_p^{0.33}$, is also exactly the same as that extracted from data given in Schubert (1985) for a 541 mechanical flotation cell at a gassing rate of Q_{GV} = 0.45vvm. This implies that the effect of solid-liquid variables on N_{js} may be independent of flotation cell design as is also the case with different impellers in stirred tanks. The effects of both solids concentration and kinematic viscosity increased slightly from the two-phase correlation and compared very well with the average findings in gassed stirred tank work. In gassed conditions, kinematic viscosity caused N_{jsg} to increase for both particle sizes, but still stronger for the finer particle size fraction, suggesting that turbulent effects, which is reduced

by increasing viscosity, play a larger role in the suspension of the smaller particles, whilst coarser particles are suspended more by fluid flow.

6.2 CONCENTRATION PROFILES

A secondary objective of this work was to evaluate the solids distribution aspect of solids suspension in a pilot scale mechanical flotation cell and to determine how it related to off-bottom suspension in terms of the critical impeller speed.

6.2.1 Evaluation of Concentration Profiles

Concentration profiles were measured at a full range of impeller speeds (300 to ~1100 rpm) for two solids size fractions (75-106μm, 150-250μm) under both two- and three-phase conditions (J_G = 0, 1 cm/s). Some qualitative observations can be made from considering these *concentration profiles*, and by applying the sedimentation-dispersion model for interpretation purposes.

The *two-phase profiles* were characterised by uniform solids distributions up to a certain height, at which level the concentrations dropped off rapidly. The suspension height can thus be clearly identified from these two-phase profiles. The suspension heights increased with impeller speed and reached a relative height of around 0.90 of T when the critical impeller speed was reached. For relative impeller speeds above approximately 60% of critical impeller speed, the concentrations in the lower (more uniform) section of the profiles were generally above the bulk average concentration and approached the bulk concentration as the impeller speed was increased and the suspension became more homogeneous. From results with the finer fraction, it can be seen that a homogeneous suspension was approached as the relative impeller speed was increased to around 150% of N_{js}. This finding agrees well with observations from stirred tanks where homogeneous suspension is taken to be between 150 and 170 % of critical [Oldshue, Herbst and Post (1995); Shaw (1992)].

The *three-phase profiles*, in the range of approximately 60% to 100% of N_{jsg}, can generally be characterised as displaying worse solids distribution in the lower and larger part of the cell, but slightly improved solids distribution in the uppermost sections when compared to the two-phase profiles at the same relative impeller speed. The concentrations in the larger and lower

part were higher and further above the bulk average concentration with the drop-off in concentrations at lower heights than for the two-phase profiles. The reduced solids distribution with gassing implies that gassing caused turbulence dampening as well as reduced fluid circulation. It therefore follows that gas addition not only negatively affected off-bottom suspension as seen in the critical impeller speed work but also reduced the effectiveness of solids distribution in the bulk of the tank. The drop-offs in solids concentration at the top of the cell were however not as steep as those obtained for two-phase conditions, indicating that the rising gas bubbles were contributing to solids distribution in the upper regions of the tank. The dispersing effect of the gas bubbles was seen to be stronger for the finer particle size fraction. It is thought that the dispersing action of the rising bubbles in the upper more quiescent region below the froth may interfere with the separation of gangue minerals from the bubble-particle aggregates, and thus may play some role in entrainment.

In testing the '*solids concentration above the base*' N_{js} criterion it was seen that some criterion does seem to exist but that it related to a relative impeller speed far below the critical impeller speed (~ 60 % of N_{js}). This agrees with Ayazi Shamlou and Koutsakos (1989) also finding that this criterion predicts N_{js} values below the visually measured critical impeller speeds.

Applying the *sedimentation-dispersion* model contributed somewhat to the mechanistic understanding of solids distribution in that it highlighted the opposing effects of the downward solids sedimentation flux versus the upwards solids dispersion flux [Schubert (1999)]. Its practical application to describe vertical solids distributions in stirred tanks has however mainly been restricted to idealized turbulent suspensions (two-phase, low solids concentrations, small vessels), and also from this work it seems as if its practical application to model the solids distribution in larger flotation cells, operating at higher solids concentration under gassed conditions is limited. Nonetheless, some mechanistic observations can be made by applying the concepts of upwards solids dispersion and downwards sedimentation.

- For the two-phase profiles the turbulent dispersion action of the impeller was totally controlling in most of the cell, causing uniform vertical profiles, up to the suspension height at which height the impeller action reduced abruptly and the sedimentation of particles became controlling leading to sharp drop-offs in solids concentrations.

- In three-phase conditions the dispersion action was not only due to the impeller action, but also due to the dispersing action of the rising gas bubbles, which became more significant in the lower turbulent conditions at the top of the cell and for finer particles.
- For most of the three-phase profiles at relative impeller speeds between approximately 60 and 100% of critical, the dispersing action of the impeller was controlling leading to almost uniform profiles up to approximately 60% of the height. In the upper 30% of the cell the impeller action dropped off and was replaced by the dispersing action of the rising gas bubbles. Yet, at higher impeller speeds (N > ~115% N_{js}) the impeller action became more controlling in the upper section of the cell, leading to more uniform solids concentrations extending further up in the cell.

6.2.2 Effectiveness of Solids Suspension

The *effectiveness of solids suspension* was evaluated quantitatively by using solids suspension measures that could be derived from the concentration profiles. These measures included extent of off-bottom suspension, suspension heights, and variation within the distribution. The first measure relates to off-bottom suspension whilst the other two relate to solids distribution aspects. Together these measures give a complete quantitative picture of the effectiveness of solids suspension and distribution in the vessel. When these solids suspension criteria were benchmarked against relative impeller speed in terms of percentage of critical impeller speed (N/N_{js}), definite trends emerged. The extent of off-bottom suspension was obtained by comparing the average profile concentration at different impeller speeds, and as would be expected the extent of off-bottom suspension was complete at or above N_{js}. It was further seen that dramatic sedimentation was evident as N/N_{js} dropped to below 60%. This would suggest that a flotation cell should be operated above at least 60% of N_{jsg} in order to prevent significant sanding losses. Suspension heights (h_s) were determined from the concentration profiles at the height where the concentration drops below 50% of the bulk solids concentration and also showed significant reductions when the impeller speed dropped below 60% of N_{js}, from which follows that, in addition to off-bottom suspension, the extent of vertical solids distribution was also significantly reduced as the impeller speed dropped below 60% of critical. Similar to some findings in stirred tanks, the just suspended condition agreed consistently with a vertical suspension height equivalent to 90% of the tank

diameter, which suggests that suspension height measurements may be a considered as an alternative criterion to the visual 1s criterion for determining N_{js} in flotation cells. This should however be applied with caution as many stirred tank studies have found that h_s is not a very consistent N_{js} criterion. The homogeneity of the solids distribution as depicted by the relative standard deviation *RSD* of the solids concentrations in the profile showed a constant value at the just suspended condition and a consistent trend under two-phase conditions. However, with gas addition the trend was less clear.

In summary,

- *A Critical impeller speed (N_{jsg}) correlation, relating complete off-bottom suspension to the effects of solid-liquid-gas variables, was for the first time developed for a mechanical flotation cell. This correlation incorporates the effects of d_p, X, $\Delta\rho/\rho_L$, ν_L, and J_G (or Q_{GV}) and fitted the experimental data of this work very well ($r^2 = 0.92$).*
- *Particle size, density difference, and air addition was found to have the largest effects on N_{jsg}. The effects of d_p and especially $\Delta\rho/\rho_L$ were also found to be stronger than the results obtained in standard stirred tanks. The stronger influences are thought to be related to the proximity of the stator to the impeller in a mechanical flotation cell, which reduces fluid flow in favour of increased turbulence. The effect of fluid flow (circulation) extends further away from the impeller for solids suspension considerations.*
- *Gas addition caused a linear increase in N_{jsg} with gas addition rate and the slope of the increase was found to be proportional to N_{jsu}.*
- *Solids concentration and liquid kinematic viscosity were found to have small effects on N_{jsg} and their effects were similar to that found in stirred tank work.*
- *Gas addition affected the effects of solid-liquid variables in three-phase conditions. After an initial increase in the effects of all variables at around $Q_{GV} = 1.1$ vvm, the effects of the solid-liquid variable decreased on further increased aeration.*
- *Solids distribution deteriorated with increased particle size and gassing. Increasing d_p increases the terminal settling velocity of the particles, whereas increased gassing reduces the solids suspension action of the impeller due to turbulence dampening and reduced impeller discharge mass flow.*
- *With N below N_{js} (60-100% N_{js}), the impeller action controlled solids distribution in approximately the lower 2/3 of the cell, with the dispersing action of the rising gas bubbles becoming more prevalent in the upper more quiescent areas of the cell. This dispersing action of the gas bubbles is stronger for finer particles and is thought possibly to influence the separation of valuables and gangue particles in this area just below the froth. The impeller action extended more and more into the upper third of the cell as the impeller speed was increased above N_{js}.*
- *The sedimentation-dispersion was not found to be of practical use to model vertical solids distribution in this flotation cell, but was used in the mechanistic description.*

- *The effectiveness of solids suspension in terms of extent of off-bottom, suspension height, and variation showed that common trends emerged for the different criteria, when benchmarked against percentage of critical impeller speed (% N_{js}). This demonstrated the leading role that N_{js} plays in solids suspension, both off-bottom and solids distribution.*
- *The effectiveness of solids suspension is generally good at the critical impeller speed (100% N_{js}), but deteriorated dramatically with N dropping below 60 % N_{js}. To the other end, a homogeneous suspension (perfect solids suspension) was approached as the impeller speed increased to 150-170 % N_{js}.*

REFERENCES

Ahmed, N and Jameson, GJ, 1989. Flotation kinetics. *Miner. Process. Extract. Metall. Rev.*, 5: 77-99.

Aldrich, C and Van Deventer, JSJ, 1995. Modelling of induced aeration in turbine aerators by use of radial basis function neural networks. *The Canadian Journal of Chemical Engineering*, 73: 808.

Anon, 1998. Svedala Flotation Machines. *Svedala marketing brochure.*

Anon, 2003a. Metso Minerals Flotation Machines RCS. *Brochure (No. 1010-10-01-MP/Sala-Englisch), Sweden.*

Anon, 2003b. Wemco SmartCell Flotation Machines. *Brochure (GL&V/EMC3327)*, USA.

Anon, 2004. Outokumpu Flotation Technologies. *Brochure (3007EN Libris, Apr 2004)*, Helsinki, Finland.

Arbiter, N and Harris, CC, 1962. Flotation machines, in *Froth Flotation*, Ed(s): D.W. Fuerstenau, pp 347-364, AIME, New York.

Arbiter, N and Steininger, J, 1962. Hydrodynamics of flotation cells, in *Proceedings 6th International Mineral Processing Congress, Cannes (English version given in Mineral Processing, 1965)*, pp 595-608, Pergamon Press, New York.

Arbiter, N, 1984. The flotation cell - a critique, in *Principles of mineral flotation*, pp 301-311.

Arbiter, N, 1999. Development and scale-up of large flotation cells, in *Proceedings SME Annual Meeting*, pp 345-352, Denver.

Arbiter, N, Harris, CC and Yap, RF, 1969. Hydrodynamics of flotation cells. *SME Transactions*, 244: 134-148.

Armenante, PM and Uehara Nagamine, E, 1998. Effect of low off-bottom impeller clearance on the minimum agitation speed for complete suspension of solids in stirred tanks. *Chemical Engineering Science*, 53: 1757-1775.

Ayazi Shamlou, P and Koutsakos, E, 1989. Solids suspension and distribution in liquids under turbulent agitation. *Chemical Engineering Science*, 44: 529-542.

Baldi, G, Conti, R and Alaria, E, 1978. Complete suspension of particles in mechanically agitated vessels. *Chemical Engineering Science*, 33: 21-25.

Barresi, A and Baldi, G, 1987a. Solid dispersion in an agitated vessel. *Chemical Engineering Science*, 42: 2949-2956.

Barresi, A and Baldi, G, 1987b. Solid dispersion in an agitated vessel: effect of particle shape and density. *Chemical Engineering Science*, 42: 2969-2972.

Bohnet, M and Niesmak, G, 1980. Distribution of solids in stirred suspensions. *German Chemical Engineering*, 3: 57-65.

Bourne, JR and Sharma, RN, 1974., in *Proceedings First European Conference on Mixing*, pp B3-25 to B3-38, BHRA, Cranfield, in Chapman *et al.*, 1983. *op cit.*.

Bujalski, W, Konno, M and Nienow, AW, 1988., in *Proceedings 6th European Conference on Mixing, BHRA*, pp 389-398, Cranfield, in Nienow, 1992. *op cit.*

Bujalski, W, Nienow, AW and Huoxing, L, 1990. The use of upward pumping 45° pitched blade turbine impellers in three-phase reactors. *Chemical Engineering Science*, 45: 415-421.

Buurman, C, Resoort, G and Plaschkes, A, 1986. Scaling-up rules solids suspension in stirred vessels. *Chemical Engineering Science*, 41: 2865-2871.

Calderbank, PH, 1958. Physical rate processes in industrial fermentation. Part I: The interfacial area in gas-liquid contacting with mechanical agitation. *Trans. Inst. Chem. Eng.*, 36: 443-460, in Rewatkar, Deshpande, Pandit and Joshi, 1993.

Chapman, CM, Nienow, AW, Cooke, M and Middleton, JC, 1983a. Particle-gas-liquid mixing in stirred vessels. Part 1: Particle-liquid mixing. *Chemical Engineering Research & Design*, 61: 71-81.

Chapman, CM, Nienow, AW, Cooke, M and Middleton, JC, 1983b. Particle-gas-liquid mixing in stirred vessels. Part 2: Gas-liquid mixing. *Chemical Engineering Research & Design*, 61: 82-95.

Chapman, CM, Nienow, AW, Cooke, M and Middleton, JC, 1983c. Particle-gas-liquid mixing in stirred vessels. Part 3: Three phase mixing. *Chemical Engineering Research & Design*, 61: 167-181.

Chapman, CM, Nienow, AW, Cooke, M and Middleton, JC, 1983d. Particle-gas-liquid mixing in stirred vessels. Part 4: Mass transfer and final conclusions. *Chemical Engineering Research & Design*, 61: 182-185.

Chatzi, E, Boutris, CJ and Kiparissides, C, 1991. On-line monitoring of drop size distributions in agitated vessels. 2. Effect of stabilizer concentration. *Ind. Eng. Chem. Des.*, 30: 1307, In: Mezaki, Mochizuki and Ogawa, 2000. *op cit.*

Chudacek, MW, 1986. Relationship between solids suspension criteria, mechanics of suspension tank geometry, and scale-up parameters in stirred tanks. *Ind. Eng. Chem. Fundam.*, 25: 391, in Rewatkar, 1991. *op cit.*

Coulson, JM and Richardson, JF, 1990. Pumping of Fluids, in *Chemical Engineering, Volume 1, Fourth Edition*, Ed(s): J.M. Coulson, J.F. Richardson, J.R. Backhurst and J.H. Harker, pp 261-311, Pergamon Press, Oxford.

De Nevers, N, 1991. *Fluid Mechanics for Chemical Engineers*, Second Edition Edition, Chapter 13, pp 433-447, McGraw-Hill, New York.

Deglon, DA, 1998. *PhD Thesis, University of Cape Town.*

Deglon, DA, Egya-Mensah, D and Franzidis, JP, 2000. Review of hydrodynamics and gas dispersion in flotation cells on South African platinum concentrators. *Minerals Engineering*, 13: 235-244.

Degner, VR and Treweek, HB, 1976. Large flotation cell design and development, in *Flotation, A. M. Gaudin Memorial Volume*, Ed(s): M.C. Fuerstenau, pp 816-837, A.I.M.E., New York.

Dickey, DS, 1992. Dimensional analysis, similarity and scale-up, in *Proceedings AIChE 1992 Annual Meeting, Nov 1-6*, pp 1-13, Miami Beach.

Dohi, N, Takahashi, T, Minekawa, K and Kawase, Y, 2003. Power consumption and solid suspension performance of large-scale impellers in gas-liquid-solid three-phase stirred tank reactors. *Chemical Engineering Journal*, Article in press: 1-12.

Dutta, NN and Pangarkar, VG, 1995. Critical impeller speed for solid suspension in multi-impeller three-phase agitated contactors. *The Canadian Journal of Chemical Engineering*, 73: 273-283.

Edwards, MF and Baker, M, 1992. Mixing of liquids in stirred tanks, in *Mixing in the process industries, Second edition*, Ed(s): N. Harnby, M.F. Edwards and A.W. Nienow, pp 137-157, Butterworth Heinemann, Oxford.

Einenkel, W, 1980. Influence of physical properties and equipment design on the homogeneity of suspensions in agitated vessels. *German Chemical Engineering*, 3: 118-124.

Fallenius, K, 1976. Outokumpu flotation machines, in *Flotation, AM Gaudin Memorial Volume*, Ed(s): M.C. Fuerstenau, pp 838-861, AIME, New York.

Frijlink, JJ, Bakker, A and Smith, JM, 1990. Suspension of solid particles with gassed impellers. *Chemical Engineering Science*, 45: 1703-1718.

Gates, LE, Morton, JR and Fondy, PL, 1976. Selecting agitator systems to suspend solids in liquids. *Chemical Engineering*, May: 144-150.

Gilbert, CG, 2004. Bateman Flotation Equipment: Round BQR Cells. *Memorandum (30 June 2004)*, Germiston, South Africa.

Godfrey, JC and Zhu, ZM, 1994. Measurement of particle-liquid profiles in agitated tanks, in *Industrial Mixing Technology: Chemical and Biological Applications, AIChE Symposium Series, Vol. 90*, Ed(s): G.B. Tatterson, R.V. Calabrese and W.R. Penney, pp 181-185, AIChE, New York.

Griffiths, M, 1998. *Of Mines and Men: Australia's 20th Century Mining Miracle 1945-1985*, Kangaroo Press, Sydney.

Harris, CC, 1974. Impeller speed, air, and power requirements in flotation machine scale-up. *International Journal of Mineral Processing*, 1: 51-64.

Harris, CC, 1976. Flotation Machines, in *Flotation, AM Gaudin Memorial Volume*, Ed(s): M.C. Fuerstenau, pp 753-815, AIME, New York.

Herringe, RA, 1979. The behaviour of mono-size particle slurries in fully baffled turbulent mixers, in *Proceedings Third Euro. Conf. Mixing*, pp 199, in Rewatkar, 1991. *op cit.*

Hicks, MT, Myers, KJ and Bakker, A, 1997. Cloud height in solids suspension agitation. *Chemical Engineering Communications*, 160: 137-155.

Hirsekorn, FS and Miller, SA, 1953. Agitation of viscous solid-liquid suspensions. *Chemical Engineering Progress*, 49: 459-466.

Hixson, AW *et al.*, 1942. *Industr. Engng. Chem. (Industr.)*, 34: 120, 194, in Zwietering, 1958. *op cit.*

Holtham, P and Cheng, T, 1991. Study of the probability of detachment of particles from bubbles in flotation. *Trans. Inst. Min. Metall.*, 100: C147-C153.

Hudcova, V, Nienow, AW, Haozhung, W and Huoxing, L, 1987. On the effect of liquid height on the flooding/loading transition. *Chemical Engineering Science*, 42: 375-377.

Hughmark, G, 1980. *Ind. Eng. Chem. Proc. Des. Dev.*, 19: 638, in Joshi, Pandit and Sharma, 1982. *op cit.*

Hui, S and Ahmed, N, 1998a. The effect of energy dissipation on coarse particle flotation, in *Innovations in Mineral and Coal Processing*, Ed(s): S. Atak, G. Onal and M. Celik, pp 113-118, Balkema, Rotterdam.

Hui, S and Ahmed, N, 1998b. The effect of vessel geometry on mixing hydrodynamics and coarse particle flotation, in *Proceedings 26th Australasian Chemical Engineering Conference (Chemeca 98)*, Port Douglas, Australia.

Hui, S and Ahmed, N, 1999. Hydrodynamics of coarse particle flotation, in *Proceedings 27th Australasion Chem. Eng. Conf. (Chemeca 99)*, pp 1-6, Newcastle, Australia.

Jonaitis, AJ, 1999. Design, development, application, and operating benefits of 100 m^3+ Outokumpu TankCell flotation cells, in *Advances in Flotation Technology*, Ed(s): B.K. Parekh and J.D. Miller, pp 371-380, SME, Littleton, USA.

Joshi, JB, 1981. Axial mixing in multiphase contactors. *Trans. Inst. Chem. Eng.*, 59: 139, in Rewatkar and Joshi, 1991. *op cit.*

Joshi, JB, Pandit, AB and Sharma, MM, 1982. Mechanically agitated gas-liquid reactors. *Chemical Engineering Science*, 37: 813-844.

Kim, SD, Kim, HS and Han, JH, 1992. Axial dispersion characteristics in three-phase fluidized beds. *Chemical Engineering Science*, 47: 3419-3426.

Kneule, F and Weinspach, PM, 1967. Suspendieren Von Festoffpartikeln in Ruhrgefass, in *Verfahrenstechnik*, pp 531, Mains, in Rewatkar, 1991. *op cit.*

Kneule, F, 1956. *Chem. Ing. Tech.*, 28: 221, in Zwietering, 1958. *op cit.*

Koch, P, 1975. Die einflusse der konstruktion und betriebsweise von ruhrern in mechanischen flotationsapparaten auf die hydrodynamik des dreiphasensystem und den flotationserfolg. *Freiberg Forschunghefte*, 546: 5-80, in Inoue, Nonaka and Imaizumi, 1986. *op cit.*

Kolar, V, 1967a. *Coll. Czech. Chem. Commun.*, 32:, in Chapman, Nienow, Cooke, and Middleton, 1983a. *op cit.*

Kolar, V, 1967b. *Coll. Czech. Chem. Commun.*, 32: 526, in Rieger and Ditl, 1994. *op cit.*

Laskowski, JS, 1993. Frothers and flotation froths. *Miner. Process. Extract. Metall. Rev.*, 12: 61-89.

Lehn, MC, Myers, KJ and Bakker, A, 1999. Agitator design for solids suspension under gassed conditions. *The Canadian Journal of Chemical Engineering*, 77: 1065-1071.

Levenspiel, O, 1972. Nonideal flow, in *Chemical Reaction Engineering, Second Edition*, pp 253-325, John Wiley & Sons, New York.

Lewis, J, 2003. *MSc Thesis, University of Cape Town.*

Matsumoto, T, Hidaka, N, Takebayasi, Y and Morooka, S, 1997. Axial mixing and segregation in gas-liquid-solid three-phase fluidized bed of solid particles of different sizes and densities. *Chemical Engineering Science*, 52: 3961-3970.

Matsumura, M, Masunaga, H, Haraya, K and Kobayashi, J, 1978. Effect of gas entrainment on the power requirement and gas holdup in an aerated stirred tank. *J. Ferment. Technol.*, 56: 128, in Mezaki, Mochizuki and Ogawa, 2000. *op cit.*

Mavros, P, 1992. Mixing and hydrodynamics in flotation cells, in *Innovations in Flotation Technology*, Ed(s): P. Mavros and K.A. Matis, pp 211-234, Kluwer Academic Publishers, The Netherlands.

Mehrotra, SP and Saxena, AK, 1983. Effects of process variables on the residence time distribution of a solid in a continuously operated flotation cell. *International Journal of Mineral Processing*, 10: 255-277.

Mezaki, R, Mochizuki, M and Ogawa, K, 2000. *Engineering Data on Mixing*, Elsevier, Tokyo.

Middleton, JC, Edwards, MF and Stewart, L, 1980. Recommended standard terminology and nomenclature for mixing, IChemE, Rugby, as reprinted from. *The Chemical Engineer*, Aug/Sep: 557, In: Chapman, Nienow, Cooke and Middleton, 1983b. *op cit.*

Mika, TS and Fuerstenau, DW, 1968. A microscopic model of the flotation process, in *Proceedings VIII Int. Miner. Process. Cong.*, pp 246-269, Leningrad, in Ahmed and Jameson, 1989. *op cit.*

Molerus, O and Latzel, W, 1987a. Suspension of solid particles in agitated vessels - Archimedes numbers < 40. *Chemical Engineering Science*, 42: 1423-1430.

Molerus, O and Latzel, W, 1987b. Suspension of solid particles in agitated vessels - II. Archimedes numbers > 40. Reliable prediction of minimum stirrer angular velocities. *Chemical Engineering Science*, 42: 1431-1437.

Musil, L and Vlk, J, 1978. Suspending solid particles in an agitated conical-bottom tank. *Chemical Engineering Science*, 33: 1123-1131.

Musil, L, 1976. *Coll. Czech. Chem. Commun.*, 41: 839, in Chapman *et al.*, 1983. *op cit.*

Nagata, S, 1975. *Mixing principles and applications*, Chapter 6, Agitation in Solid-Liquid Systems, pp 249-295, John Wiley & Sons, New York.

Narayanan, S, Bhatia, VK, Guha, DK and Rao, MN, 1968. *Chemical Engineering Science*, 24: 223, in Baldi, Conti and Alaria, 1978. *op cit.*

Nienow, AW, 1968. Suspension of solid particles in turbine agitated baffled vessels. *Chemical Engineering Science*, 23: 1453-1459.

Nienow, AW, 1992. The suspension of solid particles, in *Mixing in the process industries, Second edition*, Ed(s): N. Harnby, M.F. Edwards and A.W. Nienow, pp 364-393, Butterworth-Heinemann, Oxford.

Nienow, AW, Wisdom, DJ and Middleton, JC, 1977., in *Proc. Second Conf. Mixing*, pp F1-1, BHRA, Cranfield, in Chapman, 1983. *op cit.*

Oldshue, JY, 1983a. Solids suspension, in *Fluid Mixing Technology*, Mc Graw - Hill, New York.

Oldshue, JY, 1983b. Continuous flow in mixing processes, in *Fluid Mixing Technology*, pp 338-358, Mc Graw - Hill, New York.

Oldshue, JY, Herbst, NR and Post, TA, 1995. *A guide to fluid mixing*, Lightnin, New York.

Parthasarathy, R, Jameson, GJ and Ahmed, N, 1991. Bubble breakup in stirred vessels - predicting the Sauter mean diameter. *Trans IChemE*, 69A: 295, In: Mezaki, Mochizuki and Ogawa, 2000. *op cit.*

Patwardhan, AW and Joshi, JB, 1999. Design of gas-inducing reactors. *Ind. Eng. Chem. Res.*, 38: 49-80.

Raghava Rao, KSMS, Rewatkar, VB and Joshi, JB, 1988. Critical impeller speed for solid suspension in mechanically agitated contactors. *AIChE Journal*, 34: 1332-1340.

Ralston, J, Fornasiero, D and Hayes, R, 1999. Bubble-particle attachment and detachment in flotation. *International Journal of Mineral Processing*, 56: 133-164.

Reilly, IG, Scott, DS, De Bruijn, TJW, MacIntyre, D and Piskorz, J, 1990. Axial solids concentrations in three-phase bubble columns. *Chemical Engineering Science*, 45: 2293-2299.

Rewatkar, VB and Joshi, JB, 1991. Critical impeller speed for solid suspension in mechanically agitated three-phase reactors. 2. Mathematical model. *Ind Eng Chem Res*, 30: 1784-1791.

Rewatkar, VB, Raghava Rao, KSMS and Joshi, JB, 1989. Some aspects of solids suspension in mechanically agitated reactors. *AIChE Journal*, 35: 1577, in Rewatkar, 1991. *op cit.*

Rewatkar, VB, Raghava Rao, KSMS and Joshi, JB, 1991. Critical impeller speed for solid suspension in mechanically agitated three-phase reactors. 1. Experimental part. *Ind Eng Chem Res*, 30: 1770-1784.

Rieger, F and Ditl, P, 1994. Suspension of solid particles. *Chemical Engineering Science*, 49: 2219-2227.

Rodrigues, WJ, Leal Filho, LS and Masini, EA, 2001. Hydrodynamic dimensionless parameters and their influence on flotation performance of coarse particles. *Minerals Engineering*, 14: 1047-1054.

Rogers, GFC and Mayhew, YR, 1988. *Thermodynamic and Transport Properties of Fluids*, 4th Edition, Basil Blackwell, Oxford, UK.

Sawant, SB and Joshi, JB, 1979. Critical impeller speed for the onset of gas induction in gas inducing types of agitated contactors. *Chemical Engineering Journal*, 18: 87.

Schubert, H and Bischofberger, C, 1978. On the hydrodynamics of flotation machines. *International Journal of Mineral Processing*, 5: 131-142, .

Schubert, H and Bischofberger, C, 1981. On the optimization of hydrodynamics in flotation processes, in *Proceedings Thirteenth Int. Miner. Process. Congr., Warsaw, June 4-9, 1979, Part B*, pp 1261-1284, in Hui and Ahmed, 1998. *op cit.*

Schubert, H and Bischofberger, C, 1998. On the microprocesses air dispersion and particle-bubble attachment in flotation machines as well as consequences for the scale-up of macroprocesses. *International Journal of Mineral Processing*, 52: 245-259.

Schubert, H, 1985. On some aspects of the hydrodynamics of flotation processes, in *Flotation of Sulphide Minerals*, Ed(s): K.S.E. Forssberg, pp 337-355, Elsevier, Amsterdam.

Schubert, H, 1999. On the turbulence-controlled microprocesses in flotation machines. *International Journal of Mineral Processing*, 56: 257-276.

Schubert, H, Bischofberger, C and Koch, P, 1982a. On the influence of the hydrodynamics in flotation processes. *Aufbereitungs-Technik*, 16: 306-315.

Schubert, H, Bischofberger, C and Koch, P, 1982b. On the influence of hydrodynamics in flotation processes, in *Proceedings XIV International Mineral Processing Congress*, pp 17, Toronto, Canada.

Schulze, H, 1989. Hydrodynamics of bubble-mineral particle collisions. *Miner. Process. Extract. Metall. Rev.*, 5: 43-76.

Schulze, HJ, 1982. Dimensionless number and approximate calculation of the upper particle size of floatability in flotation machines. *International Journal of Mineral Processing*, 9: 321-328.

Schulze, HJ, 1984. *Physico-Chemical Elementary Processes in Flotation*, Elsevier, Amsterdam.

Sharma, RN and Shaikh, AA, 2003. Solids suspension in stirred tanks with pitched blade turbines. *Chemical Engineering Science*, 58: 2123-2140.

Shaw, JA, 1992. Succeed at Solids Suspension. *Chemical Engineering Progress*, 88: 34-41, in Hicks, Myers and Bakker, 1997. *op cit.*

Skillen, A, 1993. Froth flotation - New technologies bubbling under. *Ind. Miner.*, Feb: 48-54.

Smith, DN and Ruether, JA, 1985. Dispersed solids dynamics in a slurry bubble column. *Chemical Engineering Science*, 40: 741-754.

Soong, Y, Gamwo, IK, Blackwell, AG, Schehl, RR and Zarochak, MF, 1995. Measurements of solids concentration in a three-phase reactor by an ultrasonic technique. *The Chemical Engineering Journal*, 60: 161-167.

Stanley, GG, 1987. Plant Design and Commissioning, in *The Extractive Metallurgy of Gold in South Africa, Vol. 2, SAIMM Monograph Series M7, The Chamber of Mines of South Africa*, Ed(s): G. G. Stanley, pp 966, Johannesburg.

Staudinger, G and Moser, F, 1976. *Chem. Ing. Tech.*, 48: 1071, in Bohnet and Niesmak, 1980. *op cit.*

Stolojanu, V and Prakash, A, 1997. Hydrodynamic measurements in a slurry bubble column using ultrasonic techniques. *Chemical Engineering Science*, 52: 4225-4230.

Taggart, AF, 1945. *Handbook of Mineral Dressing, Ores and Industrial Minerals (2nd Edition)*, Wiley, New York.

Tatterson, GB, 1991. *Fluid mixing and gas dispersion in agitated tanks*, Chapter 1, Mixing geometries, pp 1-17, McGraw-Hill, New York.

Thomas, DG, 1965. Transport characteristics of suspension: VIII. A note on the viscosity of Newtonian suspensions of uniform spherical particles. *Journal of Colloid Science*, 20: 267-277.

Voit, H and Mersmann, A, 1985. *Chemical Engineering Technology*, 57: 692, in Rieger and Ditl, 1994. *op cit.*

Wang, M, Dorward, A, Vlaev, D and Mann, R, 1999. Measurements of gas-liquid mixing in a stirred vessel using electrical resistance tomography (ERT), in *Proceedings 1st World Congress on Industrial Process Tomography*, pp 78-83, Buxton, Greater Manchester.

Warmoeskerken, MMCG and Smith, JM, 1985. Flooding of disc turbines in gas-liquid dispersions: A new description of the phenomenon. *Chemical Engineering Science*, 40: 2063-2071, in Wong *et al.*, 1987. *op cit.*

Weber, A, Walker, C, Redden, L, Lelinski, D and Ware, S, 1999. Scale-up and design of large-scale flotation equipment, in *Advances in Flotation Technology*, Ed(s): B.K. Parekh and J.D. Miller, pp 353-369, SME, Littleton, USA.

Weisman, J and Efferding, LE, 1960. Suspension of slurries by mechanical mixers. *AIChE Journal*, 6: 419-426.

Weiss, T and Schubert, H, 1989. On optimum hydrodynamics of coarse particle flotation. *Aufbereitungs-Technik*, 30: 657-663.

White, AM and Summerford, SD, 1933. *Industr. Engng. Chem. (Industr.)*, 25: 1025, in Zwietering, 1958. *op cit.*

Wichterle, K, 1988. Conditions for suspension of solids in agitated vessels. *Chemical Engineering Science*, 43: 467-471.

Wills, BA, 1997. *Mineral Processing Technology, Sixth Edition*, pp 258-341, Butterworth Heinemann, Oxford.

Wong, CW, Wang, JP and Huang, ST, 1987. Investigations of fluid dynamics in mechanically stirred aerated slurry reactors. *The Canadian Journal of Chemical Engineering*, 65: 412-419.

Woodburn, ET, King, RP and Colborn, RP, 1971. The effect of particle size distribution on the performance of a phosphate flotation process. *Metallurgical Transactions*, 2: 3163-3174.

Yianatos, J, Bergh, L, Condori, P and Aguilera, J, 2001. Hydrodynamic and metallurgical characterization of industrial flotation banks for control purposes. *Minerals Engineering*, 14: 1033-1046.

Young, P, 1982. Flotation Machines. *Mining Magazine*, 146: 35-59.

Yung, CN, Wong, CW and Chang, CL, 1979. Gas holdup and aerated power consumption in mechanically stirred tanks. *The Canadian Journal of Chemical Engineering*, 57: 672, in Mezaki, Mochizuki and Ogawa, 2000. *op cit.*

Zwietering, TN, 1958. Suspending of solid particles in liquid by agitators. *Chemical Engineering Science*, 8: 244-253.

APPENDIX A. CRITICAL IMPELLER SPEED DATA

APPENDIX A. CRITICAL IMPELLER SPEED DATA 229

A.1 CRITICAL IMPELLER SPEED RAW DATA 230
A.2 CRITICAL IMPELLER SPEED TWO-PHASE DATA 233
A.3 CRITICAL IMPELLER SPEED THREE-PHASE DATA 237
A.4 CRITICAL IMPELLER SPEED TWO- AND THREE-PHASE DATA 242
A.5 MULTIPLE LINEAR REGRESSION RESULTS 245

A.1 CRITICAL IMPELLER SPEED RAW DATA

Table A.1 Critical Impeller Speed Raw Data

Run #	Njs rpm	dp, min µm	dp, max µm	X %	ρS kg/l	ρL kg/l	TL °C	µL x10^{-3} kg/m/s	vL x10^{-6} m2/s	JG cm/s	ΦG %
-3	480	106	150	5.0	2.65	1.000	16.0	1.107	1.107	0.0	0.0
-2	560	106	150	5.0	2.65	1.000	19.0	1.026	1.026	1.0	10.4
-1	755	106	150	5.0	2.65	1.000	18.7	1.033	1.033	1.5	13.7
1	478	106	150	5.0	2.65	1.000	24.6	0.893	0.893	0.0	0.0
2	570	106	150	5.0	2.65	1.000	26.0	0.864	0.864	1.0	10.7
2*	570	106	150	5.0	2.65	1.000	21.9	0.954	0.954	1.0	10.4
1*	487	106	150	5.0	2.65	1.000	25.0	0.885	0.885	0.0	0.0
2*	600	106	150	5.0	2.65	1.000	24.7	0.891	0.891	1.0	12.6
3	798	106	150	5.0	2.65	1.000	24.6	0.893	0.893	1.5	16.7
4	900	106	150	5.0	2.65	1.000	25.0	0.885	0.885	2.0	21.6
5	525	106	150	10.0	2.65	1.000	26.1	0.862	0.862	0.0	0.0
6	665	106	150	10.0	2.65	1.000	25.5	0.875	0.875	1.0	12.2
7	845	106	150	10.0	2.65	1.000	24.8	0.889	0.889	1.5	15.9
8	927	106	150	10.0	2.65	1.000	24.8	0.889	0.889	2.0	18.4
9	545	106	150	15.0	2.65	1.000	25.5	0.875	0.875	0.0	0.0
10	695	106	150	15.0	2.65	1.000	25.6	0.873	0.873	1.0	10.4
11	875	106	150	15.0	2.65	1.000	25.9	0.866	0.866	1.5	16.9
12	1010	106	150	15.0	2.65	1.000	24.9	0.887	0.887	2.0	22.1
13	587	106	150	19.9	2.65	1.000	24.9	0.887	0.887	0.0	0.0
14	865	106	150	19.9	2.65	1.000	24.5	0.896	0.896	1.0	14.4
15	985	106	150	19.9	2.65	1.000	24.7	0.891	0.891	1.5	17.9
16	1048	106	150	19.9	2.65	1.000	26.4	0.856	0.856	2.0	22.0
17	585	150	250	5.0	2.65	1.000	26.5	0.854	0.854	0.0	0.0
18	777	150	250	5.0	2.65	1.000	25.3	0.879	0.879	1.0	14.6
19	920	150	250	5.0	2.65	1.000	24.7	0.891	0.891	1.5	18.6
20	975	150	250	5.0	2.65	1.000	26.1	0.862	0.862	2.0	21.5
21	625	150	250	10.0	2.65	1.000	25.2	0.881	0.881	0.0	0.0
22	850	150	250	10.0	2.65	1.000	26.6	0.852	0.852	1.0	13.3
23	960	150	250	10.0	2.65	1.000	25.5	0.875	0.875	1.5	17.1
24	1035	150	250	10.0	2.65	1.000	25.0	0.885	0.885	2.0	20.6
25	656	150	250	15.0	2.65	1.000	26.3	0.858	0.858	0.0	0.0
26	937	150	250	15.0	2.65	1.000	26.3	0.858	0.858	1.0	14.4
27	1030	150	250	15.0	2.65	1.000	25.3	0.879	0.879	1.5	18.1
28	1115	150	250	15.0	2.65	1.000	25.1	0.883	0.883	2.0	21.9
29	675	150	250	19.9	2.65	1.000	26.4	0.856	0.856	0.0	0.0
30	1016	150	250	19.9	2.65	1.000	26.3	0.858	0.858	1.0	15.0
30*	1012	150	250	19.9	2.65	1.000	26.5	0.854	0.854	1.0	13.9
31	1107	150	250	19.9	2.65	1.000	24.8	0.889	0.889	1.5	17.3
32	1100	150	250	19.9	2.65	1.000	25.1	0.883	0.883	2.0	21.5

Run #	Njs rpm	dp, min µm	dp, max µm	X %	ρS kg/l	ρL kg/l	TL °C	µL x10^{-3} kg/m/s	vL x10^{-6} m2/s	JG cm/s	ΦG %
29*	670	150	250	19.9	2.65	1.000	16.5	1.093	1.093	0.0	0.0
30*	990	150	250	19.9	2.65	1.000	16.5	1.093	1.093	1.0	15.6
31*	1060	150	250	19.9	2.65	1.000	16.5	1.093	1.093	1.5	20.0
33	756	250	500	5.0	2.65	1.000	26.5	0.854	0.854	0.0	0.0
34	991	250	500	5.0	2.65	1.000	28.2	0.822	0.822	1.0	
35	1105	250	500	5.0	2.65	1.000	28.4	0.818	0.818	1.5	
37	820	250	500	10.0	2.65	1.000	25.5	0.875	0.875	0.0	0.0
38	1089	250	500	10.0	2.65	1.000	27.4	0.837	0.837	1.0	16.7
41	850	250	500	15.0	2.65	1.000	25.3	0.879	0.879	0.0	0.0
49	815	500	850	5.0	2.65	1.000	25.0	0.885	0.885	0.0	0.0
50	1030	500	850	5.0	2.65	1.000	25.7	0.870	0.870	1.0	15.9
53	900	500	850	10.0	2.65	1.000	24.6	0.893	0.893	0.0	0.0
65	440	75	106	5.0	2.65	1.000	26.0	0.864	0.864	0.0	0.0
66	526	75	106	5.0	2.65	1.000	26.0	0.864	0.864	1.0	0.0
67	750	75	106	5.0	2.65	1.000	25.0	0.885	0.885	1.5	15.4
68	855	75	106	5.0	2.65	1.000	24.0	0.906	0.906	2.0	20.4
69	485	75	106	10.0	2.65	1.000	25.8	0.868	0.868	0.0	0.0
70	600	75	106	10.0	2.65	1.000	25.8	0.868	0.868	1.0	11.2
71	795	75	106	10.0	2.65	1.000	24.8	0.889	0.889	1.5	15.5
72	885	75	106	10.0	2.65	1.000	23.9	0.909	0.909	2.0	19.4
73	505	75	106	15.0	2.65	1.000	24.9	0.887	0.887	0.0	0.0
74	670	75	106	15.0	2.65	1.000	25.0	0.885	0.885	1.0	12.2
75	847	75	106	15.0	2.65	1.000	24.5	0.896	0.896	1.5	16.7
76	965	75	106	15.0	2.65	1.000	24.5	0.896	0.896	2.0	22.3
77	500	75	106	20.0	2.65	1.000	24.9	0.887	0.887	0.0	0.0
78	782	75	106	20.0	2.65	1.000	25.0	0.885	0.885	1.0	13.7
79	905	75	106	20.0	2.65	1.000	25.5	0.875	0.875	1.5	18.1
77*	505	75	106	20.0	2.65	1.000	17.0	1.079	1.079	0.0	0.0
78*	770	75	106	20.0	2.65	1.000	17.5	1.065	1.065	1.0	15.0
79*	920	75	106	20.0	2.65	1.000	18.0	1.052	1.052	1.5	19.2
80	1000	75	106	20.0	2.65	1.000	25.5	0.875	0.875	2.0	23.1
81	663	75	106	5.0	4.20	1.000	25.8	0.868	0.868	0.0	0.0
82	983	75	106	5.0	4.20	1.000	27.6	0.833	0.833	1.0	15.8
83	1085	75	106	5.0	4.20	1.000	27.9	0.827	0.827	1.5	20.0
85	750	75	106	10.0	4.20	1.000	26.0	0.864	0.864	0.0	0.0
86	1076	75	106	10.0	4.20	1.000	26.9	0.846	0.846	1.0	16.7
86*	1084	75	106	10.0	4.20	1.000	23.5	0.917	0.917	1.0	17.7
89	778	75	106	15.0	4.20	1.000	25.0	0.885	0.885	0.0	0.0
90	1095	75	106	15.0	4.20	1.000	25.0	0.885	0.885	1.0	17.2
97	735	75	106	5.0	4.70	1.000	24.5	0.896	0.896	0.0	0.0
98	1045	75	106	5.0	4.70	1.000	25.5	0.875	0.875	1.0	16.9
101	805	75	106	10.0	4.70	1.000	28.0	0.826	0.826	0.0	0.0
105	835	75	106	15.0	4.70	1.000	28.5	0.816	0.816	0.0	0.0
113	480	75	106	18.6	2.65	1.096	25.5	1.923	1.754	0.0	0.0
114	740	75	106	18.6	2.65	1.096	25.5	1.923	1.754	1.0	20.0

Run #	Njs rpm	dp, min µm	dp, max µm	X %	ρS kg/l	ρL kg/l	TL °C	µL x10^{-3} kg/m/s	vL x10^{-6} m2/s	JG cm/s	ΦG %
115	494	75	106	17.7	2.65	1.160	25.5	4.089	3.526	0.0	0.0
116	870	75	106	17.7	2.65	1.160	25.5	4.089	3.526	1.0	18.2
119	560	150	250	18.6	2.65	1.096	21.0	2.145	1.957	0.0	0.0
120	930	150	250	18.6	2.65	1.096	22.2	2.082	1.899	1.0	26.0
121	510	150	250	17.7	2.65	1.160	24.0	4.238	3.655	0.0	0.0
122	920	150	250	17.7	2.65	1.160	25.2	4.118	3.552	1.0	22.9
125	510	150	250	17.2	2.65	1.206	25.7	8.421	6.980	0.0	0.0
126	830	150	250	17.2	2.65	1.206	25.8	8.401	6.964	1.0	21.7

Note: Phase I: Run 1-80; Phase II: Run 81-112; Phase III: Run 113-126; * - indicates duplicate runs.

A.2 CRITICAL IMPELLER SPEED TWO-PHASE DATA

Table A.2 Ungassed Critical Impeller Speed Data (All Experimental Phases, I, II, III)

# *1	Run *1	Njs rpm	dp µm	X %	ρS kg/l	ρL kg/l	(ρS-ρL)/ρL -	vL/v_w -	JG cm/s
1	-3	480	***128***	***5.0***	2.65	1.00	1.65	1.107	0.0
2	1	478	***128***	***5.0***	2.65	1.00	1.65	0.893	0.0
3	1*	487	***128***	***5.0***	2.65	1.00	1.65	0.885	0.0
4	5	525	***128***	***10.0***	2.65	1.00	1.65	0.862	0.0
5	9	545	***128***	***15.0***	2.65	1.00	1.65	0.875	0.0
6	13	587	***128***	***19.9***	2.65	1.00	1.65	0.887	0.0
7	17	585	***200***	***5.0***	2.65	1.00	1.65	0.854	0.0
8	21	625	***200***	***10.0***	2.65	1.00	1.65	0.881	0.0
9	25	656	***200***	***15.0***	2.65	1.00	1.65	0.858	0.0
10	29	675	***200***	***19.9***	2.65	1.00	1.65	0.856	0.0
11	29*	670	***200***	***19.9***	2.65	1.00	1.65	1.093	0.0
12	33	756	***375***	***5.0***	2.65	1.00	1.65	0.854	0.0
13	37	820	***375***	***10.0***	2.65	1.00	1.65	0.875	0.0
14	41	850	***375***	***15.0***	2.65	1.00	1.65	0.879	0.0
15	49	815	***675***	***5.0***	2.65	1.00	1.65	0.885	0.0
16	53	900	***675***	***10.0***	2.65	1.00	1.65	0.893	0.0
17	65	440	***91***	***5.0***	2.65	1.00	1.65	0.864	0.0
18	69	485	***91***	***10.0***	2.65	1.00	1.65	0.868	0.0
19	73	505	***91***	***15.0***	2.65	1.00	1.65	0.887	0.0
20	77	500	***91***	***20.0***	2.65	1.00	1.65	0.887	0.0
21	77*	505	***91***	***20.0***	2.65	1.00	1.65	1.079	0.0
22	81	663	91	5.0	4.20	1.00	***3.20***	0.868	0.0
23	85	750	91	10.0	4.20	1.00	***3.20***	0.864	0.0
24	89	778	91	15.0	4.20	1.00	***3.20***	0.885	0.0
25	97	735	91	5.0	4.70	1.00	***3.70***	0.896	0.0
26	101	805	91	10.0	4.70	1.00	***3.70***	0.826	0.0
27	105	835	91	15.0	4.70	1.00	***3.70***	0.816	0.0
28	113	480	91	18.6	2.65	1.10	1.42	***1.754***	0.0
29	115	494	91	17.7	2.65	1.16	1.29	***3.526***	0.0
30	119	560	200	18.6	2.65	1.10	1.42	***1.957***	0.0
31	121	510	200	17.7	2.65	1.16	1.29	***3.655***	0.0

# *[1]	Run *[1]	Njs rpm	dp µm	X %	ρS kg/l	ρL kg/l	(ρS-ρL)/ρL -	vL/v_w -	JG cm/s
32	125	510	200	17.2	2.65	1.21	1.20	***6.980***	0.0

*[1]: Exp phase I: 17 runs out of 20 planned, plus 4 repeats, resulting in 21 tests; Exp phase II: 6 additional ungassed runs out of 8 planned; Exp phase III: 5 additonal ungassed runs out of 6 planned.

Table A.3 Ungassed Critical Impeller Speed Data (Experimental Phase I): Effect of Particle Size

#	Run	Njs rpm	dp µm	X %	ρS kg/l	ρL kg/l	(ρS-ρL)/ρL -	vL/v_w -	JG cm/s
1	65	**440**	**91**	5.0	2.65	1.00	1.65	0.864	0.0
2	-3	**480**	**128**	5.0	2.65	1.00	1.65	1.107	0.0
3	1	**478**	**128**	5.0	2.65	1.00	1.65	0.893	0.0
4	1*	**487**	**128**	5.0	2.65	1.00	1.65	0.885	0.0
5	17	**585**	**200**	5.0	2.65	1.00	1.65	0.854	0.0
6	33	**756**	**375**	5.0	2.65	1.00	1.65	0.854	0.0
7	49	**815**	**675**	5.0	2.65	1.00	1.65	0.885	0.0
8	69	**485**	**91**	10.0	2.65	1.00	1.65	0.868	0.0
9	5	**525**	**128**	10.0	2.65	1.00	1.65	0.862	0.0
10	21	**625**	**200**	10.0	2.65	1.00	1.65	0.881	0.0
11	37	**820**	**375**	10.0	2.65	1.00	1.65	0.875	0.0
12	53	**900**	**675**	10.0	2.65	1.00	1.65	0.893	0.0
13	73	**505**	**91**	15.0	2.65	1.00	1.65	0.887	0.0
14	9	**545**	**128**	15.0	2.65	1.00	1.65	0.875	0.0
15	25	**656**	**200**	15.0	2.65	1.00	1.65	0.858	0.0
16	41	**850**	**375**	15.0	2.65	1.00	1.65	0.879	0.0
17	77	**500**	**91**	20.0	2.65	1.00	1.65	0.887	0.0
18	77*	**505**	**91**	20.0	2.65	1.00	1.65	1.079	0.0
19	13	**587**	**128**	19.9	2.65	1.00	1.65	0.887	0.0
20	29	**675**	**200**	19.9	2.65	1.00	1.65	0.856	0.0
21	29*	**670**	**200**	19.9	2.65	1.00	1.65	1.093	0.0

Table A.4 Ungassed Critical Impeller Speed Data (Experimental Phase I): Effect of Solids Concentration

#	Run	Njs	dp	X	ρS	ρL	(ρS-ρL)/ρL	vL/v_w	JG
		rpm	µm	%	kg/l	kg/l	-	-	cm/s
1	65	**440**	91	**5.0**	2.65	1.00	1.65	0.864	0.0
2	69	**485**	91	**10.0**	2.65	1.00	1.65	0.868	0.0
3	73	**505**	91	**15.0**	2.65	1.00	1.65	0.887	0.0
4	77	**500**	91	**20.0**	2.65	1.00	1.65	0.887	0.0
5	77*	**505**	91	**20.0**	2.65	1.00	1.65	1.079	0.0
6	-3	**480**	128	**5.0**	2.65	1.00	1.65	1.107	0.0
7	1	**478**	128	**5.0**	2.65	1.00	1.65	0.893	0.0
8	1*	**487**	128	**5.0**	2.65	1.00	1.65	0.885	0.0
9	5	**525**	128	**10.0**	2.65	1.00	1.65	0.862	0.0
10	9	**545**	128	**15.0**	2.65	1.00	1.65	0.875	0.0
11	13	**587**	128	**19.9**	2.65	1.00	1.65	0.887	0.0
12	17	**585**	200	**5.0**	2.65	1.00	1.65	0.854	0.0
13	21	**625**	200	**10.0**	2.65	1.00	1.65	0.881	0.0
14	25	**656**	200	**15.0**	2.65	1.00	1.65	0.858	0.0
15	29	**675**	200	**19.9**	2.65	1.00	1.65	0.856	0.0
16	29*	**670**	200	**19.9**	2.65	1.00	1.65	1.093	0.0
17	33	**756**	375	**5.0**	2.65	1.00	1.65	0.854	0.0
18	37	**820**	375	**10.0**	2.65	1.00	1.65	0.875	0.0
19	41	**850**	375	**15.0**	2.65	1.00	1.65	0.879	0.0
20	49	**815**	675	**5.0**	2.65	1.00	1.65	0.885	0.0
21	53	**900**	675	**10.0**	2.65	1.00	1.65	0.893	0.0

Table A.5 Ungassed Critical Impeller Speed Data (Experimental Phases I and II): Effect of Solids Density

#	Run	Njs	dp	X	ρS	ρL	(ρS-ρL)/ρL	vL/v_w	JG
		rpm	µm	%	kg/l	kg/l	-	-	cm/s
1	65	**440**	91	5.0	**2.65**	1.00	**1.65**	0.864	0.0
2	81	**663**	91	5.0	**4.20**	1.00	**3.20**	0.868	0.0
3	97	**735**	91	5.0	**4.70**	1.00	**3.70**	0.896	0.0
4	69	**485**	91	10.0	**2.65**	1.00	**1.65**	0.868	0.0

#	Run	Njs	dp	X	ρS	ρL	(ρS-ρL)/ρL	vL/v_w	JG
		rpm	μm	%	kg/l	kg/l	-	-	cm/s
5	85	**750**	91	10.0	**4.20**	1.00	**3.20**	0.864	0.0
6	101	**805**	91	10.0	**4.70**	1.00	**3.70**	0.826	0.0
7	73	**505**	91	15.0	**2.65**	1.00	**1.65**	0.887	0.0
8	89	**778**	91	15.0	**4.20**	1.00	**3.20**	0.885	0.0
9	105	**835**	91	15.0	**4.70**	1.00	**3.70**	0.816	0.0

Table A.6 Ungassed Critical Impeller Speed Data (Experimental Phases I and III): Effect of Liquid Kinematic Viscosity

#	Run	Njs	dp	X	ρS	ρL	(ρS-ρL)/ρL	vL/v_w	JG	Njs#
		rpm	μm	%	kg/l	kg/l	-	-	cm/s	
1	77	500	91	20.0	2.65	1.00	1.65	**0.887**	0.0	251
2	77*	505	91	20.0	2.65	1.00	1.65	**1.079**	0.0	254
3	113	480	91	18.6	2.65	1.10	1.42	**1.754**	0.0	268
4	115	494	91	17.7	2.65	1.16	1.29	**3.526**	0.0	296
5	29	675	200	19.9	2.65	1.00	1.65	**0.856**	0.0	340
6	29*	670	200	19.9	2.65	1.00	1.65	**1.093**	0.0	337
7	119	560	200	18.6	2.65	1.10	1.42	**1.957**	0.0	313
8	121	510	200	17.7	2.65	1.16	1.29	**3.655**	0.0	305
9	125	510	200	17.2	2.65	1.21	1.20	**6.980**	0.0	321

Note: $Njs^{\#} = Njs/[(\rho_S-\rho_L)/\rho_L]^{0.64}$, $Njs^{\#}$ is needed to remove the effect of the simultaneous variation in the relative solid-liquid density difference due to the addition of sugar for the liquid viscosity work.

A.3 CRITICAL IMPELLER SPEED THREE-PHASE DATA

Table A.7 Gassed Critical Impeller Speed Data (Experimental Phases I, II, and III)

#	Run	Njs	dp	X	(ρS-ρL)/ρL	vL/v_w	JG	Njsu	ΔNjs	Njs/Njsu
		rpm	μm	%	-	-	cm/s	rpm	rpm	-
1	-2	560	*128*	*5.0*	1.65	1.026	**1.0**	480	80	1.17
2	-1	755	*128*	*5.0*	1.65	1.033	**1.5**	480	275	1.57
3	2	570	*128*	*5.0*	1.65	0.864	**1.0**	478	92	1.19
4	2*	570	*128*	*5.0*	1.65	0.954	**1.0**	478	92	1.19
5	2*	600	*128*	*5.0*	1.65	0.891	**1.0**	487	113	1.23
6	3	798	*128*	*5.0*	1.65	0.893	**1.5**	487	311	1.64
7	4	900	*128*	*5.0*	1.65	0.885	**2.0**	487	413	1.85
8	6	665	*128*	*10.0*	1.65	0.875	**1.0**	525	140	1.27
9	7	845	*128*	*10.0*	1.65	0.889	**1.5**	525	320	1.61
10	8	927	*128*	*10.0*	1.65	0.889	**2.0**	525	402	1.77
11	10	695	*128*	*15.0*	1.65	0.873	**1.0**	545	150	1.28
12	11	875	*128*	*15.0*	1.65	0.866	**1.5**	545	330	1.61
13	12	1010	*128*	*15.0*	1.65	0.887	**2.0**	545	465	1.85
14	14	865	*128*	*19.9*	1.65	0.896	**1.0**	587	278	1.47
15	15	985	*128*	*19.9*	1.65	0.891	**1.5**	587	398	1.68
16	16	1048	*128*	*19.9*	1.65	0.856	**2.0**	587	461	1.79
17	18	777	*200*	*5.0*	1.65	0.879	**1.0**	585	192	1.33
18	19	920	*200*	*5.0*	1.65	0.891	**1.5**	585	335	1.57
19	20	975	*200*	*5.0*	1.65	0.862	**2.0**	585	390	1.67
20	22	850	*200*	*10.0*	1.65	0.852	**1.0**	625	225	1.36
21	23	960	*200*	*10.0*	1.65	0.875	**1.5**	625	335	1.54
22	24	1035	*200*	*10.0*	1.65	0.885	**2.0**	625	410	1.66
23	26	937	*200*	*15.0*	1.65	0.858	**1.0**	656	281	1.43
24	27	1030	*200*	*15.0*	1.65	0.879	**1.5**	656	374	1.57
25	28	1115	*200*	*15.0*	1.65	0.883	**2.0**	656	459	1.70
26	30	1016	*200*	*19.9*	1.65	0.858	**1.0**	675	341	1.51
27	30*	1012	*200*	*19.9*	1.65	0.854	**1.0**	675	337	1.50
28	31	1107	*200*	*19.9*	1.65	0.889	**1.5**	675	432	1.64
29	32	1100	*200*	*19.9*	1.65	0.883	**2.0**	675	425	1.63
30	30*	990	*200*	*19.9*	1.65	1.093	**1.0**	670	320	1.48
31	31*	1060	*200*	*19.9*	1.65	1.093	**1.5**	670	390	1.58

#	Run	Njs	dp	X	(ρS-ρL)/ρL	vL/v_w	JG	Njsu	ΔNjs	Njs/Njsu
		rpm	µm	%	-	-	cm/s	rpm	rpm	-
32	34	991	***375***	***5.0***	1.65	0.822	**1.0**	756	235	1.31
33	35	1105	***375***	***5.0***	1.65	0.818	**1.5**	756	349	1.46
34	38	1089	***375***	***10.0***	1.65	0.837	**1.0**	820	269	1.33
35	50	1030	***675***	***5.0***	1.65	0.870	**1.0**	815	215	1.26
36	66	526	***91***	***5.0***	1.65	0.864	**1.0**	440	86	1.20
37	67	750	***91***	***5.0***	1.65	0.885	**1.5**	440	310	1.70
38	68	855	***91***	***5.0***	1.65	0.906	**2.0**	440	415	1.94
39	70	600	***91***	***10.0***	1.65	0.868	**1.0**	485	115	1.24
40	71	795	***91***	***10.0***	1.65	0.889	**1.5**	485	310	1.64
41	72	885	***91***	***10.0***	1.65	0.909	**2.0**	485	400	1.82
42	74	670	***91***	***15.0***	1.65	0.885	**1.0**	505	165	1.33
43	75	847	***91***	***15.0***	1.65	0.896	**1.5**	505	342	1.68
44	76	965	***91***	***15.0***	1.65	0.896	**2.0**	505	460	1.91
45	78	782	***91***	***20.0***	1.65	0.885	**1.0**	500	282	1.56
46	79	905	***91***	***20.0***	1.65	0.875	**1.5**	500	405	1.81
47	78*	770	***91***	***20.0***	1.65	1.065	**1.0**	505	265	1.52
48	79*	920	***91***	***20.0***	1.65	1.052	**1.5**	505	415	1.82
49	80	1000	***91***	***20.0***	1.65	0.875	**2.0**	505	495	1.98
50	82	983	91	5.0	***3.20***	0.833	**1.0**	663	320	1.48
51	83	1085	91	5.0	***3.20***	0.827	**1.5**	663	422	1.64
52	86	1076	91	10.0	***3.20***	0.846	**1.0**	750	326	1.43
53	86*	1084	91	10.0	***3.20***	0.917	**1.0**	750	334	1.45
54	90	1095	91	15.0	***3.20***	0.885	**1.0**	778	317	1.41
55	98	1045	91	5.0	***3.70***	0.875	**1.0**	735	310	1.42
56	114	740	91	18.6	1.42	***1.754***	**1.0**	480	260	1.54
57	116	870	91	17.7	1.29	***3.526***	**1.0**	494	376	1.76
58	120	930	200	18.6	1.42	***1.899***	**1.0**	560	370	1.66
59	122	920	200	17.7	1.29	***3.552***	**1.0**	510	410	1.80
60	126	830	200	17.2	1.20	***6.964***	**1.0**	510	320	1.63

Table A.8 Gassed Critical Impeller Speed Data, J_G = 1.0 cm/s

# [*1]	Run [*1]	Njs	dp	X	(ρS-ρL)/ρL	vL/v_w	JG	Njsu	ΔNjs	Njs/Njsu
		rpm	μm	%	-	-	cm/s	rpm	rpm	-
1	-2*	560	***128***	***5.0***	1.65	1.026	**1.0**	480	80	1.17
2	2	570	***128***	***5.0***	1.65	0.864	**1.0**	478	92	1.19
3	2*	570	***128***	***5.0***	1.65	0.954	**1.0**	478	92	1.19
4	2*	600	***128***	***5.0***	1.65	0.891	**1.0**	487	113	1.23
5	6	665	***128***	***10.0***	1.65	0.875	**1.0**	525	140	1.27
6	10	695	***128***	***15.0***	1.65	0.873	**1.0**	545	150	1.28
7	14	865	***128***	***19.9***	1.65	0.896	**1.0**	587	278	1.47
8	18	777	***200***	***5.0***	1.65	0.879	**1.0**	585	192	1.33
9	22	850	***200***	***10.0***	1.65	0.852	**1.0**	625	225	1.36
10	26	937	***200***	***15.0***	1.65	0.858	**1.0**	656	281	1.43
11	30	1016	***200***	***19.9***	1.65	0.858	**1.0**	675	341	1.51
12	30*	1012	***200***	***19.9***	1.65	0.854	**1.0**	675	337	1.50
13	30*	990	***200***	***19.9***	1.65	1.093	**1.0**	670	320	1.48
14	34	991	***375***	***5.0***	1.65	0.822	**1.0**	756	235	1.31
15	38	1089	***375***	***10.0***	1.65	0.837	**1.0**	820	269	1.33
16	50	1030	***675***	***5.0***	1.65	0.870	**1.0**	815	215	1.26
17	66	526	***91***	***5.0***	1.65	0.864	**1.0**	440	86	1.20
18	70	600	***91***	***10.0***	1.65	0.868	**1.0**	485	115	1.24
19	74	670	***91***	***15.0***	1.65	0.885	**1.0**	505	165	1.33
20	78	782	***91***	***20.0***	1.65	0.885	**1.0**	500	282	1.56
21	78*	770	***91***	***20.0***	1.65	1.065	**1.0**	505	265	1.52
22	82	983	91	5.0	***3.20***	0.833	**1.0**	663	320	1.48
23	86	1076	91	10.0	***3.20***	0.846	**1.0**	750	326	1.43
24	86*	1084	91	10.0	***3.20***	0.917	**1.0**	750	334	1.45
25	90	1095	91	15.0	***3.20***	0.885	**1.0**	778	317	1.41
26	98	1045	91	5.0	***3.70***	0.875	**1.0**	735	310	1.42
27	114	740	91	18.6	1.42	***1.754***	**1.0**	480	260	1.54
28	116	870	91	17.7	1.29	***3.526***	**1.0**	494	376	1.76
29	120	930	200	18.6	1.42	***1.899***	**1.0**	560	370	1.66
30	122	920	200	17.7	1.29	***3.552***	**1.0**	510	410	1.80
31	126	830	200	17.2	1.20	***6.964***	**1.0**	510	320	1.63

[*1]: Include 7 repeat runs (*); thus 31-7=24 test done at JG = 1.0 cm/s; Phase I: 15 out of 20 tests planned; Phase II: 5 out of 8 planned; Phase III: 5 out of 6 tests planned.

Table A.9 Gassed Critical Impeller Speed Data, J_G = 1.5 cm/s

# *1	Run *1	Njs	dp	X	(ρS-ρL)/ρL	vL/v_w	JG	Njsu	ΔNjs	Njs/Njsu
		rpm	μm	%	-	-	cm/s	rpm	rpm	-
1	-1*	755	***128***	***5.0***	1.65	1.033	**1.5**	480	275	1.57
2	3	798	***128***	***5.0***	1.65	0.893	**1.5**	487	311	1.64
3	7	845	***128***	***10.0***	1.65	0.889	**1.5**	525	320	1.61
4	11	875	***128***	***15.0***	1.65	0.866	**1.5**	545	330	1.61
5	15	985	***128***	***19.9***	1.65	0.891	**1.5**	587	398	1.68
6	19	920	***200***	***5.0***	1.65	0.891	**1.5**	585	335	1.57
7	23	960	***200***	***10.0***	1.65	0.875	**1.5**	625	335	1.54
8	27	1030	***200***	***15.0***	1.65	0.879	**1.5**	656	374	1.57
9	31	1107	***200***	***19.9***	1.65	0.889	**1.5**	675	432	1.64
10	31*	1060	***200***	***19.9***	1.65	1.093	**1.5**	670	390	1.58
11	35	1105	***375***	***5.0***	1.65	0.818	**1.5**	756	349	1.46
12	67	750	***91***	***5.0***	1.65	0.885	**1.5**	440	310	1.70
13	71	795	***91***	***10.0***	1.65	0.889	**1.5**	485	310	1.64
14	75	847	***91***	***15.0***	1.65	0.896	**1.5**	505	342	1.68
15	79	905	***91***	***20.0***	1.65	0.875	**1.5**	500	405	1.81
16	79*	920	***91***	***20.0***	1.65	1.052	**1.5**	505	415	1.82
17	83	1085	91	5.0	***3.20***	0.827	**1.5**	663	422	1.64

*1: Include 3 repeat runs; thus 17-3=14 tests done at J_G = 1.5 cm/s; Phase I: 13 out of 20 tests planned; Phase II: 1 out of 8 tests planned; Phase III: No viscosity work planned at J_G = 1.5 cm/s

Table A.10 Gassed Critical Impeller Speed Data, J_G = 2.0 cm/s

# [*1]	Run [*1]	Njs	dp	X	(ρS-ρL)/ρL	vL/v_w	JG	Njsu	ΔNjs	Njs/Njsu
		rpm	μm	%	-	-	cm/s	rpm	rpm	-
1	4	900	***128***	***5.0***	1.65	0.885	2.0	487	413	1.85
2	8	927	***128***	***10.0***	1.65	0.889	2.0	525	402	1.77
3	12	1010	***128***	***15.0***	1.65	0.887	2.0	545	465	1.85
4	16	1048	***128***	***19.9***	1.65	0.856	2.0	587	461	1.79
5	20	975	***200***	***5.0***	1.65	0.862	2.0	585	390	1.67
6	24	1035	***200***	***10.0***	1.65	0.885	2.0	625	410	1.66
7	28	1115	***200***	***15.0***	1.65	0.883	2.0	656	459	1.70
8	32	1100	***200***	***19.9***	1.65	0.883	2.0	675	425	1.63
9	68	855	***91***	***5.0***	1.65	0.906	2.0	440	415	1.94
10	72	885	***91***	***10.0***	1.65	0.909	2.0	485	400	1.82
11	76	965	***91***	***15.0***	1.65	0.896	2.0	505	460	1.91
12	80	1000	***91***	***20.0***	1.65	0.875	2.0	505	495	1.98

[*1]: 12 tests done at J_G = 2.0 cm/s; Phase I: 12 out of 20 tests planned; Phase II: 0 out of 8 tests planned; Phase III: No viscosity work planned at J_G = 2.0 cm/s

A.4 CRITICAL IMPELLER SPEED TWO- AND THREE-PHASE DATA

Table A.11 Gassed and Ungassed Critical Impeller Speed Data (Experimental Phases I, II, and III)

#	Run	Njs	dp	X	(ρS-ρL)/ρL	vL/v_w	JG	Njsu	ΔNjs	Njs/Njsu
		rpm	µm	%	-	-	cm/s	rpm	rpm	-
1	-3	480	***128***	***5.0***	1.65	1.107	***0.0***	480	0	1.00
2	-2	560	***128***	***5.0***	1.65	1.026	***1.0***	480	80	1.17
3	-1	755	***128***	***5.0***	1.65	1.033	***1.5***	480	275	1.57
4	1	478	***128***	***5.0***	1.65	0.893	***0.0***	478	0	1.00
5	2	570	***128***	***5.0***	1.65	0.864	***1.0***	478	92	1.19
6	2*	570	***128***	***5.0***	1.65	0.954	***1.0***	478	92	1.19
7	1*	487	***128***	***5.0***	1.65	0.885	***0.0***	487	0	1.00
8	2*	600	***128***	***5.0***	1.65	0.891	***1.0***	487	113	1.23
9	3	798	***128***	***5.0***	1.65	0.893	***1.5***	487	311	1.64
10	4	900	***128***	***5.0***	1.65	0.885	***2.0***	487	413	1.85
11	5	525	***128***	***10.0***	1.65	0.862	***0.0***	525	0	1.00
12	6	665	***128***	***10.0***	1.65	0.875	***1.0***	525	140	1.27
13	7	845	***128***	***10.0***	1.65	0.889	***1.5***	525	320	1.61
14	8	927	***128***	***10.0***	1.65	0.889	***2.0***	525	402	1.77
15	9	545	***128***	***15.0***	1.65	0.875	***0.0***	545	0	1.00
16	10	695	***128***	***15.0***	1.65	0.873	***1.0***	545	150	1.28
17	11	875	***128***	***15.0***	1.65	0.866	***1.5***	545	330	1.61
18	12	1010	***128***	***15.0***	1.65	0.887	***2.0***	545	465	1.85
19	13	587	***128***	***19.9***	1.65	0.887	***0.0***	587	0	1.00
20	14	865	***128***	***19.9***	1.65	0.896	***1.0***	587	278	1.47
21	15	985	***128***	***19.9***	1.65	0.891	***1.5***	587	398	1.68
22	16	1048	***128***	***19.9***	1.65	0.856	***2.0***	587	461	1.79
23	17	585	***200***	***5.0***	1.65	0.854	***0.0***	585	0	1.00
24	18	777	***200***	***5.0***	1.65	0.879	***1.0***	585	192	1.33
25	19	920	***200***	***5.0***	1.65	0.891	***1.5***	585	335	1.57
26	20	975	***200***	***5.0***	1.65	0.862	***2.0***	585	390	1.67
27	21	625	***200***	***10.0***	1.65	0.881	***0.0***	625	0	1.00
28	22	850	***200***	***10.0***	1.65	0.852	***1.0***	625	225	1.36
29	23	960	***200***	***10.0***	1.65	0.875	***1.5***	625	335	1.54
30	24	1035	***200***	***10.0***	1.65	0.885	***2.0***	625	410	1.66

#	Run	Njs	dp	X	(ρS-ρL)/ρL	vL/v_w	JG	Njsu	ΔNjs	Njs/Njsu
		rpm	μm	%	-	-	cm/s	rpm	rpm	-
31	25	656	***200***	***15.0***	1.65	0.858	***0.0***	656	0	1.00
32	26	937	***200***	***15.0***	1.65	0.858	***1.0***	656	281	1.43
33	27	1030	***200***	***15.0***	1.65	0.879	***1.5***	656	374	1.57
34	28	1115	***200***	***15.0***	1.65	0.883	***2.0***	656	459	1.70
35	29	675	***200***	***19.9***	1.65	0.856	***0.0***	675	0	1.00
36	30	1016	***200***	***19.9***	1.65	0.858	***1.0***	675	341	1.51
37	30*	1012	***200***	***19.9***	1.65	0.854	***1.0***	675	337	1.50
38	31	1107	***200***	***19.9***	1.65	0.889	***1.5***	675	432	1.64
39	32	1100	***200***	***19.9***	1.65	0.883	***2.0***	675	425	1.63
40	29*	670	***200***	***19.9***	1.65	1.093	***0.0***	670	0	1.00
41	30*	990	***200***	***19.9***	1.65	1.093	***1.0***	670	320	1.48
42	31*	1060	***200***	***19.9***	1.65	1.093	***1.5***	670	390	1.58
43	33	756	***375***	***5.0***	1.65	0.854	***0.0***	756	0	1.00
44	34	991	***375***	***5.0***	1.65	0.822	***1.0***	756	235	1.31
45	35	1105	***375***	***5.0***	1.65	0.818	***1.5***	756	349	1.46
46	37	820	***375***	***10.0***	1.65	0.875	***0.0***	820	0	1.00
47	38	1089	***375***	***10.0***	1.65	0.837	***1.0***	820	269	1.33
48	41	850	***375***	***15.0***	1.65	0.879	***0.0***	850	0	1.00
49	49	815	***675***	***5.0***	1.65	0.885	***0.0***	815	0	1.00
50	50	1030	***675***	***5.0***	1.65	0.870	***1.0***	675	355	1.53
51	53	900	***675***	***10.0***	1.65	0.893	***0.0***	900	0	1.00
52	65	440	***91***	***5.0***	1.65	0.864	***0.0***	440	0	1.00
53	66	526	***91***	***5.0***	1.65	0.864	***1.0***	440	86	1.20
54	67	750	***91***	***5.0***	1.65	0.885	***1.5***	440	310	1.70
55	68	855	***91***	***5.0***	1.65	0.906	***2.0***	440	415	1.94
56	69	485	***91***	***10.0***	1.65	0.868	***0.0***	485	0	1.00
57	70	600	***91***	***10.0***	1.65	0.868	***1.0***	485	115	1.24
58	71	795	***91***	***10.0***	1.65	0.889	***1.5***	485	310	1.64
59	72	885	***91***	***10.0***	1.65	0.909	***2.0***	485	400	1.82
60	73	505	***91***	***15.0***	1.65	0.887	***0.0***	505	0	1.00
61	74	670	***91***	***15.0***	1.65	0.885	***1.0***	505	165	1.33
62	75	847	***91***	***15.0***	1.65	0.896	***1.5***	505	342	1.68
63	76	965	***91***	***15.0***	1.65	0.896	***2.0***	505	460	1.91
64	77	500	***91***	***20.0***	1.65	0.887	***0.0***	500	0	1.00
65	78	782	***91***	***20.0***	1.65	0.885	***1.0***	500	282	1.56
66	79	905	***91***	***20.0***	1.65	0.875	***1.5***	500	405	1.81
67	77*	505	***91***	***20.0***	1.65	1.079	***0.0***	505	0	1.00

#	Run	Njs	dp	X	(ρS-ρL)/ρL	vL/v_w	JG	Njsu	ΔNjs	Njs/Njsu
		rpm	µm	%	-	-	cm/s	rpm	rpm	-
68	78*	770	***91***	***20.0***	1.65	1.065	***1.0***	505	265	1.52
69	79*	920	***91***	***20.0***	1.65	1.052	***1.5***	505	415	1.82
70	80	1000	***91***	***20.0***	1.65	0.875	***2.0***	505	495	1.98
71	81	663	91	5.0	***3.20***	0.868	***0.0***	663	0	1.00
72	82	983	91	5.0	***3.20***	0.833	***1.0***	663	320	1.48
73	83	1085	91	5.0	***3.20***	0.827	***1.5***	663	422	1.64
74	85	750	91	10.0	***3.20***	0.864	***0.0***	750	0	1.00
75	86	1076	91	10.0	***3.20***	0.846	***1.0***	750	326	1.43
76	86*	1084	91	10.0	***3.20***	0.917	***1.0***	750	334	1.45
77	89	778	91	15.0	***3.20***	0.885	***0.0***	778	0	1.00
78	90	1095	91	15.0	***3.20***	0.885	***1.0***	778	317	1.41
79	97	735	91	5.0	***3.70***	0.896	***0.0***	735	0	1.00
80	98	1045	91	5.0	***3.70***	0.875	***1.0***	735	310	1.42
81	101	805	91	10.0	***3.70***	0.826	***0.0***	805	0	1.00
82	105	835	91	15.0	***3.70***	0.816	***0.0***	835	0	1.00
83	113	480	91	18.6	1.42	***1.754***	0.0	480	0	1.00
84	114	740	91	18.6	1.42	***1.754***	1.0	480	260	1.54
85	115	494	91	17.7	1.29	***3.526***	0.0	494	0	1.00
86	116	870	91	17.7	1.29	***3.526***	1.0	494	376	1.76
87	119	560	200	18.6	1.42	***1.957***	0.0	560	0	1.00
88	120	930	200	18.6	1.42	***1.899***	1.0	560	370	1.66
89	121	510	200	17.7	1.29	***3.655***	0.0	510	0	1.00
90	122	920	200	17.7	1.29	***3.552***	1.0	510	410	1.80
91	125	510	200	17.2	1.20	***6.980***	0.0	510	0	1.00
92	126	830	200	17.2	1.20	***6.964***	1.0	510	320	1.63

Note: Phase I: Run 1-80; Phase II: Run 81-112; Phase III: Run 113-126; * - indicates duplicate runs.

A.5 MULTIPLE LINEAR REGRESSION RESULTS

Table A.12 Regression Results: Two-Phase, Phase I, II

$$\log N_{jsu} = \log K_{SL} + c.\log d_p + d.\log X + e.\log(\Delta\rho/\rho_L)$$

	log KSL	c	d	e	f	KSL	Multiple R	0.991
Fit	1.734	**0.345**	**0.123**	**0.658**		**54.2**	**R Square**	**0.982**
Std Dev	0.032	0.011	0.012	0.022			Adjust R2	0.980
+ 95 %	0.067	0.023	0.024	0.046		9.0	Std Error	0.014
- 95 %	0.067	0.023	0.024	0.046		7.7	**Observations**	**27**

Data taken from Table A.2

Table A.13 Regression Results: Two-Phase, Phase I, II, III (viscosity)

$$\log N_{jsu} = \log K_{SL} + 0.345.\log d_p + 0.123.\log X + 0.658.\log(\Delta\rho/\rho_L) + f.\log(\nu_L/\nu_w)$$

	log KSL	c	d	e	f	KSL	Multiple R	0.153
Fit	**1.733**	0.345	0.123	0.658	**-0.013**	**54.1**	**R Square**	**0.023**
Std Dev	0.004				0.016		Adjust R2	-0.009
+ 95 %	0.007				0.033	0.9	Std Error	0.020
- 95 %	0.007				0.033	0.9	**Observations**	**32**

Data taken from Table A.2

Table A.14 Regression Results: Three-phase, JG = 1.0 cm/s, Phase I, II

$$\log(N_{jsg}/(1+0.40.J_G)) = \log N_{jsu'} = \log K_{SL'} + c'.\log d_p + d'.\log X + e'.\log(\Delta\rho/\rho_L)$$

	log KSL'	c'	d'	e'	f'	KSL'	Multiple R	0.975
Fit	1.449	**0.389**	**0.249**	**0.845**		**28.1**	**R Square**	**0.950**
Std Dev	0.070	0.025	0.022	0.054			Adjust R2	0.943
+ 95 %	0.147	0.053	0.046	0.112		11.3	Std Error	0.026
- 95 %	0.147	0.053	0.046	0.112		8.1	**Observations**	**25**

Data taken from Table A.8

Table A.15 Regression Results: Three-phase, JG = 1.0 cm/s, Phase I, II, III (viscosity)

$$\log(N_{jsg}/(1+0.40.J_G)) = \log N_{jsu'} = \log K_{SL'} + 0.389.\log d_p + 0.249.\log X + 0.845.\log(\Delta\rho/\rho_L) + f'.\log(\nu_L/\nu_w)$$

	log KSL'	c'	d'	e'	f'	KSL'	Multiple R	0.668
Fit	1.458	0.389	0.249	0.845	**0.128**	**28.7**	**R Square**	**0.447**
Std Dev	0.006				0.026		Adjust R2	0.428
+ 95 %	0.012				0.054	0.8	Std Error	0.032
- 95 %	0.012				0.054	0.8	**Observations**	**31**

Data taken from Table A.8

Table A.16 Regression Results: Three-phase, JG = 1.5 cm/s, Phase I, II

$$\log(N_{jsg}/(1+0.40.J_G)) = \log N_{jsu'} = \log K_{SL'} + c'.\log d_p + d'.\log X + e'.\log(\Delta\rho/\rho_L)$$

	log KSL'	c'	d'	e'	f'	KSL'	Multiple R	0.970
Fit	1.907	**0.266**	**0.139**	**0.607**		**80.7**	**R Square**	**0.941**
Std Dev	0.060	0.022	0.016	0.061			Adjust R2	0.927
+ 95 %	0.131	0.048	0.034	0.131		28.3	Std Error	0.015
- 95 %	0.131	0.048	0.034	0.131		21.0	**Observations**	**17**

Data taken from Table A.9

Table A.17 Regression Results: Three-phase, JG = 2.0 cm/s, Phase I, II

$$\log(N_{jsg}/(1+0.40.J_G)) = \log N_{jsu'} = \log K_{SL'} + c'.\log d_p + d'.\log X + e'.\log(\Delta\rho/\rho_L)$$

	log KSL'	c'	d'	e'	f'	KSL'	Multiple R	0.972
Fit	2.267	**0.168**	**0.109**			**184.9**	**R Square**	**0.945**
Std Dev	0.043	0.020	0.012				Adjust R2	0.821
+ 95 %	0.098	0.044	0.028			47.0	Std Error	0.010
- 95 %	0.098	0.044	0.028			37.5	**Observations**	**12**

Data taken from Table A.10

Table A.18 Regression Results: Three-phase, JG = 1.0, 1.5, 2.0 cm/s, Phase I, II

$$\log(N_{jsg}/(1+0.40.J_G)) = \log N_{jsu'} = \log K_{SL'} + c'.\log d_p + d'.\log X + e'.\log(\Delta\rho/\rho_L)$$

	log KSL'	c'	d'	e'	f'	KSL'	Multiple R	0.937
Fit	1.719	**0.313**	**0.184**	**0.731**		**52.4**	**R Square**	**0.878**
Std Dev	0.059	0.022	0.017	0.047			Adjust R2	0.871
+ 95 %	0.118	0.044	0.034	0.094		16.4	Std Error	0.030
- 95 %	0.118	0.044	0.034	0.094		12.5	**Observations**	**55**

Data taken from Table A.7

Table A.19 Regression Results: Three-phase, JG = 1.0, 1.5, 2.0 cm/s, Phase I, II, III (viscosity)

$$\log(N_{jsg}/(1+0.40.J_G)) = \log N_{jsu'} = \log K_{SL'} + 0.313.\log d_p + 0.184.\log X + 0.731.\log(\Delta\rho/\rho_L) + f'.\log(\nu_L/\nu_w)$$

	log KSL'	c'	d'	e'	f'	KSL'	Multiple R	0.521
Fit	1.725	0.313	0.184	0.731	**0.114**	**53.1**	**R Square**	**0.272**
Std Dev	0.004				0.024		Adjust R2	0.259
+ 95 %	0.008				0.049	1.0	Std Error	0.031
- 95 %	0.008				0.049	1.0	**Observations**	**60**

Data taken from Table A.7

Table A.20 Regression Results: Two- and Three-phase, JG = 0.0, 1.0, 1.5, 2.0 cm/s, Phase I, II

$$\log(N_{jsg}/(1+0.40.J_G)) = \log N_{jsu'} = \log K_{SL'} + c'.\log d_p + d'.\log X + e'.\log(\Delta\rho/\rho_L) + f'.\log(\nu_L/\nu_w)$$

	log KSL'	c'	d'	e'	f'	KSL'	Multiple R	0.955
Fit	1.711	**0.331**	**0.165**	**0.695**		**51.4**	**R Square**	**0.912**
Std Dev	0.040	0.015	0.013	0.030			Adjust R2	0.909
+ 95 %	0.079	0.029	0.025	0.059		10.3	Std Error	0.027
- 95 %	0.079	0.029	0.025	0.059		8.6	**Observations**	**82**

Data taken from Table A.11

Table A.21 Regression Results: Two- and Three-phase, JG = 0.0, 1.0, 1.5, 2.0 cm/s, Phase I, II, III (viscosity)

$$\log(N_{jsg}/(1+0.40.J_G)) = \log N_{jsu'} = \log K_{SL'} + 0.331.\log d_p + 0.165.\log X + 0.695.\log(\Delta\rho/\rho_L) + f'.\log(\nu_L/\nu_w)$$

	log KSL'	c'	d'	e'	f'	KSL'	Multiple R	0.272
Fit	1.712	0.331	0.165	0.695	**0.047**	**51.6**	**R Square**	**0.074**
Std Dev	0.003				0.018		Adjust R2	0.064
+ 95 %	0.007				0.035	0.8	Std Error	0.031
- 95 %	0.007				0.035	0.8	**Observations**	**92**

Data taken from Table A.11

APPENDIX B. CONCENTRATION PROFILE DATA

APPENDIX B. CONCENTRATION PROFILE DATA 249

B.1 SOLIDS CONCENTRATION PROFILE TWO-PHASE DATA 250

B.2 SOLIDS CONCENTRATION PROFILE THREE-PHASE DATA 251

B.1 SOLIDS CONCENTRATION PROFILE TWO-PHASE DATA

Table B.1 Solids Concentration Profile Two-Phase Data

#	Run*1	N	Njs	%Njs	d_p	Xact	ρS	ρL	vL	JG	ΦG	X_{h95}	X_{h85}	X_{h75}	X_{h65}	X_{h55}	X_{h45}	X_{h35}	X_{h25}	X_{h15}	X_{h05}	Xm	Xms	Xm /Xms	hs / T	RSD
		rpm	rpm	%	µm	%	kg/l	kg/l	x10-6m2/s	cm/s	%	%	%	%	%	%	%	%	%	%	%	%		%		%
1	77	300	500	60	91	20.0	2.65	1.00	0.906	0.0	0.0	0.0	0.0	0.8	20.7	23.8	23.7	24.6	24.2	24.8	24.8	16.7	19.9	84.0	0.70	68
2	77	450	500	90	91	20.0	2.65	1.00	0.902	0.0	0.0	0.3	15.4	22.6	22.6	22.4	22.1	22.4	22.2	22.8	22.2	19.5	19.9	97.9	0.88	36
3	77	500	500	100	91	20.0	2.65	1.00	0.887	0.0	0.0	1.5	20.5	22.5	22.3	22.3	22.3	22.2	22.0	22.0	21.7	19.9	19.9	100.0	0.91	33
4	77	600	500	120	91	20.0	2.65	1.00	0.898	0.0	0.0	15.8	20.5	20.8	20.5	20.4	20.3	20.3	20.3	19.9	19.8	19.9	19.9	99.7	1.00	7
5	77	750	500	150	91	20.0	2.65	1.00	0.893	0.0	0.0	16.9	20.2	20.5	19.9	19.6	19.6	19.7	19.5	19.2	18.7	19.4	19.9	97.3	1.00	5
6	29	300	675	44	200	19.9	2.65	1.00	0.889	0.0	0.0	0.0	0.0	0.0	3.6	7.3	8.3	8.8	8.8	9.0		5.1	19.5	26.1	0.10	82
7	29	450	675	67	200	19.9	2.65	1.00	0.891	0.0	0.0	0.0	0.0	6.9	25.4	25.8	25.5	25.5	25.7	25.1	24.9	18.5	19.5	94.8	0.73	61
8	29	600	675	89	200	19.9	2.65	1.00	0.891	0.0	0.0	0.3	11.5	23.6	23.6	22.7	21.9	21.8	21.7	21.4	20.9	18.9	19.5	97.1	0.87	39
9	29	675	675	100	200	19.9	2.65	1.00	0.856	0.0	0.0	3.9	20.7	22.9	22.0	21.7	20.8	20.8	21.4	20.7	19.9	19.5	19.5	100.0	0.92	28
10	29	750	675	111	200	19.9	2.65	1.00	0.887	0.0	0.0	14.7	21.3	21.8	20.6	19.7	19.7	20.8	19.9	19.4	18.2	19.6	19.5	100.7	1.00	10

*1: Run no's as per critical impeller speed work

B.2 SOLIDS CONCENTRATION PROFILE THREE-PHASE DATA

Table B.2 Solids Concentration Profile Three-Phase Data

#	Run**	N	Njs	%Njs	d_p	Xact	ρS	ρL	vL	JG	ΦG	X_{h95}	X_{h85}	X_{h75}	X_{h65}	X_{h55}	X_{h45}	X_{h35}	X_{h25}	X_{h15}	X_{h05}	Xm	Xms	Xm /Xms	hs / T	RSD
		rpm	rpm	%	µm	%	kg/l	kg/l	x10-6m2/s	cm/s	%	%	%	%	%	%	%	%	%	%	%	%		%		%
21	78	300	782	38	91	20.0	2.65	1.00	0.887	1.0	4.9	9.2	9.3	9.5	10.1	11.5	11.8	11.9	12.1	12.4		10.9	21.5	50.5	0.58	12
22	78	450	782	58	91	20.0	2.65	1.00	0.887	1.0	8.2	6.9	10.1	18.6	22.4	23.6	23.3	24.0	23.8	24.8	25.0	20.2	21.5	94.2	0.84	32
23	78	600	782	77	91	20.0	2.65	1.00	0.887	1.0	11.3	5.8	13.5	20.3	23.1	24.1	24.0	24.6	24.8	25.5	25.5	21.1	21.5	98.3	0.88	31
24	78	750	782	96	91	20.0	2.65	1.00	0.885	1.0	13.0	5.6	12.5	20.2	23.1	23.8	24.3	24.5	24.5	25.3	25.0	20.9	21.5	97.1	0.87	32
25	78	782	782	100	91	20.0	2.65	1.00	0.885	1.0	13.7	6.5	14.4	21.1	23.3	24.3	24.6	25.1	24.7	25.7	25.3	21.5	21.5	100.0	0.89	29
26	78	900	782	115	91	20.0	2.65	1.00	0.885	1.0	15.1	12.0	18.8	21.4	22.8	23.5	23.1	23.9	24.1	24.5	24.2	21.8	21.5	101.6	0.97	18
27	30*	300	1012	30	200	19.9	2.65	1.00	0.868	1.0	4.1	1.0	1.2	1.4	1.4	2.1	2.0	2.2	2.5	3.9		2.0	20.3	9.7	0.10	45
28	30*	450	1012	44	200	19.9	2.65	1.00	0.873	1.0	6.7	1.9	3.6	6.9	12.5	15.9	17.1	16.7	18.6	20.6	23.0	13.7	20.3	67.4	0.69	53
29	30*	600	1012	59	200	19.9	2.65	1.00	0.875	1.0	10.3	2.3	5.2	14.8	20.8	22.4	22.6	23.9	24.3	24.7	25.1	18.6	20.3	91.7	0.80	45
30	30*	750	1012	74	200	19.9	2.65	1.00	0.875	1.0	11.9	2.6	7.8	16.7	21.8	23.1	23.0	24.5	24.6	24.9	24.9	19.4	20.3	95.7	0.83	41
31	30*	900	1012	89	200	19.9	2.65	1.00	0.868	1.0	13.2	3.0	11.6	18.4	22.4	23.8	23.7	24.6	24.5	25.0	24.1	20.1	20.3	99.2	0.87	36
32	30*	1012	1012	100	200	19.9	2.65	1.00	0.854	1.0	13.9	3.8	14.5	19.4	24.0	24.0	23.1	24.3	23.7	23.6	22.4	20.3	20.3	100.0	0.89	32

*1: Run no's as per critical impeller speed work